Methods for the Efficient and Accurate Simulation of Marine and Aerospace Electrical Power Networks

Patrick J. Norman

Submitted for the Degree

of

Doctor of Philosophy

Institute for Energy and Environment

Department of Electronic and Electrical Engineering

University of Strathclyde

Glasgow G1 1XW

Scotland, UK

August 2009

Abstract

The role of modelling and simulation to the development of marine and aerospace electrical power distribution systems is becoming increasingly important as these industries embrace the more-electric concept. The large penetration of novel technologies employed in these designs places a great need on identifying key operating deficiencies and issues at an early stage in the design process. However, this thesis identifies that existing techniques which are potentially suitable for the modelling and simulation of marine and aerospace electrical power distribution systems primarily suffer from being either very time intensive to implement of numerically unstable during simulated fault conditions. Such challenges can limit the potential usefulness of modelling and simulation as part of the overall design process.

As such, this thesis addresses the need for methods which enable the efficient simulation of electrical network architectures with a significant penetration of power electronics. Two new simulation methods are developed which address the different shortcomings of existing techniques. These methods are also complementary and compatible with other existing simulation techniques.

The first method presented, Multi-Level Model Discretization, is a framework which enables the development of a power system model as a conventional continuous model before applying a range existing techniques tailored to reduce the overall computational burden of associated simulations. This can be readily achieved even if the model developer does not have extensive prior modelling and simulation knowledge and expertise.

The second method, Advanced Functional Modelling, incorporates novel functionality into the existing functional modelling method in order to overcome the occurrence of numerical instability during simulated fault conditions, whilst still facilitating efficient simulation of networks with a significant penetration of power electronics.

Contents

Figures

Tables

Acknowledgements

I would like to take this opportunity to thank my colleagues within the AES group for their continued support and encouragement. In particular I would like to thank Stuart Galloway for his valuable guidance in both the completion of this thesis and my research career as a whole.

I also owe a huge thank you to my family, especially my beautiful wife Lisa for being so understanding when many of our evenings together were lost to my never ending write up and for constantly listening to my woes and stresses. You have loyally stood by me over the last six years, and for that I am incredibly grateful, I couldn't have done this without you.

To my two wonderful children, thank you Matthew for providing an immovable deadline for the completion of the first draft of this thesis. Thank you too Emma for providing the second immovable deadline to complete my viva and corrections. If either of you decide to study for a PhD in the future, hopefully I can repay your contributions in the future with some loving guidance and support.

Chapter 1 – Thesis Outline and Principal Contributions

This thesis investigates the challenges faced in the dynamic simulation of more-electric marine and aerospace electrical distribution networks. On the basis of this investigation, novel abstraction techniques for power electronic converter models are developed to facilitate accurate and computationally efficient simulation of the aforementioned networks. The techniques developed will be demonstrated on models of representative marine and aerospace more-electric architectures.

1.1 Chapter Overview

This chapter will briefly introduce the more-electric aircraft and ship concepts, discussing the technologies utilised, potential benefits and the challenges faced in their development. The importance of modelling and simulation to these application areas will be discussed and an outline of some of the challenges faced will be given. The principal contributions described within this thesis are then summarised and finally, a chapter-by-chapter outline of the thesis is given. This concludes with a list of related publications by the author.

1.2 Background and Justification for Research

The marine and aerospace industries are experiencing a significant step change in technological development to embrace the more-electric concept [1, 2]. This change

sees the partial or complete replacement of the traditional bulky and heavy mechanical, hydraulic and pneumatic based power distribution systems with a common electrical power system. The more-electric concept is expected to provide potentially significant benefits in system efficiency, capability and flexibility.

Such a significant step change in technologies brings with it many new challenges and difficulties, and although the development of individual technologies is still a key issue, it is the integration of these that will provide perhaps the biggest challenges [3, 4]. For example, the absence of any grid connection to marine and aerospace power distributions systems (unless connected to a shore supply or ground cart respectively) distinguishes them from conventional land based systems. They are instead, finite inertia islanded systems. As such they are also particularly sensitive to network disturbances (e.g. load changes and faults). Furthermore, the significant penetration of power electronic converters within marine and aerospace more-electric networks requires that particular care must be taken in the coordination and control of separate systems to avoid instability and other unfavourable operating conditions [5, 6].

Modelling and simulation will play a key part in supporting the development of marine and aerospace more-electric systems by allowing the network-level behaviour of these architectures to be investigated [7]. It will enable the study of interactions between the network systems and will facilitate the identification and correction of adverse operating conditions, de-risking the novel technologies utilised.

However, there are many challenges that currently prevent the full capabilities of the modelling and simulation from being realised. One particular challenge is the extensive computational burden of dynamic network-level simulations, which often causes slow running and failed simulations. Techniques which improve the computational efficiency of dynamic simulations whilst retaining the key model characteristics are invaluable to the development of more-electric systems [7]. Indeed, the efficient simulation of power electronic converter models is especially important as these impose a particularly substantial burden on the computation of the overall network model [8]. However, because of their key role in determining the underlying behaviour of many marine and aerospace more-electric networks, the behaviour of the power electronic converters must still be accurately captured to ensure that representative simulation results are produced.

This thesis investigates those techniques currently available for improving the efficiency of simulating power electronic converters within the context of larger electrical network models. It assesses their suitability to network-level dynamic simulations of marine and aerospace more-electric architectures, identifying the best suited methods and discussing their key strengths and limitations. Building on this knowledge, novel techniques are proposed in this thesis to facilitate an improved simulation capability for network-level simulations of marine and aerospace more-electric architectures during both normal and fault conditions.

Note that although marine and aerospace more-electric applications appear to be significantly different in nature, many of the key challenges faced are concurrent and so the core research themes laid out in this thesis are relevant to both applications.

1.3 Research Objectives

The research presented in this thesis addresses the following objectives:

- To analyse the requirements and challenges faced in the modelling and simulation of marine and aerospace more-electric power distribution network architectures.
- To investigate existing options for improving simulation efficiency of electrical power distribution networks with a significant penetration of power electronics whilst retaining appropriate levels of accuracy, identifying those techniques and methods which are best suited for this domain.
- To fully assess the capabilities and limitations of these techniques and make recommendations for their use.
- To develop novel methods to improve the computational efficiency of simulating electrical power distribution networks with a significant penetration of power electronics in order to maximise the potential benefit of modelling and simulation to the development of marine and aerospace more-electric systems.

1.4 Principal Contributions

The principal contributions of this thesis are summarised as follows:

- Unique challenges are identified with respect to the modelling and simulation of marine and aerospace more-electric network architectures. These stem from the difficulties of achieving computationally efficient and yet accurate dynamic simulations of the electrical networks containing power electronics. Functional based modelling approaches are identified as being the most suited for use within more-electric applications.
- The barrier presented by algebraic loops to the effective simulation of larger 'more-electric' type networks is analysed. This is a result of their adverse impact on the accuracy and numerical stability of functional converter modelling approaches and other modelled systems commonly found in marine and aerospace electrical network models.
- The functional modelling approach is shown to be unreliable for simulating electrical faults in network-level models of marine and aerospace more-electric architectures. This is the result of a detailed analysis of the capabilities, limitations and resulting suitability of the functional modelling technique for marine and aerospace more-electric networks.
- A novel modelling approach, Multi-Level Model Discretization (MLMD), is developed to facilitate the efficient and accurate simulation of more-electric marine and aerospace electrical networks. It is also numerically stable during simulated electrical fault conditions. This technique cannot represent the time averaged behaviour of converters though.

- A second modelling technique, Advanced Functional Modelling (AFM), is developed to model the time-averaged representation of power electronic converters and maintain stability under simulated fault conditions. AFM builds upon the existing functional modelling approach but includes novel features to address its existing weaknesses during simulated fault studies.

1.5 Thesis Outline

This section will summarise core technical chapters of this thesis.

Chapter two reviews more-electric marine and aerospace technologies, discussing the opportunities and unique challenges faced in each application. It also addresses the core technologies employed within more-electric marine and aerospace networks before discussing the underlying common challenges faced in both domains.

Chapter three outlines the role of modelling and simulation in supporting the development of more-electric technologies. The challenges faced in this field are discussed with particular aspects such as accurate and efficient dynamic simulations being recognised as key difficulties. To overcome these aspects, the need for techniques which improve the computational efficiency of simulating electrical power networks with a significant penetration of power electronics is identified. Existing techniques are reviewed and the functional modelling technique is identified as being particularly suited for this task. The strengths and weaknesses of this technique (as discussed in existing literature) are considered before a research path forward is proposed.

Chapter four introduces algebraic loops and provides examples of their presence within functional converters and other models common to marine and aerospace electrical networks. Through detailed analysis, it demonstrates how iterative solvers are necessary to solve models containing algebraic loops and discusses the negative impact these have on simulation efficiency. Techniques to lessen the adverse impact of algebraic loops are reviewed in detail, with the positive and negative qualities of each being considered. These techniques are analysed further in order to identify their best use within marine and aerospace more-electric architecture models.

Chapter five investigates the capabilities and limitations of the functional modelling technique for the simulation of marine and aerospace more-electric networks. Weaknesses are found relating to poor accuracy and numerical instability during simulated electrical fault studies. Conclusions are drawn regarding its usefulness for the specified application areas.

Chapter six proposes an alternative approach for modelling electrical networks with a high penetration of power electronics. This new approach builds on the findings of the previous two chapters. The technique, Multi-Level Model Discretization, facilitates computationally efficient and accurate network-level dynamic simulations, even during fault conditions. Example case studies are included to demonstrate both its effectiveness and limitations. The chapter closes with a discussion regarding the application of this technique to models of marine and aerospace more-electric network architectures.

Chapter seven proposes an additional novel technique, Advanced Functional Modelling, developed to improve the fault performance of functional models. This technique can be utilised to implement both pulsed output and time-averaged output converter models which maintain accuracy during fault conditions. Detailed analysis and case studies are utilised to demonstrate its effectiveness. The chapter concludes by considering the capabilities and limitations of this technique and outlining how the method could be developed further.

Chapter eight reviews the contribution made by this thesis and draws conclusions on the use of the Multi-Level Model Discretization and Advanced Functional Modelling techniques for use within marine and aerospace more-electric network simulation.

1.6 Related Publications

Publications by the author and related to this thesis are:

P. Norman, G. Dudgeon, J. R. McDonald, "A Review of the Current and Future Role of Power Electronics within Marine More-Electric Environments," in *Proc. 38th International Universities Power Engineering Conference (UPEC)*, Thessaloniki, Greece, 2003, pp 197 – 200.

P. J. Norman, G. J. W. Dudgeon, J. R. McDonald, "Assessment and recommendations for the modelling of faults and interactions within power

electronics based power systems," *in Proc. Ninth IEEE Workshop on Computers in Power Electronics COMPEL 2004*, University of Illinois, August 2004.

P. J. Norman, C.D. Booth, J.D. Schuddebeurs, G.M. Burt, J.R. McDonald, J.M Apsley, M. Barnes, A.C Smith, S. Williamson, E. Tsoudis, P. Pilidis, R. Singh, "Integrated electrical and mechanical modelling of integrated-full-electric-propulsion systems," *in Proc. The 3rd IET Power Electronics Machines and Drives conference (PEMD 2006),* April 2006, Dublin, Ireland.

P. J. Norman, C. D. Booth, J. D. Schuddebeurs, S. J. Galloway, G. M. Burt, J. R. McDonald, A. Villasenor, R. Todd, J. M Apsley, M. Barnes, A.C Smith, S. Williamson, E. Tsoudis, P. Pilidis, R. Singh, "Simulating IFEP Systems," *Marine Engineering Review (MER)*, pp. 26 – 31, October 2006.

I. M. Elders, **P. J. Norman**, J. D. Schuddebeurs, C. D. Booth, J. R. McDonald, J. Apsley, M. Barnes, A. Smith, A. Forsyth, S. Loddick, I. Myers, "Modelling and analysis of electro-mechanical interactions between prime-mover and load in a marine IFEP system," *IEEE Electric Ship Technologies Symposium (ESTS)*, May 2007.

P. J. Norman, S. J. Galloway, and J. R. McDonald, "Simulating electrical faults within future aircraft networks," *IEEE Transactions on Aerospace and Electronic Systems*, Vol. 44, no. 1, pp. 99 – 110, January 2008.

P. J. Norman, S. J. Galloway, G. M. Burt, D. R. Trainer, M. Hirst, "Transient analysis of the more-electric engine electrical power distribution network," *The 4th International Conference on Power Electronics Machines and Drives 2008 (PEMD 2008)*, 2nd-4th April 2008, York.

P. J. Norman, S. J. Galloway, G. M. Burt, J. E. Hill, D. R. Trainer, "Evaluation of the dynamic interactions between aircraft gas turbine engine and electrical system," *The 4th International Conference on Power Electronics Machines and Drives 2008 (PEMD 2008)*, 2nd-4th April 2008, York.

J. D. Schuddebeurs, **P. J. Norman**, S. J. Galloway, G. M. Burt, J. R. McDonald, J. Apsley, "A high fidelity integrated system model for marine power systems," *The 2nd Annual IEEE International Systems Conference*, 7th – 10th April 2008, Montreal.

P. J. Norman, S. J. Galloway, G. M. Burt, J. R. McDonald, "Functional converter models for electrical fault simulations within aircraft power systems," *submitted to IEEE Transactions on Aerospace and Electronic Systems*.

In addition to the research papers listed above, numerous other technical reports relating the modelling and simulation of marine and aerospace more-electric networks have also been produced.

1.7 References

[1] D.S. Parker and C.G. Hodge, "The electric warship", *Trans IMarE*, vol. 108, part 2, pp. 109-125, 1996.

[2] Lester F. Faleiro, "Trends towards a more electrical aircraft," Liebherr-Aerospace. Available: http://www.poa-project.com/53.asp

[3] A. D. Crane, R. E. Maltby, M. Benatmane, Capt. J. M. Newell, "Naval power and propulsion system: the intricacies of integration", *World Maritime Technology Conference*, March 2006.

[4] Gareth E. Moore, Nnamdi Okaeme, David Trainer, Stephen Long, "Electrical mechanical interaction study," Rolls-Royce internal report. Document number DNS 124710.

[5] CDR John V. Amy Jr, "Modern, high-converter-populations argue for changing how to design naval electric power systems," *Proceedings of the 2005 IEEE Electric Ship Technologies Symposium (ESTS)*, Philadelphia, July 2005, pp 280 – 283.

[6] S.D. Sudhoff, S.F. Glover, P.T. Lamm, D.H. Schmucker, D.E. Delisle, "Stability analysis of dc power electronics based distribution system using admittance space constraints," *IEEE Trans. on Aerospace and Electronic Systems*, Vol. 36, no. 3, pp. 965 – 973, July 2000.

[7] Graham J. W. Dudgeon, James R. McDonald, "Simulation challenges for the all electric ship – form micro-second to macro-second," *Proc. IMarEST Electric Warship IX Seminar*, December 2003, pp. 42 – 54.

[8] A. M. Gole, Albert Keri, C. Nwankpa, E. W. Gunther, H. W. Dommel, I. Hassan, J. R. Marti, J. A. Martinez, K. G. Fehrle, L. Tang, M. F.

McGranaghan, O. B. Nayak, P. F. Ribeiro, R. Iravani, R. Lasseter, "Guidelines for modeling power electronics in electric power engineering applications," *IEEE Trans. on Power Delivery*, Vol. 12, No. 1, pp. 505 – 514, January 1997.

Chapter 2 – Overview of Marine and Aerospace More-Electric Applications

2.1 Chapter Overview

Marine and aerospace industries are poised for significant technological step changes in the near future as the more-electric concept is applied to system designs within both of these application areas [1 - 3]. This concept sees the traditionally mechanical, hydraulic and pneumatic power distribution systems replaced to a varying degree by power dense electric equivalents offering potentially significant space and weight savings. The advanced electrical power distribution employed in these systems should also provide a greater system capability, operational efficiency and increased design flexibility than was previously capable with the traditional approach.

This chapter will give a general overview of how the more-electric concept is being applied to the marine and aerospace industries, outlining the key developments in recent years. Looking at each application in turn, it will describe the individual novel technologies utilised, discussing the potential benefits and challenges these technologies bring. Power electronics underpin the successful utilisation of many of these novel technologies and the evolution of their role within marine and aerospace more-electric architectures is discussed. The chapter concludes by highlighting the commonality between marine and aerospace more-electric applications and

discussing the key research challenges faced in the development of both of these areas.

2.2 Marine More-Electric Systems

In the marine sector, the more-electric concept is being incorporated into new designs of both commercial and naval vessels giving competitive advantages over traditional designs [1]. It also represents a key stage in the progression towards the all-electric ship. Figure 2.1 illustrates conventional and more-electric marine power systems

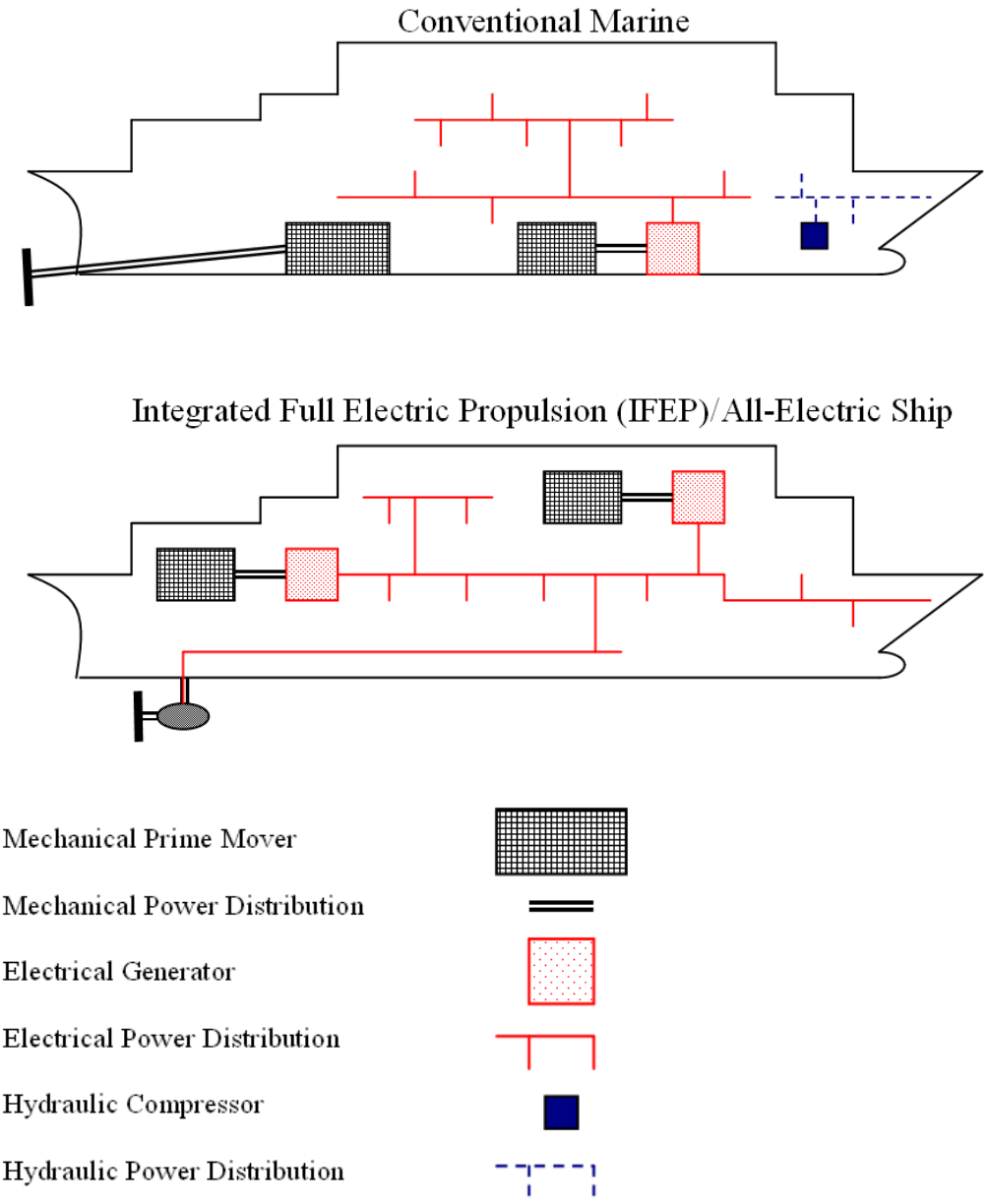

Fig. 2.1. Evolution of ship power distribution technologies

Figures 2.2 and 2.3 provide examples of the power distribution systems of traditional and Integrated Full Electric Propulsion (IFEP)/all-electric vessel designs.

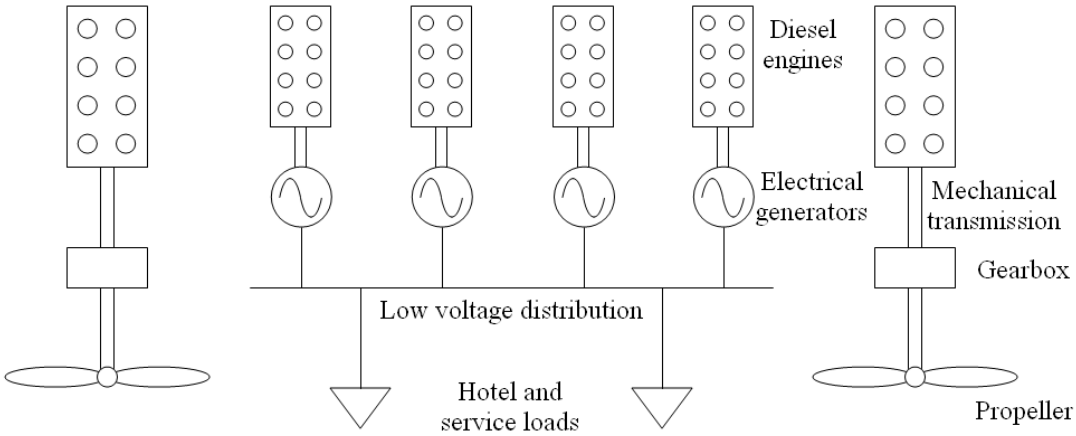

Fig. 2.2. Example traditional marine power distribution system

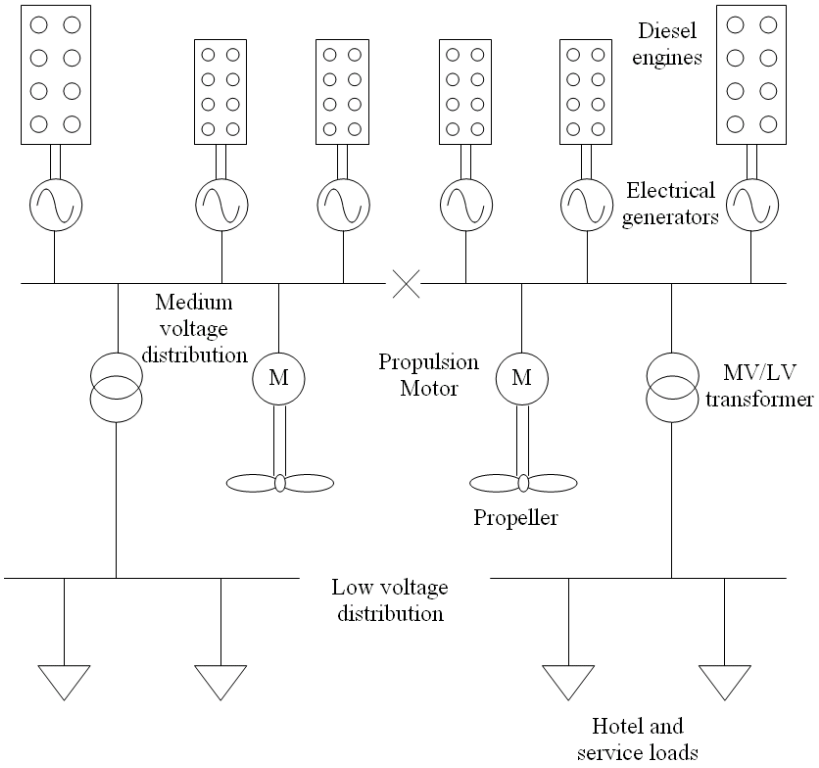

Fig. 2.3. IFEP/All-electric equivalent of the network shown in figure 2.2.

Figures 2.1 and 2.2 illustrate how conventional ship power systems see the use of dedicated prime movers to mechanically power the ship's propulsion systems and separate smaller prime movers to drive electrical generators. This electrical power is

then distributed throughout the ship to the various electrical loads by means of a (traditionally) low voltage distribution network. This approach offers high efficiency operation for vessels which spend a large proportion of their service life travelling at a constant cruising speed, such as tankers and ferries. The technologies utilised are mature and reliable and as such, the mechanical direct-drive approach is well established in most types of marine vessel [1].

Figures 2.1 and 2.3 illustrate how IFEP utilises a single prime mover set to drive electrical power generation in order to supply both the ship's propulsion systems and electrical hotel loads. Additionally, it sees many significant non-electrical loads (such as hydraulic and pneumatic systems) replaced by electrical equivalents [1].

This approach provides a number of key benefits. Firstly, the main prime movers no longer have to be located close to the ship's propellers, thus providing increased design flexibility [1, 4]. This gives the option for locating the prime movers close to the deck of the vessel in order to provide better access for maintenance as well as easier ducting for air inlet and exhaust outlets. This also frees up space within the hull of the vessel for other more beneficial usage.

Secondly, many new IFEP vessels build upon this design flexibility and employ podded propellers [4], where the propulsion motor and drive is embedded in a streamlined pod, located outside the hull of the vessel. This approach allows even more space to be vacated within the vessel's hull. The propeller pods can also be rotated to provide improved vessel manoeuvrability at low speeds.

Another key benefit of IFEP is the greater flexibility in generator scheduling provided by the common set of prime movers. This enables higher system efficiencies at lower cruising speeds and part-load operation [1], and hence makes IFEP particularly suited to vessel types with a widely varied operational profile such as cruise liners, yachts and naval vessels.

The main drawbacks to utilising the IFEP approach are an increased build cost, decreased efficiencies at full load operation, higher network voltage levels (to accommodate the increased installed power levels) and the utilisation of newer, less proven technologies [1].

Figure 2.4 shows an example IFEP network layout and loading [5].

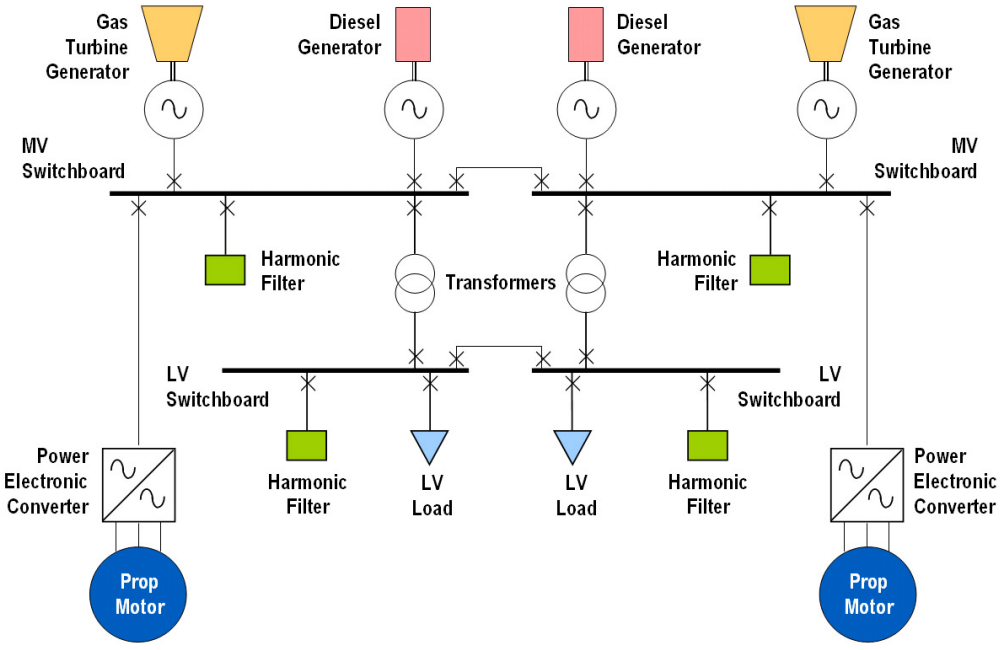

Fig. 2.4. Example IFEP network

(source: "A short power system appreciation course", UTC internal document)

The network depicted in figure 2.4 is an example network for one particular application. The size and nature of the more-electric vessel in question will dictate particular network aspects such as the number and configuration of medium voltage (MV) and low voltage (LV) switchboards, the voltage levels employed, generation options, and the available redundancy in supply (e.g. through tie-lines).

There is no existing standard for the propulsion motor although multiphase permanent magnet synchronous motors and advanced induction motors are two favourable options [6]. The power electronic motor drives are generally designed around the requirements of the motor type and often employ multi-level or series connected architectures in order to operate at the voltage levels of the MV switchboards [7].

At the LV switchboard there is some considerable debate over whether to utilise ac or dc power distribution [8, 9]. The advantages of dc distribution include fewer power conversion stages and greater power transfer through existing cables. However, current dc circuit breaker technology is much bulkier and heavier than its ac counterpart. Alternatively, ac power distribution utilises more proven technologies but presents greater challenges in providing redundancy through fast acting reconfiguration.

Finally, IFEP systems are aiming towards the utilisation of more power electronic interfaced loads and sources to provide greater network control and flexibility [10]. An example of this is the use of power electronic converters to actively limit or block

fault current contributions in order to reduce the large variations in fault level that are common within IFEP networks [11]. However, this also requires the implementation of revised network protection strategies in order to accommodate the resulting non-standard fault characteristics of the network.

Finally, with respect to figure 2.1, the all-electric ship represents the final stage of the evolutionary process where all the significant power systems on the ship will be electrical. This concept is mainly aimed at naval vessels, which may also utilise electromagnetic aircraft launches and pulsed electrical weapons [12, 13]. Opportunities for novel functionality and features such as intelligent post-fault network reconfiguration have also been considered for all-electric ships [14].

2.3 Aerospace More-Electric Systems

Within the aerospace sector, the application of the more-electric concept sees the replacement of the mechanical aircraft systems such as wing flaps, engine guide vanes and air conditioning systems by electrical equivalents. With space and weight at an even greater premium than in marine electrical systems, this substitution of the bulky and heavy mechanical equipment with lighter, more compact electrical systems could provide users of the more-electric aircraft with potentially significant savings in fuel consumption [2, 3]. This aspect is particularly relevant amid the concerns over the growing pollution from commercial air travel.

Although not yet a reality, the more-electric aircraft concept when fully developed, could also provide increased flexibility in the design of the power distribution system and increased levels of safety through improved system redundancy [2, 3].

One example of research in this area is the Power Optimised Aircraft (POA) programme, a European consortium aiming to develop a ground-based technology demonstrator to investigate the potential challenges and benefits of the more-electric approach [15]. The POA concept is illustrated in figure 2.5, which also highlights the core aspects of the more-electric aircraft.

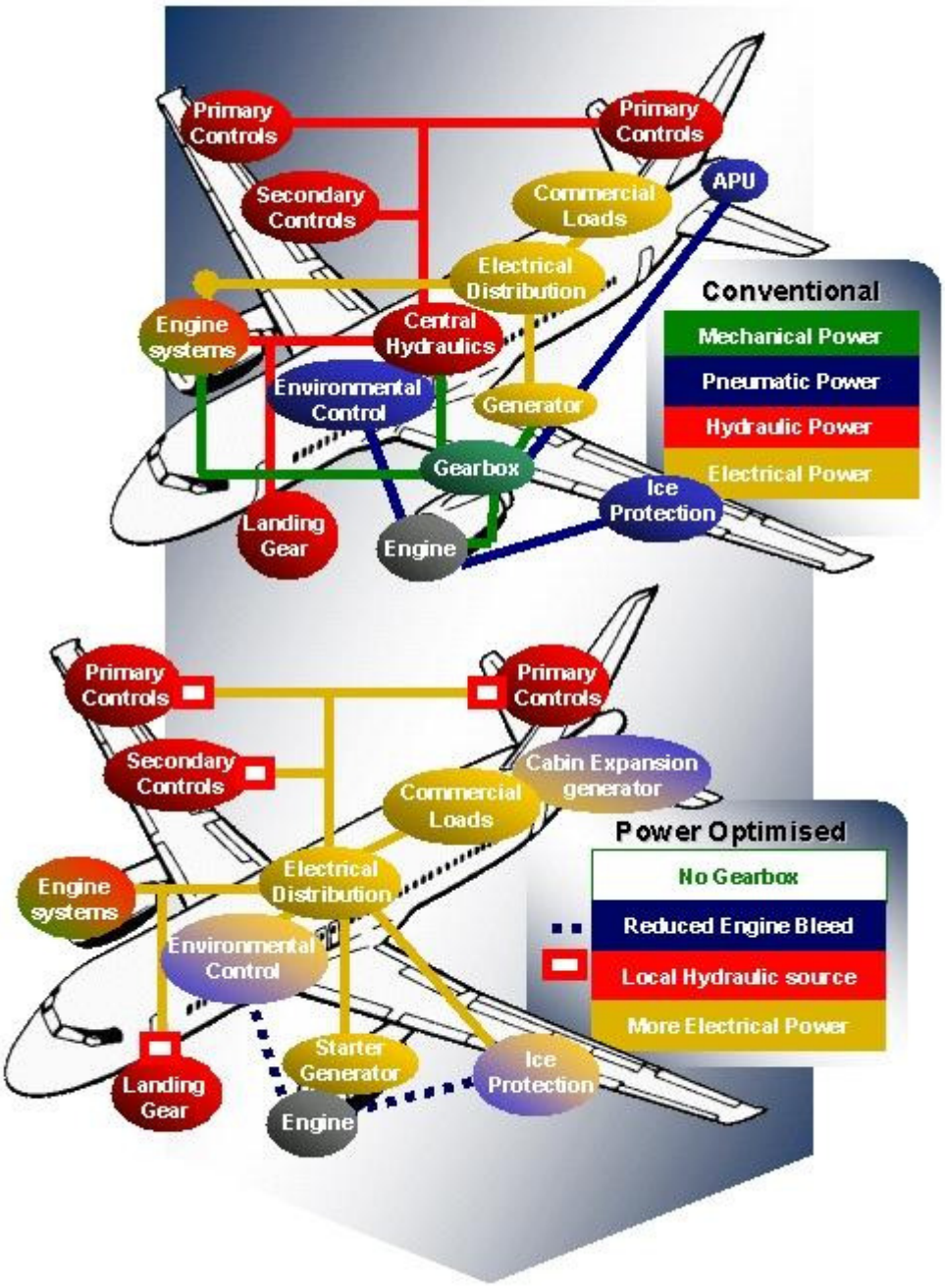

Fig. 2.5. Power Optimised Aircraft (POA) concept

Source: www.poa-project.com

Although the traditional mechanical systems have not been completely replaced, figure 2.5 illustrates how the POA concept incorporates a much greater penetration

of electrical systems, which will allow for a high level of equipment and concept de-risking.

A core stage of the POA program and indeed more-electric aircraft concept is the more-electric engine [16]. A high level schematic of this is shown in figure 2.6 (note that the intermediate pressure shaft of the gas turbine engine and its components have been omitted for greater clarity).

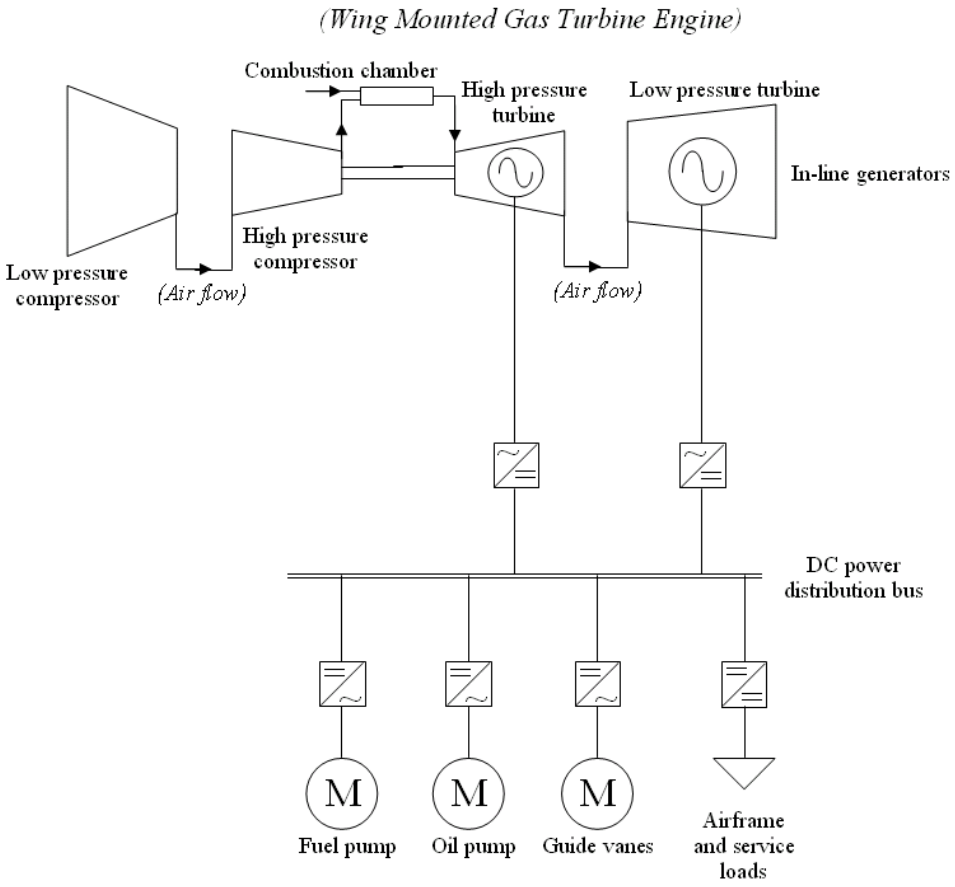

Fig. 2.6. Typical More-Electric Engine Network and Technologies

Figure 2.6 illustrates how within the more-electric engine, inline electrical generators are utilised, allowing the removal of the bulky and heavy engine-mounted gearboxes.

Many of the engine support systems (fuel pump, oil pump and guide vanes) have also been replaced by electrical equivalents, interfaced through power electronic converters. Permanent magnet synchronous machines are proving popular in the early concept stages of the more-electric engine as these provide power dense options for the electrical pumps, motors and generators [16, 17]. Switched reluctance machines are also being considered for both motor loads and generation due to their robust nature and high power density [16, 18].

Options for proposed designs of the power distribution network within the more-electric aircraft vary widely. A mixture of ac (fixed and variable frequency) and dc power distribution could be utilised, with architecture options ranging from fully interconnected networks (utilising paralleled generation) right through to multiple islanded power systems being considered. Much research still needs to be conducted in order to find the design which provides the optimal combination of weight, robustness, and availability of supply to critical loads [19, 20].

The choice of which of the turbine shafts to mount the electrical generators onto and draw power from is also a subject of much debate [16]. Power may be drawn from more than one shaft, although aspects such as power sharing and whole system optimisation during different stages of the flight cycle require further research.

Lastly, one of the greatest challenges faced in making the more-electric aircraft concept a reality is the immaturity of many of the key technologies [2, 16]. These are largely still in the development stage and as such are not fully proven. In such a

safety critical environment, it is essential to have full confidence in the technologies utilised, as there is no room for error within this particular application.

2.4 The Evolving Role of Power Electronic Converters in Marine and Aerospace Applications

Both the marine and aerospace more-electric networks see a significant increase in the utilisation of power electronic converters within the electrical power distribution networks over more conventional systems. In addition to this, the role of power electronics within these networks is also evolving.

In conventional power distribution networks, power electronics have found common use as motor drives, active filters and interfaces for small generation sources. The behaviour of the converters in these applications is well understood. However, in marine and aerospace more-electric applications, power electronic converters are finding increased use in many other applications [1, 17]. Examples of this include interfaces to novel generator technologies and energy storage systems, advanced propulsion drives, and power flow control and regulation devices.

As a result of their novel nature, the response of many of these converters to network transients and fault conditions is not well understood. The characteristics of these very responses will significantly impact upon the dynamic behaviour of the overall network and as such it is essential to consider the behaviour of the power electronic

converters when evaluating of network-level dynamics of marine and aerospace more-electric power distribution networks [21].

2.5 Underlying Research Challenges in the Development of the More-Electric Concept

Although the more-electric ship and the more-electric aircraft appear to be significantly different, they do in fact share many common research challenges in their development. The following section discusses some of the unique characteristics of these systems that contribute to a network behaviour which is very different to that of the more conventional land based systems. The research and development challenges associated with each characteristic are also briefly discussed.

The absence of any grid connection in both marine and aerospace more-electric networks means that they possess only finite inertias. Indeed, this islanded nature makes them significantly more sensitive to large network state changes compared to the more robust land based power systems [21 - 23]. Highly dynamic load variations can potentially lead to voltage and frequency regulation issues and even network instability [12]. Loads of this nature are commonly found in marine and aerospace systems (e.g. bow thrusters, propulsion drives, wing flap actuation systems) creating a need for improved network operation and management [24]. In addition to these aspects, marine and aerospace architectures are separated by only short cable lengths of very low impedance. As such, there is a high potential for interactions between the separate systems, even including interaction between the mechanical prime movers

and electrical network systems [25, 26]. This is especially relevant in IFEP applications at present, where large loading variations can lead to poor dynamic operation of the prime movers reducing their life span and potentially leading to unexpected shutdowns of plant.

Within aerospace applications, the aspect of interactions between the prime mover and electrical systems has so far been of a lower concern. This is due to the electrical loading forming only a small proportion of the total loading on the prime mover (with the propulsion of the aircraft being the dominant load) [2]. However, with the increasing levels of electrical loading being proposed for future generations of aircraft, there is a growing need to identify the electrical-mechanical interactions that could potentially occur [26]. Given the criticality of the prime mover to the safety of the aircraft, it is essential that appropriate measures be taken to eliminate all the problematic interactions so that the safe and reliable operation of that prime mover is ensured. A good network-level understanding of the system is hence required to minimise the effects of the electrical-mechanical interactions within aerospace (and indeed marine) more-electric architectures and improve the robustness of these designs.

The implementation of effective fault detection and protection schemes for marine and aerospace more-electric networks represents a significant research challenge. Aspects such as highly variable fault levels, a high penetration of power electronic converters, mixed ac and dc distribution, novel generation and load systems and unearthed/high impedance earthed network parts all combine to produce fault

behaviour characteristics which are very different in nature to those of land based systems [27, 28]. As such, conventional protection schemes have a much-reduced effectiveness in marine and aerospace more-electric applications. The development of new schemes particularly suited to marine and aerospace networks is hence of great importance. In addition, the criticality of many of the electrical loads produces a real requirement for reconfiguration capabilities to be built into the network [28, 29].

Space and weight are at a premium within marine and aerospace applications. The smaller the electrical power generation, distribution and load technologies are, the greater the space that is freed up within the body of the ship/aircraft to be used for other purposes. In addition, a smaller, lighter ship/aircraft consumes less fuel, providing reduced operating costs. Hence, there is a great need for the continued development of novel technologies whose purchase cost may be higher than conventional technologies, but whose power dense characteristics (achieved through reductions in weight in size) will give rise to reduced through-life costs [1, 16]. The successful integration of these novel technologies into the power distribution network will also present further challenges though.

Lastly, the unique characteristics of marine and aerospace more-electric networks listed above place an increased requirement on the use of modelling and simulation to support the design and development of these systems [30, 31]. This is particularly true for network-level studies, where there is a great need to capture the dynamic behaviour of large parts of, or even the whole network, to facilitate the identification

of key operational deficiencies at an early stage in the design and development process. However, the time constants present in marine or aerospace more-electric networks range from a few microseconds for power electronics and protection systems right through to a few seconds for mechanical prime movers and loads. As a result, the effective and efficient modelling of such highly dynamic networks presents many significant challenges [31, 32]. Indeed, the requirement to model such large networks in an efficient manner is often beyond the capabilities of existing simulation software and methods. Hence, whilst the challenges described above are of little concern for smaller and simpler models (for example, single motor drive systems), the model size and complexity required to fully capture interactions in marine and aerospace more-electric networks makes these challenges very significant [31]. This issue is explored further in the next chapter.

Given the importance of modelling and simulation to the overall system development process, the associated challenges outlined above must be addressed in order to maximise its role. This aspect is indeed the focus of this thesis, which proposes novel methods for the more effective modelling and simulation of electrical networks with a high penetration of power electronics, typical of those found in marine and aerospace more-electric applications.

2.6 Chapter Conclusions

This chapter has given a brief overview of the more-electric concept as applied to marine and aerospace technologies. It has reviewed the novel technologies used in each application, discussing the benefits and challenges associated with them. Power

electronic converters were identified as being essential to the operation of more electric marine and aerospace systems by providing both the means to interface other novel technologies to the electrical distribution network as well as facilitate the control and conditioning of electrical power around the network. The chapter concluded by discussing the challenges faced in the development of marine and aerospace more-electric systems.

2.7 References

[1] D.S. Parker and C.G. Hodge, "The electric warship", *Trans IMarE*, vol. 108, part 2, 1996, pp. 109-125.

[2] Lester F. Faleiro, "Trends towards a more electrical aircraft," Liebherr-Aerospace. Available: http://www.poa-project.com/53.asp (accessed 13/10/2008)

[3] "Beyond the More Electric Aircraft," *Aerospace America*, pp 35 – 39, September 2005.

[4] Julia King, Ian Ritchey, "Marine propulsion: The transport technology for the 21st century." Available at www.raeng.org.uk/news/publications/ingenia/issue12/King.pdf (accessed 11/05/2009)

[5] D. Vanderpump, M. Benatmane, P. T. Murray, "The Type 45 destroyer power and propulsion system", *Proc 6th International Naval Engineering Conference and Exhibition (INEC)*, April 2002.

[6] P .J. Norman, C.D. Booth, J.D. Schuddebeurs, G.M. Burt, J.R. McDonald, J.M Apsley, M. Barnes, A.C Smith, S. Williamson, E. Tsoudis, P. Pilidis, R. Singh, "Integrated electrical and mechanical modelling of integrated-full-electric-propulsion systems," *Proc. The 3rd IET Power Electronics Machines and Drives conference (PEMD 2006)*, Dublin, Ireland, April 2006.

[7] David Gritter, Swarn S. Kalsi, Nancy Henderson, "Variable speed electric drive options for electric ships," *Proc. IEEE Electric Ship Technologies Symposium (ESTS)*, Philadelphia, Pennsylvania, USA, July 2005, pp. 347 – 354.

[8] Cdr C.G. Hodge and D.J. Mattick, "The electric warship II", *Trans IMarE*, vol. 109, part 2, 1997.

[9] Mesut E. Baran, Nikhil Mahajan, "System reconfiguration on shipboard DC zonal electrical system," *Proc. Of IEEE Electric Ship Technologies Symposium (ESTS)*, Philadelphia, Pennsylvania, USA, July 2005, pp. 86 – 92,

[10] C. G. Hodge, "Modern applications of power electronics to marine propulsion systems," *2002 IEEE International Symposium on Power Semiconductor Devices and ICs (ISPSD).* Available: http://www.ship.org.tw/Upload/ISPSD_2002_Paper.pdf (accessed 11/05/2009)

[11] M. E. Baran, N. R. Mahajan, "Overcurrent protection on voltage-source-converter based multiterminal DC distribution systems," *IEEE Trans. Power Delivery*, vol. 22, no. 1, pp. 406 – 412, January 2007.

[12] Zimin W. Vilar, Roger A. Dougal, "Effectiveness of generator control strategies on meeting pulsed load requirements in ship electric systems," *in Proc. IEEE Electric Ship Technologies Symposium (ESTS)*, Philadelphia, Pennsylvania, USA, July 2005, pp. 459 – 462,

[13] Hamid A. Toliyat, Salman Talebi, Patrick McMullen, Co Huynh, Alexei Filatov, "Advanced high-speed flywheel energy storage systems for pulsed power applications," *Proc. 2005 IEEE Electric Ship Technologies Symposium (ESTS)*, Philadelphia, July 2005, 379 – 386.

[14] Karen Butler-Purry, "Self-healing shipboard electric power systems," *Proc. ASNE Reconfiguration and Survivability Symposium*, Atlantic Beach, Florida, February 2005.

[15] Liebherr Aerospace, "Power Optimised Aircraft," Available at: www.poa-project.com (accessed 13/10/2008)

[16] Richard Newman, "The more electric engine concept," *SAE Technical Papers*, document number: 2004-01-3128.

[17] "Vehicle power electronics and electric machines – 2001 annual progress report." Available: http://www1.eere.energy.gov/vehiclesandfuels/pdfs/program/2001_pr_vehicle_power.pdf (accessed 11/05/2009)

[18] David A. Torrey, "Switched reluctance generators and their control," *IEEE Trans. on Industrial Electronics*, vol. 49, no. 1, pp 3 – 14, February 2002.

[19] Alan T. Bernier, "Advanced electrical power distribution network," *SAE Technical Papers*, document number: 2000-01-3640.

[20] S. Mollov, A. Forsyth, M. Bailey, "System modelling of advanced electrical power distribution architectures for large aircraft," *SAE Technical Papers*, document number: 2001-01-3631.

[21] CDR John V. Amy Jr, "Modern, high-converter-populations argue for changing how to design naval electric power systems," *Proc. 2005 IEEE Electric Ship Technologies Symposium (ESTS)*, Philadelphia, July 2005, pp. 280 – 283.

[22] S.D. Sudhoff, S.F. Glover, P.T. Lamm, D.H. Schmucker, D.E. Delisle, "Stability analysis of dc power electronics based distribution system using admittance space constraints," *IEEE Trans. on Aerospace and Electronic Systems*, Vol. 36, no. 3, pp. 965 – 973, July 2000.

[23] J. O. Flower, C. G. Hodge, "Stability of power-electronics based dc-distribution systems," *Proc. IMarEST Electric Warship IX Seminar*, December 2003, pp. 86 – 97.

[24] Stuart Galloway, Patrick Norman, "Additional Engine Start-up and Endurance Cycle Studies Report" University of Strathclyde internal report. Document number RR/MEE/TR/2006-004.

[25] A D Crane, R E Maltby, M Benatmane, Capt. J M Newell, "Naval power and propulsion system: the intricacies of integration", *Proc. World Maritime Technology Conference*, March 2006.

[26] Gareth E Moore, Nnamdi Okaeme, David Trainer, Stephen Long, "Electrical mechanical interaction study," Rolls-Royce internal report. Document number DNS 124710.

[27] C. Booth, G. Dudgeon, J.R. McDonald, A. Kinson, J. Hill, "Protection of modern marine power systems: challenges and solutions", *Eighth IEE International Conference on Developments in Power System Protection,* pp. 825 – 828, April 2004.

[28] S. A. Long, D. R. Trainer, "Ultra-compact intelligent electrical networks," *1st SEAS DTC Technical Conference*, Edinburgh, 2006. Available: http://www.seasdtc.com/downloads/pdf/conf_material_06/propulsion_power_generation_and_energy_management/ppem007.pdf (accessed 11/05/2009)

[29] Dave Mattick, Martin Butcher MEng (Hons), "Demonstrating re-configuration of electrical systems at the electric ship technology demonstrator." Available at:

http://www.caps.fsu.edu/ASNE_Conference/Thur_Presentations/Thur_4/Testbeds/Mattick.pdf (accessed 26/01/2009)

[30] P. J. Norman, S. J. Galloway, and J. R. McDonald, "Simulating electrical faults within future aircraft networks," *IEEE Transactions on Aerospace and Electronic Systems*, Vol. 44, no. 1, pp. 99 – 110, January 2008.

[31] Graham J W Dudgeon, James R McDonald, "Simulation challenges for the all electric ship – form micro-second to macro-second," *Proc. IMarEST Electric Warship IX Seminar*, December 2003, pp. 42 – 54.

[32] P. J. Norman, C. D. Booth, J. D. Schuddebeurs, S. J. Galloway, G. M. Burt, J. R. McDonald, A. Villasenor, R. Todd, J. M Apsley, M. Barnes, A.C Smith, S. Williamson, E. Tsoudis, P. Pilidis, R. Singh, "Simulating IFEP Systems," *Marine Engineering Review (MER)*, pp. 26 – 31, October 2006.

Chapter 3 – Research Justification and Literature Review

3.1 Chapter Overview

In the review of marine and aerospace more-electric systems conducted in Chapter 2, the significance of modelling and simulation to the development of these systems was discussed. More specifically, it was argued that there is a great need to utilise network-level dynamic simulations to identify key operating deficiencies and issues at an early stage in the design process. Thereby, de-risking the system to some extent. The size and complexity of the modelled systems however, presents significant barriers to their efficient and accurate simulation [1]. Appropriate methods and techniques are hence required to overcome the difficulties faced and maximise the contribution of modelling and simulation to the development of future marine and aerospace systems.

This chapter discusses the role of network-level modelling and dynamic simulation in the development of marine and aerospace more-electric systems and explores the challenges faced which limit its effectiveness. It investigates the consequences of having significant levels of penetration of power electronic converters within these networks and identifies how this leads to computationally inefficient simulations. As a result, the potential benefit of modelling and simulation to the design and development of marine and aerospace more-electric architectures is not achieved in full.

This chapter presents a review of the existing literature covering suitable methods which could improve the efficiency of simulating multi-converter network architectures. Whilst several of the methods reviewed show real promise for this type of application, all have key factors limiting their effectiveness. This chapter hence identifies that there is still a requirement to develop novel methods for this purpose.

3.2 The Importance of Modelling and Simulation to the Development of More-Electric Systems

This section will discuss in detail the role of modelling and simulation to the development of marine and aerospace more-electric systems and its importance in this process. By considering this aspect, and later, the challenges faced which limit the potential benefit of modelling and simulation to the overall design process, it is intended that this section will provide the context from which the methods in existing literature can be properly evaluated.

As discussed previously in Chapter 2, one of the key underlying challenges faced in the successful development of more-electric network architectures for marine and aerospace applications is the uncertainty concerning the integration of so many new technologies into a single low inertia network [2, 3]. Little is known about how these technologies will interact and what the subsequent impact on the operation and management of the rest of the network will be [4]. A good example of this is the negative impedance phenomenon deriving from the use of constant power loads in dc distribution networks [5, 6]. Whilst the performance of these load types is perfectly

robust in isolated test environments, their reaction to other network events can potentially lead to the collapse in voltage across the entire electrical power network.

As such, whilst the need still remains for device level modelling (i.e. the representation of single loads/generators and/or converters), there is now an emerging need for network-level modelling of these systems (i.e. the representation of large sections of, or even the whole of the power distribution network) in order to characterise the interactions between individual systems and evaluate the dynamic response of the electrical power network [1, 4]. Indeed, it is in this area, that modelling and simulation could provide an especially valuable role by derisking more-electric architectures at an early stage of their development.

3.2.1 The Challenge of Computational Efficiency

There is one key challenge which prevents the benefits of network-level modelling and dynamic simulation being fully realised though. In order to accurately represent the behaviour of a large number of active systems, interconnected through an electrical network, a complex model is often required [1, 4]. The key challenge of this complexity is the significant associated computational burden and the slow running simulations that result from this. The latter aspect is particularly disadvantageous for network level modelling and simulation, where large numbers of separate simulations often have to be conducted to achieve the result required [1, 4]. For example, if modelling and simulation is used as the first stage of designing an electrical protection system, the impact of all possible fault types on the network must first be considered [7]. The completion time of the simulations conducted must

be reasonably short if this and other similar tasks are to be completed over a practical time scale.

Slow running simulations are also problematic when longer transient events such as a generator restart or propeller torque oscillations are simulated [1, 4]. For investigations such as these, it is important that the true behaviour of every system affected by the transient event is accurately captured. However, this requirement can lead to long running simulations if the model utilised is very complex in nature.

Marine and aerospace more-electric architectures face an additional challenge in their efficient simulation. Many of the active systems within these networks are interfaced through power electronic converters. As discussed in Chapter 2, the behaviour of these converters is often very influential on the response of the overall network [3, 8]. As such it is necessary to represent the dynamic behaviour of these devices accurately if the simulation results produced are to be representative of the real system. Models of power electronic converters require small simulation step sizes to be utilised in order to accurately represent their typically high frequency switching behaviour [9, 10]. This aspect in itself is not a significant limiting factor though. The efficient simulation of a single converter system over a period of a few milliseconds can be readily achieved without the need to employ techniques to improve simulation efficiency [11].

The difficulties arise when models of power electronic converters are incorporated into large electrical networks (such as those utilised in marine and aerospace

applications) where there are other systems with much slower responses. Table 3.1 illustrates the typical range of system responses that might be found in marine and aerospace applications [12].

Table 3.1. Typical system response times

System	Response Time
Semiconductor switch commutation	~1μs
PWM period	0.5ms – 2ms
Rotor time constant	50ms – 1s
Propeller run up time	20s – 60s
Mechanical disturbance	10s – 100s

Hence, in order to fully capture the dynamic behaviour of the electrical network containing systems with a wide range of response times, it is often necessary to simulate transient events over periods of several seconds or more. As such, the models of the power electronic converters are also simulated over this period, but using a finer resolution so that the behaviour of the converters is accurately modelled. Simulations of this nature thus have a high computational requirement and as a result run very slowly. This behaviour is particularly undesirable for network-level simulations of marine and aerospace more-electric architectures as it prevents the full benefit of modelling and simulation to the design and development of these systems from being realised.

Whilst there is some comfort from the developments in microprocessor technologies providing improved computing power, the ever increasing demands on modelling and simulation are likely to go some way to cancelling out any gains from these [4].

In essence, as computing power increases, the complexity of models utilised often also increases, effectively providing no net benefit. As such, there is a clear need to identify and utilise methods which can reduce the computational burden of simulating electrical networks with a significant penetration of power electronic converters whilst still maintaining an appropriately high degree of accuracy. Achieving this will maximise the potential benefits of modelling and simulation to the design and development of marine and aerospace more-electric systems.

3.3 Literature Review

Existing literature on the modelling and simulation of power electronic converters is very extensive, addressing a variety of research challenges relating to a wide range of applications [13, 14]. As such, only the literature concerned with improving computational efficiency of simulating power electronic converters utilised in the setting of a larger electrical network will be considered as this aspect is the most relevant to marine and aerospace domains. It is worth noting that there is a relatively small range of such methods in comparison to the multitude of work being conducted on small power electronic systems. This reflects the fact that the requirement to perform network-level dynamic simulations of marine and aerospace more-electric architectures (and indeed other network types) is an emerging application [1, 4, 15].

3.3.1 Model Abstraction Methods and Solver Considerations

This section will first consider model abstraction methods. These involve representing devices or systems at a low level of detail so that the primary behavioural aspects of interest are represented whilst other aspects which are of

lesser interest are neglected [1]. It then reviews solver options for effective and efficient simulation of electrical power networks containing power electronics, examining how these may be different to those of small converter systems (i.e. those typically containing one or two converters).

The authors in [14] provide guidelines for modelling power electronics in electrical power applications. These are aimed at power engineers who wish to incorporate power electronics into their power systems models. The core theme of this paper is utilising model abstraction methods to reduce the computational burden of simulating power electronics within an electrical power network model. Through abstraction, the governing equations of the converter model are simplified, and the computational requirement associated with it is reduced. This in turn leads to quicker simulations.

The paper gives several good examples of how the abstraction of power electronic converters within electrical power systems models can be achieved. Of the methods given, there are a few which are particularly relevant to marine and aerospace applications. These are given below.

The first method utilises simplified semiconductor switch models instead of detailed models to characterise the power electronics. The paper argues that when conducting network-level simulations, the loss in accuracy incurred by representing the turn-on and turn-off characteristics of the converter switches in a simplified linear fashion is negligible. This method is particularly relevant for marine and aerospace applications

where the longer term controlled response of the power electronic converters in relation to some other network event or transient is usually the aspect of interest. Whilst the operation of the semiconductor switches within these converters is the means for which the response of the controller can be realised, the specific transitional behaviour of these switches is usually of a lesser importance. In this manner, as long as the dynamic response of the modelled converters is not affected significantly, errors in their high frequency pulsed outputs are often acceptable in light of the reductions in simulation computation that can be achieved.

An example of this first method is illustrated in figure 3.1, which shows detailed switching characteristic of a diode (part (a)) and the simplified equivalent characteristic (part (b)) [14].

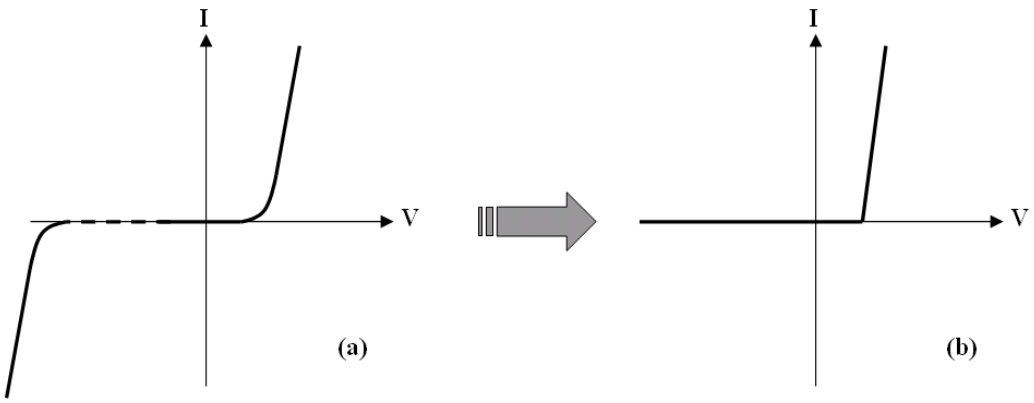

Fig. 3.1. Detailed and simplified representations of a diode static characteristic

Part (a) of figure 3.1 incorporates aspects such as reverse breakdown, leakage current and forward voltage drop. These aspects are represented in a simplified manner or

neglected altogether in part (b), which illustrates the characteristics of a simplified model with reduced computational requirements.

A second method listed in [14] involves representing groups of similar power electronics interfaced loads as a single scaled equivalent (where feasible). This method significantly reduces the number of converter models within the network, hence reducing the level of computation associated with it. In marine and aerospace applications, it is common to find groups of similar power electronics loads such as pumps, small motor drives and actuator systems [3, 8, 16]. By representing these similar systems as a single unit, the underlying dynamic response of the group of converters as a whole can still be captured accurately. Meanwhile, the number of converter models being simulated is significantly reduced, resulting in notable reductions in computational burden. Some of the higher fidelity model behaviour will be lost by grouping converters together like this, but this loss of detail is likely to be acceptable for most applications.

This second method is illustrated in figure 3.2, which shows how a model of an electrical power network from a marine vessel [17] can be simplified by grouping the four 300kVA pump loads into a single 1.2MVA equivalent.

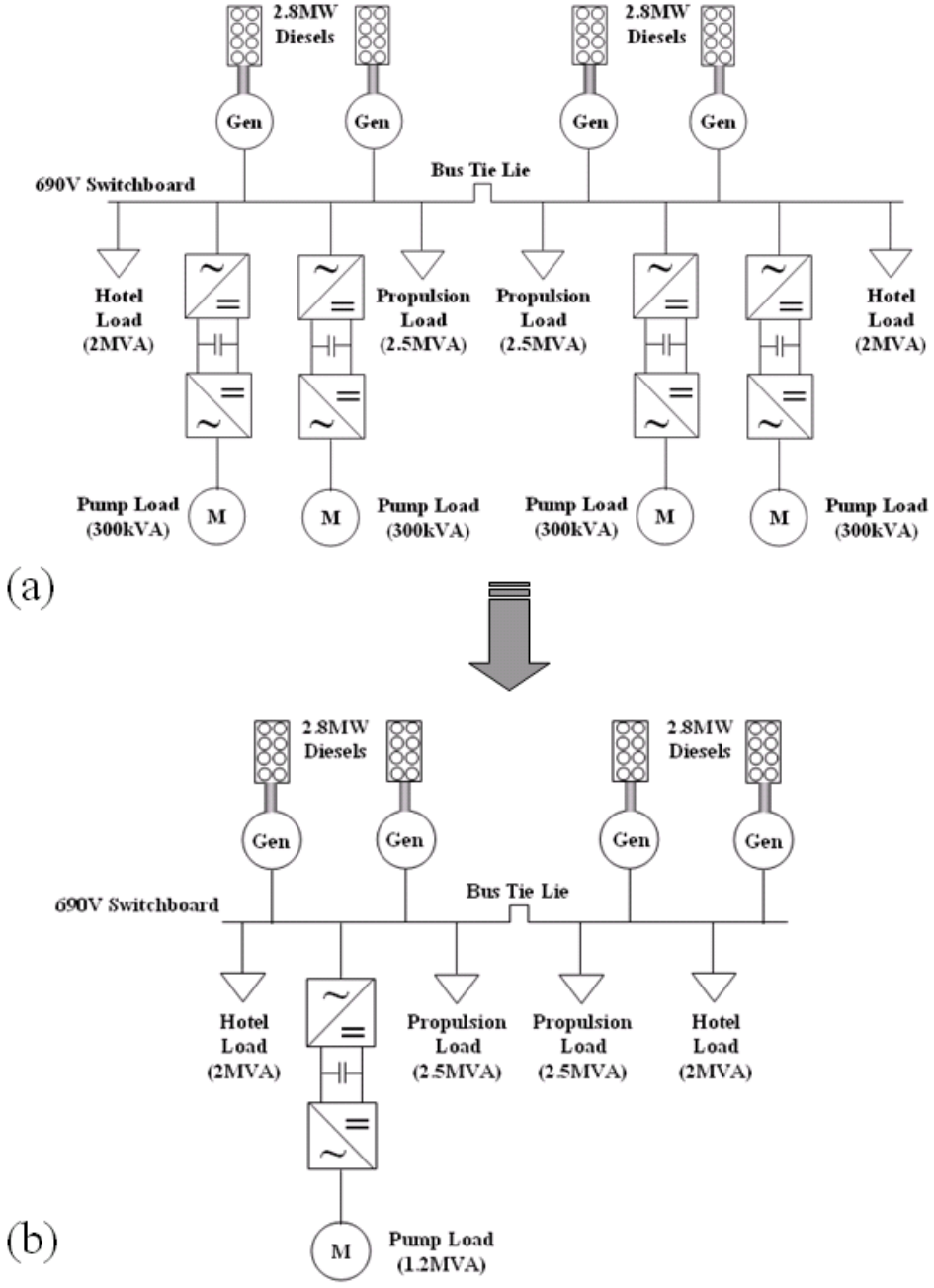

Fig. 3.2. Grouping of pump loads within a marine electrical network

A third method given in [14] suggests representing only the front end of a drive system when the impact of its interface with the rest of the network is the primary interest. In a similar manner to the previous example, this method reduces the simulation computation of a network model by effectively reducing the number of

power electronic converter models present within it. Again, this approach may be feasible in some marine and aerospace applications where there are two-stage converters (e.g. rectifier-inverter combination) interfacing to other systems which are out with the scope of investigation. This method also appears to be particularly compatible with the previous one.

Figure 3.3 illustrates how the third method suggested in [14] can be implemented on an ac:dc:ac motor drive system.

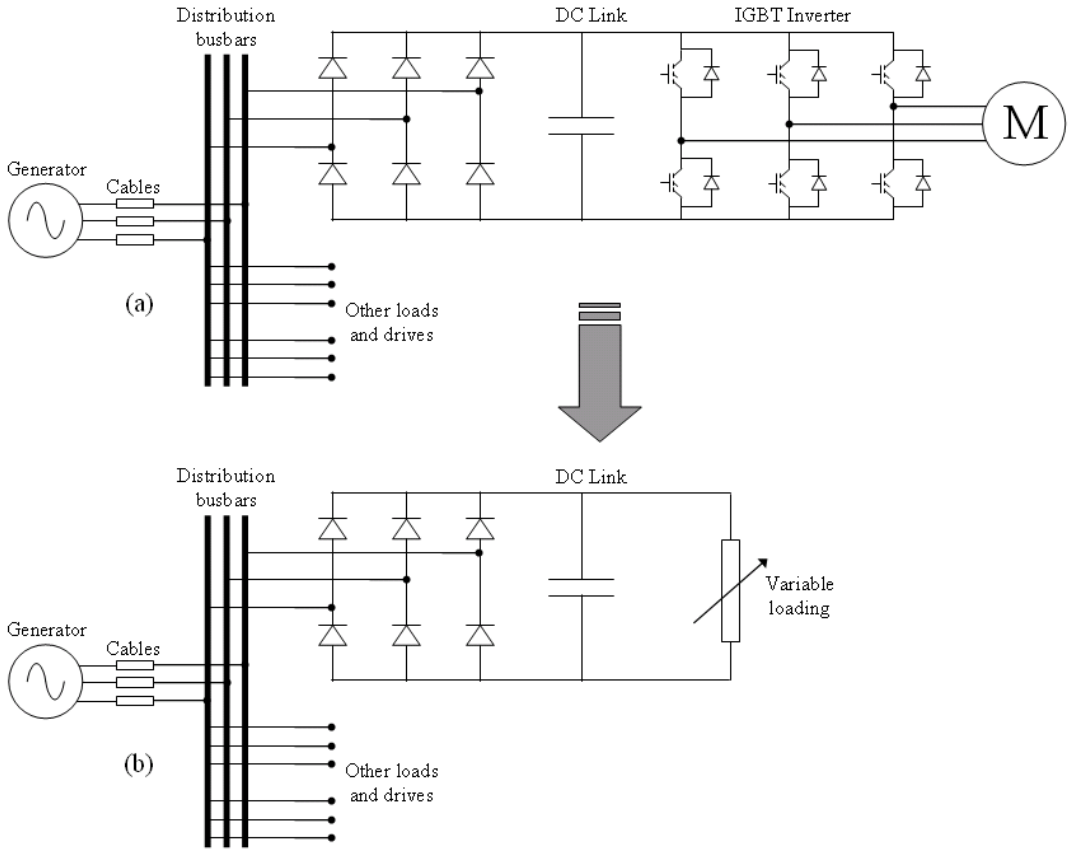

Fig. 3.3. Simplification of a motor drive system to a front end only system

In the example shown in figure 3.1, the diode bridge front end of the converter is retained so that the impact of its operation on the remainder of the busbar connected loads and systems is accurately represented. However, by removing the inverter and motor from the model of the drive system, the associated computational requirement is greatly reduced.

The paper then provides a small number of examples to illustrate how the methods described can be implemented. These examples are typically only of one or two converters but the methods put forward are readily transferable to multi-converter systems such as those found in marine and aerospace more-electric architectures.

Overall, the methods put forward in [14] are focused on reducing the computational burden of multiple power electronic converter models within the context of a larger electrical network model. Additionally, these methods can be readily implemented, are not limited to specific software packages or modelling approaches, and offer potentially significant savings in computational effort of network-level simulations. Hence, these methods (and indeed the theme of abstraction in general) are very relevant to the network level modelling and simulation of marine and aerospace more-electric systems. More generally, from [14], it is apparent that when investigating the response of the electrical network, detailed models of power electronic converters provide more detail than is often actually necessary. As such, there is a real potential for the abstraction of these models without creating significant levels of error in the simulation results. This theme should be investigated in further research work.

It is worth noting however, that the methods put forward in [14] do require some thought in their implementation. For example, it can be difficult to ascertain whether grouping several power electronic loads as a single system will lead to unacceptable levels of error or not. In a marine or aerospace network where there is often little cable impedance between separate loads (this was discussed in Chapter 2), the interaction between these similar systems under certain network operating states may then impact on the overall network behaviour. By grouping these power electronics loads together in the manner described in [14], this impact on the network response would be lost. As such, it seems that the model abstraction methods suggested must be implemented carefully (requiring some degree of technical appreciation) so that unacceptable levels of error are not introduced.

The authors in [14] do make one more interesting point. They review different types of simulation software and discuss which is best for the modelling and simulation of electric power networks containing power electronics. Dedicated power systems transient simulation tools (for example ATP [18], PSCAD [19] and SimPowerSystems [20]) are recommended for this task. They claim that whilst these packages are not as capable as dedicated power electronics simulation tools (for example PSIM [21], Caspoc [22] and ORCAD [23]) for modelling detailed converter behaviour, their simpler converter models are still sufficient for network-level studies. Additionally, with their typically extensive model libraries and general flexibility, they are far more capable at modelling the rest of the electrical network than the dedicated power electronics simulation tools.

As such, the authors feel that power systems transient simulation tools represent the best overall choice for modelling electrical power networks containing power electronics. On this basis, power systems transient simulation tools are likely to be the first choice platform for network-level modelling and dynamic simulation of marine and aerospace architectures. As such, any novel methods identified should ideally be compatible with these packages. It is acknowledged that the selection of simulation software is often a personal choice with many other factors impacting on the final decision. However, to identify or later develop novel methods for the simulation of multi-converter networks which are not compatible with power systems transients simulation tools would be to severely limit the possible scope of application of such methods.

A good example of this limited scope of application is the method presented in [24]. The authors put forward a method for the real time simulation of a small high-voltage dc (HVDC) power electronic system. It utilises a custom solver algorithm for the fixed step simulation of detailed converter models. This algorithm re-adjusts the model architecture using hidden computational steps to maintain accuracy at switch transitions whilst minimising the computational requirement of the overall simulation. Whilst this method is clearly successful in reducing the computational requirement of simulating a power electronic system, it would be difficult to implement within power systems transient simulation tools, which employ their own solver algorithms. As such, the method presented in [24] is only truly applicable only in a limited range of software tools. In addition, these tools are also unlikely to be preferred choice for modelling marine and aerospace more-electric systems.

Additionally in [24], the use of fixed and variable step solvers for the simulation of power electronic converter models is discussed. It states that variable step solvers provide a greater level of accuracy than fixed step solvers by reducing the simulation step size taken during periods of the simulation in which the model exhibits highly dynamic behaviour. However, the simulation step size is increased during periods of almost steady state behaviour so that the overall computational effort required is minimised. Indeed, achieving the same level of accuracy with a fixed step solver, would require the application of a very small, constant step size throughout the entire simulation, and would hence be less efficient. In addition to this, the use of a fixed step solver in power electronics applications causes the switching transitions within converters to be delayed to coincide with the solver time steps, reducing the accuracy of the simulation results. The authors of [10] also discuss similar findings.

Interestingly, both [10] and [24] claim that in some cases of power electronics simulation, the application of a fixed step solver may actually be more efficient than a variable step solver! They argue that by being able to fix the solver step size taken, it is possible to prevent small simulation steps being taken around switch transitions, reducing the computation required to simulate a converter model. Both papers warn that this approach produces notable errors in the results produced but state that in some applications, where the underlying lower frequency behaviour of the converters is the main aspect of interest, these errors may be acceptable. In these cases, reductions in the overall computational requirement of the simulation can be achieved.

Whilst variable step solvers are often preferred for small converter systems where the accuracy in the detailed behaviour of the converter is necessary, the opposite is true for larger power networks containing multiple converters. For these applications, the level of error produced by the use of a fixed step solver operating with a relatively large time step is often acceptable in light of the computational savings achieved. This issue is clearly a complex one, and given that many power systems transient simulation tools provide options for the use of variable step or fixed step solvers, it is also very relevant to the network-level simulation of marine and aerospace more-electric systems. As such, this issue is explored further in Chapter 6.

3.3.2 Real Time Simulation Methods

It is worth noting that whilst the method presented in [24] is not necessarily suited for use in marine and aerospace applications (as a result of its incompatibility with power systems transient simulation tools), it is working towards a very similar set of objectives as those laid out at the start of section 3.3. In order to achieve real-time performance of a simulated power electronic system, the authors were seeking to develop a method which either significantly reduced the computational requirement of the simulated electrical network or significantly improved the efficiency of this computation (or preferably both). These requirements also hold true for the network-level modelling and dynamic simulation of marine and aerospace more-electric systems.

On this basis, Section 3.3.2 considers other papers which present methods specifically developed to achieve real time or near real time simulation of power electronics and power distribution systems. Whilst real-time simulation is not a specific requirement for network-level simulations of marine and aerospace more-electric architectures, the methods and techniques employed could still be utilised to achieve significant increases in simulation speed (i.e. to achieve near real time simulation speeds).

Four separate methods which facilitate real time or near real time simulation of power systems and power electronics are reviewed in this section. These are listed below.

- The first example presented in [25] utilises clustered computer processors in order to deliver increased computational capabilities for achieving real time simulation of power electronics systems. In conjunction with this, a number of methods for refining models to reduce their computational requirement are also presented. In line with the guidance given in [14], these methods include utilising grouped network impedances and simplified switch models within the converters. The refined model is then split into fast and slow parts, forming a multi-rate model whose computation is split over several machines. Using this approach, the paper presents a model of a twelve-pulse rectifier-inverter motor drive, constructed within a commercially available power systems simulation software package (the SimPowerSystems block set of Matlab Simulink [11]) and simulated in real time.

- A second publication on the real time simulation of power electronics [26] maintains the theme of model partitioning but this time using a single computational machine (compared to the clustered approach demonstrated in [25]). The method described isolates the equations defining the converter from the remainder of the network model. In this way, each switching action of the converter does not impact on the larger network equation set allowing more efficient computation of the model to be achieved.

- The method put forward in [27] facilitates the real time simulation of AC motor drives. Again, the core issues of achieving computationally efficient simulation of power electronics systems are discussed throughout the paper. However, in contrast to [25, 26], this paper argues that partitioning a model across two or more computational engines results in stability issues and that the use of a single simulator is much more robust. The paper focuses on reducing the computational burden of power electronics simulation by combining the converter and motor models in order to achieve real time simulation of an AC drive system.

- Whilst not striving towards real-time simulation capabilities, a clustering based approach similar to the methods discussed above is presented in [28]. This paper puts forward a software framework, Distributed Heterogeneous Simulation (DHS), which facilitates the integration of various models (even developed in different software packages), into a single combined model. The computation of this integrated model is then split across multiple processors

in order to achieve substantial reductions in simulation time. At this stage, it appears that a significant manual effort is still required to configure the models for use in the DHS framework. However, the capability to integrate multiple software packages is particularly appealing for some aspects of network-level modelling of marine and aerospace architectures where investigations into interactions between electrical and mechanical systems are being conducted [2, 29]. Indeed, some of the applications of this technique listed for DHS in [30] *are* marine and aerospace systems. Perhaps the most interesting aspect of this technique is that (unlike other real time techniques) it does not attempt to improve the simulation efficiency of individual models, but rather reduces the simulation time by spreading the simulation computation across multiple processors. As such, computational reduction methods such as those presented in [14] will be compatible with the DHS method, offering even greater potential savings in simulation run time.

The four methods presented above for the real time or near real time simulation of power systems and power electronics are very effective at reducing the computational requirement and/or increasing the computational efficiency of simulations, providing potentially significant improvements in simulation completion times. These improvements are obtained without incurring unacceptable levels of error for the nature of the studies conducted. Indeed, some of the methods presented actually produced much lower levels of error than would be considered necessary for network-level modelling and simulation of large power networks. In addition to these aspects, the methods presented are compatible with power systems transient

simulation tools and often with other tools as well. All these attributes make these methods very applicable to the network-level modelling and dynamic simulation of marine and aerospace more-electric architectures. However, there is one key drawback which prevents their wide scale adoption to these domains at this point in time.

In every method reviewed, a substantial build effort is required to refine the composition of the models into a format that is suitable for the real time methods to be applied. This refinement is largely a manual process, requiring a good knowledge and understanding of the real time or near real time simulation method in order to implement it properly and maximise the benefits achieved. This aspect is especially concerning given that most of the methods reviewed are demonstrated on electrical networks with only one or two power electronic converters without any real discussion on the practical implications of expanding these methods to cover multi-converter systems.

Ideally, any methods employed for the network-level modelling and dynamic simulation of marine and aerospace more-electric applications should be capable of being readily implemented whilst providing significant reductions in computational burden. At this point in time, the real time methods do not deliver on both of these requirements. As such, this author does not believe that these methods are fully suitable for the marine and aerospace more-electric domains just yet. The long model build and development time far out weigh the computational benefits offered by these methods. In the future when these capabilities have been developed further and

the refinement/formatting process is more automated, and as a result much quicker, it is believed that these methods will become common place, transforming the potential capabilities and benefits of modelling and simulation to marine and aerospace more-electric (and indeed other) applications. However, because this potential is still some way off, there is a requirement for intermediate techniques. Ideally, these should be compatible with the real time or near real time methods discussed so that whilst the two methods are developed in parallel, the benefits of each may eventually be combined.

3.3.3 Behavioural Modelling Methods

This section will now consider four papers discussing an additional type of abstraction method for power electronic converters. This method, behavioural modelling is generally applied to networks with one or two converters in the existing literature but is scaleable to accommodate multi-converter networks. It is also compatible with power systems transient simulation tools, and real time simulation methods making it a particularly flexible and adaptable method. The applicability of the behavioural modelling approach to marine and aerospace more-electric systems is discussed at the end of this section.

In line with the guidelines given in [14], the author in [10] states that detailed switch models are not necessary for network-level simulations. This author argues rather, that it is the external behaviour of the power electronic converter that is often the main focus of interest during studies of this type. The paper then presents a group of modelling methods which are able to replicate the external behaviour of the

converter without specifically modelling the internal switching action. The paper claims that by doing this, the computational requirement associated with the converter model is reduced, while the behavioural aspects of interest (i.e. the external behaviour of the converter) are retained. This group of methods are another form of model abstraction (as discussed in [1] and [14]).

The three separate methods described in [10] are termed behavioural modelling methods. These methods each achieve a different level of abstraction and are described below.

- The first of these is the ideal-model method. This method involves representing the semiconductor devices of the converter with linear equivalents whilst neglecting any small stray impedances. Note that this method follows the same principles as one of the guidelines given in [14] regarding the representation of power electronic converters in a simplified fashion. The paper claims that both aspects of this method greatly reduce the computational burden of the converter model. It also points out that this is the most easily and readily implemented technique, and as such is the most commonly utilised. Note that according to the definition given by the author earlier in this paper, this first method is not actually a true behavioural modelling method as the internal behaviour of the converter is still represented, albeit in a slightly simplified form. The remaining two methods presented, do meet the author's definition of a behavioural modelling method however.

- The functional model approach is the second method listed. This method sees the replacement of the switched converter model with an arrangement of controlled current and voltage sources. Using the control and pulse generation circuits of the original switched converter model, the voltage and current sources can be operated in such a manner as to replicate the external terminal conditions of this switched model. However, by neglecting the internal behaviour of the converter, its computational requirement is reduced significantly (even more so than with the ideal model approach). The paper highlights that with this approach, the high-frequency content of the converter model's output is successfully retained. However, it does also indicate that it is not possible to monitor the internal voltages and currents of the converter and that any dead-time switching effects [31] can not be accommodated. In accordance with the guidelines given in [14] though, these aspects are often of little consequence for network-level modelling of large systems. It is worth noting that in-line with guidelines given in [14], the functional modelling approach could also be utilised to implement just the front end of a converter, whereby the load or source conditions at the non-represented end would be assumed to be constant or modelled by some simple function. This approach greatly simplifies the equations of operation and provides further reductions in the computation of any associated simulations.

- The third method listed in the paper is the average model approach. This method neglects the high frequency component of the converter, choosing instead to only represent the underlying low frequency components. This is

achieved through the use of controlled voltage and current sources in the same manner as the functional modelling approach, but this time with the behaviour of the converter being represented in a time-averaged fashion. The paper describes how by only modelling the low frequency components of the converter model outputs, its computation is greatly simplified and larger solver step sizes can also be employed, further reducing its computational requirement. The author of the paper quickly points out that the switching harmonics are lost with this approach though. However, because the averaged output of the converter is derived from its original control and pulse generation functions, its dynamic response is still maintained. Hence, the author claims that this approach still enables accurate investigations into the interactions between network connected systems whilst only requiring only a minimal level of computation to simulate it. To illustrate this aspect, the paper includes a number of worked examples where the averaged model approach is shown to simulate up to 30 times faster than the detailed switch model.

The authors in [13] echo these views on the benefits of the averaged model approach. Whilst this paper is more focused on low power applications rather than networks of a similar size and nature to marine and aerospace systems, the same underlying concepts of detailed models, ideal models and averaged models are discussed. Indeed the authors in [13] feel that the averaged model approach is the ideal method for investigations into converter control and network response, and that the non-averaged methods listed provide far more detail than is often necessary. The paper

uses an example of a dc-dc boost converter to illustrate how the higher frequency effects of the converter (such as the switching ripple) are lost through this approach, while the core underlying low frequency behaviour is unaffected. This is established by comparing the results of a time-averaged model to that of a detailed switching model.

It is worth noting that this approach of comparing the response of a behavioural converter model to that of the equivalent detailed switch model appears to be the accepted method to validate the accuracy of that behavioural model. Indeed, this approach is also used in [10]. Some care should be taken using this approach though as it does not necessarily confirm that the response of the behavioural model matches that of the real hardware converter. The behaviour of the detailed model must be validated first to ensure this. Hence, although the response of the behavioural model may be an accurate representation of the detailed switch model, it may still be completely unrepresentative of the real device.

In the absence of hardware rigs to achieve full validation of every converter model however, comparing the response of the behavioural model to that of an accredited switch model (i.e. one whose general operation has been checked by an expert to confirm that it is indeed representative of the real system [32]) offers a useful method to assess its accuracy.

The remaining two papers to be reviewed in this chapter provide examples of the application of the behavioural modelling approach to network-level modelling and

simulation of electric power systems containing power electronic converters. By addressing issues that are relevant to the marine and aerospace domains, these papers will provide further insight into the utilisation of this method for these applications.

The authors in [33] present a model of a space station electrical network. With multiple dc-dc converters incorporated and a desire to study the dynamic behaviour of the full network as efficiently as possible, functional converter models with time-averaged outputs are recognised as a being particularly suited to this application. In line with the approach taken in [13] and [14], the performance of the functional converter models within the network is compared to that of the original switched models (which have been validated against the hardware system). This is done for different load change conditions and other network transients in order to validate their behaviour. Negligible differences between the functional and detailed models are demonstrated. Once again, significant reductions in the computational requirement of network simulation are reported.

In addition to the case studies presented, the authors in [33] make some interesting observations on the application of time-averaged functional models to network-level simulation studies of electrical power systems. Firstly, they recommend retaining any circuit based filters for the power electronic converters when using behavioural models. This remains the case even if time-averaged models are utilised. In the absence of high frequency switching effects, it would appear that these filters are redundant. However, the authors of this paper point out that it is necessary to retain

the filter circuits so that their impact on the underlying dynamics of the electrical network is not lost.

Additionally, the authors discuss the possibility of building hybrid network models which contain both detailed switch and functional converter models. If the investigations into the behaviour of a single converter within the network model are such that a detailed model of this converter must be used, the authors recommend against utilising detailed models for the remainder of the converters in the network. Instead, they state that utilising functional models for these remaining converters will reduce the computational requirement of an overall network model without having any notable impact on the response of the detailed converter being studied. Although the simulation step size may have to be much smaller than is typically required by functional or time-averaged functional models, the use of these models will still serve to improve the simulation speed in comparison to a network where all the converters are modelled as detailed switch models (which have a higher computational requirement than functional models). It is also possible that this approach could be beneficial if there is one particular converter within the network model that is difficult to represent in a functional manner (for example, if it has complex circuit topology or the relationship between its input and output is not easily defined [10]).

The authors in [9] present functional models of matrix converters for marine applications. In line with previous papers reviewed, the authors of this paper claim that the functional modelling approach is ideal for developing control methods for

converters and for assessing their behaviour within larger electrical networks. Indeed, the novel control strategies presented in the paper are demonstrated using results obtained from a functional model of a matrix converter.

In contrast to the other papers discussing behavioural or functional modelling methods, the authors of this paper include some discussions of the limitations of the functional modelling approach. Unfortunately, these discussions are not reinforced with mathematical proof or simulation results and as such would require further analysis to validate the claims made. However, these limitations are worth considering as they will give a fuller appreciation of the applicability of behavioural and functional methods to the network-level modelling and simulation of marine and aerospace more-electric systems. The limitations identified in [9] are listed below.

- Functional models are not accurate for some modes of operation. One example of this is when all the semi-conductor switches within the converter are switched off.
- Converters whose mode of operation is dependant on external circuit conditions are difficult to represent in a functional manner.
- Functional converter models are not accurate under fault conditions [9] (although the paper fails to elaborate on this point any further).

With reference to the first limitation, when the converter is operating in this particular state, it is not possible to replicate the open circuit conditions normally created by a switched converter model with the controlled voltage sources of the

functional equivalent model. This limitation does not have a particularly significant impact on the applicability of the functional modelling method for marine and aerospace systems though and is probably very straight forward to overcome.

The second limitation listed above affects naturally commutating converters (e.g. diode and thyristor converters) and some types of resonant converters [31]. The authors in [11] and [34] discuss similar findings where it is noted that in order for functional type models of diode bridge rectifiers to be accurate, a knowledge of the circuit and power source conditions are required so that the switch transitions of the rectifier could be calculated in advance. Failing this, the co-dependancy between the operating state of the network and the converter results in highly erroneous model behaviour and even failed simulations. The authors in both papers quickly point out that for islanded systems such as a marine electrical power distribution networks operating with highly dynamic load conditions, this requirement for knowledge about the circuit and power source (or sources) is nearly impossible to meet. As such, the authors decide on the use of a simplified switch model for the given marine application.

Hence, the limitation of the functional modelling approach identified in [11, 34] with regards to diode and thyristor converters has notable consequences on the application of functional models in marine and aerospace domains where such converters are common place. For electrical network models containing converters of this type, it is likely that the hybrid based approach described in [33] would have to be employed. This method suggests the utilisation of ideal switch models for any converters which

cannot be represented in a functional manner. This approach may still provide useful reductions in simulation computation, as the typical operating frequencies of naturally commutating devices such as diodes and thyristors are of the same order of magnitude as the fundamental circuit frequencies. It is expected that the ideal switch models of these converters could operate using similar simulation time steps to those required by averaged functional models of other converters (although with higher computational requirements). As such, the overall impact on the simulation running speed may not be particularly detrimental.

With regards to the third limitation listed in [9], it is interesting that this aspect is not raised in [33] where a case study of a fault scenario is even given. However, it is possible that the current limiting control loop added to the functional converter model in [33] may have masked this behaviour. However, given that not all converters operate with such control schemes, this issue of potential inaccuracy has a notable impact on the applicability of the functional modelling to marine and aerospace more-electric domains where investigative fault simulations are of great importance (as discussed in Chapter 2). This aspect is not mentioned in any of the other publications considered (including those not mentioned in this review) and as such it is difficult to ascertain the reasons for this limitation.

Initially neglecting the limitations of the behavioural and functional modelling approaches described above, these methods seem ideally suited for use within marine and aerospace applications. They can be implemented readily, are compatible with power system transient simulation tools (and also with the real time methods listed

earlier) and are scalable to accommodate any size of network with a significant penetration of converters. In addition, the potential reductions in the computational requirement per converter are significant, especially if time-averaged representations are implemented.

The limitations of the behavioural and functional approaches listed above cannot be completely overlooked though. The implications of these are such that in the network-level modelling and simulation of marine and aerospace more-electric architectures, there will be some converter topologies and some simulation study types which are simply not compatible with these methods. Under these conditions, switched models of the converters (either ideal or detailed) must be utilised and the reductions in the simulation computation of the networks considered are lost.

3.4 Conclusions

From the review of existing literature, it is apparent that there is no single technique which will facilitate a significant increase in the computational efficiency of simulating electric power networks with a significant penetration of power electronics. Whilst the guidelines laid out in [14] present some good abstraction options for reducing the computational requirement of models of multi-converter networks, these alone are unlikely to be sufficient to achieve this aim.

The real time and near real time techniques reviewed attempt to improve upon this position by employing methods to perform the required computation in more efficient ways. This is generally achieved through partitioning of models and by

delivering an increased computational capability through the use of paralleled processors. These methods offer substantial rewards in terms of increased simulation speed and would be ideally suited to the network-level modelling and simulation of marine and aerospace networks if it were not for the long model build time and expertise presently required to implement models on real time platforms. As such, although it is anticipated that these methods will be the future standard for modelling and simulation, it is this author's opinion they are not at that stage yet.

The behavioural modelling approach seems ideally suited to marine and aerospace applications for the reasons given in the previous section. The inability to represent natural commutation devices is not a significant shortcoming if the hybrid approach is adopted. However, the reported poor accuracy during simulated fault conditions severely limits the options for the use of the behavioural modelling approach. This is disappointing because the computational savings resulting from this technique and its modularity (making it suitable for multi-converter networks) would otherwise make it ideal for application to the network-level modelling and dynamic simulation of marine and aerospace more-electric networks.

As such, there still remains a need for an effective method which enables efficient simulation of electrical network architectures with a significant penetration of power electronics. The absence of such a method presently places an effective limit on the potential contribution that can be made by modelling and simulation in the design and development of marine and aerospace more-electric architectures.

On the basis of this review, two recommendations can be made. Firstly, whilst the reasons behind the difficulties of modelling naturally commutated converters in a functional manner are well documented [34], there is lack of similar information regarding the inaccuracy of functional models under simulated fault conditions. There is hence an opportunity to investigate this poor quality model behaviour in order to identify and inform the research community of the reasons behind this. Such analysis could then direct further efforts into refining the functional modelling approach so that it is more reliable under the given operating conditions. Secondly, other methods should be also be developed to reduce the computational burden of electrical networks with a significant penetration of power electronics in order to produce a method or group of methods that will enhance the value of modelling and simulation to the design and development of marine and aerospace more-electric systems.

3.5 References

[1] Graham J. W. Dudgeon, James R. McDonald, "Simulation challenges for the all electric ship – form micro-second to macro-second," *Proc. IMarEST Electric Warship IX Seminar*, December 2003, pp. 42 – 54.

[2] A. D. Crane, R. E. Maltby, M. Benatmane, Capt. J. M. Newell, "Naval power and propulsion system: the intricacies of integration", *World Maritime Technology Conference*, March 2006.

[3] Richard Newman, "The more electric engine concept," *SAE Transactions: Journal of Aerospace*, vol. 113, no.1 , pp. 1656 – 1661, 2004.

[4] Scott Graham, Ivan Wong, Won-Zon Chen, Alex Lazarevic, Keith Cleek, Eric Walters, Charles Lucas, Oleg Wasynczuk, Peter Lamm, "Distributed Simulation of an Uninhabited Aerial Vehicle Power System," *SAE 2004 Transactions: Journal of Aerospace*, pp. 1916 – 1921, 2004.

[5] S.D. Sudhoff, S.F. Glover, P.T. Lamm, D.H. Schmucker, D.E. Delisle, "Stability analysis of dc power electronics based distribution system using admittance space constraints," *IEEE Trans. on Aerospace and Electronic Systems*, Vol. 36, no. 3, pp. 965 – 973, July 2000.

[6] J. O. Flower, C. G. Hodge, "Stability of power-electronics based dc-distribution systems," *Proc. IMarEST Electric Warship IX Seminar*, December 2003, pp. 86 – 97.

[7] C. Booth, G. Dudgeon, J.R. McDonald, A. Kinson, J. Hill, "Protection of modern marine power systems: challenges and solutions", *Eighth IEE International Conference on Developments in Power System Protection,* pp. 825 – 828, April 2004.

[8] C. G. Hodge, "Modern applications of power electronics to marine propulsion systems," *2002 IEEE International Symposium on Power Semiconductor Devices and ICs (ISPSD)*. Available: http://www.ship.org.tw/Upload/ISPSD_2002_Paper.pdf (accessed 11/05/2009)

[9] J. Clare, P. Zanchetta, P. Wheeler, L. Empringham, "Modelling and design of matrix converter solutions for shipboard applications," *Proc. IMarEST Electric Warship IX Seminar*, December 2003, pp. 20 – 34.

[10] H. Jin, "Behaviour-mode simulation of power electronic circuits," *IEEE Trans. on Power Electronics*, Vol. 12, no. 3, pp. 443 – 452, May 1997.

[11] *Using Matlab*, The Mathworks Inc., 3 Apple Hill Drive, Natick, MA, USA, 2002.

[12] A. Gonzalez Villasenor, J. M. Apsley, M. Barnes, A. C. Smith, S. Williamson, J.D. Schuddebeurs, P. J. Norman, C. D. Booth, G.M. Burt, J. R. McDonald, "Propulsion drive models for full Electric marine propulsion systems," *IEEE International Electric Machines and Drives Conference (IEMDC)*, May 2007.

[13] Dragan Maksimović, Aleksandar M. Stankovic, Joseph V. Thottuvelil, George C. Verghese, "Modeling and simulation of power electronic converters," *Proceedings of the IEEE*, vol. 89, No. 6, pp. 898 – 912, June 2001.

[14] A. M. Gole, A. Keri, C. Nwankpa, E. W. Gunther, H. W. Dommel, I. Hassan, J. R. Marti, J. A. Martinez, K. G. Fehrle, L. Tang, M. F. McGranaghan, O. B. Nayak, P. F. Ribeiro, R. Iravani, Lasseter, "Guidelines for modeling power

electronics in electric power engineering applications," *IEEE Trans. on Power Delivery*, Vol. 12, No. 1, pp. 505 – 514, January 1997.

[15] CDR John V. Amy Jr, "Modern, high-converter-populations argue for changing how to design naval electric power systems," *Proc. 2005 IEEE Electric Ship Technologies Symposium (ESTS)*, Philadelphia, July 2005, pp 280 – 283.

[16] A. M. Cross, A. J. Forsyth, "Simulation and evaluation of high-voltage power systems for civil aircraft," *SAE Transactions: Journal of Aerospace*, vol. 113, no.1, pp. 1861 – 1870, 2004.

[17] I. M. Elders, P. J. Norman, J. D. Schuddebeurs, C. D. Booth, G. M. Burt, J. R. McDonald, J. Apsley, M. Barnes, A. Smith, S. Williamson, S. Loddick and I. Myers, "Modelling and analysis of electro-mechanical interactions between prime-mover and load in a marine IFEP system," *Proc. 2007 IEEE Electric Ship Technologies Symposium (ESTS)*, 2007, Arlington, Virginia, 2007.

[18] M. Kizilcay, "Alternative Transients Program." Available at: http://www.emtp.org (accessed 11/05/2009)

[19] Manitoba HVDC Research Centre, "PSCAD." Available at: http://www.pscad.com (accessed 11/05/2009)

[20] The Mathworks, "SimPowerSystems." Available at: http://www.mathworks.com/products/simpower/ (accessed 11/05/2009)

[21] Powersim inc., "PSIM." Available at: http://www.powersimtech.com (accessed 11/05/2009)

[22] Integrated Engineering Software, "Power Electronics and Electrical Drives Modelling and Simulation." Available at: http://www.integratedsoft.com/caspoc (accessed 11/05/2009)

[23] Cadence, "ORCAD PCB Design Tools." Available at: http://www.cadence.com/orcad/index.html (accessed 11/05/2009)

[24] Pedrag Pejović, Dragan Maksimović, "A method for fast time-domain simulation of networks with switches," *IEEE Transactions on Power Electronics*, vol. 9, no. 4, pp. 449 – 456, July 1994.

[25] Lok-Fu Pak, Omar Faruque, Xin Nie, Venkata Dinavahi, "A versatile cluster-based real-time digital simulator for power engineering research," *IEEE Transactions on Power Systems*, vol. 21, no. 2, May 2006, pp. 455 - 465.

[26] Bruno De Kelper, Handy Fortin Blanchette, Louis-A Dessaint, "Switching time model updating for the real-time simulation of power-electronic circuits and motor drives," *IEEE Transactions on Energy Conversion*, vol. 21, no. 1, March 2005, pp. 181 - 186.

[27] Roger Champagne, Louis-A. Dessaint, Handy Fortin-Blanchette, Gilbert Sybille, "Analysis and validation of a real-time AC drive simulator," *IEEE Transactions on Power Electronics*, vol. 19, no. 2, March 2004, pp. 336 - 345.

[28] Scott Graham, Ivan Wong, Won-Zon Chen, Alex Lazarevic, Keith Cleek, Eric Walters, Charles Lucas, Oleg Wasynczuk, Peter Lamm, "Distributed Simulation of an Uninhabited Aerial Vehicle Power System," *SAE 2004 Transactions: Journal of Aerospace*, pp. 1916 – 1921, 2004.

[29] P. J. Norman, C. D. Booth, J. D. Schuddebeurs, S. J. Galloway, G. M. Burt, J. R. McDonald, A. Villasenor, R. Todd, J. M Apsley, M. Barnes, A.C Smith, S. Williamson, E. Tsoudis, P. Pilidis, R. Singh, "Simulating IFEP Systems," *Marine Engineering Review (MER)*, pp. 26 – 31, October 2006.

[30] "Distributed Heterogeneous Simulation (DHS)." Available at: http://new.pcka.com/products/distsim.html (accessed 11/05/2009)

[31] Barry W. Williams, *Power electronics: devices, drivers, applications, and passive components*. Available http://www.eee.strath.ac.uk/~bwwilliams (accessed 11/05/2009)

[32] "DEF STAN 61-22 Issue 1. Definition of Modelling Standards – Draft. Marine Electrical Power Systems." MOD Document.

[33] Kwa-Sur Tam, Lifeng Yang, "Functional models for space power electronic circuits," *IEEE Transactions on Aerospace and Electronic Systems*, Vol. 31, No. 1, pp. 288 – 296, January 1995.

[34] A. Gonzalez Villasenor, R. Todd, M. Barnes, "Rectifier and DC-Link Simulation Models for Marine Power Systems," Technical report for the Advanced Marine Electrical Propulsion Systems (AMEPS) project, August 2006.

Chapter 4 – Analysis of Algebraic Loops

4.1 Chapter Overview

Algebraic loops occur commonly within many different dynamic models including those of marine and aerospace electrical power systems. They also feature heavily in the functional model representations of power electronic converters discussed in the previous chapter and are a key issue throughout this whole thesis. It will be shown that when algebraic loops are present, the model states become dependant on both system inputs and outputs, requiring the use of computationally expensive iterative solvers to find a solution. This consequence can often limit the operating capabilities of many models and also cause difficulties during dynamic simulations. Identifying methods to address the problems caused by algebraic loops is hence vital to improving the capability of modelling and simulation to support the development of marine and aerospace more-electric systems.

This chapter will discuss the concept of algebraic loops, providing examples of how they may occur within network-level models of marine and aerospace more-electric architectures (including within functional models of power electronic converters). It will then describe the how these algebraic loops can be solved, examining the difficulties of this process as well as the resulting impact on simulation efficiency and accuracy. Commonly utilised methods for removing algebraic loops will be compared and contrasted. Through this analysis, the chapter will show that one of these removal methods does not in fact remove the algebraic loop, but actually serves to lessen the impact of its presence, which alters the ways in which this method

should be utilised. To conclude the chapter, the marine and aerospace algebraic loop examples are revisited and the process of determining which removal method is best suited to each is outlined.

Currently, there is only limited literature available on the subject of algebraic loops in power systems simulation, but it is believed that they are one of the reasons that many simulations fail. As such, this chapter makes a notable contribution to the understanding of the impact of algebraic loops upon dynamic network-level simulations of power systems.

4.2 Introduction to algebraic loops

This section will introduce algebraic loops, discuss the forms in which they might occur within network-level models of marine and aerospace more-electric systems and outline why their presence may be problematic for the efficient computation of such models. The concepts presented in this section will form the basis for further analysis and discussions in later sections.

An algebraic loop is a feedback loop containing only functions with direct feed-through characteristics (i.e. those which have no inherent delay). As a result, the input of each function in the loop is directly dependant on its own output at any instant [1, 2]. In this manner, a co-dependency between the input and output of each function is created.

It is important at this stage to make a distinction between the two main ways in

which algebraic loops can occur within power system simulation. The first results from the manner in which some non-linear components are modelled within power systems simulation tools [3]. The outputs and operating state of these models are co-dependant, and as such they cannot be computed in a linear fashion with dedicated inputs and outputs.

A good example of this is a diode, which possesses a turn-on characteristic driven by its terminal voltage and a turn-off characteristic driven by its output current. These interdependent characteristics make the diode difficult to model efficiently [4]. For example, if the model is configured such that the input is the terminal voltage and the output is the current conducted, the turn-on instant of the diode will be readily obtainable but the turn-off instant will be much more difficult to determine. This is because the diode should turn off when the current output of the model reaches zero. However, this requires that the current output of the model be fed back to form a second input so that state of the diode can be determined. This instantaneous feedback loop is an example of an algebraic loop.

The algebraic loop of the type described above occurs in most circuit simulator packages and is largely solved out of sight of the end user [3] (although Chapter 6 shows that this is not easily and efficiently achieved though). As a result, this type will not be considered in this chapter.

The second way in which algebraic loops can occur is in the development of active models. These models have some control or behavioural characteristics that are a

function of external parameters (e.g. functional converter models). As will be illustrated later in this chapter, this feedback system can lead to the development of algebraic loops. These types of algebraic loops are common to all simulation packages, but are not usually out of sight of the end user. As such, this type will be the key focus of this chapter.

Some simulation packages deal with the presence of this second type of algebraic loop by inserting delays into all measurement functions (i.e. those which provide information regarding the state of the modelled electrical system) [5]. This is in an attempt to break the causal dependence of the loop. However, this chapter will show that whilst this approach is an effective method for removing algebraic loops, it can also have a negative impact on the stability of the overall model, potentially leading to erroneous or even failed (i.e. divergent) simulations. As a result, although hard coding this solution method into the software tool keeps the issue of algebraic loops out of site of the end user, it is not always the best suited solution for a model. It can also have a significant impact on the effectiveness of the behavioural converter methods described in the previous chapter.

Formally, an algebraic loop may be expressed mathematically as

$$y(t) = f\big(t, y(t)\big), \qquad (4.1)$$

where $y(\cdot)$ and $f(\cdot, \cdot)$ are continuous real valued functions of variable t. A simple example of an algebraic loop is shown in figure 4.1.

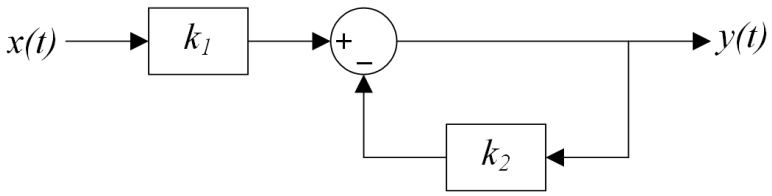

Fig. 4.1. Simple example of an algebraic loop

This system is a linear feedback system and is defined mathematically as

$$y(t) = k_1 x(t) - k_2 y(t), \qquad (4.2)$$

where k_1 and k_2 are constants and $x(\cdot)$ is a continuous real valued function of variable t. The dependency of $y(t)$ upon itself is evident in this equation. Whilst in the case of equation (4.2), a simple rearrangement will express the equation in standard form, this type of co-dependency can make more complex functions difficult to solve, often requiring the use of additional solver algorithms to find an approximate solution. This aspect will be explored in more detail later in the chapter.

This chapter will now consider some examples of algebraic loops commonly found in models of marine and aerospace more-electric architectures. It is intended that these examples will provide some context for the later theoretical sections of this chapter as well as illustrate the impact on simulation efficiency and accuracy that the various forms of algebraic loop might have.

4.3 Examples of Algebraic Loops in Marine and Aerospace Models

Within marine and aerospace power system models, algebraic loops are typically found embedded within representations of active devices or as part of control systems [6]. The following section describes three examples of algebraic loops commonly found within dynamic models of marine and aerospace more-electric architectures. These examples will be revisited at the end of the chapter to evaluate their impact on the network-level modelling of these applications in light of the analysis conducted later.

4.3.1 Control System Example

Consider the example shown in figure 4.2 of an electrical generator connected through a switched rectifier interface to a DC distribution busbar.

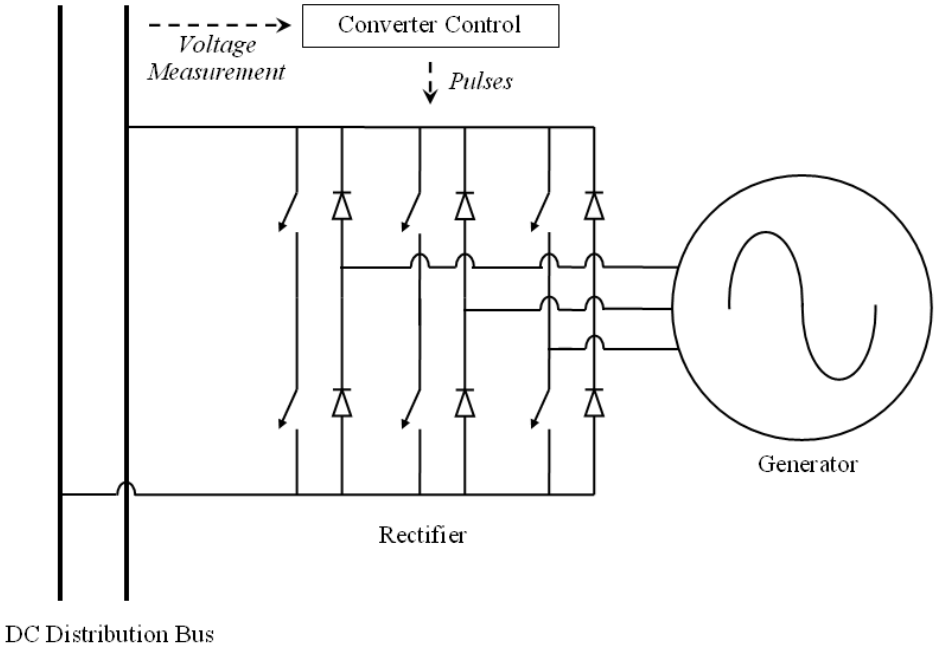

Fig. 4.2. Power electronics interfaced generator system

This system is typical of the generators utilised on the More-Electric Engine as part of the Power Optimised Aircraft (POA) program (described in Chapter 2 and depicted in figure 2.6) [7]. In this application, the converter control system receives a measurement of the DC busbar voltage magnitude and controls the converter switching pattern to regulate the current output of the converter and maintain this voltage at the required level [8, 9]. Within the hardware system, there will be delays in the measurement process, controller response and the actuation of the converter switching. However, within the modelled system, unless these delays are explicitly accounted for (and are often neglected in abstracted network-level dynamic models), all stages of this feedback loop could exhibit direct numerical feed-through and result in the creation of an algebraic loop.

Whilst the characteristics of this loop ultimately depend on the nature of the control system in operation, algebraic loops of this type are generally slow acting and stable in nature. In other words, any change in conditions external to the loop will typically only result in a slow and small change in the state of the loop. As will be discussed later in this chapter, loops of this type cause only minor difficulties in modelling and simulation.

4.3.2 Surge Arrestor Example

A surge arrestor is designed to protect electrical equipment from transient over-voltages. This type of device operates by rapidly decreasing its internal impedance when the voltage across its terminals exceeds a threshold level. By doing so, it forms an effective short circuit, rapidly diverting the main flow of current away from the equipment it is protecting. During all other times, it maintains a high-impedance, non-conducting state so that there is little leakage current during periods of normal voltage conditions. Surge arrestors are often employed within various electrical applications to provide protection against high magnitude voltage transients which can be potentially damaging to the power electronic converters and other sensitive equipment types found within these networks [10, 11, 12].

Figure 4.3 shows a cross section of a Raycap StrikeSorb 80-20 surge arrestor [13], which has been fitted to the Engine Systems Validation Rig (ESVR) as part of the POA program [7].

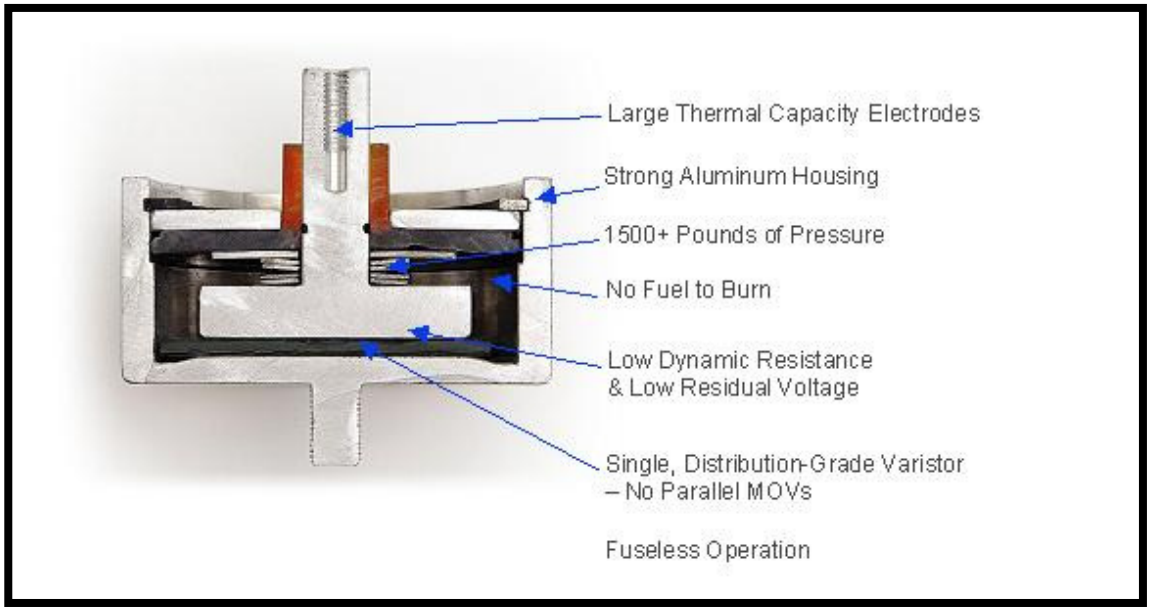

Fig. 4.3. Cross Section of a Raycap StrikeSorb 80-20 surge arrestor (www.raycap.com)

For network-level simulations, it is often not desirable to model the internal physics of the device as this approach could be very computationally demanding. Instead, an abstracted model is often utilised (this aspect is discussed in Chapter 3) [14, 15]. This can be implemented using a voltage-controlled current source, which allows the straight forward implementation of the manufacturer's supplied V/I device characteristics into the model. This approach is shown in figure 4.4.

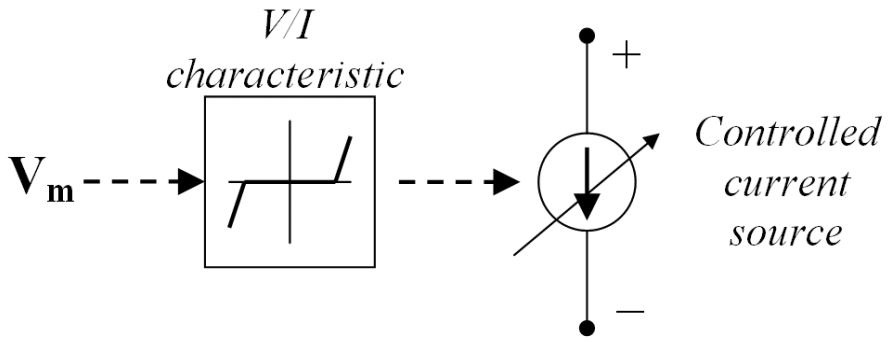

Fig. 4.4. Schematic of a look-up table based surge arrestor model

The model operates by monitoring its own terminal voltage, V_m, and then derives the required level of current to be sunk by the controlled current source based on the implemented V/I curve. In this way, when the threshold terminal voltage is exceeded, the controlled current source is operated to draw current in order to reduce this voltage.

To demonstrate the effectiveness of this device, figure 4.5 shows the line voltage generated in a simple test circuit model when the surge arrestor is not in use. Figure 4.6 shows the line voltage and current drawn by the surge arrestor when it is included in this test circuit. It demonstrates the voltage being suppressed to less than 600V by the action of the surge arrestor sinking current.

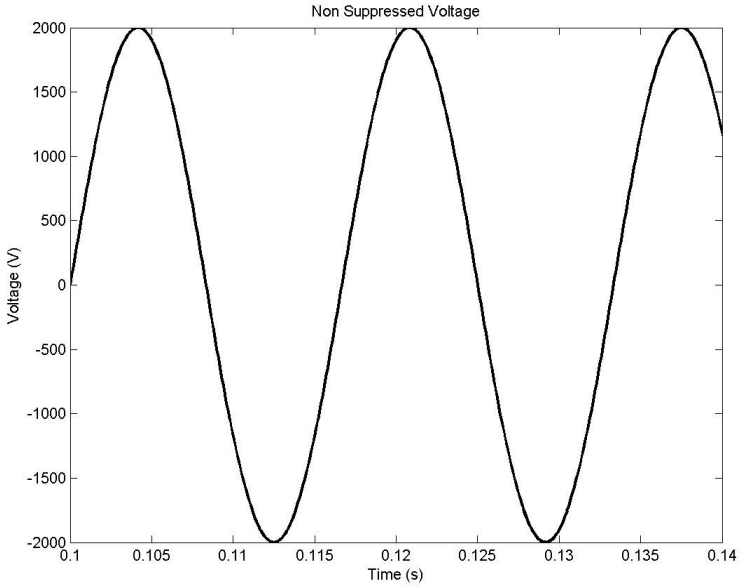

Fig. 4.5. Line voltage with the surge-arrestor not in use

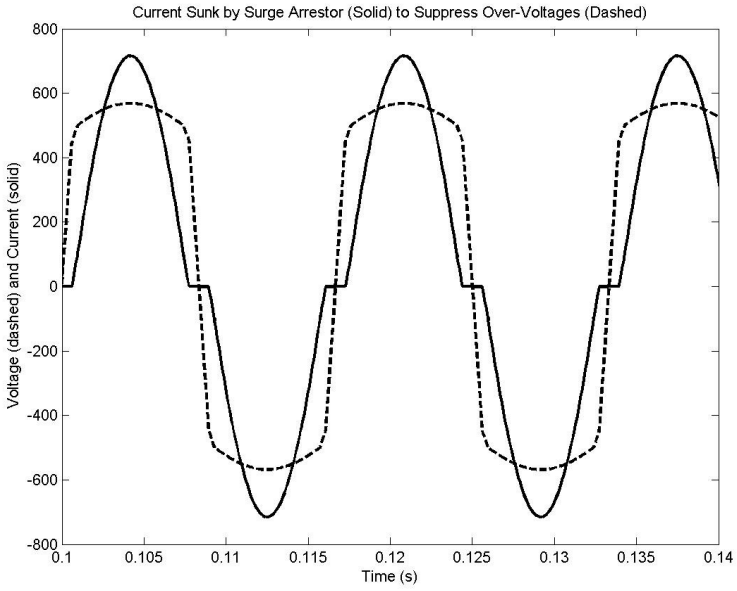

Fig. 4.6. Suppressed line voltage (dashed line) and current sunk by surge arrestor (solid line)

This type of surge arrestor model contains a single algebraic loop. The current sunk by the device is a function of the terminal voltage at that instant. However, this voltage in turn is directly affected by the current sunk; thereby creating a co-

dependency between device voltage and current. In reality, the device would have a short operating delay, typically of the order of a few hundred nanoseconds at most. However, as almost all network-level simulations of marine and aerospace more-electric networks are conducted using simulation time steps of at least one order of magnitude greater, the surge arrestor is usually represented as an instantaneous device in this setting. This in turn leads to the formation of an algebraic loop.

Due to the high current sensitivity of the device during transient over-voltage conditions and the potential impact its operation can have on the behaviour of a number of other systems within the modelled network, the algebraic loop present within the surge arrestor model can be very computationally intensive to solve. It will be shown later that this aspect causes many difficulties when trying to utilise the device in larger marine and aerospace network models.

4.3.3 Functional Model Example

The implementation of the functional approach to modelling power electronic converters outlined in the previous chapter also creates algebraic loops [6, 15]. Although this aspect will be covered in greater detail in Chapter 5, it is necessary to also consider it in this chapter in order to gain a better appreciation of the impact of the algebraic loop on this modelling approach.

Figures 4.7 and 4.8 show schematics of a three-phase inverter and its functional equivalent model.

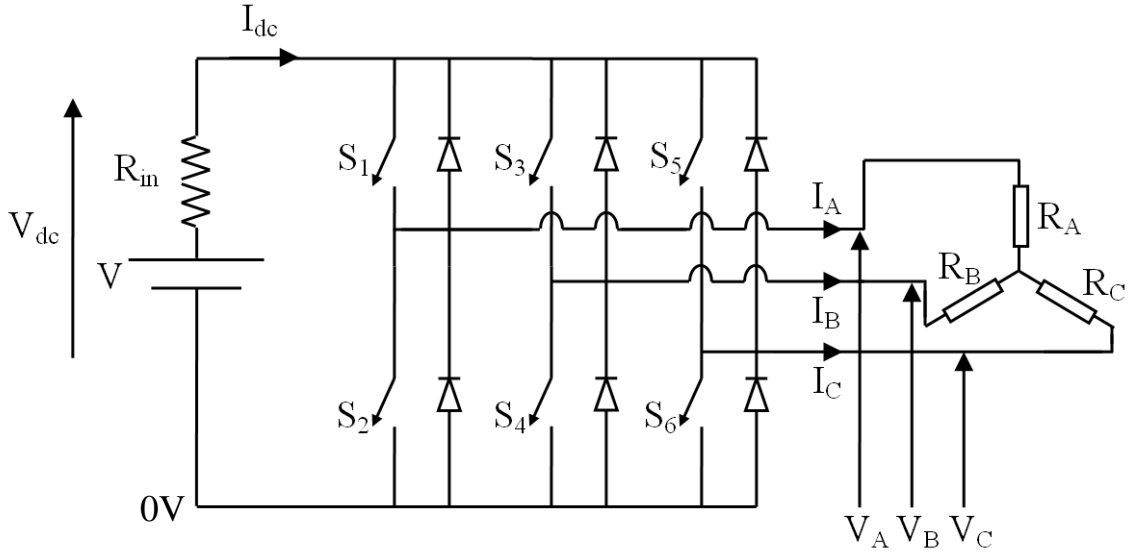

Fig. 4.7. Switched model representation of a three-phase inverter

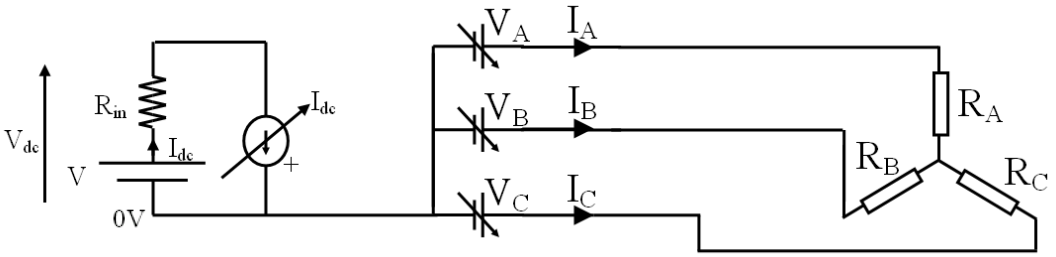

Fig. 4.8. Functional model representation of a three-phase inverter

The governing equations for both models are

$$V_A = S_1 V_{dc} \tag{4.3}$$

$$V_B = S_3 V_{dc} \tag{4.4}$$

$$V_C = S_5 V_{dc} \tag{4.5}$$

$$V_{dc} = V - I_{dc} R_{in} \tag{4.6}$$

$$I_{dc} = S_1 I_A + S_3 I_B + S_5 I_C , \tag{4.7}$$

where V_A, V_B, V_C and I_A, I_B, I_C are the ac side voltages and currents of the inverter. The voltage V_{dc} is the magnitude of the non-ideal dc voltage source (derived from the ideal dc source magnitude V, and the product of the dc side current I_{dc} and source internal resistance R_{in}). The impedances R_A, R_B and R_C are the ac side loads. The term S_j is the j-th switch state and is defined as

$$S_j = \begin{cases} 1 & if \quad closed \\ 0 & otherwise \end{cases} \qquad \text{for } j = 1,2,3,4,5,6\,. \qquad (4.8)$$

The states of switches S_2, S_4 and S_6 are defined as,

$$S_2 = 1 - S_1 \qquad (4.9)$$

$$S_4 = 1 - S_3 \qquad (4.10)$$

$$S_6 = 1 - S_5\,. \qquad (4.11)$$

As discussed in Chapter 3, the functional equivalent model replicates the terminal behaviour of the switched converter model without specifically simulating the operation of its semi-conductor switches, providing significant reductions in computational requirement. It also readily interfaces with the same control and pulse generation systems as utilised by the switched model.

However, a key disadvantage of the functional approach to modelling power electronic converters is that the functional converter models contain one or more

algebraic loops (depending on the converter topology). To illustrate this, figure 4.9 shows the simplified process diagram of three-phase functional inverter model.

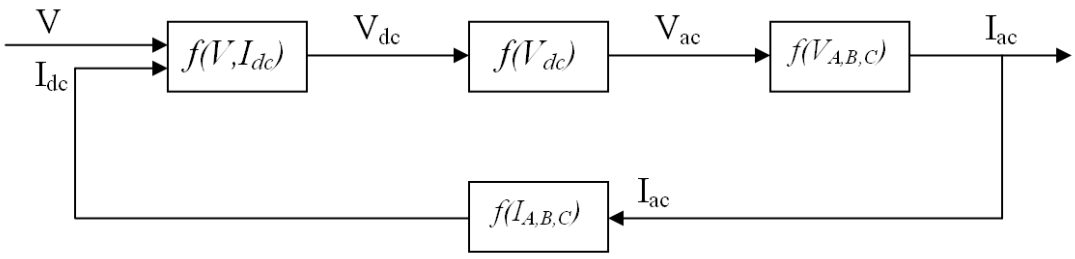

Fig. 4.9. Simplified process diagram of the three-phase functional inverter model

By considering equations (4.3) through to (4.11) and figure 4.9 it is evident that the magnitude of the non-ideal dc source voltage (V_{dc}) is a function of the ideal source voltage (V) and the dc source current (I_{dc}). This voltage determines the magnitudes of the ac side voltages (V_A, V_B and V_C). These in turn, impact directly on the ac side load currents (I_A, I_B and I_C) which then determine the dc current (I_{dc}) magnitude. Hence, the dc side voltage (V_{dc}) is effectively dependant upon itself and an algebraic loop is thus present.

In practice, because the ac side of the inverter has three phases, there are actually three parallel algebraic loops present in this model. Like the surge arrestor model, these are fast acting loops and are often governed by particularly complex equations of operation, especially when the converter is part of a larger network, making them more difficult to solve.

4.4 Root Finding Techniques

Given the complexity of solving algebraic loops within larger network models, most simulation packages utilise iterative solver algorithms to perform this task [1, 16]. These algorithms estimate input and output values of all the functions within a loop, in this way seeking to reduce the error at each step until every function holds true to a specified tolerance. Some of the most common methods utilised are adaptations of root finding techniques.

This section will introduce root finding techniques, providing some illustrative examples of their use. These descriptions form the basis for the following section which illustrates how these methods can be adapted to solve algebraic loops within network-level models of marine and aerospace more-electric systems.

Roots of an equation $f(x) = 0$, are the values of x for which the equation is satisfied [17]. Figure 4.10 illustrates this concept where the roots for the non-linear function $f(x) = 0$, are marked A, B, C.

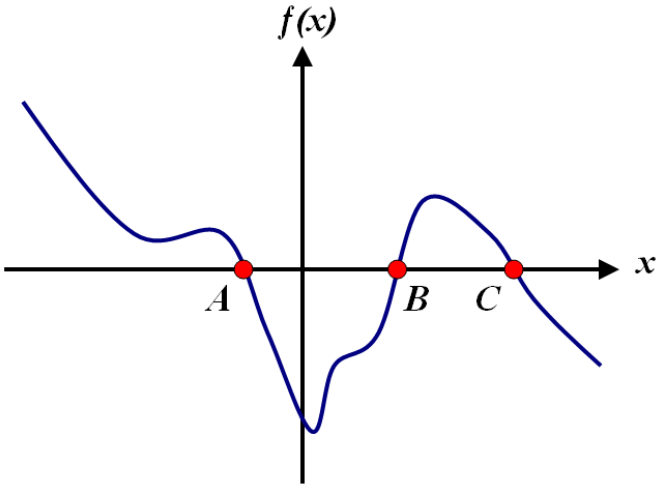

Fig. 4.10. Roots of $f(x)=0$

For equations utilising simple functions, it is often possible to find the roots algebraically. However, for equations with more complex functions (such as those arising from algebraic loops within marine and aerospace electrical network models) this is not usually possible. Under these circumstances it is necessary to utilise a dedicated solver routine. Two such routines are described in the following sections.

4.4.1 The Bisection Method

The first root finding technique considered is the bisection method [18]. This method iteratively converges upon a root within a given region by evaluating the equation in question at the boundaries of the region and then again at its midpoint. By considering the sign of the solution from all three points, it is possible to determine in which of the two subintervals the root lies. At this stage, the process is repeated with the bisection of the subinterval containing the root. In this manner, the region under consideration is halved at each iteration until it reaches a predefined size and

the root is approximated. One stage of the bisection method is illustrated in figure 4.11.

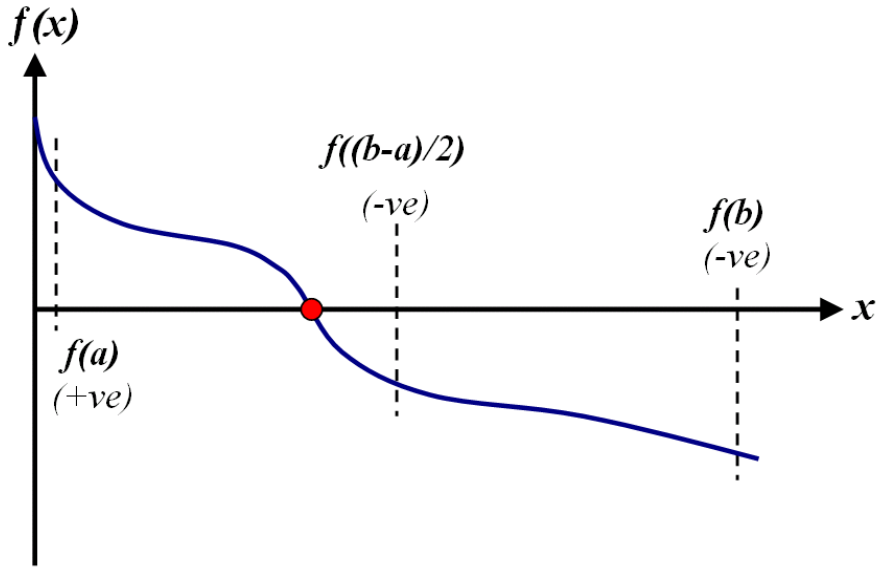

Fig. 4.11. Bisection method

In the figure shown, the function $f(x)$ is considered in the region (a, b). The sign of this function is evaluated at the end points of the region and again at its midpoint, indicating that the root of $f(x) = 0$ lies in the region $(a, \frac{1}{2}(b-a))$. This process will then be repeated on the new region for the corresponding boundary points and midpoint, and so on until convergence on the root occurs (to within a predefined tolerance).

Clearly, the larger the initial region, the more iterations are required to find the root. If more than one root exists within the region, an additional decision algorithm or a suitably augmented version of the bisection method is required to avoid non-convergence. This is illustrated in figure 4.12.

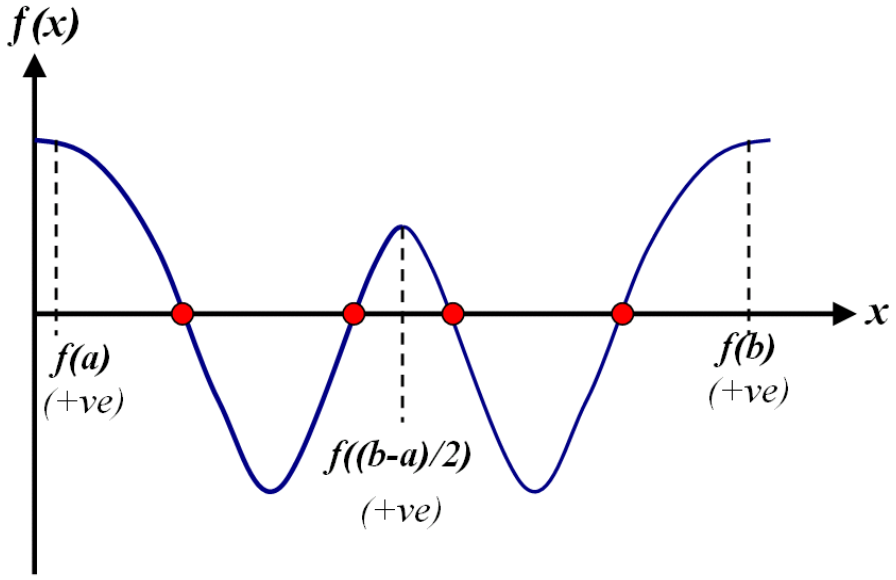

Fig. 4.12. Failed convergence of the bisection method

In this second example, the region being considered is again *(a, b)*. However, the analysis of the function *f(x)* at the end points and the midpoint of the region does not indicate which sub-region contains a root of *f(x) = 0*. In this case, the region specified contains four roots and is hence too large. Under these conditions, the bisection method would fail to converge on a root. A possible solution would be to investigate the two subregions *(a, ½(b-a))* and *(½(b-a), b)* separately.

The bisection method is not however affected by the shape of the function. If only one root exists within the region, the number of iterations required to find the root will always be determined by the size of the region under consideration and the predefined tolerance. In this way, the bisection method is a robust root finding method but it is not necessarily very computationally efficient.

4.4.2 Newton's Method

A second root finding method is Newton's Method (NM). This method is more computationally efficient than the bisection method. As such, it is the favoured root finding method in many commercial software packages [1]. It should also be noted that these commercial packages often utilise more complex adaptations of NM than that discussed in this and the following sections. However, these methods are based on the fundamental concepts of NM and as such, the description and case studies given provide a useful illustration of the use of similar iterative methods to solve algebraic loops.

To locate the roots of a real valued function *f(x)*, $x \in \Re$, the discretized form of the NM iteration formula is

$$x_{n+1} = x_n - \frac{f(x_n)}{f'(x_n)}, \qquad (4.12)$$

where x_n and x_{n+1} are successive estimates of the root of *f(x)* [16, 19], and *f'(x)* is the derivative of *f(x)*.

NM operates by taking iterative calculations from an initial trial point in order to converge upon a root of the function being considered. The first trial point, x_0, is specified either manually or by some additional algorithm. From this, $f(x_0)$ and $f'(x_0)$ are calculated and then used in the NM iteration formula specified above in equation (4.12). This formula provides a value for x_1, the next trial point. This process is

repeated, iteratively updating estimates of trial points until one of the stopping criteria is reached. Two commonly used stopping criteria are:

A When NM has failed to achieve convergence within a preset number of iterations. This can often occur if the gradient of a trial point is zero or close to zero, an aspect which will be explored in more detail later. The limit to the number of iterations is usually put in place to prevent NM running indefinitely under these circumstances.

B When NM achieves convergence. A number of methods can be implemented to indicate this. A common example is

$$\left|x_{n+1} - x_n\right| < \varepsilon , \qquad (4.13)$$

where ε is a predefined tolerance level.

The NM iteration formula works by initially finding $f(x)$ for a specified value of x. The tangent to $f(x)$ at this point is calculated. Geometrically, in terms of the algorithm, this tangent is extended to the x-axis and the value of x at which this occurs becomes the new trial point. The whole process is then repeated until one of the stopping criteria is achieved.

This conceptual consideration of NM is illustrated in figure 4.13 which shows a stage by stage operation of NM converging on a root of $f(x) = 0$. An accompanying explanation of this example is given following the figure.

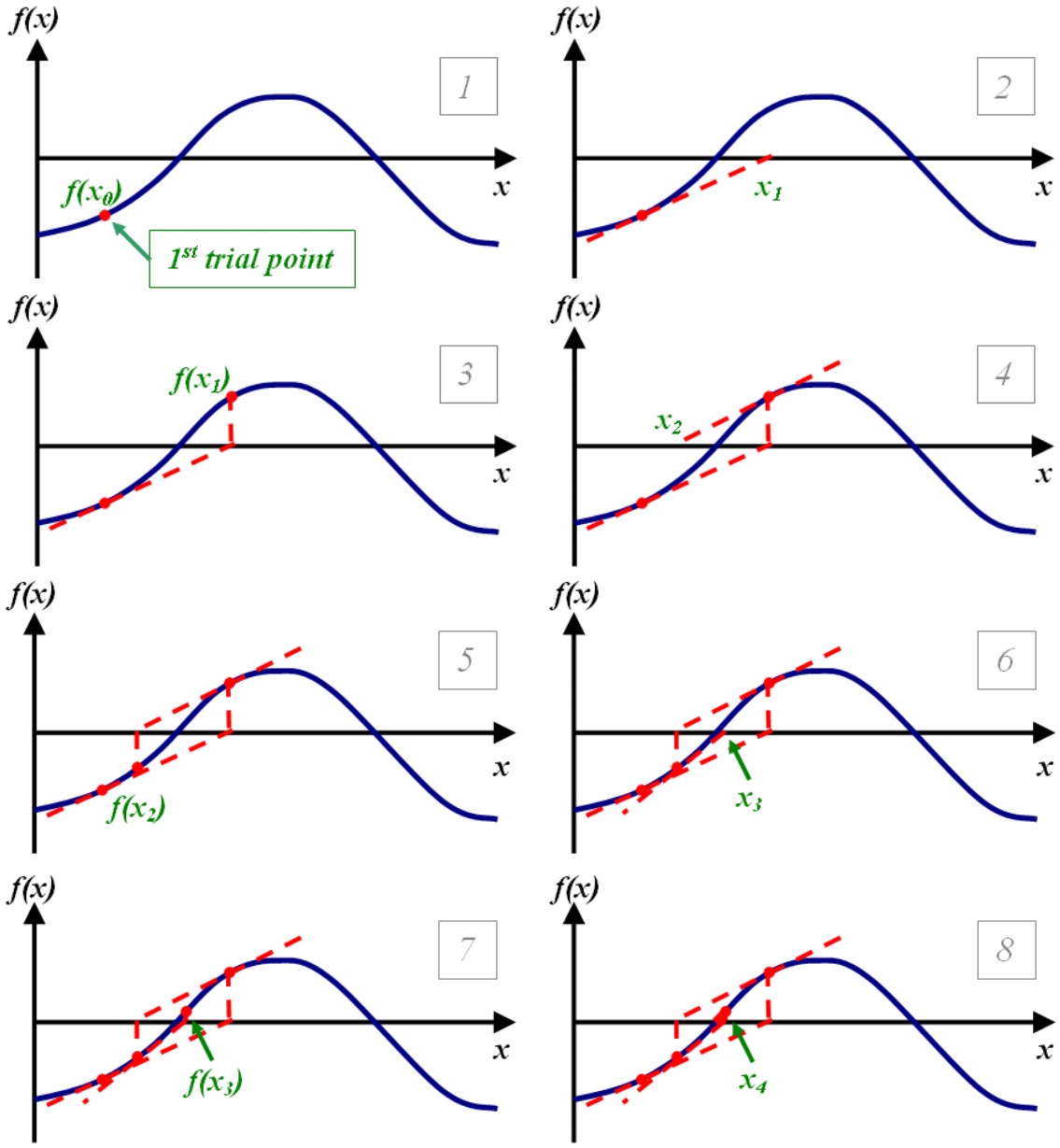

Fig. 4.13. Graphical illustration of Newton's Method converging on a root

In stage one, x_0 is specified for the first trial point and $f(x_0)$ is calculated from this. In stage 2, the tangent to $f(x_0)$ is extended to the x-axis to find x_1. In stage 3, $f(x_1)$ is found using this new trial point. In stages 4 and 5, x_2 and $f(x_2)$ are found by extending the tangent from $f(x_1)$ to the x-axis. In stage 6, x_3 is generated from the tangent to $f(x_2)$. This point lies very close to a root of $f(x)$. Within this region, $f(x)$ is almost

linear. As a result, the tangent generated to $f(x_3)$ (in stages 7 and 8) follows the same path as $f(x)$. In this manner, x_4 is a very close approximation to the root of $f(x) = 0$ and the subsequent stages would meet the stopping criteria 'B' (given on page 95), for convergence on a root.

Note that for NM to find the second root of the $f(x) = 0$ shown in figure 4.13, a different initial trial point would have to be specified. This is illustrated in figure 4.14

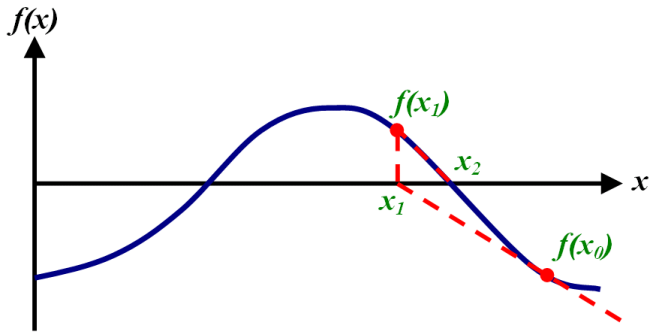

Fig. 4.14. NM finding the second root

The last example illustrates one of the weaknesses of NM. It may find a root of the function, but not necessarily the one sought. An additional algorithm is needed to evaluate whether the located root is the desired one (where possible) and to appropriately vary the initial trial point if it is not. Note that this process can also be performed manually. Convergence on the wrong root can lead to erroneous simulation results and potential numerical instability for other subsequent computations.

If the initial trial point selected is too far from a root, or there are local maxima or minima present in the function, NM is likely to take a large number of iterations to converge on this root (increasing the computational burden of the associated simulation). In some cases, NM may not even converge on the root at all! This is illustrated graphically in figure 4.15, where the presence of the local maximum turning point produces an almost zero gradient, causing the NM iterations to actually diverge from the root. As highlighted earlier as part of stopping criteria 'A', it is common to set an upper limit to the number of iterations taken by NM before declaring a failed attempt. This is to prevent NM taking an unnecessarily large number of iterations to find a root, as might be the case in the example shown in figure 4.15.

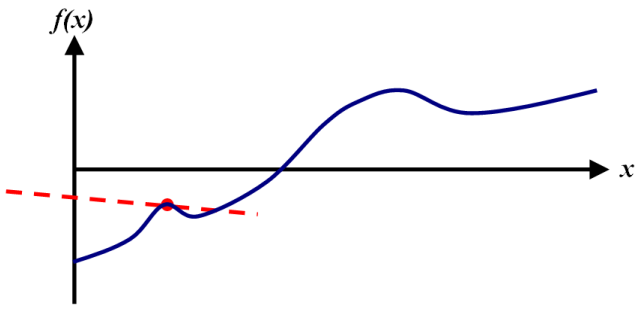

Fig. 4.15 NM failing to converge on a root

Note that if a trial point falls exactly on a turning point, where the derivative of the function is zero, this will create a division by zero in the NM iteration formula causing it to fail unless some additional preventative algorithm is employed.

4.5 Utilising NM to Solve Algebraic Loops

This section will describe how NM can be utilised to solve algebraic loops within power systems (and indeed other) simulations. This will be achieved through the use of two case studies which will also highlight the detrimental effect on simulation efficiency and accuracy that arises from utilising an iterative solver algorithm such as NM to solve algebraic loops. Additionally, the case studies will form the basis for understanding how one of the loop removal methods discussed later (insertion of a small filter) serves to lessen this detrimental effect.

4.5.1 Simple Feedback System Example

The first example is based on the simple feedback system given by equation (4.2). Although in reality, this system can be readily solved algebraically to yield a solution for *y(t)*, applying NM to this simple example allows many of the core features of NM to be clearly demonstrated before a more complicated case study is considered.

The first stage of using NM to solve algebraic loops is to perform some algebra on the equations for the loop in order to convert them into a suitable format for later use. Equation (4.2), can be rewritten as

$$y^{(a)} = k_1 x - k_2 y^{(b)}, \qquad (4.14)$$

where $y^{(b)}$ is an estimate for the original variable y, and $y^{(a)}$ is the resultant of this estimate. When these are equal, a valid solution for the algebraic loop has been

found. Note that in equation (4.14), y and x are still functions of t, but t is being held constant for one particular sampling interval. As a result, x is also treated as a constant during the NM iteration process. The $y^{(b)}$ term is a variable that will be modified in order to find suitable values for y which will give a valid solution for the algebraic loop at that sampling interval.

Mathematically, a valid solution for the algebraic loop is found when

$$G_n = y_n^{(a)} - y_n^{(b)} = 0 . \qquad (4.15)$$

Substituting the expression for $y^{(a)}$, given in equation (4.14) and performing some algebra gives

$$k_1 x - y_n^{(b)}(1 + k_2) = 0 . \qquad (4.16)$$

The NM iteration formula can then be applied, adjusting trial points of $y^{(b)}$ until a root of $G = 0$ is found. When this is achieved, $y^{(b)}$ will represent a value for the variable y which achieves a valid solution for the algebraic loop expressed in equation (4.2) at the sampling interval being considered.

This process is repeated at each sampling interval of the simulation, where the valid solution for the current sampling interval is used as the initial trial point for the next [2]. When the dynamic model is unperturbed and resting in a steady state, the initial trial point at each sampling interval will actually provide the valid solution for the

next sampling interval. For small changes in the model state, the initial trial point at each sampling interval will be close to the valid solution for the loop at that interval. Under these conditions the NM will only need to take a few iterations to converge on a solution. For larger perturbations in the model state or periods of highly dynamic behaviour, a greater number of iterations may be required to achieve convergence. As such, this operating condition will be much more computationally demanding than the steady state conditions discussed above and as a result will lead to slow running simulations during periods of this nature.

Writing the general NM iteration formula for this unity feedback system case study gives

$$y_{n+1}^{(b)} = y_n^{(b)} - \frac{G_n}{G_n'} \ , \qquad (4.17)$$

where

$$G_n = k_1 x - y_n^{(b)}\left(1 + k_2\right) \ , \qquad (4.18)$$

and

$$G_n' = \frac{d}{dy_n^{(b)}}\left(G_n\right) = -\left(1 + k_2\right). \qquad (4.19)$$

For greater clarity in this particular case study, x, k_1 and k_2, will all arbitrarily

assigned the value of 1. This gives

$$G_n = 1 - 2y_n^{(b)} \quad , \tag{4.20}$$

and

$$G_n' = -2 \, . \tag{4.21}$$

The first stage of the NM iteration process is to select an initial trial point, $y_0^{(b)}$, which in this case will be chosen to take the value of zero. Using this value to find G_0 gives

$$G_0 = 1 - 2y_0^{(b)} = 1. \tag{4.22}$$

NM can then be applied to find the next trial point

$$y_1^{(b)} = y_0^{(b)} - \frac{G_0}{G_0'} = 0 - \frac{1}{(-2)} = \frac{1}{2} \, . \tag{4.23}$$

The entire process is now repeated using this new trial point.

$$G_1 = 1 - 2y_1^{(b)} = 1 - 1 = 0 \tag{4.24}$$

$$y_2^{(b)} = y_1^{(b)} - \frac{G_1}{G_1'} = \frac{1}{2} - \frac{0}{(-2)} = \frac{1}{2} \, . \tag{4.25}$$

The repeated value for $y^{(b)}$ indicates convergence on a root of $G = 0$ (indeed, equation (4.2) can be solved algebraically to verify this). As $y(t)$ (and hence G) is linear and therefore only possesses one root, selecting other initial trial points will lead to NM converging on the same root. Also, this analysis shows that for linear functions, NM will always find the root of the function in one step regardless of the initial guess (although a second iteration may be necessary for the algorithm to confirm that convergence on a root has occurred). This is because the tangent at any point on a linear function will always cross the x-axis at the root of the linear function.

4.5.2 Non-Linear Feedback Loop Case Study

Whilst the previous case study clearly demonstrates the application of NM to solving algebraic loops, it does not provide an appreciation of the complexities associated with solving non-linear algebraic loops. This section will present a second case study which is more representative of the modelled systems found in marine and aerospace more-electric architectures in order to better explore this aspect. It will also argue that it is necessary to remove all algebraic loops from complex models such as those of marine and aerospace more-electric systems in order to achieve more computationally efficient simulations.

The governing equation of the non-linear feedback loop for this second case study is

$$y(t) = 2x(t) - \left(y(t)\right)^2 . \qquad (4.26)$$

The dependence of *y(t)* upon itself in equation (4.26) indicates the presence of an algebraic loop. As before, NM can be utilised to find valid solutions for this system. The first stage of this analysis is to modify equation (4.26) into a form that can be accommodated by NM. This is achieved in the same manner as before where $y^{(a)}$ and $y^{(b)}$ (the estimated and resultant values of the original variable *y*) are incorporated and *t* is held constant.

$$y_n^{(a)} = 2x - \left(y_n^{(b)}\right)^2. \qquad (4.27)$$

The next stage is to develop the expression for *G* which in this case gives

$$G_n = y_n^{(a)} - y_n^{(b)} = 2x - \left(y_n^{(b)}\right)^2 - y_n^{(b)}. \qquad (4.28)$$

The derivative of *G* with respect to $y_n^{(b)}$ therefore is

$$G_n' = \frac{d}{dy_n^{(b)}}(G_n) = -2y_n{}^{(b)} - 1. \qquad (4.29)$$

For greater clarity in this particular case study, the values of *x* and $y_0^{(b)}$ will be chosen to be *2* and *0* respectively. NM can now be employed. Table 4.1 illustrates the implementation of NM to find a root of *G = 0* described in its original form by equation (4.28).

Table 4.1. NM applied to the nonlinear case study

Trial Number	$y_n^{(b)}$	G	G'	$y_{n+1}^{(b)} = y_n^{(b)} - \frac{G}{G'}$
0	0	4	-1	4
1	4	-16	-9	2.2222
2	2.2222	-3.1604	-5.4444	1.6147
3	1.6147	-0.3369	-4.2834	1.5631
4	1.5631	-6.4×10^{-3}	-4.1262	1.5616
5	1.5616	-1.9456×10^{-4}	-4.1232	1.5616
6	1.5616	-1.9456×10^{-4}	-4.1232	1.5616

Convergence is achieved by the sixth iteration. An additional initial trial point is required to find the second root of this function, which in this case occurs when $y^{(b)} = -2.56$. This aspect is illustrated in figure 4.16, which shows the function G, and the two roots for $G = 0$. For initial trial points to the right of the minimum turning point (which occurs at $y^{(b)} = -0.5$), NM will converge on the first root found in the analysis above. For trial points to the left of this minimum turning point, NM will converge on the second root. Also note that initial trial points close to the minimum turning point will result in very large magnitudes of $y^{(b)}$ at the next iteration. However, for a parabolic function such as the one considered in this case study, the absence of any other turning points means that it is unlikely that this initial divergent behaviour will cause any longer term convergence problems.

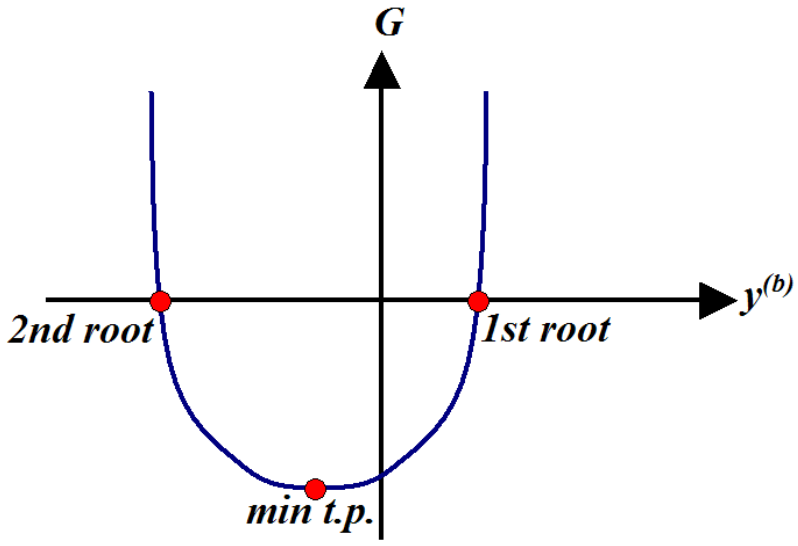

Fig. 4.16. Graphical illustration of the nonlinear NM case study

Comparing this case study to the previous one of section 3.6 demonstrates that whilst convergence will occur within a relatively small number of steps for functions that are linear or very close to being linear, more complex functions with localised maxima and minima may cause NM to take a substantially more iterations to achieve convergence. By requiring a greater number of iterations at each sampling interval, the computational burden of a particular simulation will be substantially increased. This in turn will lead to lengthened simulation completion times for associated power system problems which can be particularly disadvantageous if the model is already a complex, computationally intensive model. Some simulations may also fail if the algebraic loop(s) cannot be solved within the predefined number of iterations.

In summary, when simulating simpler, more convenient models, it is often acceptable to leave any algebraic loops in place as the governing equations defining these loops can usually be solved with just a few iterations of NM. However, within

more complex models such as power electronics dense marine and aerospace electrical network models, the governing equations of any algebraic loops present will be far more complex in nature due to the interaction between the various functions of the network model. These loops will require a greater number of iterations to solve, causing a substantial increase in the simulation computation and increasing the risk of failed simulations if convergence is not achieved. As a result, it is hence a necessity to remove all algebraic loops from a complex model if reliable and computationally efficient simulations are to be achieved.

4.6 Removing Algebraic Loops

Given the need outlined above to remove all algebraic loops from network-level models of marine and aerospace more-electric architectures in order to achieve more accurate, faster running simulations, this section will discuss and contrast the three main methods listed in the literature which facilitate this. By doing so, the key strengths and limitations of each method will be outlined, providing guidelines for their implementation.

There are three main methods listed in literature that enable the removal of algebraic loops in order to produce more stable, faster running simulations [1, 2, 5]. These are:

- Reducing the loop to a feed-forward equivalent system
- Inserting a unit delay into the loop
- Inserting a simple low pass filter into the loop

Each of these methods will be considered in turn in the following subsections.

4.6.1 Feed-Forward Equivalent System

In some cases, the algebraic loop is simple enough to be re-expressed as a feed-forward equivalent function, where the removal of the feedback path negates the effects of the algebraic loop. To illustrate this, consider the feedback system described in equation (4.2). As mentioned earlier, this linear equation can be solved algebraically for *y(t)* in a straight forward manner, giving

$$y(t) = \frac{k_1 x(t)}{(1 + k_2)}, \qquad (4.30)$$

which is effectively now a feed forward equivalent system. The new form of this system is illustrated in figure 4.17.

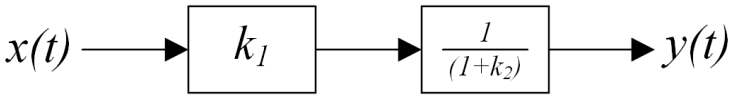

Fig. 4.17. Feed-forward equivalent of the simple feedback system

Some commercial simulation software packages utilise embedded algorithms to identify any simple algebraic loops in a model prior to its computation and replace these with feed-forward equivalent functions [2]. However, feedback systems of a greater complexity are much more difficult to reduce to feed-forward equivalents. This is especially true in more-electric marine and aerospace systems where the complex nature of the electrical network and the equations governing it often make it impossible to implement this solution method.

4.6.2 Utilisation of a Unit Delay

An alternative to the feed-forward equivalent system method is the placement of small delays into the algebraic loop, typically of the order of one simulation time step (or unit). By delaying the data fed around the loop, the input of a particular function now becomes dependant on it own output from the previous simulation sampling interval, effectively breaking the direct feed-through of the loop. Some existing power system software packages utilise this method in all measurement type functions (i.e. those which provide information regarding the state of the modelled electrical system) to prevent any algebraic loops occurring [5]. However, as will be discussed below, this solution method is not always the most appropriate and can lead to numerically unstable models.

To illustrate this, consider the example system described by equation (4.2). If a single unit delay is placed into the feedback path, the expression for the output *y(t)* becomes

$$y(t) = \begin{cases} k_1 x(t) & \text{for } t = 0 \\ k_1 x(t) - k_2 y(t-1) & \text{otherwise} \end{cases}, \qquad (4.31)$$

where *y(t)* is some integer function.

This approach is readily achievable in almost all cases. It should be noted though, that adding delays into feedback loops marginally reduces their stability and can potentially compromise the dynamic performance of the entire models, especially

those with larger simulation step sizes [20]. Indeed, the governing equation for the delayed feedback system given in (4.31) is an example of a first order recurrence relation and has finite limits to its numerical stability. To illustrate this, consider the general solution to equation (4.31) which is

$$y^{(N)} = k_1 x \sum_{i=0}^{N} (-1)^i k_2^i , \qquad (4.32)$$

for y at $N+1$ stages. Note that $x(t)$ has been considered as a constant in order to simplify the expression for y and provide a clearer illustration of the impact of the unit delay method on numerical stability.

In terms of numerical stability, if $|k_2| > 1$, equation (4.32) becomes unbounded and any simulation containing loops of this type would be unstable. Naturally, the magnitude of k_2 is dependant upon the algebraic loop in question but this example illustrates the risks associated with utilising the unit delay method. The use of this method in functional converter models is explored in more detail in Chapter 5.

4.6.3 Utilisation of a Simple Filter

The insertion of a filter is the third solution method mentioned in existing literature for the removal of algebraic loops [2]. Like the unit delay method, the filter method is easy to implement although the impact of its presence is very different to the former method. However, this section will argue, that contrary to the view presented in the existing literature [1, 2], the filter method *does not* actually remove the

algebraic loop within the model, but rather aids the numerical convergence of iterative solvers such as NM. As such, it will be shown that the effectiveness of the filter method is very much dependant on the nature of the algebraic loop and the surrounding model.

To illustrate the use of the filter method, consider the mathematical expression for the simple feedback loop given in equation (4.2) but with a first order low pass filter inserted into the feedback path. The governing equation of this new feedback system is given by

$$y(t) = k_1 x(t) - k_2 a(t), \qquad (4.33)$$

where *y(t)* is some integer function and *a(t)* is the function of the modified feedback path (where *y(t)* is fed through a first order low pass filter). The function *a(t)* takes the following form

$$a(t) = k_f \left(y(t) - y_0 \right) + y_0, \qquad (4.34)$$

where y_0 is the magnitude of *y(t)* prior to a perturbation and is considered constant. When the algebraic loop is resting in a steady state, $y_0 = y(t)$ and equation (4.33) is equal to equation (4.2). The effective gain of the low pass filter is represented by k_f and is defined by

$$k_f = 1 - \exp\left(\frac{-(t - t_0)}{\tau}\right), \qquad (4.35)$$

where t_0 is the time instant at which the initiation of any perturbation from a previously steady state condition occurs, and τ is the time constant of the filter. The step response of this function is illustrated in figure 4.18.

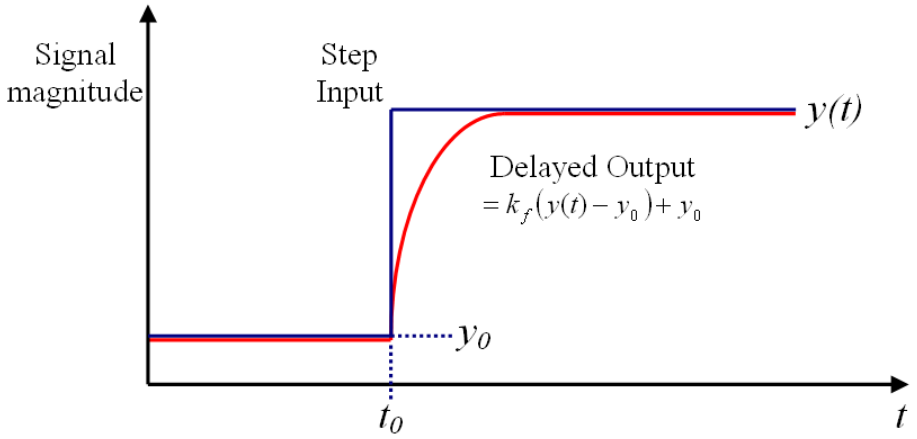

Fig. 4.18. Time domain response of a low pass filter

Considering the expression for k_f (given in equation (4.35) and illustrated in figure 4.14 earlier), it can be seen that the effective gain (k_f) of a low pass filter on the change in $y(t)$ (i.e. $y(t) - y_0$) is almost zero following a perturbation on the function. This gain increases as a non-linear function of time until some point later when it reaches unity again. The key point to note here is that the function does not become discontinuous as a result of the inclusion of the low pass filter. In this manner, the use of a low pass filter will not remove the presence of an algebraic loop either. This aspect can be illustrated by substituting for $a(t)$ in equation (4.33) to obtain the following

$$y(t) = k_1 x(t) - k_2\left(k_f\left(y(t) - y_0\right) + y_0\right). \qquad (4.36)$$

Equation 4.36 shows that the dependence of *y(t)* upon itself is only removed when k_f has a magnitude of zero. This is only true when $t = t_0$, i.e. when the perturbation occurs (consider the definition of k_f given in equation (4.35)). At all other times there will be some interdependence of *y(t)* upon itself and the algebraic loop will exist.

Despite the fact that the filter method does not remove the algebraic loop, it is still an effective method in reducing the computational burden of solving algebraic loops and as such is still an effective counter-measure. For example, in the sampling interval immediately following a perturbation in system, the effective gain of the low pass filter in the feedback loop is almost zero. As such, the feedback component of the loop remains largely unchanged and the desired root is easily found. To illustrate this, consider the expression for the non-linear function $y^{(a)}$ given earlier in equation (4.27). If a low pass filter were added to the feedback loop of this function, the effective magnitude of the $(y^{(b)})^2$ term would be constant following a perturbation in the function input (x). As such, the expression for G' given in equation (4.29) would be almost constant (indicating that the function G is nearly linear), for which the roots could be readily found by NM.

At successive sampling intervals after the perturbation has been applied, as the effective gain of the low pass filter in the feedback loop increases, the feedback system moves towards its original unfiltered form. This behaviour should result in progressively more iterations being taken to achieve convergence on the desired

solution of the root. However, as stated earlier in section 4.5, iterative solvers such as NM utilise the solution to the loop from the previous sampling interval as the initial trial point for the next. In this manner, as the effective gain of the low pass filter in the feedback loop increases, the solution to the loop at each sampling interval will usually lie close to the initial trial point used by the iterative solver and the number of iterations required to achieve convergence will be minimised.

In contrast to this, if a significant perturbation was applied to the same system with the low pass filter removed, there would be a substantial change in the valid solution to the algebraic loop from one sampling interval to the next. The solution at the sampling interval before the perturbation would not provide a good initial trial point for the iterative solver at the next (post-perturbation) interval. A larger number of iterations would hence be required to achieve convergence on a valid solution after the perturbation (resulting in an increased computational burden) and there would also be the likely possibility of a failed convergence occurring.

In this manner, the low pass filter method serves primarily to aid the numerical convergence of the iterative solver by slowing the transition of the algebraic loop from one state to the next and be providing good initial trial points as the loop is restored to its original unfiltered form following this change. It does not however actually remove the algebraic loop, like the other two solution methods discussed earlier.

This understanding of how the filter method operates also exposes some of its weaknesses. Following significant perturbations or during periods of highly dynamic variations in the model's state, this method may not sufficiently aid the iterative solver in achieving convergence if the time constant of the low pass filter chosen is too small. In some cases, failed simulations may even occur. This is because the effective gain of the low pass filter increases so rapidly that the initial trial point provided by the solution of the previous sampling interval is not close enough to the new solution to achieve convergence efficiently or even at all.

The complexity of the network model also has an impact on the effectiveness of the filter solution method. For example, a modelled subsystem containing an algebraic loop may simulate efficiently and accurately in isolation with the implementation of a low pass filter in the feedback path of the loop. However, inserting this modelled subsystem into a larger network model may lead to less efficient and even failed simulations. This is because the interactions between the loop and the surrounding model produce more complex governing equations for the loop, requiring a greater number of iterations to achieve convergence. Thus while the time constant chosen is effective for the development of the isolated subsystem model, it may prove to be too small to have any significant impact on aiding the convergence of NM in a more complex model.

To compensate for these limitations, it is necessary to increase the time constant of the filter. However, in doing so, the dynamic behaviour of the modelled system may be altered. Given that the aim of simulating marine and aerospace more-electric

architectures at a network level [21, 22] is often to assess the impact of this dynamic behaviour, such an outcome is unacceptable. Whilst higher order filters may offer further options, their effectiveness is still not guaranteed.

4.6.4 Review of Methods

The previous sections have shown that whilst the filter method improves the computational efficiency of models containing algebraic loops it does not in fact remove the algebraic loop and as such is not a guaranteed solution. The other methods presented in this chapter always remove the algebraic loop. However, given that the unit delay method increases the risk of numerical instability and the feed-forward equivalent system method is not always achievable, it is clear that the presence of algebraic loops within a model can present real difficulties in achieving efficient and accurate dynamic simulations.

As a final point, it is worth noting that there is a fourth approach that should be considered when addressing the difficulties associated with algebraic loops. Reducing the size of the period between sampling intervals (i.e. the simulation step size) taken by the simulation solver does not remove algebraic loops but is still an effective fourth option for reducing the impact they have on the efficiency of simulations. This method aids convergence in the same manner as the filter method by providing better initial trial points at each sampling interval. However, given the desire to utilise maximum levels of abstraction in order to facilitate the use of large sampling intervals in network-level dynamic simulations of marine and aerospace more-electric power networks [21, 22], the use of this method is not desirable.

4.7 Evaluation of Solution Types to Marine and Aerospace Algebraic Loop Examples

This section will revisit the marine and aerospace based power system examples of algebraic loops investigated at the start of this chapter. It will consider the potential effectiveness of each of the solution methods considered above and identify the best suited one for each example. In doing so, this section will provide useful guidelines on mitigating the effects of algebraic loops within models of marine and aerospace more-electric architectures. These guidelines have been developed based on the theoretical analysis given in earlier sections of this chapter and the personal modelling experience of this author.

It should be noted that the feed-forward equivalent method is not particularly applicable to any of these examples. This is due to either the complexity of the feedback loops themselves (control system example) or the complexity of the interactions between the loop functions and the surrounding power system (surge arrestor and functional model examples) when modelling marine and aerospace more-electric architectures.

4.7.1 Control System Example

Algebraic loops found within control systems are typically slow acting loops with a low sensitivity to changes in conditions external to the loop. As a result, the insertion of a unit delay is often the preferred solution method (this applies for both simple and complex models). It is readily implemented, is guaranteed to remove the loop and the

reduction of the stability margin will usually have little impact on the overall model stability. Alternatively, whilst not removing the algebraic loop, the use of a low pass filter is also likely to aid the numerical convergence of NM sufficiently enough to cause only a slight increase in simulation run time. However, in complex models involving many control systems, the slight increase in simulation run time resulting from solving each loop may be compounded. If this occurs, the unit delay method remains as the only viable solution.

4.7.2 Surge Arrestor Example

As discussed at the start of the chapter, the algebraic loop present within the surge arrestor model is a very fast acting, sensitive loop. In other words, any change in circuit voltage could potentially result in a significant and rapid change in the current sunk by the surge arrestor model. As a result, implementing the unit delay method will often create numerical stability problems when the surge arrestor model is not resting in a passive state. Unfortunately, implementing the filter solution is also difficult to achieve successfully. Whilst a filter with a large time constant will substantially aid the convergence of NM, the very fast dynamic response of the surge arrestor will be misrepresented. Implementing a filter with a small time constant will only produce a negligible impact on the convergence of NM and as such will have very little benefit.

The only remaining solution for achieving simulation accuracy therefore is to leave the algebraic loop in place. It is easily solved when the surge arrestor model is not active (i.e. no voltage surges are occurring) and although the use of NM during the

periods of active operation will impact significantly on the computational burden of the simulation (resulting in much increased simulation durations), these periods generally occur infrequently and usually very briefly. However, if the surge arrestor model is contained within a more complex network model (and as a result the governing equations of the algebraic loop are also very complex), it is likely that NM will not be able to converge on a valid solution for the algebraic loop, causing a failed simulation.

Hence there is a real difficulty in representing surge arrestors in dynamic models of complex electrical power networks, like those found in marine and aerospace more-electric applications. The only remaining options are to either represent the surge arrestor model behaviour very simply so that the governing equations of the algebraic loop are simplified (aiding convergence) or to substantially decrease the period between sampling intervals so that the operation of the surge arrestor is no longer considered to be instantaneous. Both of these approaches will allow the filter and unit delay methods to be utilised more effectively. However, as discussed earlier, the action of decreasing the simulation solver step size will lengthen the overall run time of the dynamic models, which is particularly undesirable for network-level models of complex systems.

4.7.3 Functional Converter Model Example

Like the surge arrestor example, the algebraic loop present within functional converter models is typically fast acting and very sensitive to changes in conditions external to the loop. As before, these characteristics make the filter method

unfavourable for this application as it is not guaranteed to prevent failed simulations. This is especially true if the converter model is utilised within the larger network models where the governing equations of the algebraic loop are complex in nature and are more difficult to solve.

In simpler network models, where the interactions between the functional converter model and other network elements are well known, it may be possible to utilise the feed-forward equivalent method. However in the larger marine and aerospace electrical network models, this method is not easily implemented and as such, the unit delay method is the only remaining solution for these applications. This latter method is easily implemented within the functional converter model and will guarantee the removal of the algebraic loop providing more efficient, faster running simulations. However, as discussed earlier in the chapter, there will be some degradation in the numerical stability of the model, which in turn could lead to erroneous or failed simulations in some operating scenarios. A full understanding of the impact of the unit delay on the behaviour of the functional converter model is essential to enabling its successful application within marine and aerospace more-electric network models. Chapter 5 will explore this issue in greater detail as part of an in-depth analysis of functional approach to modelling power electronic converters.

4.8 Chapter Conclusions

This chapter has explored the concept of algebraic loops. They have been defined and examples have been given to illustrate how they might occur within marine and

aerospace more-electric network models. This chapter has highlighted the use of iterative solvers as a popular means to overcoming the co-dependency between inputs and outputs of functions within algebraic loops. A commonly used iterative solver within power system simulation software packages is Newton's Method and this technique is both described and demonstrated using case studies in order to give a greater appreciation of the typical numerical processes involved in solving algebraic loops. One of the key disadvantages of employing iterative solvers like NM for this task is the increased computational burden resulting from the additional calculations performed. This can produce a significant increase in simulation completion times, which are particularly disadvantageous for network-level models of marine and aerospace electrical systems whose typically complex nature will exacerbate this effect. As a result, it is desirable to seek methods to remove the algebraic loops from the models in order to achieve more efficient simulation.

Three of the most popular methods for removing algebraic loops were reviewed and discussed. This chapter demonstrated that one of these, the filter method, does not in fact guarantee the removal of the algebraic loop as stated in the literature but instead serves to improve the performance of NM in converging on a valid solution, impacting on its application to network-level models of marine and aerospace more-electric architectures.

Finally, this chapter revisits the three marine and aerospace examples of algebraic loops given at the start of the chapter and considers the best solution method for each

example. This was done in order to illustrate the process of selecting the best suited solution method for each application.

4.9 References

[1] "Simulating Dynamic Systems," Available at: http://www.mathworks.com (accessed 11/05/2009)

[2] "Algebraic loops," Available at: http://www.20sim.com/webhelp/editor/Compiling/AlgebraicLoops.htm (accessed 11/05/2009)

[3] *Using Matlab*, The Mathworks Inc., 3 Apple Hill Drive, Natick, MA, USA, 2002.

[4] A. Gonzalez Villasenor, J. M. Apsley, M. Barnes, A. C. Smith, S. Williamson, J.D. Schuddebeurs, P. J. Norman, C. D. Booth, G.M. Burt, J. R. McDonald, "Propulsion drive models for full Electric marine propulsion systems," *IEEE International Electric Machines and Drives Conference (IEMDC)*, May 2007.

[5] "Electrical System Modelling," *presentation given by the Rolls-Royce University Technology Centre of Manchester at the Modelling Workshop on 8th November 2006*.

[6] P. J. Norman, S. J. Galloway, and J. R. McDonald, "Simulating electrical faults within future aircraft networks," *IEEE Transactions on Aerospace and Electronic Systems*, Vol. 44, no. 1, pp. 99 – 110, January 2008.

[7] Liebherr Aerospace, "Power Optimised Aircraft." Available at: www.poa-project.com (accessed 11/05/2009)

[8] Lester F. Faleiro, "Trends towards a more electrical aircraft," Liebherr-Aerospace. Available at: http://www.poa-project.com/53.asp (accessed 11/05/2009)

[9] F. Barruel, N. Retiere, J. L. Schanen, A. Caisley, "Stability approach for vehicle dc power networks; application to aircraft on-board system," *Proc. IEEE Power Electronics Specialists Conference (PESC)*, Recife, Brazil, June 2006.

[10] A Haddad, P Naylor, D M German, R T Waters, "A fast transient test module for ZnO surge arresters,"
Available at http://ej.iop.org/links/rPlsX8A2h/iuYq22xi2xG-Jqyrav5vpA/mt950517.pdf (accessed 8/10/2008)

[11] F. Fernandez, R. Diaz, "Metal-oxide surge arrester model for fast transient simulations," Available at http://www.ipst.org/TechPapers/2001/IPST01Paper144.pdf (accessed 11/05/2009)

[12] R. Diaz, F. Fernandez, J. Silva, "Simulation and tests on surge arresters in high-voltage laboratory," Available at http://www.ipst.org/TechPapers/2001/IPST01Paper145.pdf (accessed 11/05/2009)

[13] Raycap, "Raycap transient voltage surge suppression system." Available at: http://www.raycap.com/surge/rayvoss.htm (accessed 11/05/2009)

[14] The Mathworks, "Matlab surge arrestor help file." Available at: http://www.mathworks.com/ (accessed 13/10/2008)

[15] H. Jin, "Behaviour-mode simulation of power electronic circuits," *IEEE Trans. on Power Electronics*, Vol. 12, no. 3, pp. 443 – 452, May 1997.

[16] Ian Jacques, Colin Judd, "Numerical Analysis", *Chapman and Hall*, New York, 1987.

[17] Eric W. Weisstein, "Root." Available at: http://mathworld.wolfram.com/Root.html (accessed 11/05/2009)

[18] Eric W. Weisstein, "Bisection," Available at: http://mathworld.wolfram.com/Bisection.html (accessed 11/05/2009)

[19] Eric W. Weisstein, "Newton's Method." Available at: http://mathworld.wolfram.com/NewtonsMethod.html (accessed 11/05/2009)

[20] Jacqueline Wilkie, Michael Johnson, Reza Katebi, *Control Engineering*, Palgrave, Basingstoke, 2002.

[21] Graham J W Dudgeon, James R McDonald, "Simulation challenges for the all electric ship – form micro-second to macro-second," *Proc. IMarEST Electric Warship IX Seminar*, December 2003, pp. 42 – 54.

[22] Scott Graham, Ivan Wong, Won-Zon Chen, Alex Lazarevic, Keith Cleek, Eric Walters, Charles Lucas, Oleg Wasynczuk, Peter Lamm, "Distributed Simulation of an Uninhabited Aerial Vehicle Power System," *SAE 2004 Transactions: Journal of Aerospace*, pp. 1916 – 1921, 2004.

Chapter 5 – Analysis of Functional Converter Model Behaviour

5.1 Chapter Overview

In Chapter 3 the capabilities and limitations of the functional modelling approach (as described in existing literature) were discussed. Its ease of implementation (without the requirement of prior specialist simulation expertise) and resulting large reductions in model computational requirement were considered to make this technique well suited to the network-level modelling and simulation of marine and aerospace more-electric architectures.

Chapter 3 also discussed the shortcomings of the functional modelling technique during some operating conditions as indicated in existing literature. In order to fully assess its suitability to marine and aerospace applications, an in-depth analysis of the functional modelling technique must be conducted.

This chapter will hence investigate the capabilities and more importantly, the limitations of the functional approach for modelling power electronics converters and consider the implications of these for marine and aerospace application areas. This chapter represents a significant contribution of the thesis.

This chapter is divided into two main parts. The first evaluates general functional converter behaviour and investigates which behavioural functions of the real converters are and are not accurately represented. It investigates what features are

required to address these aspects and evaluates the impact of these on the overall simulation efficiency. The second part considers the impact of the algebraic loops found in functional models (as outlined in Chapter 4) and assesses the implications for the numerical stability within marine and aerospace more-electrical applications.

5.2 Definition of Functional Converter Models

As described in Chapter 3, functional type power electronic converter models derive from the behavioural modelling approach where the characteristics of a converter are represented without specifically modelling the switching action of its semi-conductor switches. This is achieved by utilising controlled voltage and current sources to replicate the terminal conditions of the converter, greatly reducing the computation required to simulate the model. By utilising the same control and pulse generation systems that would be employed by a switched converter model, the dynamic behaviour of the converter is retained [1, 2].

5.3 Examples of Functional Converter Models

This section will provide examples of functional models of the following converter topologies:

- Three-phase inverter/switched rectifier
- DC-DC forward converter
- Diode bridge rectifier

It is acknowledged that other converter topologies are also utilised within marine and aerospace network architectures [3, 4]. However, these are too numerous to consider individually and the core principles from the examples provided can be readily applied to these other topologies.

5.3.1 Inverter/Switched Rectifier Functional Model

Consider the three-phase inverter shown in figure 5.1.

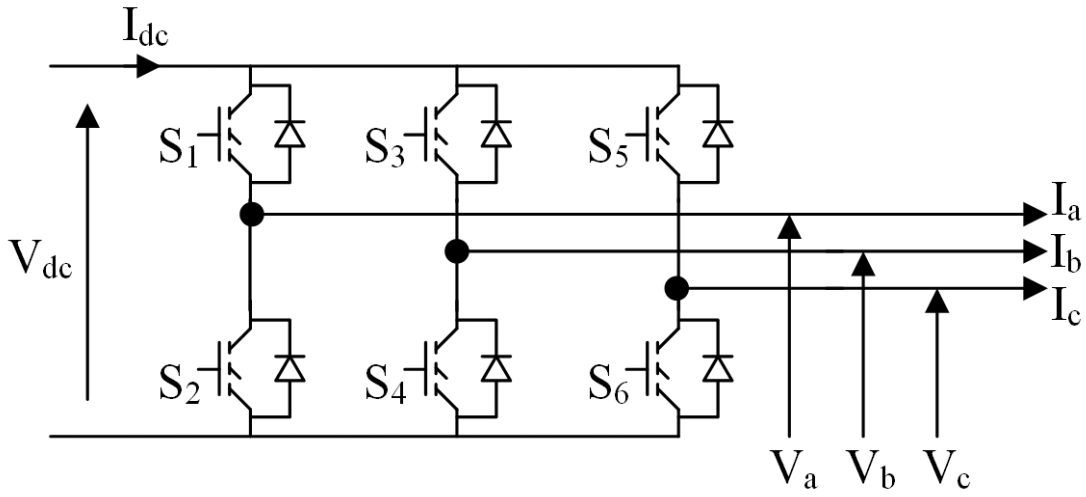

Fig. 5.1. Three-phase inverter schematic

The behaviour of this converter is described by

$$V_A = S_1 V_{dc} \tag{5.1}$$

$$V_B = S_3 V_{dc} \tag{5.2}$$

$$V_C = S_5 V_{dc} \tag{5.3}$$

$$I_{dc} = S_1 I_A + S_3 I_B + S_5 I_C , \tag{5.4}$$

where V_A, V_B and V_C are the ac side phase voltages of the inverter and V_{dc} is the voltage across the dc terminals of the converter. The term S_j is the j-th switch state and is defined as

$$S_j = \begin{cases} 1 & if \quad closed \\ 0 & otherwise \end{cases} \qquad \text{for } j = 1,2,3,4,5,6\,. \qquad (5.5)$$

The states of switches S_1, S_3 and S_5 are determined by the converter control system. The states of switches S_2, S_4 and S_6 result from these, and are described by the expressions below,

$$S_2 = 1 - S_1 \qquad (5.6)$$

$$S_4 = 1 - S_3 \qquad (5.7)$$

$$S_6 = 1 - S_5\,. \qquad (5.8)$$

Now consider the functional equivalent circuit of the three-phase inverter shown in figure 5.2.

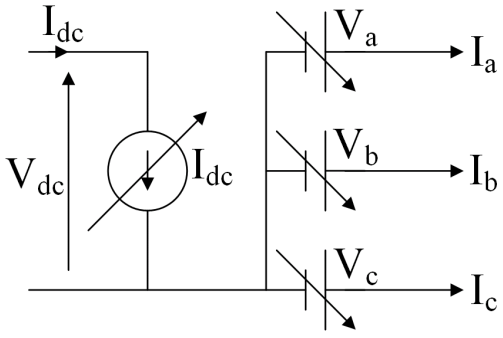

Fig. 5.2. Functional equivalent model of a three-phase inverter

In this representation, the switched model is replaced by three controlled voltage sources and a single controlled current source. The equations describing the operation of this model remain the same as for the switched model except that the controlled sources now replicate the terminal conditions of the inverter without explicitly simulating the operation of the switches. As discussed in Chapter 3, this achieves large gains in computational efficiency which in turn leads to a reduction in overall simulation run times.

If the switching functions S_1, S_3 and S_5 are replaced by the continuously varying modulation waves of the pulse generation circuit, the time-averaged output of the converter will be represented. Figure 5.3 illustrates this process of pulse averaging.

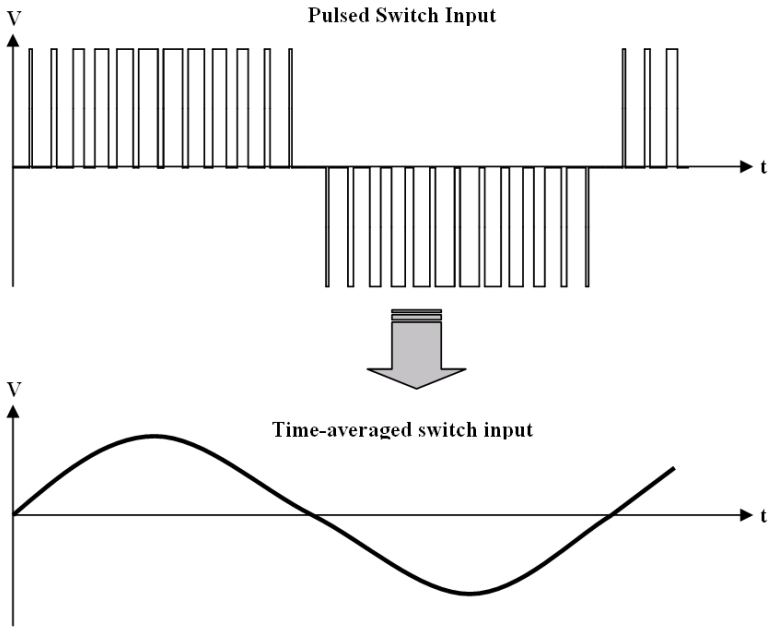

Fig. 5.3. Illustration of pulse averaging

Utilising time-averaged converter behaviour permits larger solver step sizes to be utilised further reducing the overall simulation computation.

5.3.2 DC/DC Forward Converter Functional Model

Consider the circuit schematic of the dc-dc forward converter shown in figure 5.4.

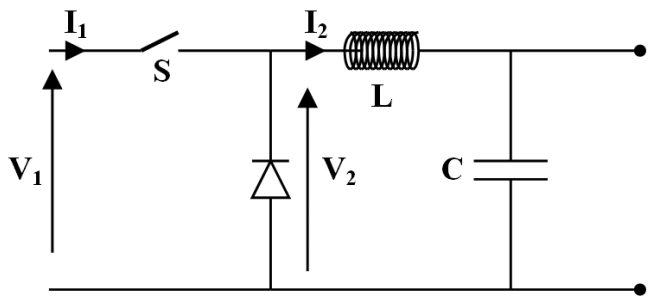

Fig. 5.4. DC-DC forward converter schematic

The behaviour of this forward converter is described by

$$V_2 = SV_1 \qquad (5.9)$$

$$I_1 = SI_2, \qquad (5.10)$$

Where V_1, V_2 and I_1, I_2 are the input and output voltages and currents of the converter. S is the switch state and is defined as

$$S = \begin{cases} 1 & if \quad closed \\ 0 & otherwise \end{cases} . \qquad (5.11)$$

Figure 5.5 shows the functional equivalent model of the DC-DC forward converter.

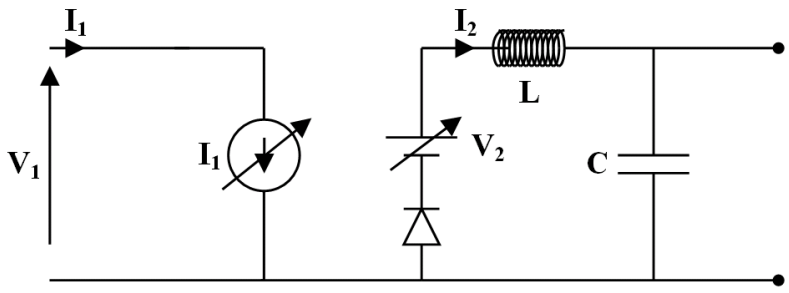

Fig. 5.5. Functional equivalent model of a DC-DC forward converter

In this representation, the switched model of the forward converter is replaced by a controlled voltage source and a controlled current source. The diode is required to prevent the load current reversing in direction when the output of the V_2 is zero. As with the inverter functional model, the controlled sources now replicate the terminal conditions of the converter without explicitly simulating the operation of the semiconductor switch. Unlike the inverter however, this functional model will deliver only marginal increases in simulation efficiency due to the low switch count in the original switched model. However, representing more complex DC-DC converter topologies with functional model representations will provide more substantial gains in simulation efficiency.

5.3.3 Diode Bridge Rectifier Functional Model

In Chapter 4, the difficulties associated with modelling diodes were discussed. The dependence of the diode's state on its own terminal conditions requires the use of an iterative solver to produce accurate results. This problem extends to functional

models of diode bridge converters where the decoupling of the ac and dc sides of the converter limits the capabilities of the model [5] or it leads to inaccurate behaviour of the model, including the creation of rapidly oscillating model outputs in some operational modes [2]. Unless the turn-on and turn-off times are easily predicted in advance (for example if the diode bridge is supplied by an ideal three-phase source), a functional representation of a diode bridge rectifier will be very inaccurate. As it is unlikely that an ideal source will be used in network-level models of marine and aerospace more-electric architectures, this poor behaviour necessitates the use of switched diode bridge models (which do not decouple the two sides of the converter) in these applications.

However, because of the typically low switching frequency of diode bridges, the computation required for a switched model of this converter type is much less than for other fully-controlled topologies. As such, the potential benefits of employing a functional representation of a diode bridge converter are low in comparison to other converter types. In this manner, utilising both switched diode rectifier models and functional representations of the other converter topologies within a single network models represents a suitable compromise (as suggested in [6]). With this approach, the minimum level of accuracy is retained whilst the reduction in simulation computation is maximised.

5.4 Demonstration of Functional Modelling on an IFEP Case Study

This section will consider a marine electrical network containing a single power electronic converter, comparing the accuracy and efficiency of switched, functional and averaged functional representations of that converter.

The modelled system is an electrical network of an LV diesel electric vessel [7], driven by four diesel generators. The network loading consists of fixed hotel loads, electric propulsion loads as well as an LV pump system driven by a back-to-back switched rectifier-inverter motor drive. The single line network diagram for this system is shown in figure 5.6.

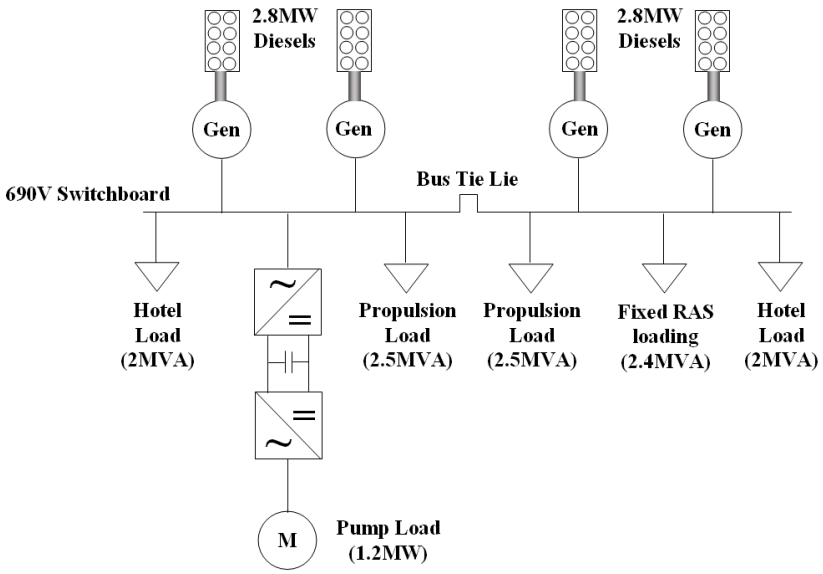

Fig. 5.6. Network diagram of the modelled LV diesel electric vessel

Note that the pump load is in fact a representation of four separate 300kW pump loads. However, for the purposes of these investigations, it is acceptable to group them together into a single equivalent system in order to reduce the overall computation required to solve this model. This is in line with the guidance given by [6], discussed in Chapter 3.

Three simulations were performed with the model whilst maintaining consistent external conditions. The first employs a switched converter model, the second a functional converter model and the third a time averaged functional converter model. In these simulations, a step change in pump load from 250kW to 1MW takes place after 20s. Table 5.1 lists the details of the comparative simulations, including the respective completion times (averaged over five separate simulations). Note that all simulations were conducted using a $2^{nd}/3^{rd}$ order Runge-Kutta variable step solver and the completion times were measured using Matlab functionality [8]. Figures 5.7, 5.8 and 5.9 illustrate the line current of the pump load for the switched, functional and time-averaged functional models respectively over the same time period. Figures 5.10, 5.11 and 5.12 illustrate the frequency response of the electrical network during the step change in pump load for the switched, functional and time-averaged functional models respectively.

Table 5.1. Details of comparative simulation completion times

Case Number	Average Simulation Completion Time (for a 35 second simulation)	Average Simulation Completion Time as a % of Case 1
1. Switched converter model	35491 seconds	100%
2. Functional converter model	15848 seconds	44.65%
3. Time-averaged functional converter model	778.5 seconds	2.19%

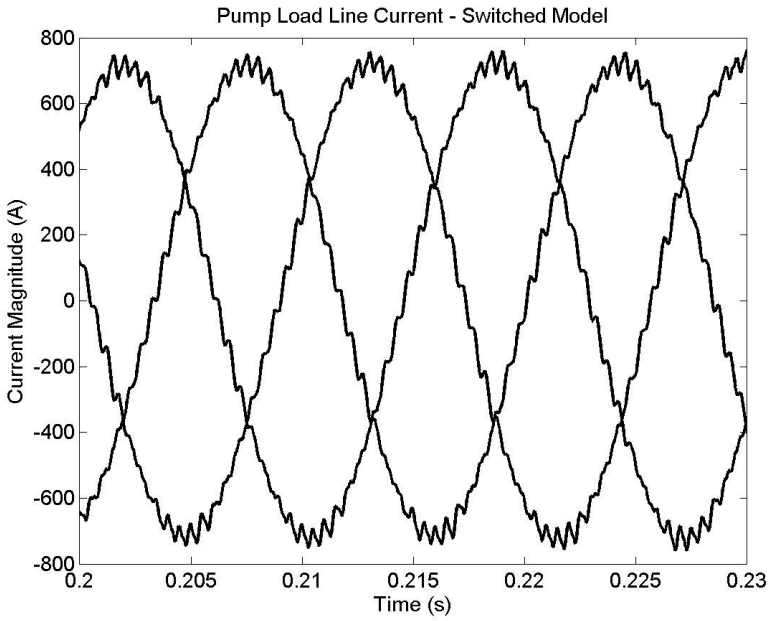

Fig. 5.7. Switched model line current

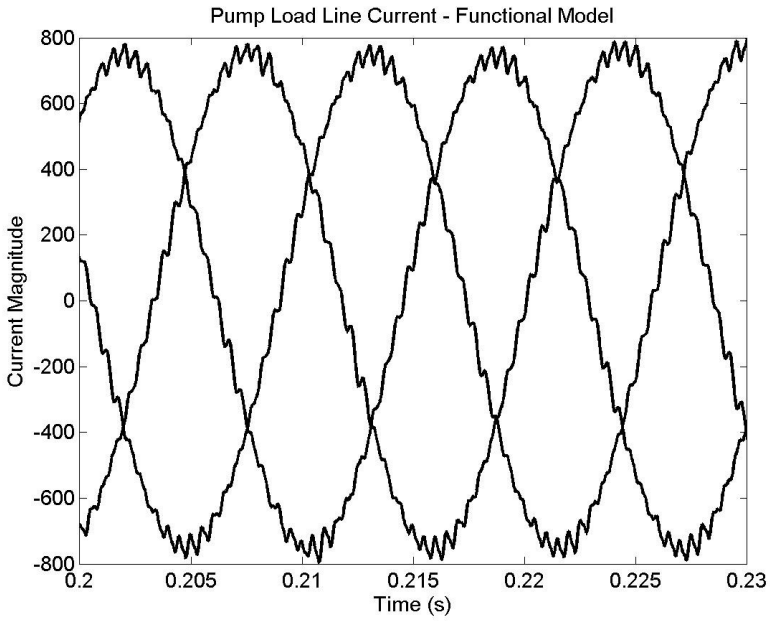

Fig. 5.8. Functional model line current

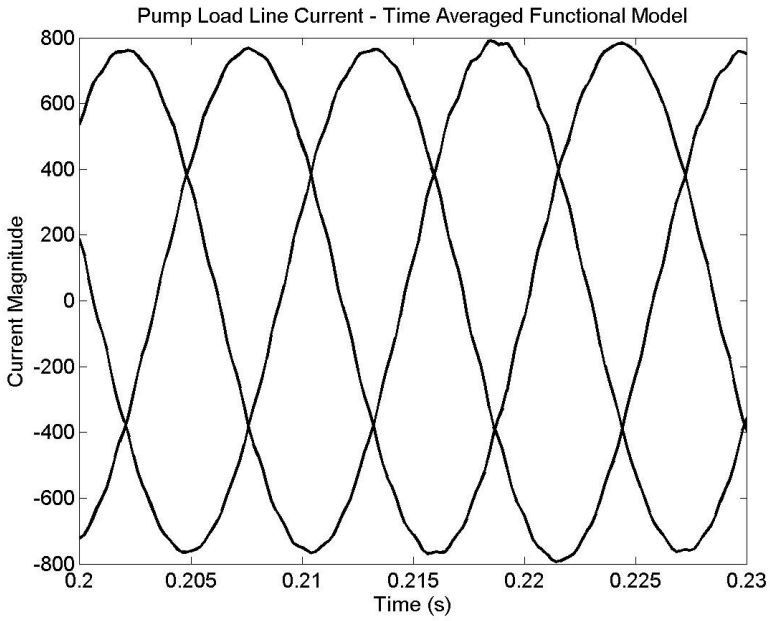

Fig. 5.9. Time-averaged functional model line current

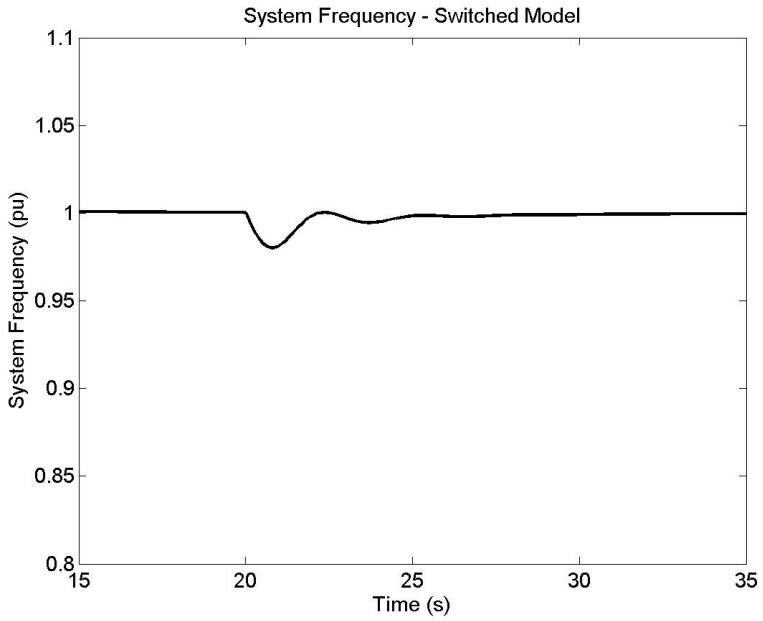

Fig. 5.10. Switched model system frequency

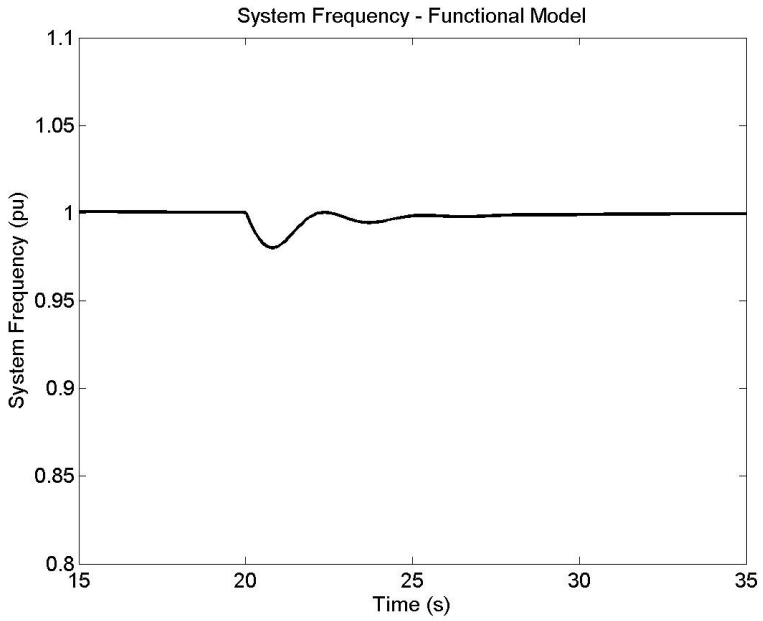

Fig. 5.11. Functional model system frequency

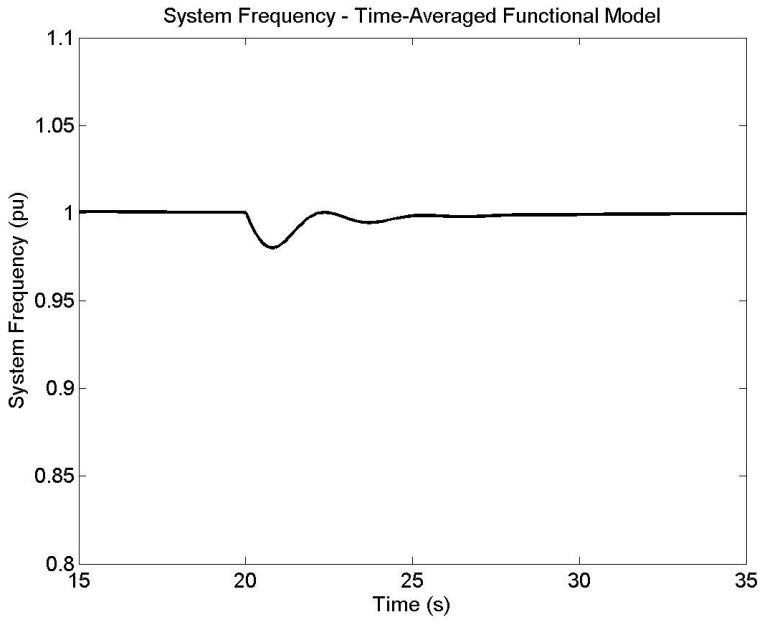

Fig. 5.12. Time-averaged functional model system frequency

Table 5.1 illustrates how both the functional modelling approach and time-averaged functional modelling approach offer reductions in simulation completion time although the latter method is far more effective in this aspect. Indeed a simulation completion time of just under thirteen minutes offered by this technique is very favourable compared to that of almost ten hours for the switched model. Note that these times not only reflect the reduced computation and larger simulation time steps of the time-averaged functional modelling approach, but also the reduced data storage requirements resulting from these larger time steps.

From figures 5.7, 5.8 and 5.9 it can be seen that the functional converter model closely matches the behaviour of its switched equivalent. Note however, that the peak current is slightly larger with the functional model. This is as a result of the effects of the semiconductor switch forward voltage and the on-state resistance being

omitted in the functional model. Also observe how the switching effects are not apparent in figure 5.10 as this is the time averaged converter output. However, the underlying lower frequency component of the line current is still replicated adequately.

Perhaps the most interesting outcome of the comparative studies can be observed in figures 5.10 through to 5.12, where despite the small differences in output of the different converter representations, there are no noticeable differences in the plots of the system frequency, whose time constant is several orders of magnitude greater than that of the switching frequency of the converters. This is especially remarkable in the case of the averaged functional model, which shows that the high frequency components of an electrical system model can often be neglected without sacrificing any accuracy in the underlying behaviour of the network and the interactions between systems. The reductions in completion times of the simulations however, clearly illustrate the benefit of using functional and more significantly, averaged functional modelling techniques to study longer transient events within models of marine and aerospace networks.

5.5 Analysis of the General Behaviour of Functional Converter Models

The examples of functional converter models given in the previous section have illustrated how it is possible to replicate the terminal of switched converters without explicitly modelling the semiconductor switches. The IFEP case study illustrated in

the previous section supported this analysis by demonstrating how the underlying behaviour of the converter was retained with the functional modelling approach but at the same time achieving significant reductions in simulation completion times.

It is important to consider however, not only the capabilities of the functional modelling approach but also its limitations. This complete picture will provide a better appreciation of the suitability of this approach for use in the modelling and simulation of marine and aerospace more-electric networks. With the exception of the difficulties of modelling diode bridge converters, which has been addressed separately, further conceptual consideration of the functional modelling approach gives rise to some general limitations, the main examples of which are as follows:

- The forward voltages and on-state impedances of the semiconductor switches within the converters are not represented.
- The non-linear transition of semiconductor switches is also not represented
- The voltage and current limits of the semiconductor switches are not represented.
- The effects of any anti-parallel diodes within a converter are not represented.
- Converter turn-off (i.e. where all the semiconductor switches are opened) cannot be properly replicated with a functional model. Under these conditions, a switched model would create open-circuit conditions at both ends of the converter, preventing any current flowing. However, any controlled voltage sources employed within a functional model will still

allow the flow of electrical current when a zero voltage is applied, creating erroneous results.

The first three limitations usually have little impact on the accuracy of network-level simulations of large systems [9]. As such, their absence in functional representations of converter models is not considered important. However, the last two limitations listed above could potentially cause more significant problems in the application of functional converter models to marine and aerospace more-electric networks. For example, if an electrical fault simulated on a dc network model (containing power electronic converters) causes the voltage at the terminals of a converter to reverse in polarity, it would be expected that any anti-parallel diodes present in the converter would conduct. However, the functional converter models would fail to represent this aspect. Additionally, the ability to turn-off converters when simulating electrical fault conditions is also of significant importance.

Given these significant limitations of the functional modelling approach, it would seem that it is necessary to resort back to utilising the more computationally demanding switched converter models during cases in which they are inaccurate. However, by including additional components within the functional models, many of the existing limitations can be overcome. For example, by incorporating additional mathematical functions into the expressions for output voltage/current, the forward voltages and on-state impedances of the converter models can be accounted for. These forward voltages or on-state impedances would be represented as the total voltage drop occurring at the converter terminals. For example, the expression for the

phase ‘A’ output voltage of the functional inverter given by equation (5.1) could be modified to incorporate these additional factors, giving

$$V_A = S_1 V_{dc} - k_A - k_B I_A, \qquad (5.12)$$

where k_A and k_B are the forward voltage and on-state resistance of the active semiconductor switches. This revised expression for V_A clearly impacts on all other associated system equations.

Other limitations can be overcome by employing additional circuit features externally to the functional models. For example, the operation of anti-parallel diodes during periods of voltage reversal can be represented by placing an additional diode model across the terminals of the functional converter model. This approach also avoids the difficulties of representing diodes behaviourally with the functional modelling approach. In a similar fashion, converter turn-off can be represented by placing a single controllable switch model in series with any controlled voltage sources employed and opening it whenever all the converter switches are turned off, creating the required open circuit conditions.

In conclusion it appears that almost all aspects of a converter’s behaviour can be represented with a functional model representation by employing additional mathematical expressions or external circuit features. The drawback of these however, is the increased computation required to solve these models. Hence, it is

desirable to represent only features required for the studies in question, maximising the efficiency of the overall model.

5.6 Analysis of the Impact of Algebraic Loops within a Single Phase Functional Inverter Model

There is an additional exception to the concluding points raised in the last section. The presence of algebraic loops within functional converter models and the limitations created by these cannot be simply overcome with additional mathematical expressions or external circuit features. As the previous chapter discussed, if not properly accommodated, the algebraic loops present within these models can lead to slow running or even failed simulations [10]. Both of these limitations are particularly undesirable for the functional modelling approach, which is intended to facilitate fast and stable simulations. Chapter 4 investigated potential solution methods for removing the algebraic loops present within the functional converter models and concluded that using unit delays to break the feedback loops is the only practical solution. However, the chapter indicated that this method reduced the numerical stability of the model, which may limit the application of the functional modelling approach. This section will investigate the presence of algebraic loops within functional converter models in more detail in order to assess the limitations associated with them.

The analysis will initially be conducted on a single-phase inverter in order to aid the conceptual understanding of the associated core issues before moving on to consider other converter topologies.

Consider the switched and functional representations of a single-phase inverter shown in figures 5.13 and 5.14.

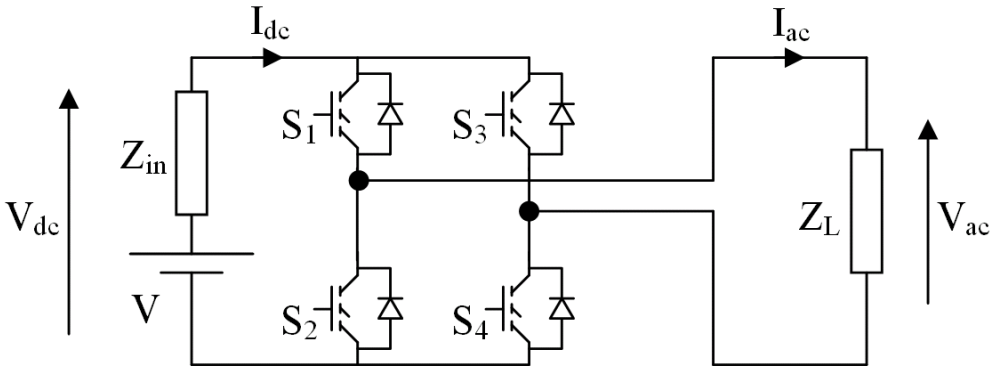

Fig. 5.13. Single-phase switched inverter model

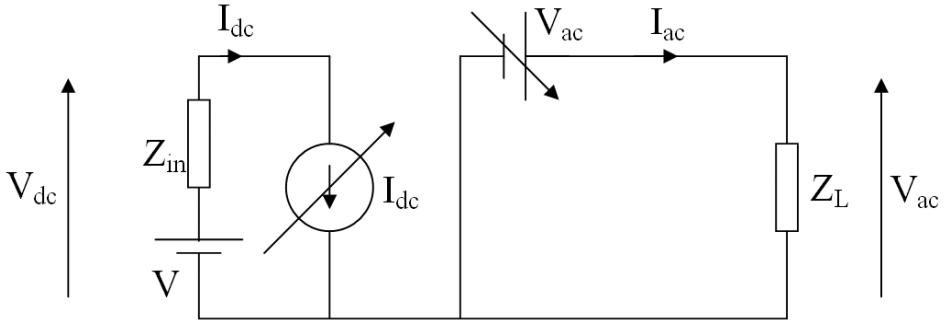

Fig. 5.14. Single-phase functional inverter model

The equations of operation for the switched model are

$$V_{ac} = k_s V_{dc} \tag{5.13}$$

$$V_{dc} = V - I_{dc} Z_{in} \tag{5.14}$$

$$I_{dc} = k_s I_{ac} \tag{5.15}$$

$$I_{ac} = \frac{V_{ac}}{Z_L}, \tag{5.16}$$

where k_s is defined as

$$k_s = (S_1 - S_3), \tag{5.17}$$

and where S_j is the j-th switch state and is defined as

$$S_j = \begin{cases} 1 & \textit{if} \quad \textit{closed} \\ 0 & \textit{otherwise} \end{cases} \qquad \text{for } j = 1,2,3,4\,. \tag{5.18}$$

The states of switches S_2 and S_4 are described by the expressions below,

$$S_2 = 1 - S_1 \tag{5.19}$$

$$S_4 = 1 - S_3\,. \tag{5.20}$$

If the functional model is implemented with a unit delay in the feedback path of I_{ac} in order to remove the algebraic loop that would otherwise be present, equations (5.13) through to (5.20) become

$$V_{ac}^{(n)} = k_s^{(n)} V_{dc}^{(n)} \tag{5.21}$$

$$V_{dc}^{(n)} = V - I_{dc}^{(n)} Z_{in} \tag{5.22}$$

$$I_{dc}^{(n)} = k_s^{(n)} I_{ac}^{(n-1)} \tag{5.23}$$

$$I_{ac}^{(n)} = \frac{V_{ac}^{(n)}}{Z_L} \tag{5.24}$$

$$k_s^{(n)} = \left(S_1^{(n)} - S_3^{(n)} \right) \tag{5.25}$$

$$S_2^{(n)} = 1 - S_1^{(n)} \tag{5.26}$$

$$S_4^{(n)} = 1 - S_3^{(n)}. \tag{5.27}$$

In this notation, superscripts *(n-1)* and *(n)* represent subsequent simulation time steps. As such, the magnitude of I_{dc} is determined by that of I_{ac} from the previous time step. Note that Z_{in}, Z_L and V are considered constant in this analysis although it is possible that they may vary from one time step to the next. However, this aspect has not been considered in the analysis conducted in order to provide greater clarity in the findings presented.

The transfer function of the functional inverter can be derived by combining equations (5.21) through to (5.24) to give

$$V_{ac}^{(n)} = k_s^{(n)} V - \left(k_s^{(n)}\right)^2 V_{ac}^{(n-1)} \frac{Z_{in}}{Z_L}, \qquad (5.28)$$

Equation (5.28) is an example of a first order recurrence relation which has the general solution (for V_{ac} at stage N),

$$V_{ac}^{(N)} = k_s^{(N)} V \sum_{i=0}^{N} \left(-1\right)^i C^i , \qquad (5.29)$$

where

$$C = \left(k_s^{(N)}\right)^2 \frac{Z_{in}}{Z_L} . \qquad (5.30)$$

If $|C|<1$, this expression is bounded and V_{ac} will move towards the equivalent solution of the non-delayed function with the error decaying to zero over time, at a rate determined by C. However, for $|C|>1$, the expression becomes unbounded at which point the model is no longer numerically stable. Under these conditions it is likely that the model will become highly erroneous and may even result in a failed simulation.

Considering the definition of k_s, it can be deduced that the maximum magnitude of this term will be unity. Hence, to guarantee numerical stability of the delayed functional model, it is necessary that the ratio of the absolute values of Z_{in} and Z_L is bounded by unity, or more simply, $Z_L > Z_{in}$. This condition is commonly met for most normal operating conditions, for which the model remains both numerically stable and accurate. However, if a low impedance short circuit fault is applied across the ac terminals of the functional inverter model, the effective value of Z_L is likely to become lower than Z_{in} producing significant errors and potential instability.

It is worth noting at this stage that simply capping the input signals to V_{ac} and I_{dc} to their maximum values (V and V/Z_{in} respectively) does not restore stability to the functional model. Rather, it causes V_{ac} and I_{dc} to alternate between these maximum values and zero at every simulation time step. In this manner, as I_{dc} reaches its maximum, V_{ac} is driven to zero causing I_{ac} also to become zero. As a result, I_{dc}, which is a function of I_{ac} then becomes zero at the subsequent time step causing V_{ac} to reach its maximum and so on.

5.7 Impact of Complex Impedances on Model Stability

In order to simplify the analysis conducted in section 5.5, the resistances, inductances and capacitances were intentionally grouped together as a combined impedance, Z. However, for a more complete understanding of the effects of algebraic loops in functional converter models it is necessary to consider the impact of the resistive, inductive and capacitive components individually.

Whilst the effective impedance of resistances are constant regardless of circuit conditions, the effective impedance of capacitances and inductances depends as much upon the circuit conditions from the previous time step as it does the present time step. This can create complications in the analysis and render the resulting stability criteria very difficult to determine. As such, conceptual consideration of the impact of inductances and capacitances is far more straight forward (and hence more effective), than can be achieved through a purely mathematical approach.

In order to demonstrate the complexity of the mathematical approach to analysing the stability of functional converters with R-L-C components and also to demonstrate the clarity provided by a more conceptual approach, an example of a single phase functional inverter will be analysed using both methods. This converter model is similar to the one analysed in section 5.5, except that some inductance has been added to the ac side of the inverter (representative of cable impedance to the load) as shown in figure 5.15.

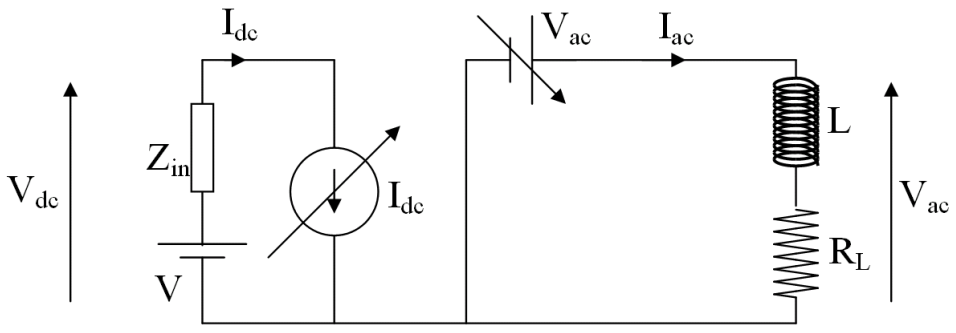

Fig. 5.15. Single-phase functional inverter model

With the mathematical approach, in order to determine the effect of the inclusion of L on the numerical stability of this model, it is necessary to first determine the expression for the ac side current I_{ac}. This can be achieved by considering Kirchoff's Voltage Law ("in travelling round any closed mesh (section) of a network (circuit), the algebraic sum of the emfs (voltages) acting in the mesh is equal to the algebraic sum of the IR voltage drops for the individual resistance in the mesh," [11]) around the circuit loop on the ac side of the inverter. This gives

$$V_a - L\frac{d}{dt}(I_a) - I_a R_L = 0. \qquad (5.31)$$

Equation (5.31) is an example of a first order Ordinary Differential Equation (ODE). Rearranging this to form an expression for I_a gives

$$I_a = \frac{V_a - L\frac{d}{dt}(I_a)}{R_L}. \qquad (5.32)$$

When this expression is included as part of the transfer function for the model, it makes the resulting stability inequality complex and hence difficult to solve. An alternative approach is to consider the rate of change of I_a as a discrete difference equation, where

$$\frac{d}{dt}(I_a) \cong \frac{I_a^{(n)} - I_a^{(n-1)}}{Ts} \qquad (5.33)$$

and where *Ts* is the magnitude of the simulation time step.

However, once again this approach makes it difficult to develop a transfer function and stability criterion as there will now be two delayed variables; V_a and I_a. This example demonstrates the difficulty in obtaining informative results regarding the numerical stability of the model from a purely mathematical analysis of the functional model.

An alternative approach is to conceptually consider the impact of inductances and capacitances upon the numerical stability of functional models by developing expressions for the effective time-varying impedances of these components. For example, in the case of an inductor, the voltage developed across it is a function of the rate of change of current flowing through it, thus

$$V_L = L\frac{d}{dt}(I_L). \qquad (5.34)$$

Therefore, the effective impedance of an inductor can be expressed as

$$Z_L = \frac{V_L}{I_L}, \qquad (5.35)$$

which by simple substitution gives

$$Z_L = \frac{L\frac{d}{dt}(I_L)}{I_L}. \qquad (5.36)$$

Equation (5.36) indicates that the effective impedance of the inductor is very high to current which is rapidly changing in nature. Conversely, the effective impedance of the inductor is very low to current which is almost steady state in nature.

The effective impedance of a capacitor can be determined in a similar manner, where the current of a capacitor is a function of the rate of change of the voltage across it.

$$I_C = C\frac{d}{dt}(V_C). \qquad (5.37)$$

Therefore, the effective impedance of a capacitor can be expressed as

$$Z_C = \frac{V_C}{I_C}, \qquad (5.38)$$

which by simple substitution gives

$$Z_C = \frac{V_C}{C\frac{d}{dt}(V_C)}. \qquad (5.39)$$

Equation (5.39) indicates that to rapidly changing voltages across the capacitor, its effective impedance is very low. Conversely, the capacitor's effective impedance to steady state voltages is very high.

The main difficulty created by capacitors and inductances surrounding functional models is that it is nearly impossible to fully establish whether stability will be maintained under certain operating conditions or not. This is because the effective impedances of these components are dependant on the network state prior to the initiation of any fault and also on the other passive components in the network. Conceptual consideration of the impact of these components and to some extent, trial and error are the only practical ways to establish the numerical stability of a particular functional model and network architecture under fault (and other) conditions.

This aspect can be illustrated by returning to the single-phase functional inverter model considered in section 5.5 and figure 5.15. It was shown that the numerical stability of this model is guaranteed if

$$Z_L > Z_{in}, \qquad (5.40)$$

where Z_L is the ac side load impedance of the inverter and Z_{in} is the dc side source impedance. Under normal operating conditions, it is expected that this condition would be easily met. However, if a short circuit fault is placed between the load and the ac terminals of the functional inverter, the effective impedance of Z_L would be

equal to the fault impedance Z_F (which would be very low for a typical short circuit fault) and would hence not be likely to meet this stability criterion.

Consider now the impact on numerical stability if an inductor is placed between the functional inverter and the fault location (e.g. representing a fault at some distance from the converter terminals) as illustrated in figure 5.16.

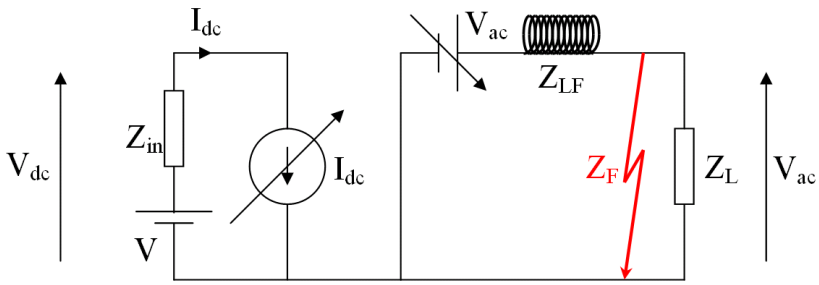

Fig. 5.16. Inductor in the fault path

In this case, following the application of the fault, the ac side impedance would effectively become $Z_F + Z_{LF}$. Under these conditions, the initial high rate of change of current would cause the Z_{LF} to act as a high impedance. In these circumstances, the ac side impedance is likely to remain greater than the dc side source impedance, therefore maintaining numerical stability. However, as the initial transient dies away and the rate of change of current through Z_{LF} decreases, the ac side impedance may become less than the dc side impedance leading to the initiation of numerical instability. Changes in the inverter's output state caused by the representation of switching may also cause a higher rate of change in the inductor current, restoring numerical stability for a short period.

However, under these conditions, although the numerical stability of the model may be periodically restored, the accuracy of the results will be poor. Note also that if the fault location lies between Z_{LF} and the functional inverter, the presence of this extra inductor will have very little impact on the numerical stability of the model as it would not lie in the fault path.

If an inductor was instead present in series with Z_{in}, representing some source inductance, this would create very different operating conditions. This circuit arrangement is shown in figure 5.17.

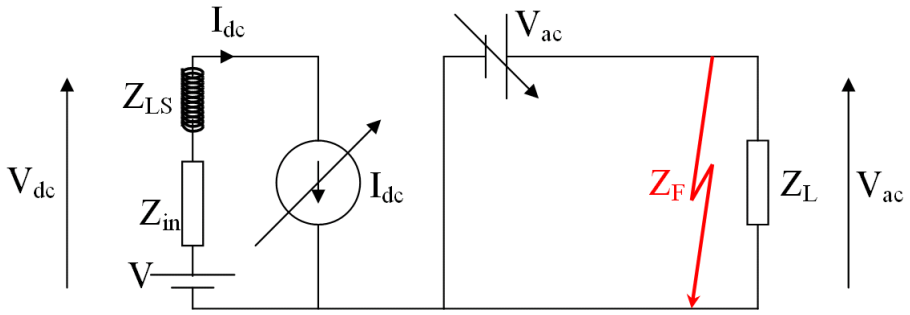

Fig. 5.17. Inductor in the source impedance

Following the application of the fault, the rate of change of current flowing through Z_{LS} becomes very high. This causes Z_{LS} to appear as a very high impedance. Under these circumstances, it is unlikely that $(Z_{in} + Z_{LS}) < Z_F$, implying that numerical stability will not be achieved. Again, as the transient dies away and the rate of change of current through Z_{LS} will fall, reducing its impedance. Note, that with the circuit configuration shown in figure 5.17, it is possible that the conditions for numerical stability may not even be met during normal operation (depending on the

magnitude of Z_{LS}). However, it is also likely that a smoothing capacitor would be applied to the dc terminals of the functional inverter which as will be shown, helps maintain the numerical stability of the model.

As a final example, consider the implementation of a smoothing capacitor at the dc terminals of the functional inverter, as illustrated in figure 5.18.

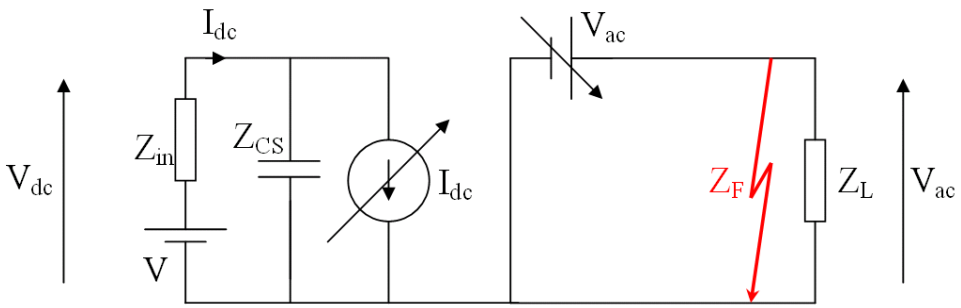

Fig. 5.18. Capacitor across the dc terminals of the functional inverter

Following the application of the ac side fault, the rate of change of I_{dc} increases suddenly. This leads to a large rate of change of the voltage across the dc smoothing capacitor, V_{dc}. Under these conditions, Z_{CS} appears as a very small impedance and the inclusion of this capacitor will aid the numerical stability of the functional inverter model. As the initial fault transient dies away, the effective impedance of Z_{CS} increases, reducing its positive impact on the numerical stability of the functional model. It has also been found through experience that unless there is some inductance on the ac side of the inverter model, the inclusion of capacitance alone is not enough to maintain numerical stability when a short circuit fault is placed on the ac side of the inverter.

The findings of sections 5.5 and 5.6 have serious implications for the use of functional converter models within network-level modelling of marine and aerospace more-electric architectures. Whilst the results presented from the single phase inverter case study clearly outline the key trends and outcomes, the next stage of this investigation is to apply the stability analysis to other functional converter topologies to consider the wider implications of the algebraic loops contained within these models.

In each of the cases presented in the next section, the impact of inductances and capacitances will only be addressed when they are a core part of the converter's operation, otherwise, combined resistive, inductive and capacitive impedances will be utilised.

5.8 Analysis of Other Functional Converter Models

The following sections will consider the stability of a three-phase inverter, a switched rectifier and a dc-dc forward converter. Once again, it is acknowledged that other converter types are utilised within marine and aerospace more-electric architectures [3, 4], but to consider each of these on a case by case basis offers limited benefit. The core concepts of the analysis applied however can be readily extended to accommodate other converter types if required.

5.8.1 Stability Analysis of a Three-Phase Functional Inverter

Consider the three-phase inverter supplying a three-phase star connected load and its functional equivalent model shown in figures 5.19 and 5.20.

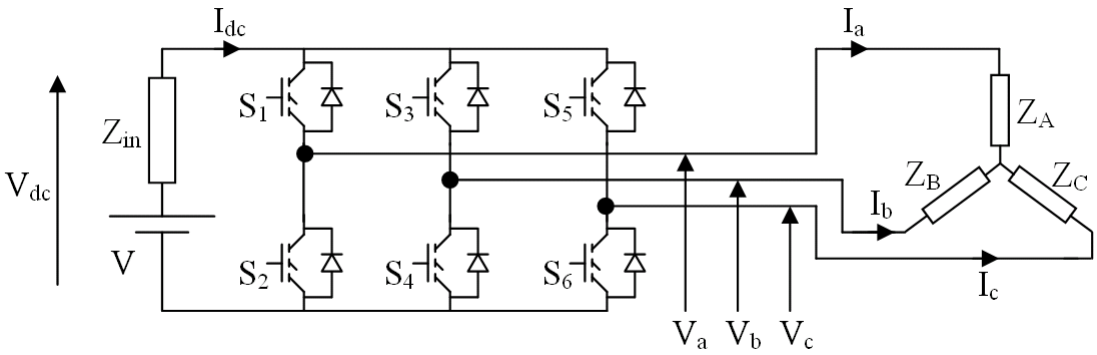

Fig. 5.19. Three-phase switched inverter model with load and source

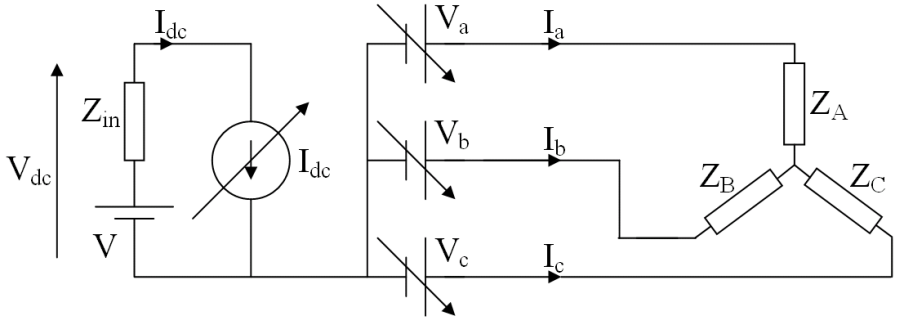

Fig. 5.20. Three-phase functional inverter model with load and source

The governing equations for the switched converter model are

$$V_a = S_1 V_{dc} \tag{5.41}$$

$$V_b = S_3 V_{dc} \tag{5.42}$$

$$V_c = S_5 V_{dc} \tag{5.43}$$

$$V_{dc} = V - I_{dc} Z_{in} \tag{5.44}$$

$$I_{dc} = S_1 I_a + S_3 I_b + S_5 I_c \,. \tag{5.45}$$

where S_j is the j-th switch state and is defined as

$$S_j = \begin{cases} 1 & if \quad closed \\ 0 & otherwise \end{cases} \qquad \text{for } j = 1,2,3,4,5,6 \,. \tag{5.46}$$

The states of switches S_2, S_4 and S_6 are defined as,

$$S_2 = 1 - S_1 \tag{5.47}$$

$$S_4 = 1 - S_3 \tag{5.48}$$

$$S_6 = 1 - S_5 \,. \tag{5.49}$$

The terms Z_A, Z_B and Z_C are the ac side load impedances and Z_{in} is the dc side source impedance. In the same manner as the single phase inverter, the three-phase functional inverter model contains algebraic loops. To remove these, unit delays are inserted into the feedback paths of I_a, I_b and I_c such that the magnitude of I_{dc} is determined by the respective magnitudes of these currents from the previous time step. With these delays incorporated, equations (5.31) through to (5.49) now become

$$V_a^{(n)} = S_1^{(n)} V_{dc}^{(n)} \tag{5.50}$$

$$V_b^{(n)} = S_3^{(n)} V_{dc}^{(n)} \tag{5.51}$$

$$V_c^{(n)} = S_5^{(n)} V_{dc}^{(n)} \tag{5.52}$$

$$V_{dc}^{(n)} = V - I_{dc}^{(n)} Z_{in} \tag{5.53}$$

$$I_{dc}^{(n)} = S_1^{(n)} I_a^{(n-1)} + S_3^{(n)} I_b^{(n-1)} + S_5^{(n)} I_c^{(n-1)} \tag{5.54}$$

$$S_2^{(n)} = 1 - S_1^{(n)} \tag{5.55}$$

$$S_4^{(n)} = 1 - S_3^{(n)} \tag{5.56}$$

$$S_6^{(n)} = 1 - S_5^{(n)}. \tag{5.57}$$

Once again, superscripts *(n-1)* and *(n)* are subsequent simulation time steps. In this manner, the magnitude of I_{dc} is determined by that of I_a, I_b and I_c from the previous time step. Once again, V, Z_{in}, Z_A, Z_B and Z_C are considered constant in this analysis to provide a greater level of clarity in the findings presented.

In order to develop a transfer function defining the behaviour of the three-phase functional inverter and its numerical stability, expressions for I_a, I_b and I_c must be developed. However, unlike balanced three-phase power systems where the neutral point of the load maintains a zero potential, ac side line currents in power electronic systems cannot be simply derived from V_{phase}/Z_{phase} [12, 13]. Instead, they are formed by considering the electrical circuit on the ac side of the inverter and employing Kirchoff's voltage and current laws. Full derivation of the ac side currents I_a, I_b and I_c is given in Appendix A. The resultant expressions are

$$I_a^{(n)} = \frac{S_A^{(n)} V_{dc}^{(n)}}{Z_{ABC} \Big/ Z_B + Z_C} \tag{5.58}$$

$$I_b^{(n)} = \frac{S_B^{(n)} V_{dc}^{(n)}}{Z_{ABC} \big/ Z_A + Z_C} \tag{5.59}$$

$$I_c^{(n)} = \frac{S_C^{(n)} V_{dc}^{(n)}}{Z_{ABC} \big/ Z_A + Z_B}, \tag{5.60}$$

where

$$Z_{ABC} = Z_A Z_B + Z_B Z_C + Z_A Z_C \tag{5.61}$$

$$S_A^{(n)} = S_1^{(n)} - S_3^{(n)} \left(\frac{Z_C}{Z_B + Z_C} \right) - S_5^{(n)} \left(\frac{Z_B}{Z_B + Z_C} \right) \tag{5.62}$$

$$S_B^{(n)} = S_3^{(n)} - S_1^{(n)} \left(\frac{Z_C}{Z_A + Z_C} \right) - S_5^{(n)} \left(\frac{Z_A}{Z_A + Z_C} \right) \tag{5.63}$$

$$S_C^{(n)} = S_5^{(n)} - S_1^{(n)} \left(\frac{Z_B}{Z_A + Z_B} \right) - S_3^{(n)} \left(\frac{Z_A}{Z_A + Z_B} \right). \tag{5.64}$$

Substituting equations (5.54), (5.58), (5.59) and (5.60) into equation (5.53) gives the transfer function for the three-phase functional inverter model as

$$V_{dc}^{(n)} = V - Z_{in} V_{dc}^{(n-1)} \left(\frac{S_1^{(n)} S_A^{(n-1)}}{Z_{ABC} \big/ Z_B + Z_C} + \frac{S_3^{(n)} S_B^{(n-1)}}{Z_{ABC} \big/ Z_A + Z_C} + \frac{S_5^{(n)} S_C^{(n-1)}}{Z_{ABC} \big/ Z_A + Z_B} \right). \tag{5.65}$$

Equation (5.65) is an example of a first order recurrence relation which has the general solution (for V_{dc} at stage N),

$$V_{dc}^{(N)} = V\sum_{i=0}^{N}(-1)^i C^i , \qquad (5.66)$$

where

$$C = Z_{in}\left(\frac{S_1^{(n)}S_A^{(n-1)}}{Z_{ABC}/Z_B + Z_C} + \frac{S_3^{(n)}S_B^{(n-1)}}{Z_{ABC}/Z_A + Z_C} + \frac{S_5^{(n)}S_C^{(n-1)}}{Z_{ABC}/Z_A + Z_B}\right). \qquad (5.67)$$

For the expression given in equation (5.67) to be bounded and hence numerically stable, it is necessary that $C < 1$. In its present form, it is difficult to ascertain the true implications of this stability criterion. Further simplification of the expression for C is needed. This can be achieved by first assuming a balanced load, where Z_A=Z_B=Z_C=Z_L. Imposing this assumption on the expressions for Z_{ABC}, S_A, S_B and S_C (equations (5.61) through to (5.64)) allows (5.67) to be reduced to

$$C = \frac{2Z_{in}}{3Z_L}\left[H_1^{(n)} + H_3^{(n)} + H_5^{(n)}\right] \qquad (5.68)$$

where

$$H_1^{(n)} = S_1^{(n)}\left(S_1^{(n-1)} - \frac{S_3^{(n-1)}}{2} - \frac{S_5^{(n-1)}}{2}\right) \tag{5.69}$$

$$H_3^{(n)} = S_3^{(n)}\left(S_3^{(n-1)} - \frac{S_1^{(n-1)}}{2} - \frac{S_5^{(n-1)}}{2}\right) \tag{5.70}$$

$$H_5^{(n)} = S_5^{(n)}\left(S_5^{(n-1)} - \frac{S_1^{(n-1)}}{2} - \frac{S_3^{(n-1)}}{2}\right). \tag{5.71}$$

At this stage there are still too many variables present to obtain a clear understanding of the model. One additional assumption will therefore be applied which will be to assume that the state of switches S_1, S_3 and S_5 (and hence S_2, S_4 and S_6) will be constant over a small number of time steps (this is especially true in time-averaged representations of the model). In this manner, for the short time period in consideration, it will be assumed that

$$S_1^{(n-1)} = S_1^{(n)} \tag{5.72}$$

$$S_3^{(n-1)} = S_3^{(n)} \tag{5.73}$$

$$S_5^{(n-1)} = S_5^{(n)}. \tag{5.74}$$

The expression for C, in equation (5.68) can hence be further reduced to

$$C = \frac{2Z_{in}}{3Z_L} H_s^{(n)}, \tag{5.75}$$

where

$$H_s^{(n)} = \left(S_1^{(n)}\right)^2 + \left(S_3^{(n)}\right)^2 + \left(S_5^{(n)}\right)^2 - S_1^{(n)}S_3^{(n)} - S_1^{(n)}S_5^{(n)} - S_3^{(n)}S_5^{(n)}. \qquad (5.76)$$

For the eight possible combinations of S_1, S_3 and S_5, Table 5.2 shows that H_S adopts a value of either 0 or 1.

Table 5.2. Evaluation of (S_1, S_3, S_5) Combinations

$\left(S_1^{(n)}, S_3^{(n)}, S_5^{(n)}\right)$	$H_s^{(n)}$
(0, 0, 0), (1, 1, 1)	***0***
(0, 0, 1), (0, 1, 0), (1, 0, 0)	***1***
(0, 1, 1), (1, 0, 1), (1, 1, 0)	***1***

Therefore, to guarantee the numerical stability of the three-phase functional inverter model under the given assumptions regarding a balanced load and constant switch states, it is necessary that

$$Z_L > \frac{2}{3} Z_{in}. \qquad (5.77)$$

Under normal network operation, this stability criterion is easily met. However, under ac side, low-impedance fault conditions this may not be the case. The requirements for the three-phase functional inverter model to achieve numerical stability under phase-to-neutral, two phases-to-neutral and three phases to neutral fault conditions (where neutral is the star point of the load) are given as

Phase-to-Neutral Fault

$$Z_L > 2Z_{in} \tag{5.78}$$

Two Phases-to-Neutral Fault

$$Z_F > \frac{1}{2}Z_{in} \tag{5.79}$$

Three Phases-to-Neutral Fault

$$Z_F > \frac{2}{3}Z_{in}, \tag{5.80}$$

where Z_F is the effective fault impedance per phase. A full derivation of equations (5.78), (5.79) and (5.80) is given in Appendix B. By considering these equations more closely, it is observed that the requirements for numerical stability become more difficult to meet as the severity of the simulated fault increases. A point to note though is that the three-phase functional inverter model may actually still be stable under single and two phases-to-neutral faults.

The analysis conducted on this model is not fully comprehensive, given the number of assumptions adopted. It does however, illustrate the clear degradation of numerical stability as the severity of the applied fault increases. In addition, the analysis could also be extended to included delta connected loads, unbalanced loads and faults, open circuit faults, dc side faults and earth faults. The impact of many of these scenarios can be established based on the procedure and findings presented above. For example, a dc side low impedance fault would effectively reduce Z_{in}, serving to improve the numerical stability of the functional converter model.

However, the analyses of these additional fault scenarios have not been considered in this thesis as they provide only limited added value to the understanding of the behaviour of functional models under simulated fault conditions.

5.8.2 Stability Analysis of a Single-Phase Functional Switched Rectifier

This section will examine the numerical stability of a single-phase functional switched rectifier model. The three-phase equivalent model will not be considered, but the analysis of this can be readily achieved using the principles applied in sections 5.7.1. and 5.8.1.

Figures 5.21 and 5.22 illustrate schematics of a single phase switched rectifier model and its functional equivalent.

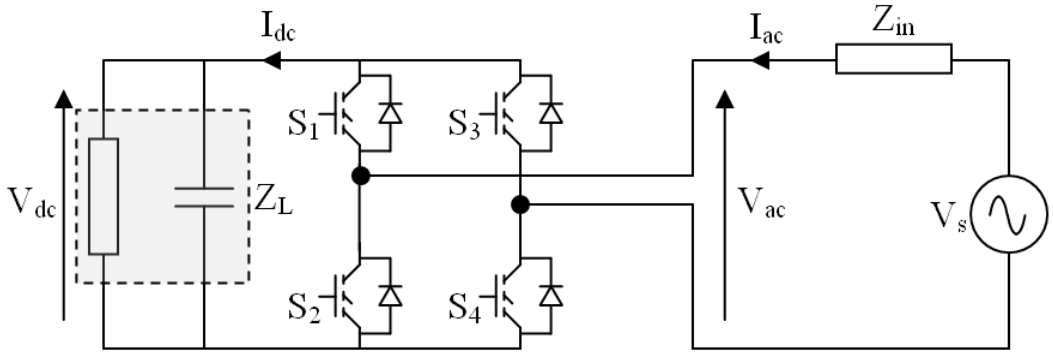

Fig. 5.21. Single phase switched rectifier

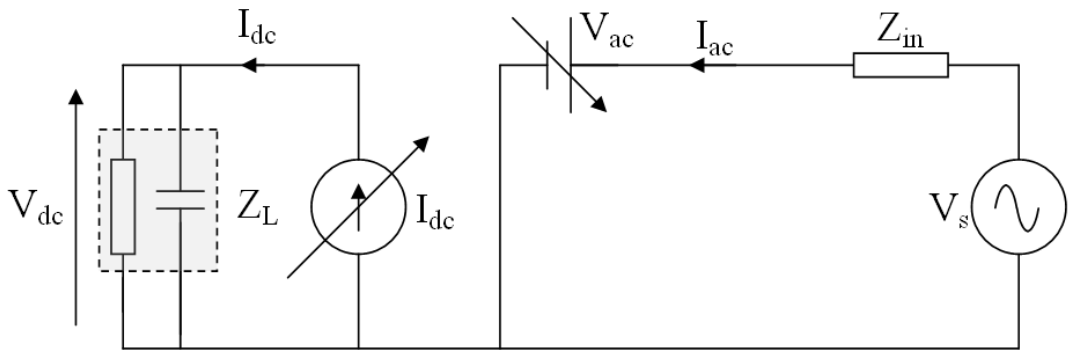

Fig. 5.22. Functional model of a single phase switched rectifier

The operation of the switched converter model is defined by

$$V_{ac} = k_s V_{dc} \tag{5.81}$$

$$V_{dc} = I_{dc} Z_L \tag{5.82}$$

$$I_{dc} = k_s I_{ac} \tag{5.83}$$

$$I_{ac} = \frac{V_s - V_{ac}}{Z_{in}}, \tag{5.84}$$

where

$$k_s = S_1 - S_3, \tag{5.85}$$

and S_j is the j-th switch state and is defined as

$$S_j = \begin{cases} 1 & if \quad closed \\ 0 & otherwise \end{cases} \qquad \text{for } j = 1,2,3,4. \tag{5.86}$$

The states of switches S_2 and S_4 are described by the expressions below,

$$S_2 = 1 - S_1 \tag{5.87}$$

$$S_4 = 1 - S_3 . \tag{5.88}$$

The functional model is implemented with a unit delay in the feedback path of I_{ac} in order to remove the algebraic loop present in the model, such that the equations defining its operation now become

$$V_{ac}^{(n)} = k_s^{(n)} V_{dc}^{(n)} \tag{5.89}$$

$$V_{dc}^{(n)} = I_{dc}^{(n)} Z_L \tag{5.90}$$

$$I_{dc}^{(n)} = k_s^{(n)} I_{ac}^{(n-1)} \tag{5.91}$$

$$I_{ac}^{(n)} = \frac{V_s^{(n)} - V_{ac}^{(n)}}{Z_{in}} , \tag{5.92}$$

$$k_s^{(n)} = S_1^{(n)} - S_3^{(n)} . \tag{5.93}$$

$$S_2^{(n)} = 1 - S_1^{(n)} \tag{5.94}$$

$$S_4^{(n)} = 1 - S_3^{(n)} . \tag{5.95}$$

where *(n-1)* and *(n)* are subsequent simulation time steps. In this manner, the magnitude of I_{dc} is determined by that of I_{ac} from the previous time step. Combining equations (5.89), (5.90), (5.91) and (5.92) gives the transfer function of the functional switched rectifier as

$$V_{ac}^{(n)} = \frac{\left(k_s^{(n)}\right)^2 Z_L}{Z_{in}} V_s^{(n-1)} - \frac{\left(k_s^{(n)}\right)^2 Z_L}{Z_{in}} V_{ac}^{(n-1)}. \qquad (5.96)$$

If V_s is considered constant over the period between *(n-1)* and *(n)*, equation (5.96) is an example of a first order recurrence relation which has the general solution (for V_{ac} at stage *N*),

$$V_{ac}^{(N)} = D\sum_{i=0}^{N}(-1)^i C^i \qquad (5.97)$$

where

$$D = \frac{\left(k_s^{(N)}\right)^2 Z_L}{Z_{in}} V_s, \qquad (5.98)$$

and

$$C = \frac{\left(k_s^{(N)}\right)^2 Z_L}{Z_{in}}. \qquad (5.99)$$

As with the single phase and three phase inverter functional model case studies, if $|C|<1$, this expression is bounded and V_{ac} will move towards the equivalent solution of the non-delayed function with the error decaying to zero over time, at a rate

determined by C. However, for $|C|>1$, the expression becomes unbounded at which point the model is no longer numerically stable.

Considering the definition of k_s it can be deduced that k_s^2 will be either 0 or 1 for functional models with a pulsed output or will vary continuously between 0 and 1 for averaged functional models. Hence, to guarantee numerical stability of the functional model, it is necessary that

$$Z_L < Z_{in}. \qquad (5.100)$$

This condition for numerical stability presents a seemingly impossible situation, whereby Z_L is highly unlikely to be of a smaller magnitude than Z_{in}, creating an inherently unstable model. However, the operation of a real switched rectifier is underpinned by the inclusion of a smoothing capacitor placed across the dc terminals of the converter (as illustrated in figures 5.21 and 5.22) allowing a voltage to be established at this location [12].

This capacitance, when subjected to rapidly changing dc voltage created by the switched rectifier effectively acts a low value impedance in parallel with Z_L. If this capacitance is suitably sized, conditions for numerical stability will be readily met.

Additionally, if a low impedance short circuit fault is placed at the ac terminals of the switched rectifier, Z_{in} will experience a substantial decrease in magnitude. The lower rate of change of voltage experienced by the dc smoothing capacitor also means that

it will assume a much higher impedance, increasing the effective magnitude of Z_L in the process. Under these conditions, the model is likely to become numerically unbounded.

5.8.3 Stability Analysis of a Functional DC-DC Forward Converter

This section will examine the numerical stability of a functional model of a dc-dc forward converter. Other dc-dc converter topologies will not be considered, but the analysis of these other converters can be readily achieved using the principles applied in this section.

Figures 5.23 and 5.24 illustrate schematics of a DC-DC forward converter model and its functional equivalent.

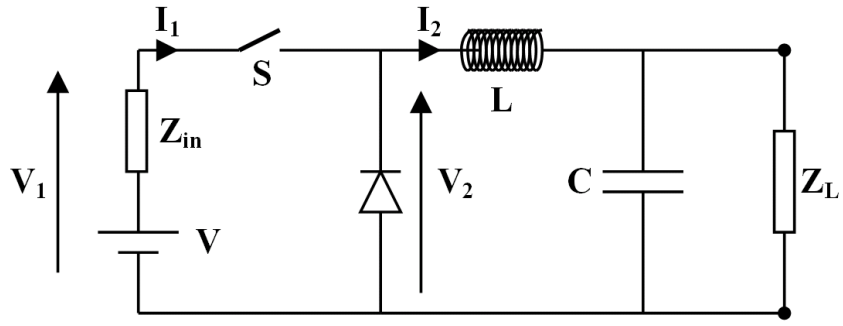

Fig. 5.23. DC-DC forward converter schematic

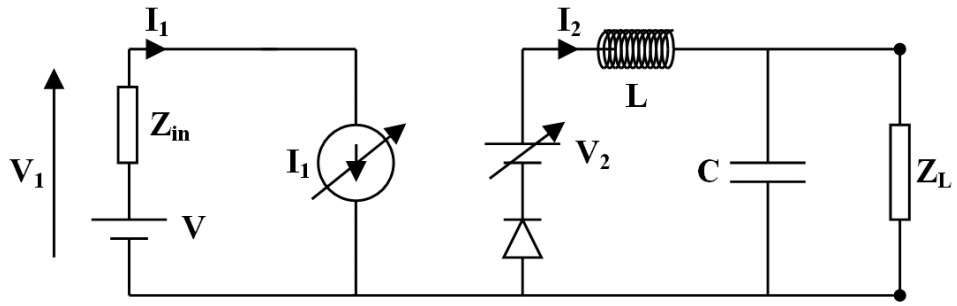

Fig. 5.24. Functional model of a single DC-DC forward converter

The governing equations for switched converter model are

$$V_2 = SV_1 \tag{5.101}$$

$$I_1 = SI_2, \tag{5.102}$$

$$V_1 = V - I_1 Z_{in} \tag{5.103}$$

$$I_2 = \frac{V_2}{Z_{out}}, \tag{5.104}$$

where S is the switch state, defined as

$$S = \begin{cases} 1 & if \quad closed \\ 0 & otherwise \end{cases} \tag{5.105}$$

and Z_{out} is the combined impedance of L, C and Z_L. As with previous examples, a unit delay is implemented in the feedback path of I_2 in order to remove the algebraic loop present in the functional converter model. Hence, the equations defining the operation of the functional model now become

$$V_2^{(n)} = S^{(n)} V_1^{(n)} \tag{5.106}$$

$$I_1^{(n)} = S^{(n)} I_2^{(n-1)}, \tag{5.107}$$

$$V_1^{(n)} = V - I_1^{(n)} Z_{in} \tag{5.108}$$

$$I_2^{(n)} = \frac{V_2^{(n)}}{Z_{out}}, \tag{5.109}$$

where the superscripts *(n-1)* and *(n)* represent subsequent simulation time steps. In this manner, the magnitude of I_1 is determined by that of I_2 from the previous time step. Combining equations (5.106), (5.107), (5.108) and (5.109) gives the transfer function of the functional forward converter as

$$V_2^{(n)} = S^{(n)} V - \left(S^{(n)}\right)^2 \frac{Z_{in}}{Z_{out}} V_2^{(n-1)}. \tag{5.110}$$

Equation (5.110) is an example of a first order recurrence relation which has the general solution (for V_2 at stage N),

$$V_2^{(N)} = S^{(N)} V \sum_{i=0}^{N} (-1)^i C^i, \tag{5.111}$$

where

$$C = \left(S^{(N)}\right)^2 \frac{Z_{in}}{Z_{out}}. \tag{5.112}$$

As before, if $|C|<1$, this expression is bounded. Hence, to guarantee numerical stability of the dc-dc forward converter functional model, it is necessary that

$$Z_{in} < Z_{out} . \qquad (5.113)$$

This condition is readily met during normal operation of the converter and so numerical stability is achieved. The presence of the inductor on the load side of the converter means that faults placed after this point are unlikely to destabilise the model. However, if a short circuit fault is placed across the output terminals of the converter, effectively short-circuiting V_2 the model will become numerically unstable. Under these operating conditions, the model will not become fully unbounded though, as the presence of the diode in series with V_2 will provide a capping effect on I_2. The impact of this effect is the same as the simple capping solution considered earlier in section 5.5, where the converter terminal conditions will become very oscillatory in nature but will remain bounded.

5.9 Demonstration of Functional Model Stability Limits

This section will illustrate the operation of a single-phase functional inverter model implemented within a power systems simulation package. Its output under normal and faulted conditions is validated against that of a switched model in order to illustrate the accuracy and numerical stability of the functional modelling technique.

5.9.1 Model Description and Parameters

Figure 5.25 shows the simulated converter system, modelled within the SimPowerSystems toolbox of Matlab Simulink [8].

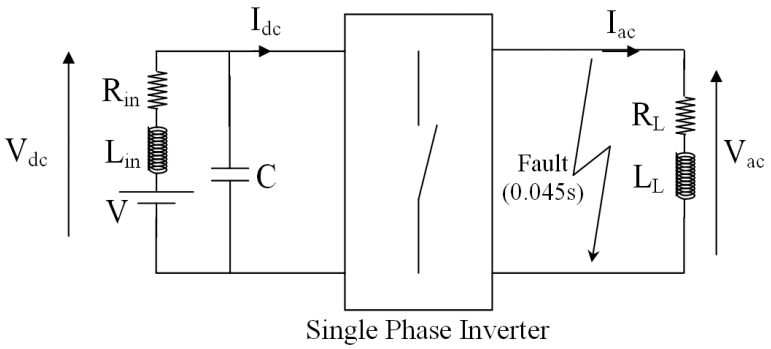

Fig. 5.25. Simulated network architecture

Note that this converter is controlled with an open loop control scheme and as such will not alter its operation following the application of the fault. This approach was taken to avoid masking the response of the converter models to the application of the fault. The parameters of this network and the inverter are described in table 5.3.

Table 5.3. Network and inverter parameters.

Parameter	**Value**
V	100V
C	100μF
R_{in}	0.1Ω
L_{in}	10μH
R_L	5Ω
L_L	1mH
Fault impedance	50mΩ (applied at 0.045s)
PWM carrier frequency	2000Hz

Figure 5.26 shows the single phase inverter switched model implemented within SimPowerSystems.

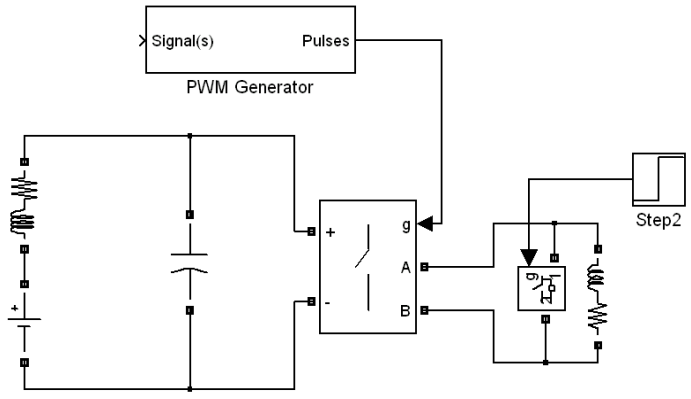

Fig. 5.26. Implemented switched model

Figures 5.27 and 5.28 show the functional equivalent model of the single-phase inverter implemented within SimPowerSystems.

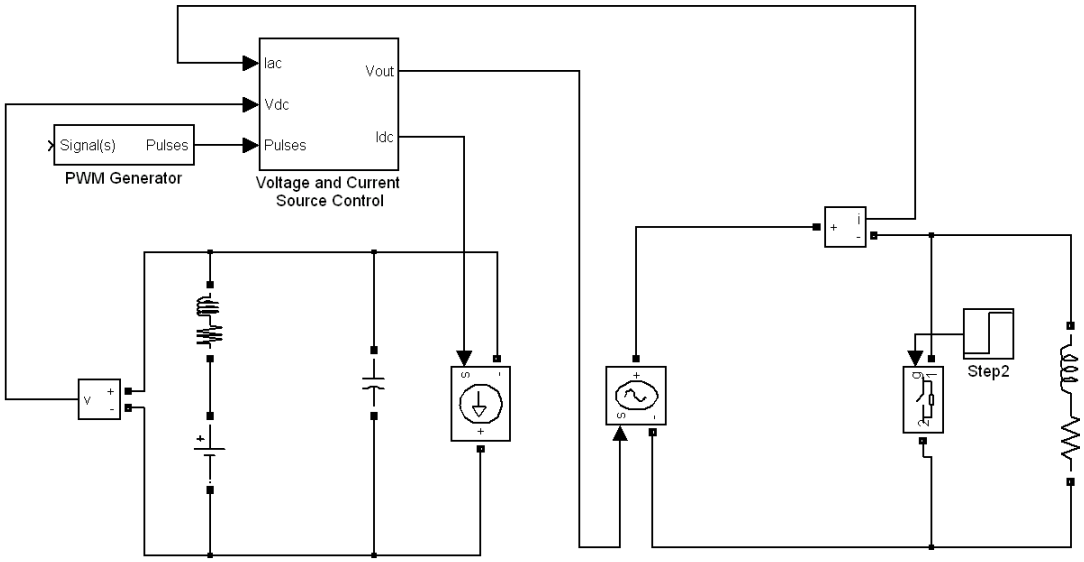

Fig. 5.27. Implemented functional inverter – main schematic

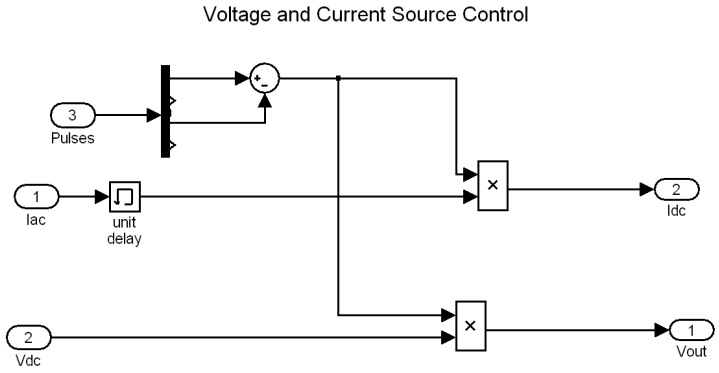

Fig. 5.28. Implemented functional inverter – voltage and current source control

5.9.2 Simulation Results

Figures 5.29, 5.30 and 5.31 illustrate the steady state ac current between 0 and 0.02 seconds of simulation time for the switched, functional and time averaged functional

inverter models respectively. These plots show the behaviour of the converter models during normal (i.e. unfaulted) operating conditions supplying an ac load of fixed impedance. Additional figures showing plots of ac side voltage, and dc side voltage and current for each of the inverter models listed above can be found in Appendix C.

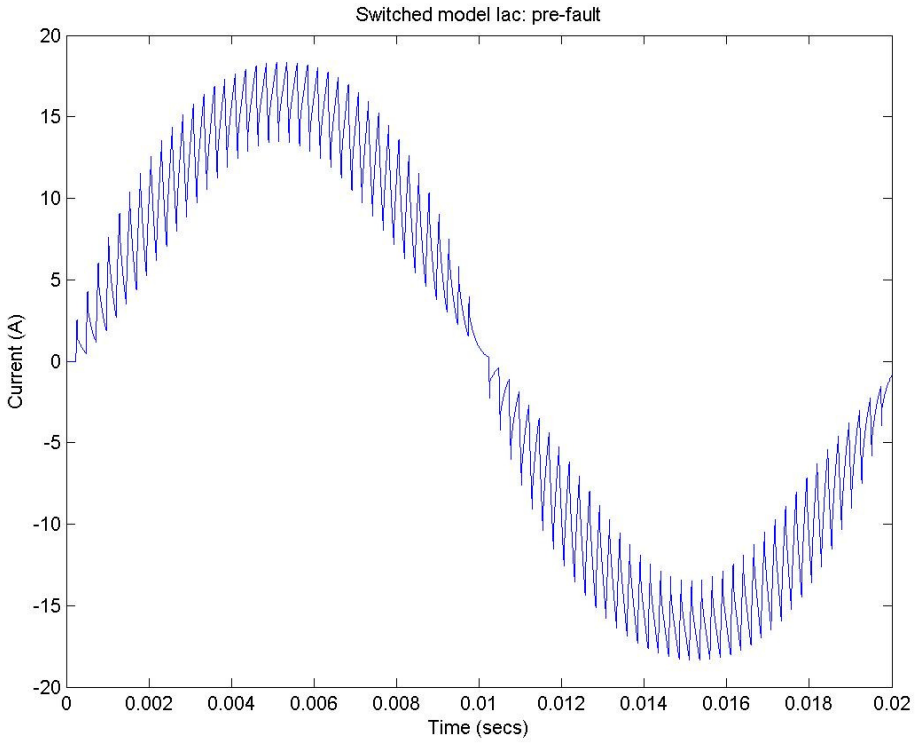

Fig. 5.29 Switched model Iac – Pre-fault

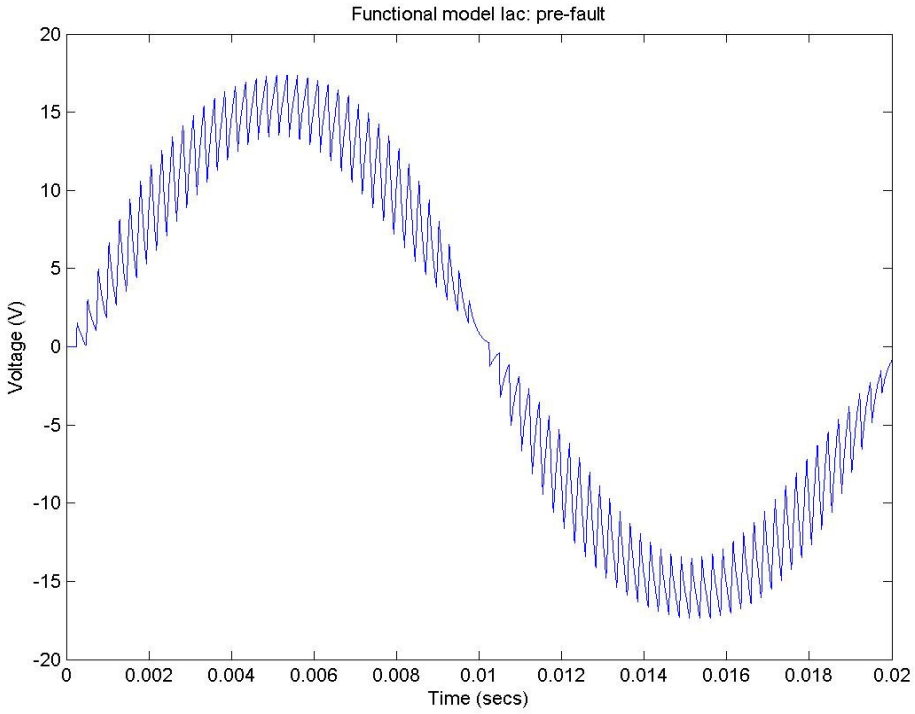

Fig. 5.30. Functional model Iac – Pre-fault

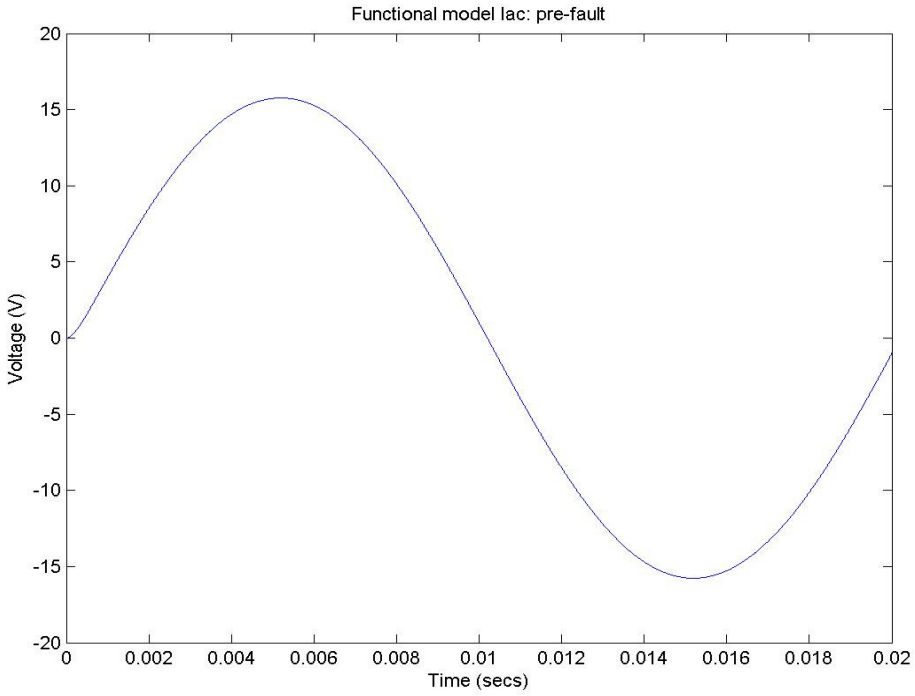

Fig. 5.31. Time-averaged functional model Iac – Pre-fault

Figures 5.32, 5.33 and 5.34 illustrate the steady state ac current between 0.06 and 0.08 seconds of simulation time for the switched, functional and time averaged functional inverter models respectively. This second group of plots shows the behaviour of the converter models after a low impedance rail to rail fault has occurred across the ac terminals of the inverter. Additional figures showing plots of ac side voltage, and dc side voltage and current for each of the inverter models listed above can be found in Appendix C.

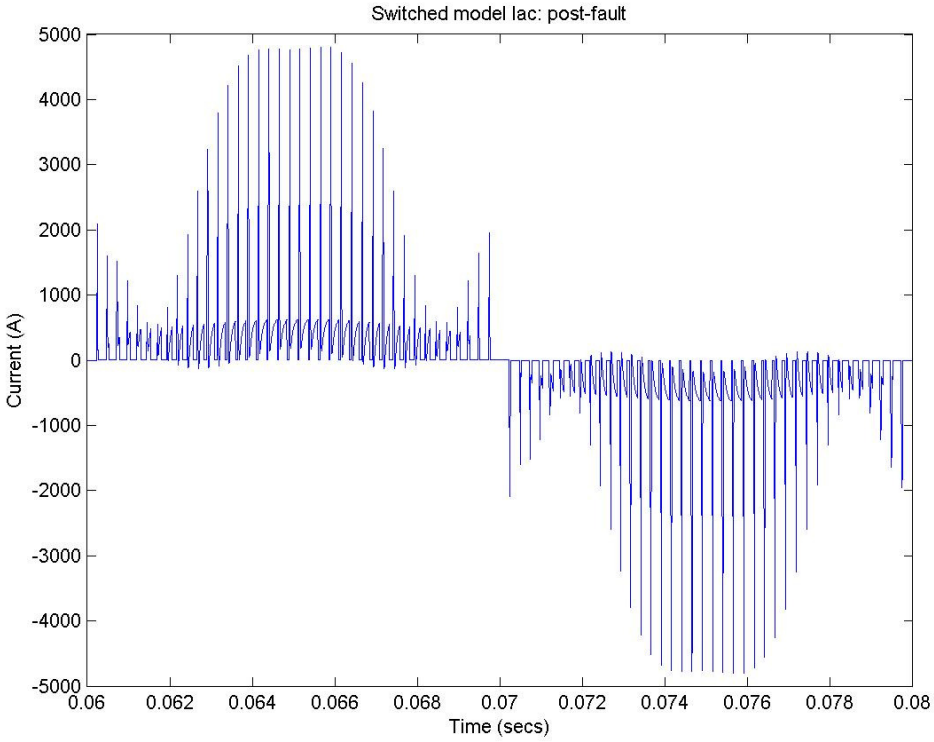

Fig. 5.32. Switched model Iac – Post-fault

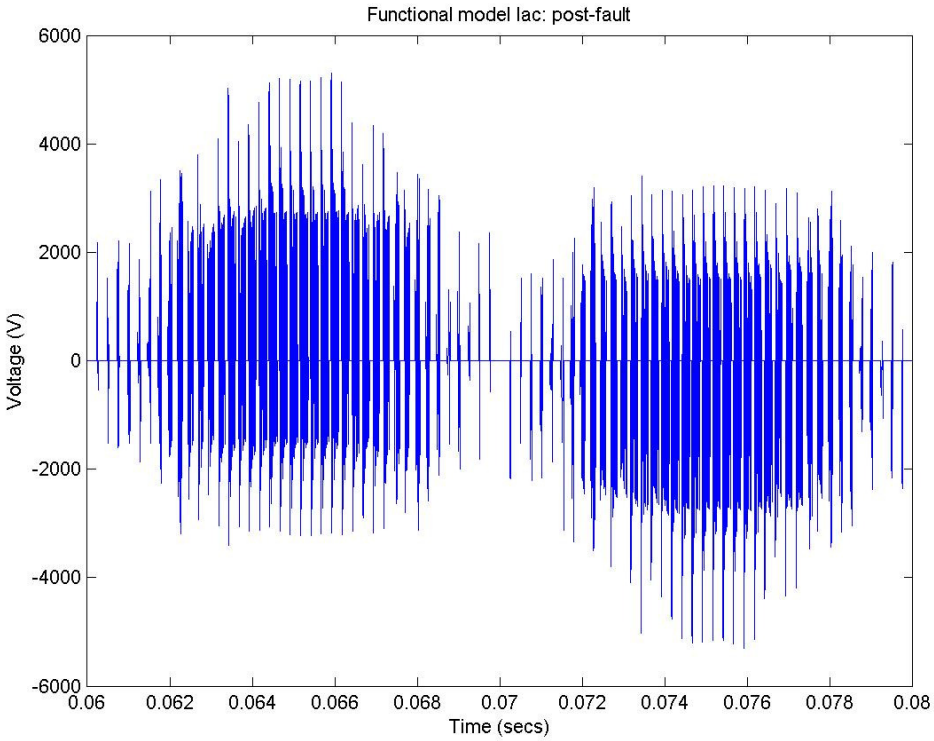

Fig. 5.33. Functional model Iac – Post-fault

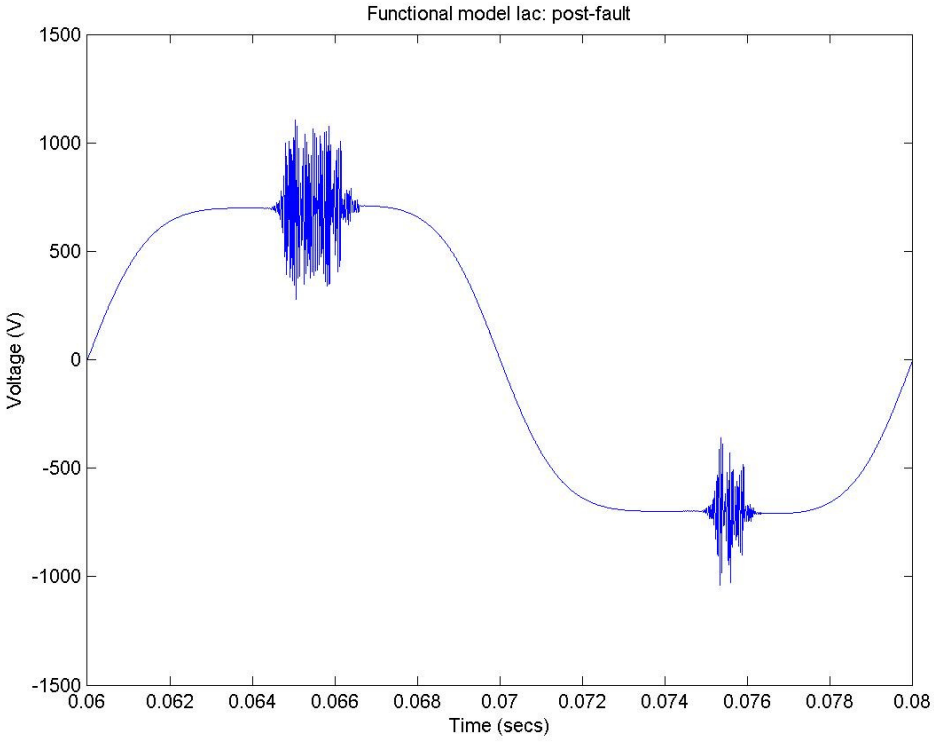

Fig. 5.34. Time-averaged functional model Iac – Post-fault

5.9.3 Summary of Findings

The results shown in figures 5.29 through to 5.31 illustrate how the inverter successfully supplies a sinusoidal current to the load prior to the application of the fault. After the application of the fault however, its behaviour changes significantly. Figure 5.32 illustrates the discharging dc side capacitance creates an ac side current surge every time an active switching vector (i.e. one that creates a non-zero magnitude of V_{ac}) is applied by the converter. Following this, the slower discharge of current from the dc voltage source is evident.

By comparing the simulation results produced by the functional inverter models (figures 5.30, 5.31, 5.33, 5.34) to those produced by the switched inverter (figures 5.29 and 5.32), the accuracy of the functional and time-averaged functional models can be assessed. It is observed that prior to the application of the fault, the functional and time-averaged functional models accurately replicate the behaviour at the terminals of the switched inverter model. However, after the fault is applied, the criterion for numerical stability (as described in Chapter 5) is not met by the functional and time-averaged functional models, leading to the creation of highly erroneous (although still bounded) outputs. It is worth noting that figure 5.34 shows that the time-averaged functional model actually remains stable for part of its operation. In line with the analysis conducted in Section 5.6 however, the model becomes erroneous when the magnitude of V_{ac} (and hence k_s) is at its greatest.

These findings reinforce the key outcomes of the analyses conducted earlier in this chapter.

5.10 Conclusions

This chapter has investigated the capabilities and limitations of the functional approach to the modelling of power electronics. The stability analyses conducted indicates that functional converter models will be stable for most operating conditions although there may be a need to utilise increased capacitances to maintain this numerical stability under some network conditions. Moreover this chapter has also provided some insight into the likely causes of numerical instability involving functional converter models, thus enabling appropriate corrective measures to be taken if such issues are experienced in practice. The consideration of the capabilities and limitations of the functional modelling approach conducted earlier in the chapter also illustrates that almost all behavioural aspects of switched converter models can be represented with functional models by incorporating additional mathematical expressions and circuit components as necessary. The examples of functional converters provided in this chapter illustrate the ease of implementing these models, and the IFEP case study provided also highlights the potential of the functional modelling technique to provide substantial gains in simulation efficiency, especially in multi-converter networks.

These advantages suggest that the functional modelling approach could be beneficial to the network-level modelling and simulation of marine and aerospace more-electric architectures. The ease of implementation and effectiveness in reducing the computational burden of simulating power electronics make functional modelling particularly appealing to this field for the reasons outlined in Chapter 3.

However, the technique as it stands, does have two significant drawbacks limiting is use to the marine and aerospace more-electric applications. Firstly, the difficulty of modelling diode bridge rectifiers as functional equivalent models represents a very significant disadvantage for this technique. In large networks containing multiple power electronic converters, the likelihood of a diode bridge rectifier being present is high. As such, this chapter recommends the use of the hybrid approach suggested in [6], where ideal switch models of diode bridge rectifiers and functional models of other converter types are combined within a single network model to achieve both accuracy and a good overall computational efficiency. There is however, a clear opportunity to improve upon this approach.

The second key drawback to the functional modelling approach is the likelihood of numerical instability during the simulation of some electrical fault conditions. In these cases, it would be necessary to resort back to using fully switched models of the converters to achieve the required numerical stability of the model. Given the importance of fault studies to network-level investigations of marine and aerospace architectures, this fallback represents a less than ideal solution though.

Recalling the literature review conducted in Chapter 3, it was concluded that the functional modelling approach was the only method at present truly suited to the network level modelling of marine and aerospace more-electric architectures. Hence it is desirable to seek ways to improve the robustness of this method for the given application areas. As such there is a requirement to develop novel methods for two separate goals. The first is to improve the robustness of functional converter models

so that the models are numerically stable under simulated fault conditions. The second is to improve the simulation efficiency of switched converter models so that any switched diode bridge rectifier models may be simulated more effectively. This second goal will also provide an alternative path forward if the desired numerical stability of functional models during fault conditions cannot be attained.

5.11 References

[1] H. Jin, "Behaviour-mode simulation of power electronic circuits," *IEEE Trans. on Power Electronics*, Vol. 12, no. 3, pp. 443 – 452, May 1997.

[2] J. Clare, P. Zanchetta, P. Wheeler, L. Empringham, "Modelling and design of matrix converter solutions for shipboard applications," *Proc. IMarEST Electric Warship IX Seminar*, December 2003, pp. 20 – 34.

[3] C. G. Hodge, "Modern applications of power electronics to marine propulsion systems," *Proc. 2002 IEEE International Symposium on Power Semiconductor Devices and ICs (ISPSD).* Available: http://www.ship.org.tw/Upload/ISPSD_2002_Paper.pdf (accessed 11/05/2009)

[4] Richard Newman, "The more electric engine concept," *SAE Transactions: Journal of Aerospace*, vol. 113, no.1 , pp. 1656 – 1661, 2004.

[5] Judith Apsley, "Motor and converter models for marine power systems – AMEPS literature review," *Technical Report*, June 2005.

[6] A. M. Gole, A. Keri, C. Nwankpa, E. W. Gunther, H. W. Dommel, I. Hassan, J. R. Marti, J. A. Martinez, K. G. Fehrle, L. Tang, M. F. McGranaghan, O. B. Nayak, P. F. Ribeiro, R. Iravani, Lasseter, "Guidelines for modeling power electronics in electric power engineering applications," *IEEE Trans. on Power Delivery*, Vol. 12, No. 1, pp. 505 – 514, January 1997.

[7] I. M. Elders, P. J. Norman, J. D. Schuddebeurs, C. D. Booth, J. R. McDonald, J. Apsley, M. Barnes, A. Smith, A. Forsyth, S. Loddick, I. Myers, "Modelling and analysis of electro-mechanical interactions between prime-mover and

load in a marine IFEP system," *Proc. IEEE Electric Ship Technologies Symposium (ESTS)*, May 2007.

[8] *Using Matlab*, The Mathworks Inc., 3 Apple Hill Drive, Natick, MA, USA, 2002.

[9] Graham J W Dudgeon, James R McDonald, "Simulation challenges for the all electric ship – form micro-second to macro-second," *Proc. IMarEST Electric Warship IX Seminar*, December 2003, pp. 42 – 54.

[10] P. J. Norman, S. J. Galloway, and J. R. McDonald, "Simulating electrical faults within future aircraft networks," *IEEE Transactions on Aerospace and Electronic Systems*, Vol. 44, no. 1, pp. 99 – 110, January 2008.

[11] Simon Carter, "Kirchoff's Laws." Available at: http://www.electronics2000.co.uk/data/itemsgl/Kirchoff.htm (accessed 11/05/2009)

[12] Barry W. Williams, *Power electronics: devices, drivers, applications, and passive components*. Available http://www.eee.strath.ac.uk/~bwwilliams (accessed 11/05/2009)

[13] Mario Cacciato, Alfio Consoli, Giuseppe Scarcella, Antonio Testa, "Reduction of common-mode currents in PWM inverter motor drives," *IEEE Transactions on Industry Applications*, vol. 35, no. 2, pp. 469 – 476, March/April 1999.

Chapter 6 – Multi-Level Model Discretization

6.1 Chapter Overview

In this chapter, a method for reducing the computational effort of modelling and simulating electrical networks with a significant penetration of power electronics (typical of marine and aerospace more-electric network architectures) using switched converter models is proposed, and is hence a major contribution of this thesis. This method, Multi-Level Model Discretization (MLMD) achieves the following benefits:

- A reduction in the computational requirement for switched converter models.
- Variable levels of model abstraction.
- Stable and accurate simulations of electrical fault conditions (an aspect in which functional equivalent models of power electronics have been previously shown to be unreliable).

Specifically, MLMD is a framework which enables the modelling of a power system as a conventional continuous model before applying a range existing techniques tailored to reduce the overall computational burden of associated simulations. This can be readily achieved even if the model developer does not have extensive prior modelling and simulation knowledge and expertise.

This chapter will discuss the use of fixed and variable step solvers, and continuous and discrete models for the dynamic simulation of marine and aerospace more-electric network architectures, highlighting the general capabilities and weaknesses of each approach. It will introduce the MLMD technique and outline its

application to the aforementioned application areas, demonstrating its capability on a case study of a typical aircraft electrical network architecture. Finally, the capabilities and limitations of MLMD will be discussed in detail.

6.2 Research Justification

Chapters 3 and 5 discuss how functional equivalent models of power electronic converters are ideally suited for use in the network-level modelling and dynamic simulation of marine and aerospace more-electric network architectures. They can be readily implemented and also provide significant computational reductions compared to detailed converter models [1, 2]. This is especially true if the time averaged behaviour, rather than the pulsed output of the converters is represented [3]. Indeed for many operating scenarios, they are the method of choice for modelling electrical networks with a significant penetration of power electronics [2, 3].

The analysis conducted in Chapter 5 however, illustrates that there are significant shortcomings of the functional modelling technique when it is utilised for electrical fault simulations. Such studies are of importance as they allow the dynamic behaviour of systems under fault conditions to be investigated, facilitating the evaluation of proposed protection schemes at a network wide level. Poor accuracy is unacceptable. As a consequence, during studies of this type, it is necessary to utilise switched models in order to ensure accurate simulation results. However, doing so produces long simulation execution times due to the increased computation associated with switched converter models [1].

Additionally, Chapter 5 also discussed the difficulties in implementing accurate functional models of diode bridge rectifiers within complex network architectures such as those found in more-electric marine and aerospace applications. In these instances, switched models of diode bridge rectifiers must be used instead if reliable simulation results are to be achieved.

Given the shortcomings of other modelling techniques outlined in chapter 3 and the inadequacy of the functional modelling technique for use in the modelling and simulation of marine and aerospace more-electric applications, a need hence exists for a technique which provides computationally efficient simulation of electrical networks with a significant penetration of power electronic converters whilst still maintaining accuracy during fault simulations. The remainder of this chapter will present a novel modelling and simulation method that meets this criterion, Multi-Level Model Discretization.

6.3 The Use of Fixed/Variable Step Solvers and Continuous/Discrete Models for the Simulation of More-Electric Network Architectures

This section will discuss the merits and drawbacks of using fixed and variable step solvers, and continuous and discrete models for use in the simulation of marine and aerospace more-electric networks.

6.3.1 Introduction to Fixed and Variable Step Solvers

A numerical solver is an algorithm that implements numerical integration methods for solving systems of equations [4, 5]. When utilised for simulation, solvers step through a time interval, computing a solution for a particular model at each specified time step [4, 5]. A variety of solvers exist for a range of purposes and applications. Solvers which are utilised for dynamic simulations can be broadly split into two categories; fixed step solvers and variable step solvers.

Fixed step solvers compute a solution for the model at regular sampling intervals, from the beginning to the end of the simulation [4, 5]. These time intervals are specified in advance and do not vary during the course of the simulation. For solvers of this type, the choice of sampling interval is a critical factor for both accuracy and simulation execution time. In this manner, utilising a smaller sampling interval produces greater levels of accuracy, but at the expense of an increased execution time, whilst utilising a larger sampling interval produces a lower computational requirement but also reduced levels of accuracy.

Variable step numerical schemes are often adopted to limit the impact of this choice on the overall simulation duration. These methods vary the simulation step size in accordance with the rate of change of the model variables in order to achieve a desired level of accuracy, or tolerance [4, 5]. In this manner, small step sizes are utilised when the model's state is rapidly changing and larger steps when it is nearly constant in nature [4, 5]. Updating the computational step in this way impacts on the global computational overhead as additional calculations must be made in order to

make an informed decision on the size of the next sampling interval. However, this is in an attempt to reduce the total number of steps required to yield a solution thereby reducing the overall computational requirement of the simulation and delivering a much reduced execution time [4, 5]. This aspect is illustrated in figure 6.1, where smaller solver steps are taken during the more dynamic regions of the plot displayed.

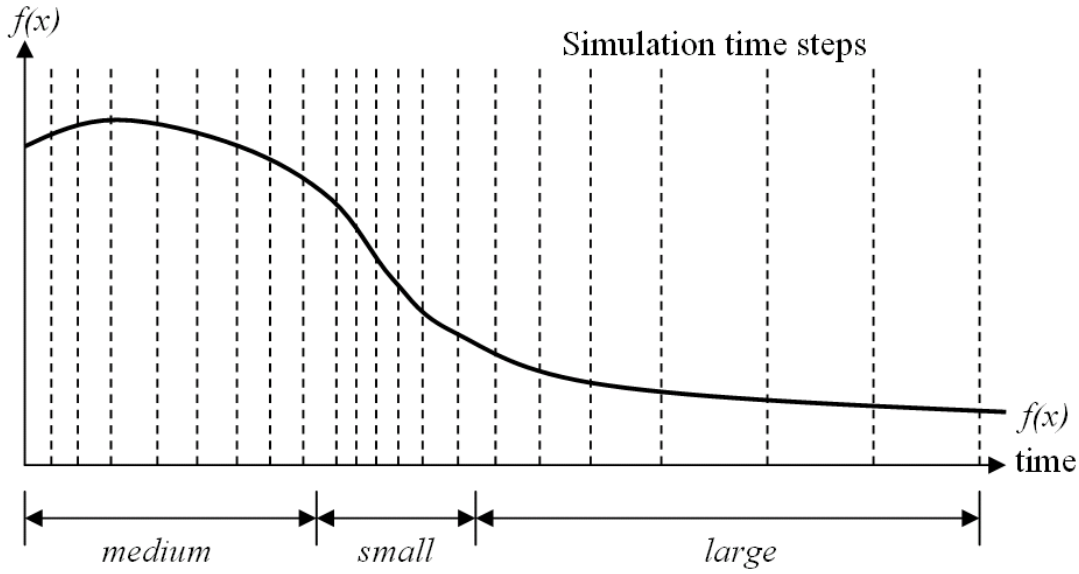

Fig. 6.1. Illustration of the variable step solver approach

The use of a variable step solver is often the favoured approach for detailed models of converters and their control systems where the very small simulation time steps taken during switch transitions and other highly dynamic periods produces very accurate results whilst minimising the overall computational requirement [1]. This approach is illustrated in figure 6.2 where the transitions in the converter switching pattern are simulated using many small steps so that the transition times are accurately captured. The constant regions however, are simulated with very large steps to minimise the overall computational requirement, providing the ideal trade

off between simulation accuracy and efficiency. Note that many more simulation steps would be taken at the transitional regions than have actually been displayed in figure 6.2, but this aspect has been simplified for illustrative purposes.

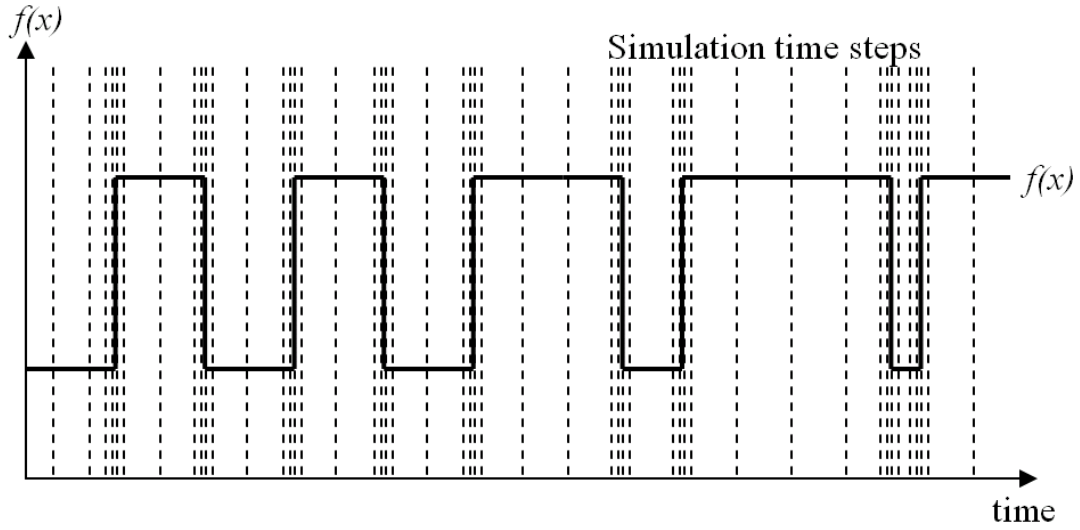

Fig. 6.2. Variable step solver applied to a switched converter output

In large, multi-converter network models, simulated over long time scales however, variable step solvers can actually provide more detail than is often necessary, which has a detrimental effect on the simulation duration [6]. This is because there are many rapidly changing variables within these models requiring the near-constant application of very small step sizes. As a result, many alternative modelling techniques have been developed to avoid modelling the specific switching of the converters in order to enable much quicker simulation times (these were reviewed in Chapter 3). The sacrifices in accuracy produced are generally acceptable within larger system models, where the higher detail level is not often required [7].

6.3.2 Introduction to Continuous and Discrete Models and Associated Solvers

Continuous models by their nature provide a continuous characterisation between system states, which is typically valid over a predefined range of states or particular interval. Continuous solvers utilise numerical integration techniques to provide the solution of a continuous model's state and as such, provide a better characterisation of system behaviour than the discrete equivalent. This improvement however is at a cost of increased computation.

In contrast discrete models represent system states at specific intervals. The transitional behaviour between these states is not captured but instead may be approximated (e.g. interpolation, splines, zero-order hold), with a lower resulting computational requirement compared to continuous models. As a result of the uncertainty introduced between states, the error in the simulated data typically increases with the size of the simulation time step taken by the discrete solver algorithm.

An example of a continuous function and its discrete equivalent are shown in Figure 6.3.

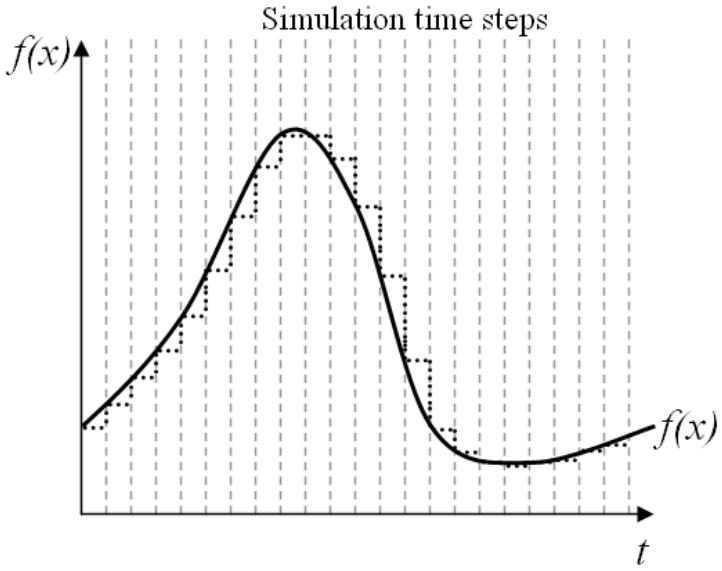

Fig. 6.3. Comparison of continuous (solid line) and discrete (dotted line) functions *f(x)*

This figure illustrates the typical errors produced by discrete models, with both under and over estimation of the integral occurring. This level of error may be unacceptable for some detailed models of devices, particularly during periods where the model states are rapidly changing. However as discussed previously, the levels of computation associated with discrete models are much lower than that associated with continuous models providing reduced execution times for any simulations conducted [6].

Despite the apparent drawbacks of fixed step models and discrete solvers, this author believes that the computational savings offered by both methods are attractive for network-level dynamic simulations of complex electrical networks, such as those found in marine and aerospace more-electric applications, where small levels of error are acceptable for types of studies typically considered. As such, this thesis proposes

a method for the network-level simulation of marine and aerospace more-electric network architectures, which embraces discrete models and fixed step solvers as its core features. This method is described in the following section.

6.4 Proposal of Multi-Level Model Discretization

The method proposed in this section, Multi-Level Model Discretization (MLMD) [9], reduces the computational burden associated with simulating switched converter models whilst achieving stable and accurate simulation results during simulated electrical fault conditions. In addition, it also facilitates variable levels of model abstraction to provide increased versatility.

The following sections will:

- Outline the core concepts of MLMD.
- Discuss its implementation and the factors involved in its successful utilisation.
- Discuss the unique challenges of its implementation to uncontrolled semiconductor devices, with case studies to demonstrate the core concepts involved.
- Demonstrate the effectiveness of MLMD in reducing the computational burden of electrical networks with a significant penetration of power electronics using a case study of a more-electric aircraft network.

The proposed technique utilises discrete equivalent models and fixed step solvers for the simulation of power electronics based, more-electric architectures. There are

risks associated with this approach, as outlined later, but it provides a means to minimise the computational requirements of dynamic simulations of the aforementioned networks.

It should be noted that in situations where the discretization of the electrical network model is not immediately possible (for example because of limitations in the capabilities of the simulation software employed), the method presented in this section can still be applied to continuous models, although this will reduce the maximum improvements in simulation efficiency possible with MLMD.

6.4.1 Implementation of Multi-Level Model Discretization

The first stage of MLMD is to develop a variable step, a continuous baseline model. The computational requirements of this model will be high in comparison to the discretized equivalent models developed later, but it will also provide the highest level of accuracy. Hence this model will be utilised as a benchmark to compare other lower fidelity equivalent models against.

From this base model, the first discretized equivalent is developed utilising an appropriate discretization algorithm (where the zero-order hold and Tustin methods are popular examples [4, 10]) and is configured for use with a fixed step solver algorithm and a small step size (typically 1-5μs). This process can be achieved using continuous to discrete conversion algorithms supplied with various commercial packages [8]. From this stage, knowing the desired purpose and functionality of the model, further discrete equivalent models utilising progressively larger step sizes can

be developed until the maximum level of acceptable error for the studies in consideration is reached. Note that some degree of expertise is required in interpreting the simulation results of each model and establishing the maximum acceptable step size for that model in question (this aspect is addressed in the following section). The larger step size models can then be utilised to study longer duration transient events (e.g. those involving the mechanical response of systems). Shorter duration transients and particular portions of the longer transients can be investigated in greater detail with appropriately initialised smaller step size models.

6.4.2 Choice of the Level of Abstraction

The choice of level of abstraction is somewhat intuitive, with a number of aspects to consider when selecting the step size (and associated model) to be utilised. First and foremost is the switching frequency of converter models within the model. The simulation step size must be suitably chosen to represent the behaviour of these to the desired level of accuracy. This choice is critical to the accuracy of the fixed step simulation because network events (e.g. switch transitions) are delayed to coincide with simulation step times [1, 6]. Changes in key quantities such as switch states and pulse generation must therefore be delayed from their intended occurrence to the next occurring simulation step. This delaying process does not usually create any significant errors when utilising variable step solvers because the solver step size is reduced around the network event (as illustrated earlier in figure 6.2). However, with fixed step solvers (for both continuous and discrete models) the simulation time step size is not flexible and the delay to network events can be significant.

This aspect is illustrated in figure 6.4, where the section of a PWM pulse train is modified by the application of the fixed step solver.

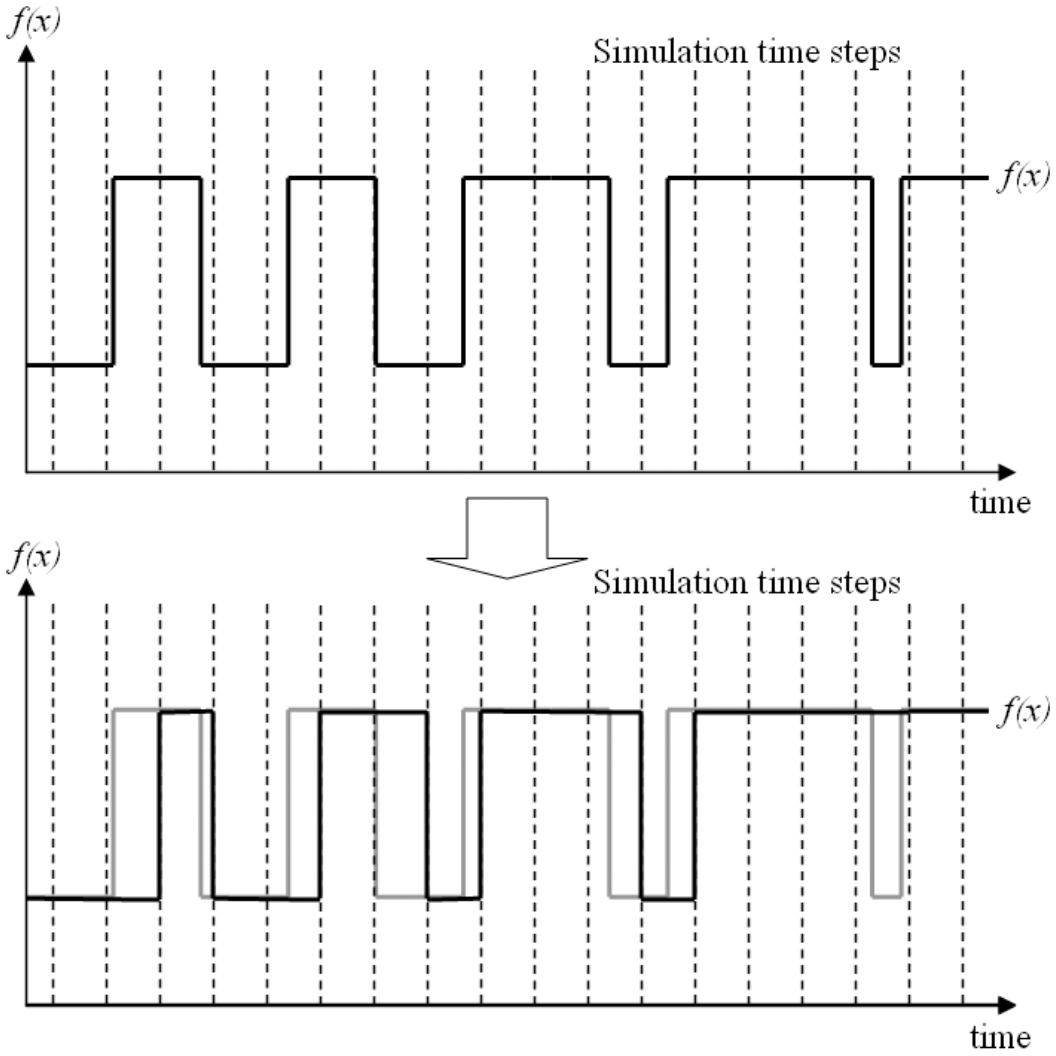

Fig. 6.4. Delaying of PWM pulse train segments by the application of a fixed step solver

Note that the fixed step size employed in figure 6.4 is intentionally large to provide a clear illustration of the delaying effect. In reality, the use of an appropriate solver step size would result in only marginal changes to the original PWM pattern. However, these delays can still result in poor representation of the model's

behaviour, the generation of extra harmonics and 'spikes' within the voltages and currents of the model, and the degradation of the model stability, by slowing the potential response of any control system.

Additionally, if the simulation step size chosen is completely inappropriate, this may result in the converter switching being poorly represented and other fast transients being missed altogether. For example, figure 6.5 shows a current trace illustrating the profile of a capacitor discharge current, typical of that experienced in DC sections of marine and aerospace more-electric architectures following the occurrence of a short circuit fault [11]. Figure 6.6 illustrates the typical results produced when this same event is simulated using a fixed step continuous (solid line) and fixed step discrete (dashed line) approach. Note that the continuous plot is overlaid in figure 6.6 to provide an easier comparison with the fixed step continuous and discrete plots.

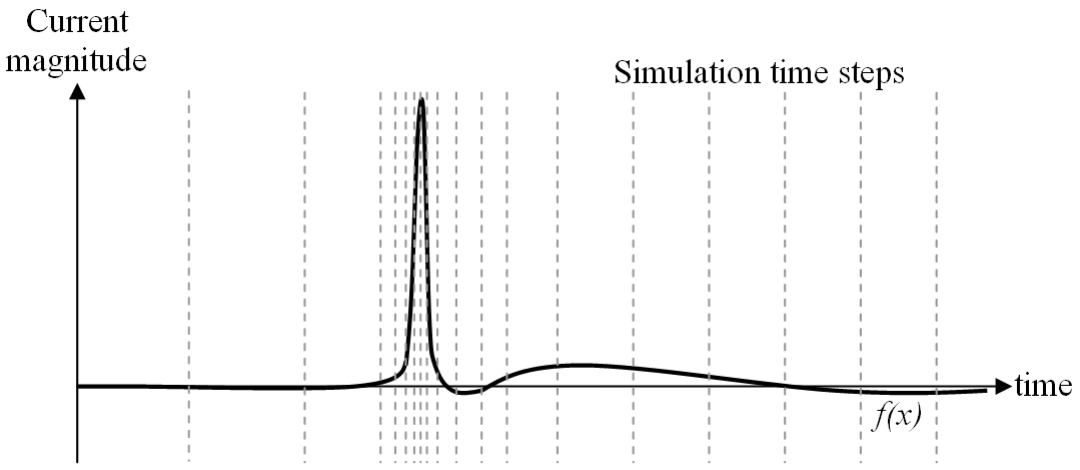

Fig. 6.5. Capacitor discharge event simulated using a variable step continuous model

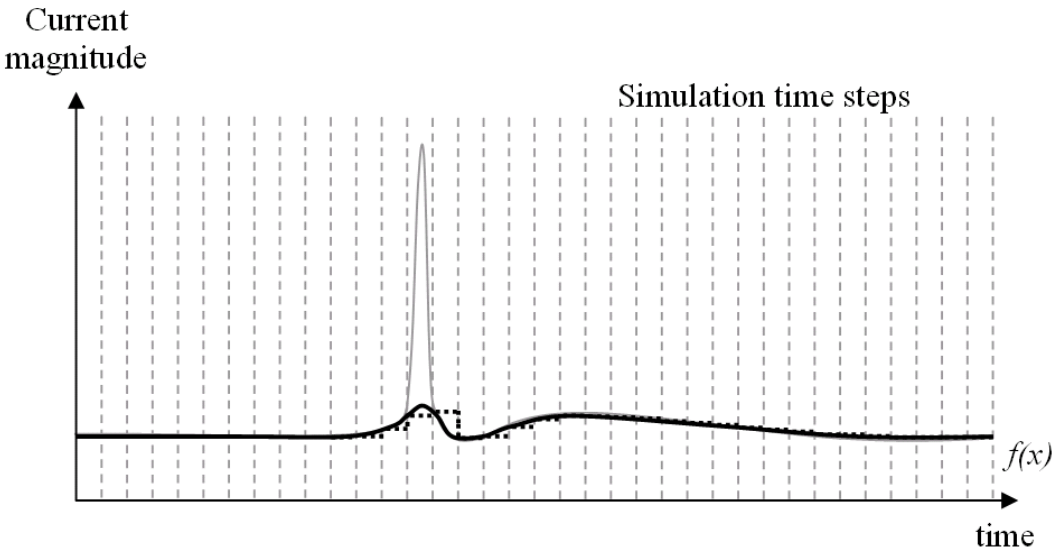

Fig. 6.6. Capacitor discharge event simulated using a fixed step continuous (bold) and discrete (dashed) solver

Although the fixed step size utilised in figure 6.6 is unrealistically large, it shows both fixed step models failing to properly represent the fast capacitor discharge event, creating unacceptable levels of error in the simulation results. This example illustrates the potential for fast transient events to be completely 'missed' by the simulation if the duration of the event is less than the fixed step size of the solver. To overcome this, the step size of the solver can be appropriately selected if some prior knowledge regarding the nature and timing of such an occurrence exists. However, if the purpose of the simulation is to identify the occurrence of such phenomena, this type of error is very difficult to eliminate, reinforcing the need for careful interpretation of simulation results when using the MLMD.

As a general rule for network-level simulations, a simulation step size that is one tenth of the typical interval between the converter switch transitions (i.e. 1/*f*, where *f*

is the switching frequency) is about the largest step size that can be used before the converter switching becomes significantly disrupted. Other fast transient events such as the capacitor discharge illustrated in figures 6.5 and 6.6 however, may require the use of smaller step sizes than this.

The performance of some controller architectures may also suffer if too large a step size is utilised, resulting in the poor regulation of electrical quantities. Additionally, harmonic studies require much smaller solver time steps so that the impact of the converters' switching (and hence the harmonic content) is accounted for accurately.

6.4.3 Multi-Level Model Discretization and Uncontrolled Semiconductor Devices

Unlike controlled semiconductor devices, whose turn-on and turn-off instances are well known, uncontrolled devices such as diodes depend on circuit parameters to determine their state and transition times. This unique behaviour has additional implications when considering the use of a fixed step solver and discrete equivalent models to simulate these devices. Indeed, the impact of this behaviour on modelling uncontrolled devices in a functional manner was also discussed in Chapter 5.

As described earlier in Chapter 3, uncontrolled devices such as diodes are represented by loop equations and require iterative solvers to compute them [5, 12]. Variable step solvers take small steps around zero crossings to ensure that each diode only switches off when the current flowing through it is zero.

When using a fixed step solver, the diode model does not stop conducting until the next time step after the current through it has reached zero. At this instant, the diode current is often negative and the simulation results presented at that instant are invalid. When the diode model is turned off, the current is forced to zero at the next time step [12, 13]. This is demonstrated in figures 6.7 and 6.8 which illustrate a typical plot of current flowing through a diode with two different solver methods applied.

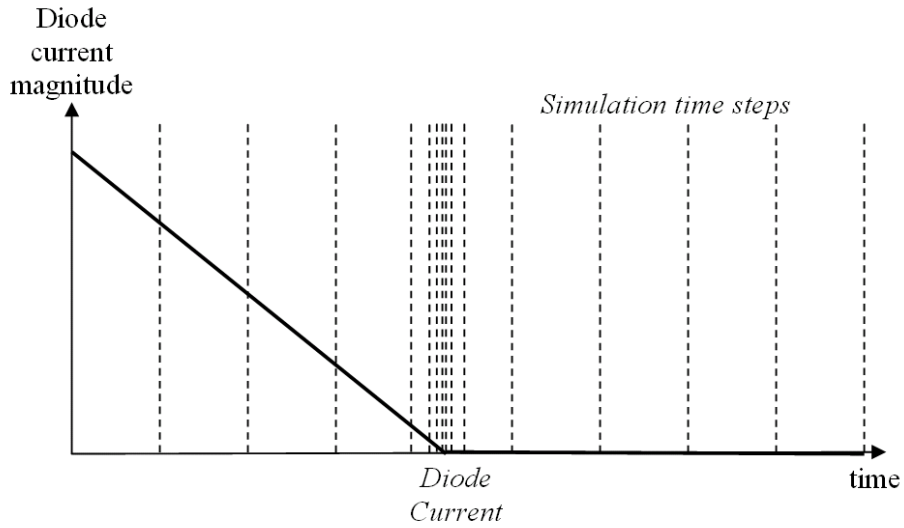

Fig. 6.7. Variable step simulation of a diode turn-off

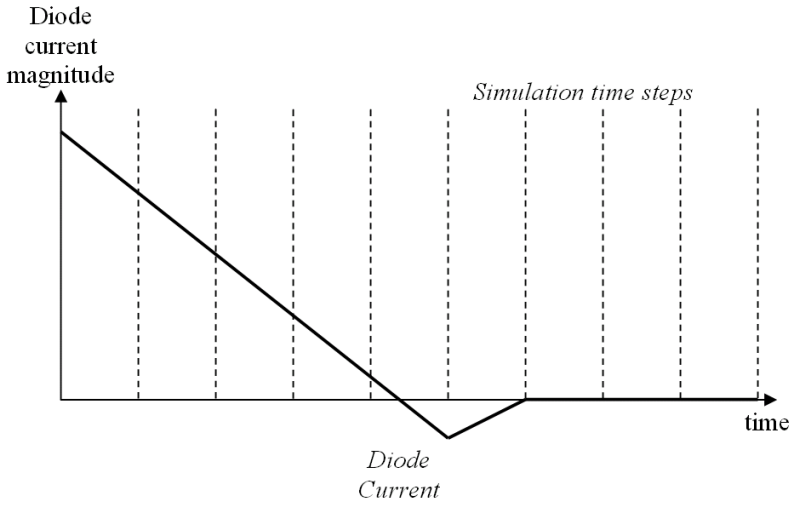

Fig.6.8. Fixed step continuous simulation of a diode turn-off

In figure 6.7, a variable step solver is employed and the diode turns off when the current through it falls to zero. In figure 6.8, the diode turns off at the time step immediately after the current reaches zero. The period when the diode current is negative does not represent the true behaviour of the diode (i.e. reverse recovery [14]) but is the result of the solver algorithm returning to a valid solution. This behaviour can create small numerical oscillations in the simulation results. In a multi-switch converter model, it can also lead to overlapping periods of conduction which can potentially lead to large numerical spikes in the line currents of the converter.

Figure 6.9 illustrates a typical plot a diode turn-off current simulated using a fixed step discrete model.

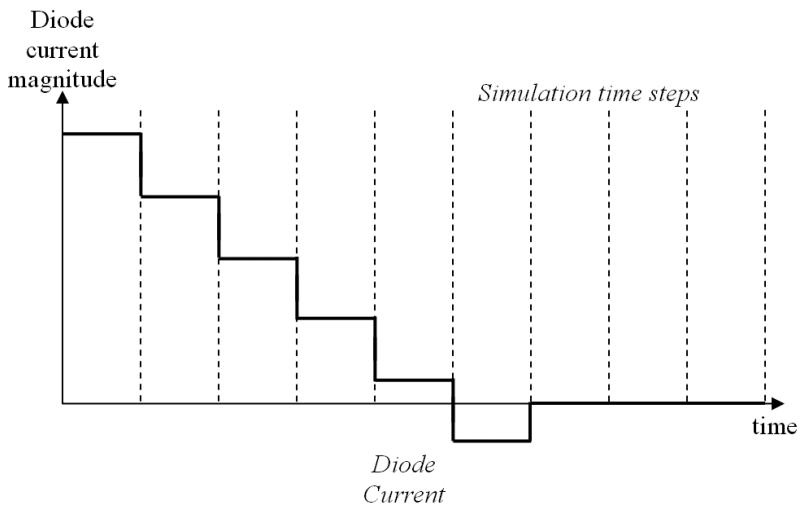

Fig.6.9. Fixed step discrete simulation of a diode turn-off

Whilst displaying the same underlying behaviour of the fixed step continuous model, the discrete model, with a higher rate of change of current experienced around the zero crossing (produced by the discretization of the model) will exacerbate any errors generated by the fixed step continuous model. Note that the solver step size chosen is in this example is unrealistically large for illustrative purposes.

If a suitably small solver step size is utilised, the erroneous behaviour described above is largely negligible for most network-level simulations. However, it will be shown in the following section that if cables or other inductive elements connected to the diode or diode-bridge are modelled, this behaviour can create additional and more significant errors. Spikes in the line currents can lead to large voltage transients across the inductors (where the voltage across an inductor is a function of the rate of change of current through it). This behaviour in turn impacts on the state of all connected diodes causing them to sporadically conduct. The resultant complex behaviour leads to switches rapidly turning on and off in an unstable manner which

is unrepresentative of the real devices [5]. This is demonstrated in the case study below.

6.4.4 Demonstration of Diode Discretization

The system shown in figure 6.10 illustrates an ac:dc:ac motor drive supplied from a 690V electrical network. This is typical of a pump system on low voltage diesel-electric IFEP vessel [15].

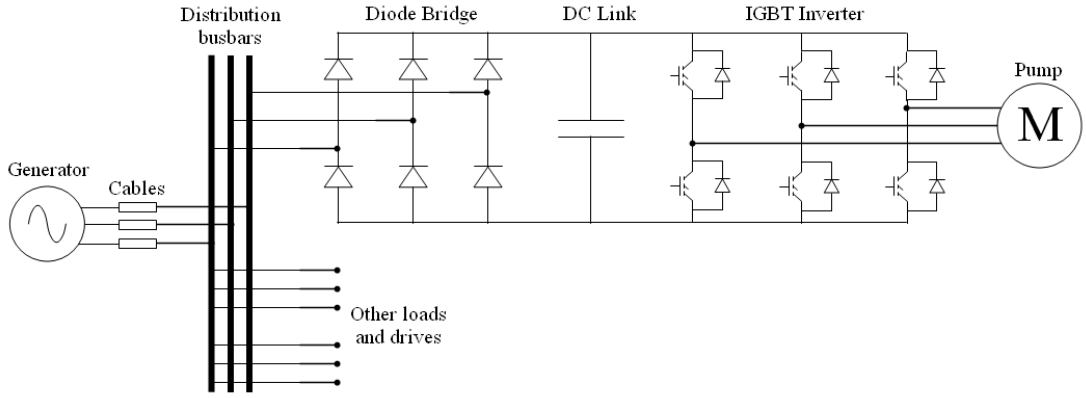

Fig. 6.10. LV IFEP Pump System

The pump motor drive consists of a 6-pulse diode rectifier, with dc link capacitor and an IGBT inverter. Figures 6.11 and 6.12 illustrate the dc link voltage profile and the phase-A load current when this system is modelled as a continuous system and computed using a variable step solver.

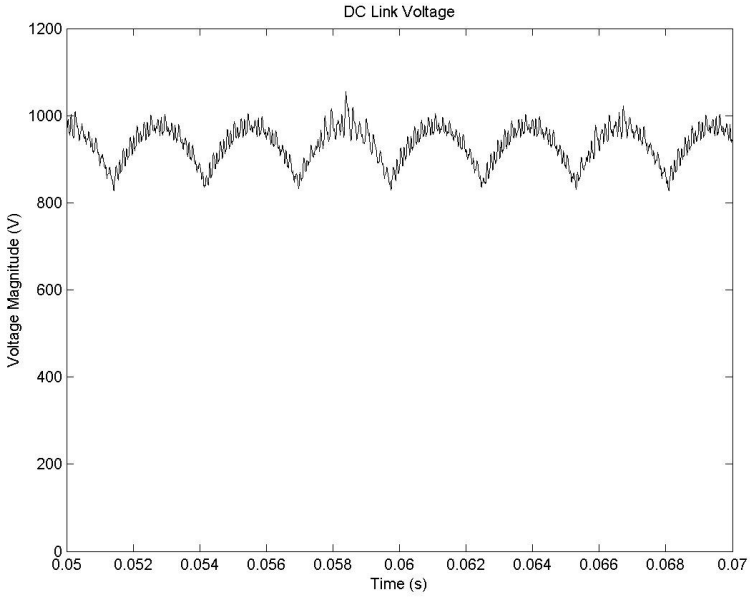

Fig. 6.11. DC link voltage profile produced from a variable step solver based continuous simulation

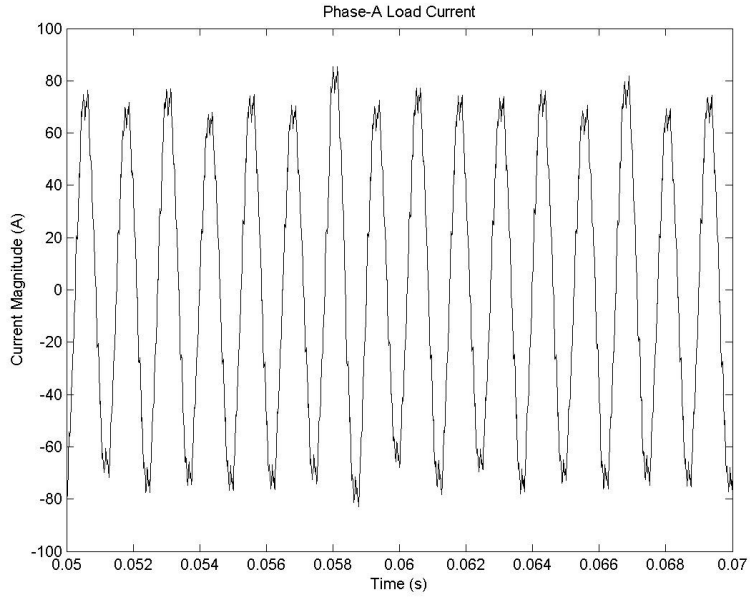

Fig. 6.12. Phase-A load current produced from a variable step solver based continuous simulation

The results presented are numerically stable and are inline with the anticipated performance of this system [14]. Note that the poor regulation of the phase-A load

current is a result of the open loop controller utilised for the inverter stage of the motor drive.

Figures 6.13 and 6.14 illustrate the dc link voltage and phase-A load current plots, this time produced using a discretized version of the original continuous model and also simulated using a fixed step solver with a step size of 10μs. Poor numerical convergence and spiking is apparent in both of these figures.

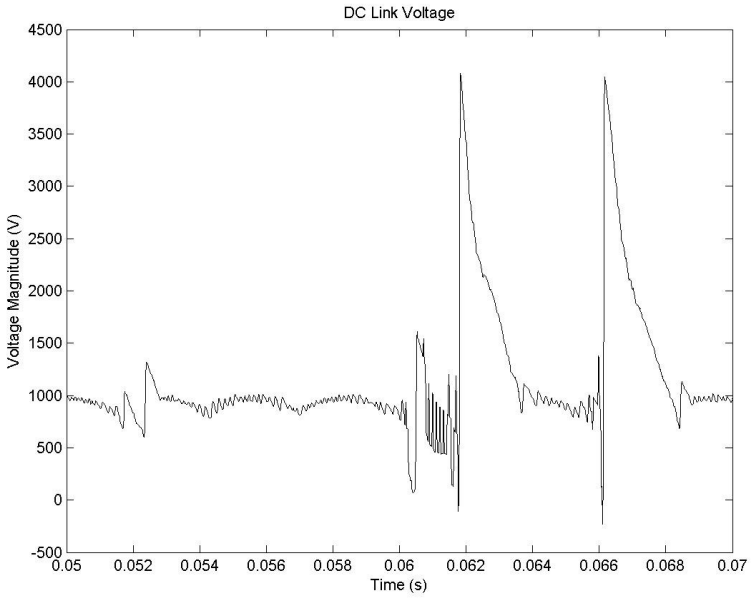

Fig. 6.13. DC link voltage profile produced from a fixed step solver based discrete simulation

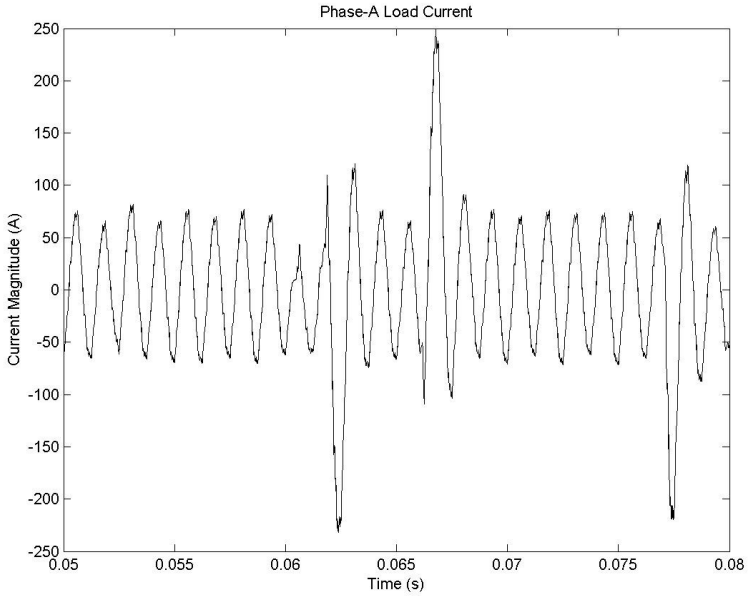

Fig. 6.14. Phase-A load current produced from a fixed step solver based discrete simulation

To achieve numerically stable simulation results similar to those generated by the continuous model and variable step solver (shown in figures 6.11 and 6.12), but using a discrete model and fixed step solver, a much smaller solver step size must be used in order to minimise the errors in the diode turn-off behaviour. Doing so negates any savings in simulation run time normally achieved using this approach though, and this path of action is hence clearly undesirable.

However, under some circumstances, it may not be necessary to utilise an undesirably small solver step size. If there are no cables between the generator and the diode bridge, the impact of the overlapping diode commutation and the current 'spiking' does not lead to significant voltage spiking (and in turn, oscillatory diode conduction). This is also true if the cables are modelled as being purely resistive, where the voltage across the resistor is directly dependant on the magnitude of the

current flowing through it. In this manner, the voltage spikes across resistive elements are of much lower magnitude than experienced when using cables with inductive elements (whose voltage is a function of the rate of change of current flowing through them). Under these conditions, the inaccurate diode behaviour has a negligible impact on the network-level accuracy of the simulation results. To demonstrate this behaviour, figures 6.15 and 6.16 show the dc link voltage and phase-A load current plots achieved when purely resistive cables are modelled. Again the model is a discrete model and is simulated using a fixed step solver with a 10μs step size. Note that there is an increased level of high frequency harmonic content present in the dc link voltage. This is due to the absence of any inductive filtering (previously provided by the cables).

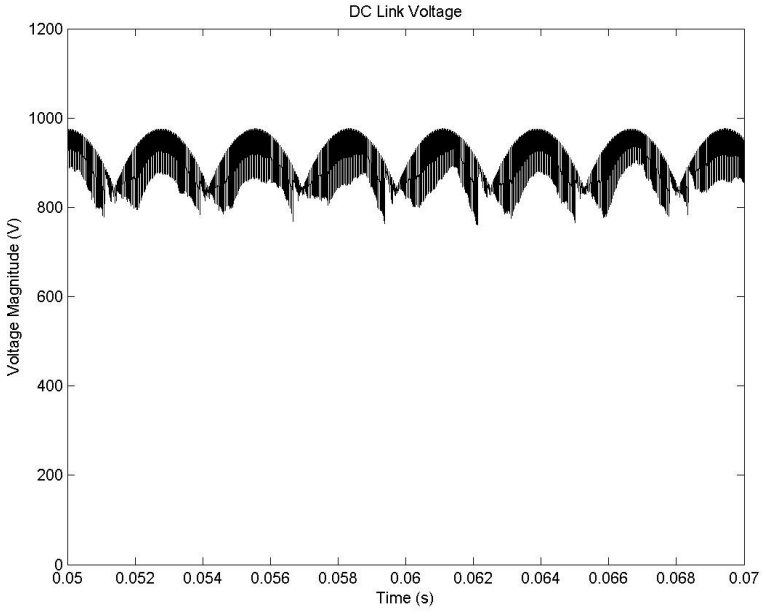

Fig. 6.15. DC link voltage profile produced from a fixed step solver based discrete simulation with purely resistive cables

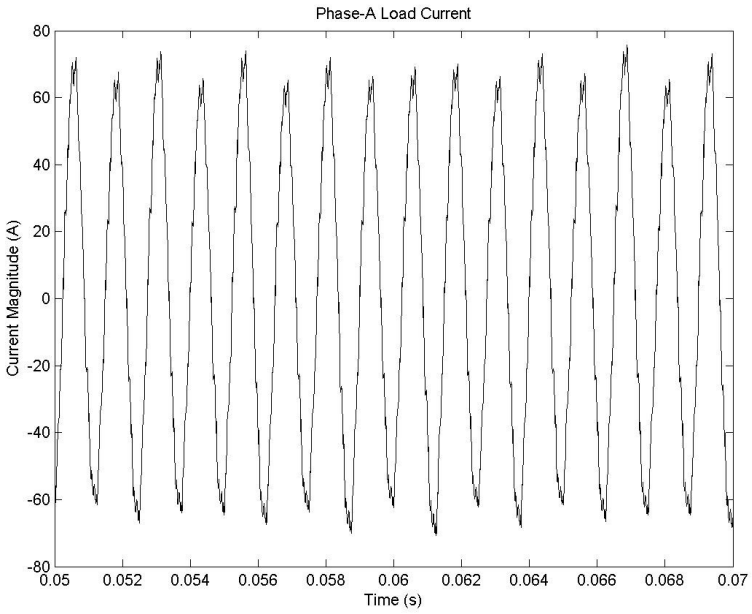

Fig. 6.16. Phase-A load current produced from a fixed step solver based discrete simulation with purely resistive cables

Given the commonality of inductive components in marine and aerospace network-level models (and indeed in many other models), there are likely to be very few instances when a larger solver step size can be satisfactorily utilised in conjunction with diode bridge rectifier models. As such, an alternative method to reducing the solver step size is required to facilitate valid simulation results when using discrete models and fixed step solvers.

The proposed approach is to use resistors placed in parallel with passive non-linear elements in the model, such as cables. As the impedance of these resistors is much higher than the circuit elements, only negligible leakage current will flow through them causing no noticeable loss in accuracy. However, the inclusion of a parallel resistive path for the current significantly reduces the voltage spiking that takes place

during the simulation. This hence aids the convergence of the simulation solver producing more accurate results [5].

The impact of this approach is demonstrated in figures 6.17 and 6.18 where 5Ω resistors have been implemented in parallel with the cable impedances and the discrete model is simulated with a fixed step solver utilising a 10μs step size.

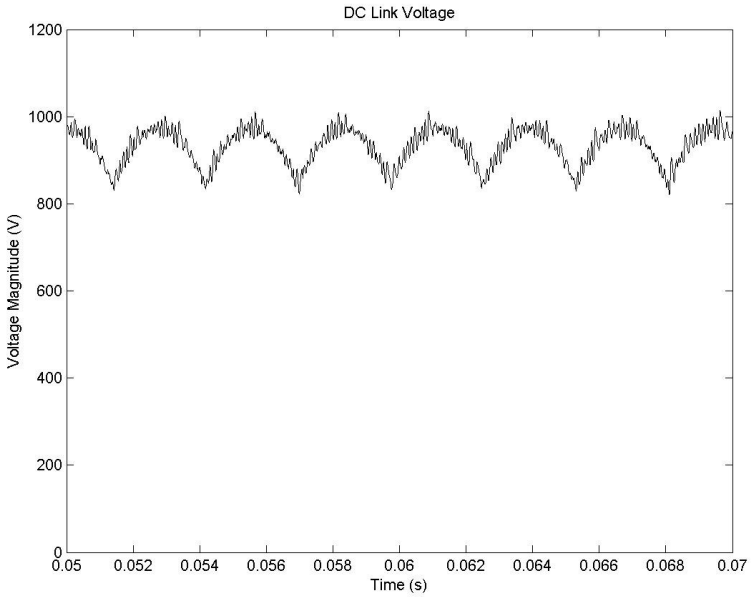

Fig. 6.17. DC link voltage profile produced from a fixed step solver based discrete simulation with parallel resistors employed

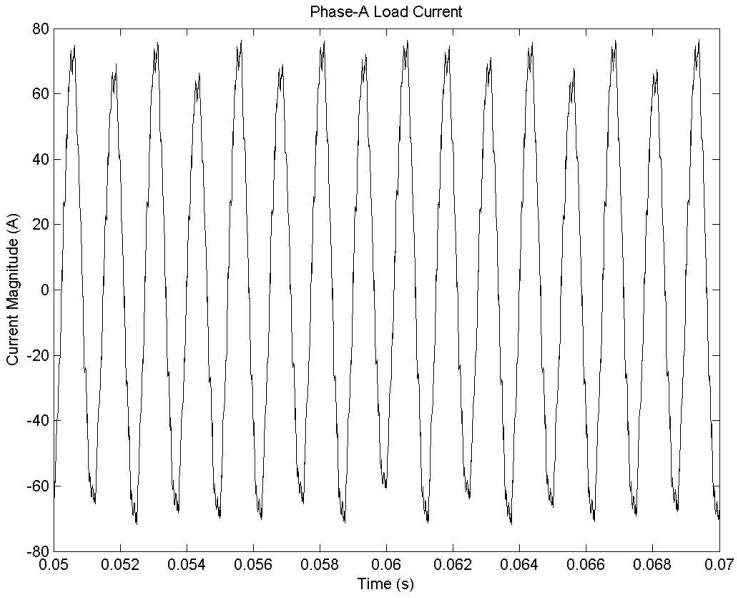

Fig. 6.18. Phase-A load current produced from a fixed step solver based discrete simulation with parallel resistors employed

In figures 6.17 and 6.18, numerical convergence is clearly restored. Note that some degradation of the simulation results is evident in these plots. This is a result of the delayed converter switching disrupting the dc link voltage and line current regulation. These small errors however, are usually acceptable in network-level simulations [7]. It is also worth highlighting, that although some degradation of simulation quality has occurred by using a discrete model and fixed step solver, much more efficient simulations are possible. In this particular example, the model simulates 8 times faster than the original continuous model simulated on a variable step solver. If more converters are present in the model, this time saving will be greater. This aspect is illustrated in Table 1 below, where simulation completion times (averaged over three separate simulations for a duration of 0.1seconds) are presented for further simulations conducted on the model depicted in figure 6.10 but with additional ac:dc:ac motor drives connected to the distribution busbar.

Table 6.1. Details of Simulations Conducted

Number of ac:dc:ac drives connected to the generator busbar	**Simulation completion time with a variable step solver based continuous simulation**	**Simulation completion time with a fixed step solver based discrete simulation**	**Completion time of discrete simulation as a percentage of that of the continuous simulation**
1	**17.30s**	**2.17s**	**12.5%**
2	**64.75s**	**5.92s**	**9.1%**
3	**164.11**	**11.72**	**7.1%**
4	**300.11s**	**20.34s**	**6.8%**
5	**503.70s**	**31.02s**	**6.2%**

Table 6.1 illustrates how the reduction in completion time offered by the fixed step solver based discrete simulations becomes more significant as greater numbers of diode bridge converters are included in the IFEP network model (although the additional reduction diminishes for every converter added).

It is worth noting that, in the same manner as the parallel resistor method, many power system simulation packages recommend the placement of snubber resistors in parallel with all semiconductor switches in order to aid numerical convergence when using discrete models and fixed step solvers [5]. This approach does indeed work satisfactorily, although this author has found the parallel resistor method to be much more effective in aiding numerical convergence. The reason for this is that the snubber resistors placed in parallel with the semiconductor switch models must have a high impedance value to prevent significant magnitudes of leakage current when

the switches are in the off state and there is a large voltage across their terminals. Resistors placed in parallel with cables however, are subjected to much lower terminal voltages and as such can be of significantly smaller magnitude whilst still only incurring a negligible amount of leakage current. The lower magnitude of resistor facilitates a much quicker numerical convergence following a diode current discontinuity. Hence, the parallel resistor method is recommended for MLMD.

It should also be noted that because the state of fully controlled devices is not directly dependant on circuit voltages and currents, these devices are much more numerically stable than uncontrolled devices when utilising discrete models and fixed step solvers. This is because spurious voltage and current spikes do not impact on the state of these devices and hence preventing the creation of further, larger spikes. However, the modelling of the anti-parallel diodes employed with some semiconductor switch types can still lead to the generation of numerical effects of this type. Under these circumstances, employing the parallel resistor method appropriately will greatly improve accuracy.

In summary, the use of discrete models and fixed step solvers as part of the MLMD technique in some power electronic based circuits (namely those with uncontrolled devices) requires the intuitive use of parallel resistors to aid convergence. However, by following the guidelines laid out above, efficient and accurate simulations can be readily achieved. This finding is in contrast to the functional modelling approach which cannot represent the terminal conditions of diode bridge converters to a satisfactory level of accuracy.

6.4.5 Demonstration of Multi-Level Model Discretization

This section aims to demonstrate the potential savings in simulation execution time that can be achieved with the use of MLMD as well as illustrating the impact of its use on the accuracy of the results produced. The model chosen for this demonstration is shown in figure 6.19 and is typical of the more-electric engine distribution network proposed for the Power Optimised Aircraft [16, 17]. The model has been developed using the SimPowerSystems toolbox of Matlab Simulink [18]. It consists of a low-pressure shaft mounted, inline ac generator feeding a central dc power distribution busbar (operating at 350V) through a switched rectifier. The model also contains inverter fed static and motor loads, representing the aircraft and engine electrical systems [16, 17]. A phase to phase fault is applied on the ac side cabling to the static engine load after 0.5 seconds resulting in a sequential discharge of all dc capacitors and a voltage collapse on the dc bus. The switching frequency of the static load inverter is 2kHz. Figure 6.19 shows the schematic for this model.

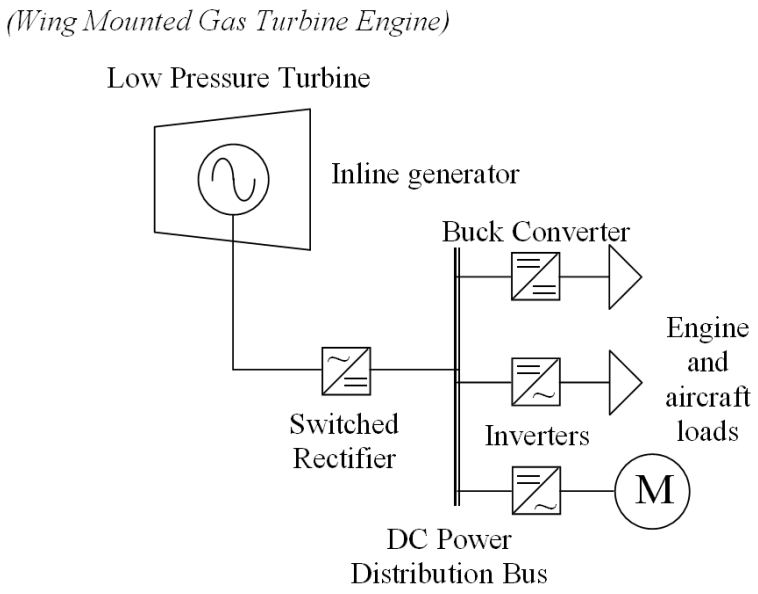

Fig 6.19. Schematic of the demonstration model

Multiple simulations have been conducted using the model whilst maintaining consistent external conditions. The simulation solver and step size are varied with each model execution to demonstrate the effect of MLMD on the simulation speed and accuracy. Table 6.1 lists the details of the comparative simulations conducted, and figures 6.20 through to 6.27 illustrate the plots of bus voltage and faulted system (ac side) line current for each of the simulations. The simulation execution times displayed in the table were measured using Matlab functionality.

It is worth noting that the level of time savings achieved by MLMD will be dependant on the nature of the model used. This aspect is discussed later. Also note that in some detailed models of power electronic converters, it is not uncommon to find a discrete control system which is simulated at a different rate to the electrical system, representing the digital aspects of the real controller [8]. This however, is primarily to achieve more realistic behaviour from the model and not to provide

reduced computation. It should be noted though that MLMD is very amenable to this approach, where a fixed step size can be readily implemented on the controllers of the network-level model whilst the network solver step size is varied.

Table 6.2. Details of Simulations Conducted

Case Number	**Electrical System**	**Control System**	**Solver Type**	**Simulation Execution Time**	**Execution Time as a % of Case 1**
1	Continuous	Continuous	2^{nd} order Runge-Kutta	5346.7 *s*	100%
2	Discrete (1μs)	Discrete (1μs)	Fixed step discrete	1918.7 *s*	35.9%
3	Discrete (10μs)	Discrete (10μs)	Fixed step discrete	53.8 *s*	1%
4	Discrete (50μs)	Discrete (50μs)	Fixed step discrete	9.7 *s*	0.18%

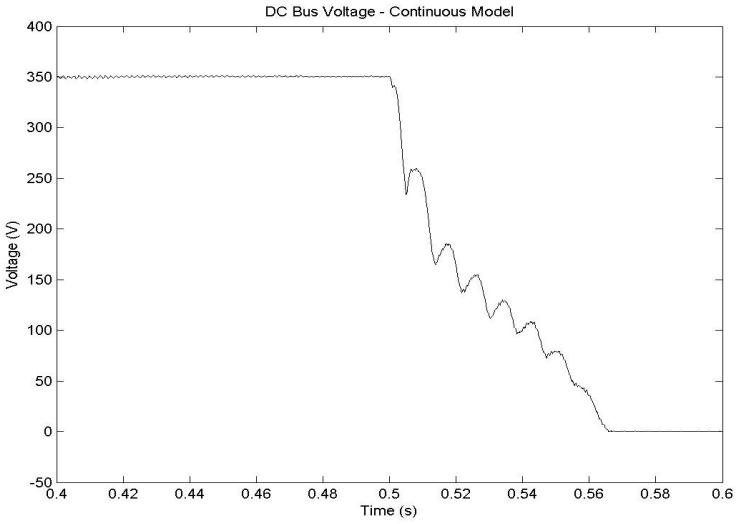

Fig. 6.20. Case 1 DC bus voltage

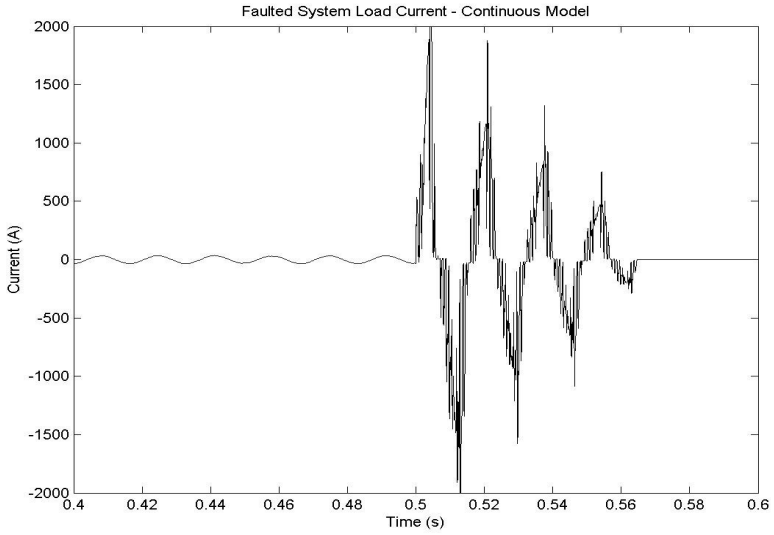

Fig. 6.21. Case 1 faulted system load current

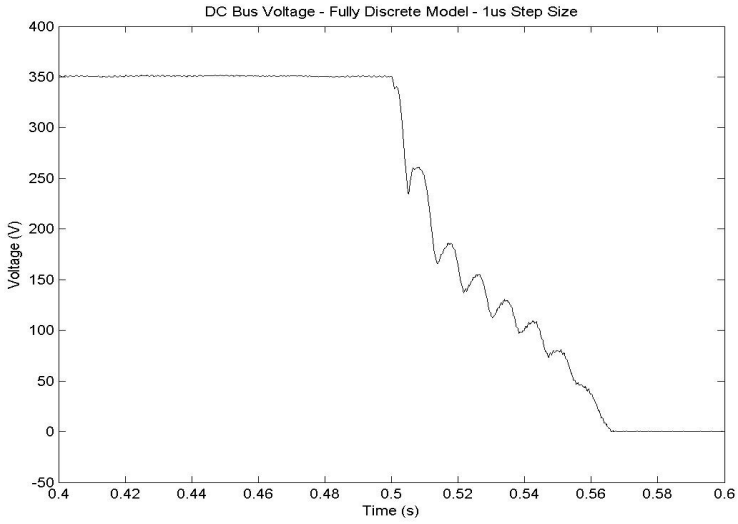

Fig. 6.22. Case 2 DC bus voltage

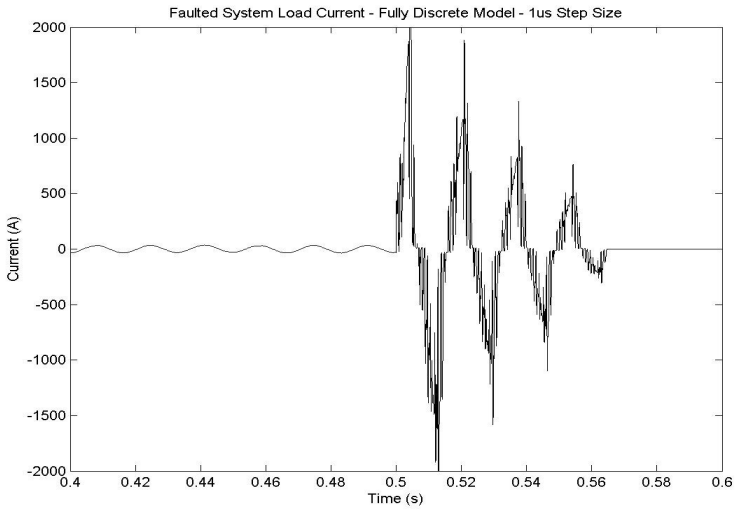

Fig. 6.23. Case 2 faulted system load current

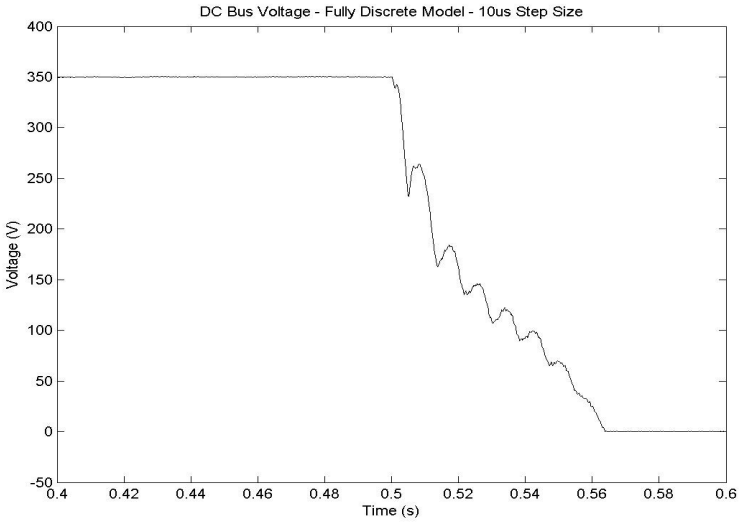

Fig. 6.24. Case 3 DC bus voltage

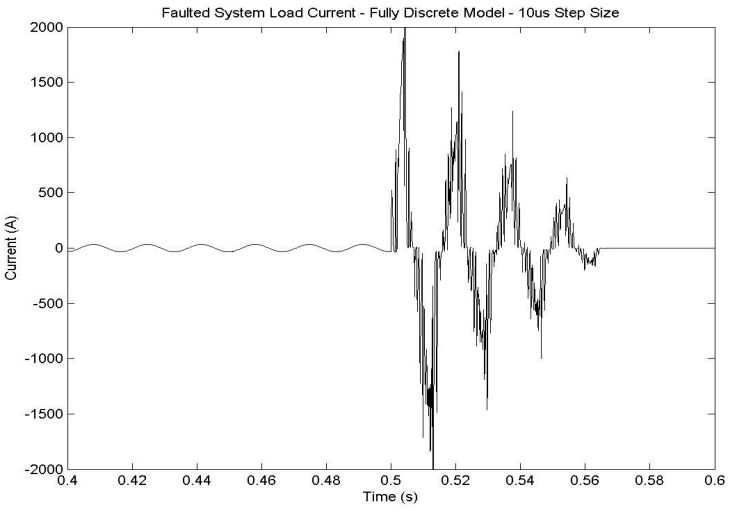

Fig. 6.25. Case 3 faulted system load current

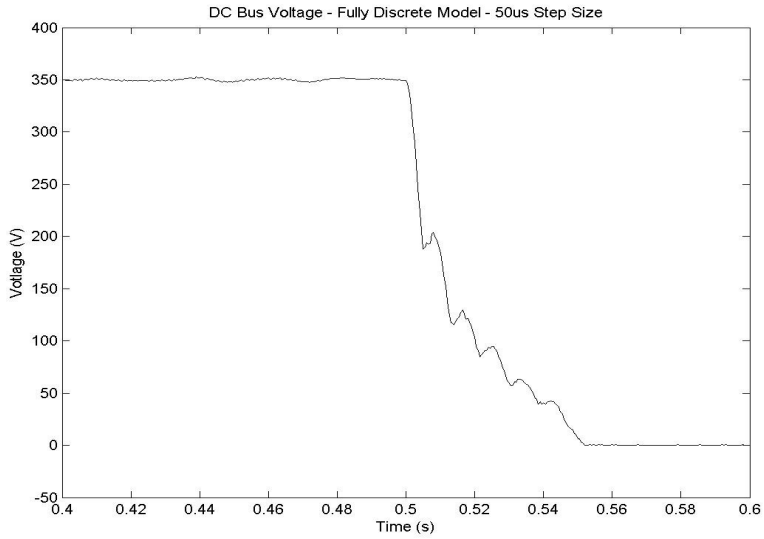

Fig. 6.26. Case 4 DC bus voltage

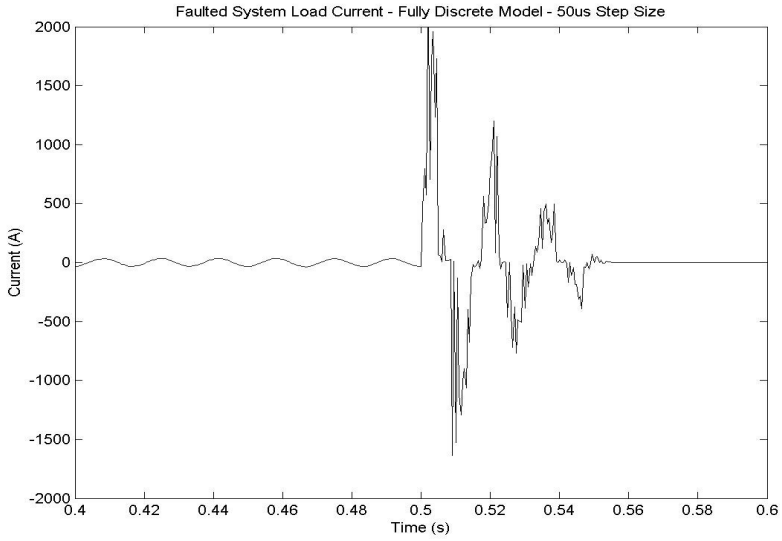

Fig 6.27. Case 4 faulted system load current

6.4.6 Discussion of Results

The trade off between simulation speed and accuracy is demonstrated in simulation results illustrated in table 6.2 and figures 6.20 through to 6.27. From these results it is observed that MLMD is an effective method for achieving computationally efficient simulations of dynamic models of complex electrical power networks with a significant penetration of power electronics, although at the expense of a loss in simulation accuracy.

Figures 6.20 and 6.21 (case 1) show the results of continuous model, simulated on a variable step solver. These are taken as the benchmark for accuracy for which to compare the results of subsequent MLMD simulations against. Figures 6.22 through to 6.27 (cases 2, 3 and 4) illustrate the degradation in the simulation accuracy as a result of the discretization process. This degradation is not particularly notable in figures 6.22 through to 6.25 however (cases 2 and 3), and indeed this level of accuracy is often satisfactory for network-level studies [7]. The purpose of case 4 (figures 6.26 and 6.27) is to demonstrate the impact of the large step size on the control system performance with both the line current and bus voltage becoming more poorly regulated. A 50μs step size in reality would often be the operating limit for MLMD, as it equates to a significant time delay in control system operation. If utilising open loop control systems, this delay can significantly alter the desired behaviour of the converter. Closed loop control systems however, show the ability to adjust set points in order to compensate and maintain the desired converter behaviour. As such, under these circumstances, a solver step size of the order of 50μs is more acceptable.

The key point to note though, is that whilst there has been some loss in accuracy, the simulation time savings are substantial. Hence, whilst a variable step solver based continuous simulation may be favourable for detailed modelling of single converter systems [1], this chapter has shown that a discrete fixed step approach is more effective for network-level simulations of large complex networks.

The reductions in simulation execution times provided by MLMD are especially valuable given that the functional converter models would fail to give valid results in the case study presented. This is demonstrated in figures 6.28 and 6.29 where the results shown have been generated from a model where all the converters have been represented as functional equivalents.

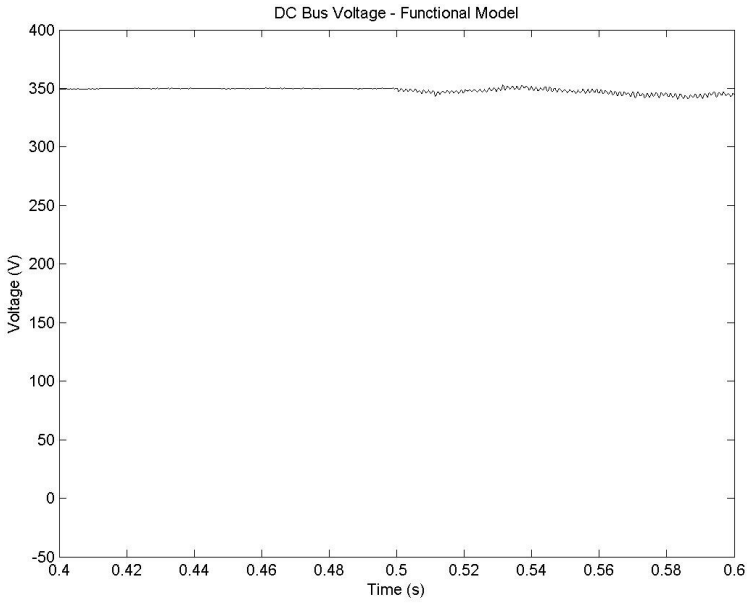

Fig. 6.28. Functional model DC bus voltage

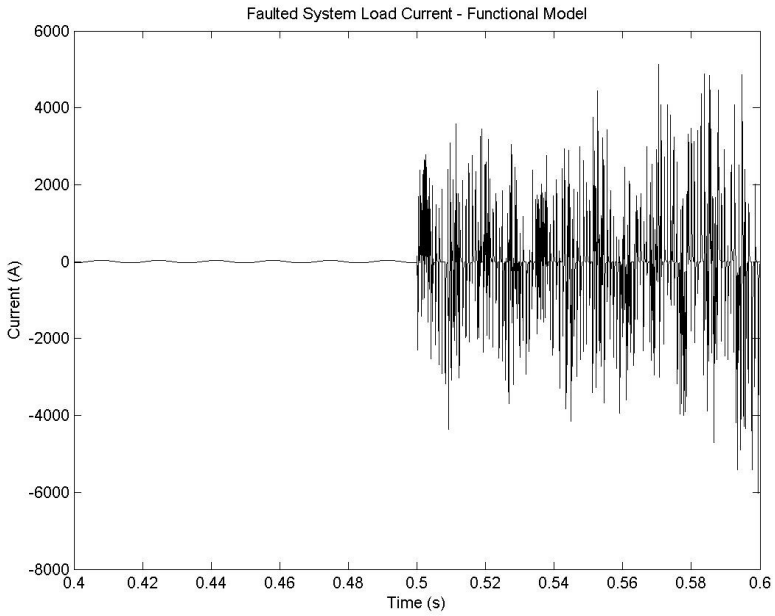

Fig. 6.29. Functional model faulted system load current

Prior to the application of the simulated fault, the model is accurate. However, after the fault is applied at 0.5 seconds, the modelled network no longer meets the criteria for numerical stability (originally derived in Chapter 5) given as

$$\frac{Z_{in}}{Z_L} < 1, \qquad (6.1)$$

where Z_{in} is the effective dc side source impedance and Z_L is the ac side load/fault impedance of the faulted inverter. As such, the load current becomes oscillatory. This does not become unbounded, but is clearly inaccurate. Furthermore, the changed nature of the fault current does not cause the dc bus voltage to collapse, which in turn impacts on the post-fault behaviour of the remaining systems on the bus.

6.5 Conclusions

The results shown in section 6.4 demonstrate that MLMD can be very effective in reducing simulation execution times of complex power system models with a significant penetration of power electronic interfaces (of which marine and aerospace more-electric systems are prime examples). The capability of delivering different levels of abstraction from a single base model also greatly improves the reusability of the model and allows a high computational efficiency to be achieved for a range of simulation scenarios. In addition to this, MLMD can be readily implemented in a wide range of simulation software packages. This aspect is indeed a key advantage of this technique in comparison to many others (for example the real time power electronics simulation techniques outlined in Chapter 3) and can represent a benefit which is almost as important as the reductions in computational burden.

It is worth noting that MLMD is also compatible with many of the real time simulation methods reviewed in Chapter 3 [19, 20]. By reducing the computational requirements of the models used, MLMD will further enhance the effectiveness of these methods.

This author still believes that functional models can provide even greater benefits than MLMD for network-level dynamic simulations of complex electrical networks such those found in marine and aerospace more-electric applications, if (and only if) the instability issues associated with electrical fault studies and inaccuracy aspects associated with diode bridge models can be overcome. Their modularity provides the capability to readily interchange between detailed switch models, functional models

and averaged functional models to best meet the requirements of the simulations being conducted. Additionally, time-averaged functional models could provide even greater reductions in the computational burden of simulations than MLMD, providing further reduced simulation execution times.

As such, although extending MLMD to be part of a multi-rate simulation approach is the most obvious follow-up to the work presented in this chapter, it will not in fact be pursued at all. This thesis will instead focus on the development of more robust functional models of power electronic converters in an to attempt to realise the significant computational gains that could be achieved. It is recognised however, that this capability will be difficult to fully develop, and that MLMD hence provides a robust and effective intermediate technique for the network-level modelling and dynamic simulation of marine and aerospace more-electric architectures.

6.6 References

[1] H. Jin, "Behaviour-mode simulation of power electronic circuits," *IEEE Trans. on Power Electronics*, Vol. 12, no. 3, pp. 443 – 452, May 1997.

[2] Kwa-Sur Tam, Lifeng Yang, "Functional models for space power electronic circuits," *IEEE Trans. on Aerospace and Electronic Systems*, Vol. 31, No. 1, pp. 288 – 296, January 1995.

[3] J. Clare, P. Zanchetta, P. Wheeler, L. Empringham, "Modelling and design of matrix converter solutions for shipboard applications," *Proc. IMarEST Electric Warship IX Seminar*, December 2003, pp. 20 – 34.

[4] "Solvers," *Using Matlab*, The Mathworks Inc., 3 Apple Hill Drive, Natick, MA, USA, 2002.

[5] J. Arrillaga, N. R. Watson, *Computer modelling of electrical power systems*, 2nd Edition, Wiley, 2001.

[6] Bruno De Kelper, Handy Fortin Blanchette, Louis-A Dessaint, "Switching time model updating for the real-time simulation of power-electronic circuits and motor drives," *IEEE Transactions on Energy Conversion*, vol. 21, no. 1, pp. 181 – 186, March 2005.

[7] A. M. Gole, A. Keri, C. Nwankpa, E. W. Gunther, H. W. Dommel, I. Hassan, J. R. Marti, J. A. Martinez, K. G. Fehrle, L. Tang, M. F. McGranaghan, O. B. Nayak, P. F. Ribeiro, R. Iravani, Lasseter, "Guidelines for modeling power electronics in electric power engineering applications," *IEEE Trans. on Power Delivery*, Vol. 12, No. 1, pp. 505 – 514, January 1997.

[8] Clare D. McGillem, George Cooper, *Continuous and Discrete Signal and System Analysis*, Holt, Rinehart, and Winston, 1984.

[9] P. J. Norman, S. J. Galloway, and J. R. McDonald, "Simulating electrical faults within future aircraft networks," *IEEE Trans. on Aerospace and Electronic Systems*, Vol. 44, no. 1, pp. 99 – 110, January 2008.

[10] Tihamér Adám, Samad Dadvandipour, József Futás, "Influence of discretization method on the digital control system performance," *Acta Monanistica Slovaca*, vol. 8, no. 4, pp. 197 – 200, 2003.

[11] T. Robbins, "Fuse model for over-current protection simulation of dc distribution systems," *in Proc. INTELEC 1993.*

[12] Ming Zou, Jen Mahseredjian, Geza Joos, Benoît Delourme, Luc Gérin-Lajoie, "Interpolation and reinitialization for the simulation of power electronic circuits," *International Conference on Power Systems Transients – IPST*, 2003, New Orleans.

[13] Kai Strunz, "Flexible Numerical Integration for Efficient Representation of Switching in Real Time Electromagnetic Transients Simulation," *IEEE Trans. on Power Delivery*, Vol. 19, No. 3, pp. 1276 – 1283, July 2004.

[14] Barry W. Williams, *Power electronics: devices, drivers, applications, and passive components*. Available http://www.eee.strath.ac.uk/~bwwilliams (accessed 11/05/2009)

[15] I. M. Elders, P. J. Norman, J. D. Schuddebeurs, C. D. Booth, G. M. Burt, J. R. McDonald, J. Apsley, M. Barnes, A. Smith, S. Williamson, S. Loddick and I. Myers, "Modelling and analysis of electro-mechanical interactions between prime-mover and load in a marine IFEP system," *Proc. 2007 IEEE Electric Ship Technologies Symposium (ESTS)*, 2007, Arlington, Virginia, 2007.

[16] Liebherr Aerospace, “Power Optimised Aircraft”, Available at: http://www.poa-project.com (accessed 13/10/2008)

[17] Richard Newman, “The more electric engine concept,” *SAE Technical Papers*, document number: 2004-01-3128.

[18] *Using Matlab*, The Mathworks Inc., 3 Apple Hill Drive, Natick, MA, USA, 2002.

[19] Lok-Fu Pak, Omar Faruque, Xin Nie, Venkata Dinavahi, “A versatile cluster-based real-time digital simulator for power engineering research,” *IEEE Trans. on Power Systems*, vol. 21, no. 2, May 2006, pp. 455 - 465.

[20] Roger Champagne, Louis-A. Dessaint, Handy Fortin-Blanchette, Gilbert Sybille, “Analysis and validation of a real-time AC drive simulator,” *IEEE Trans. on Power Electronics*, vol. 19, no. 2, March 2004, pp. 336 - 345.

7 Advanced Functional Modelling

7.1. Chapter Overview

This chapter proposes a new technique for the modelling and simulation of power electronic converters which is based upon the existing functional modelling approach [1, 2] described in Chapter 5, and is thus a major contribution of this thesis. This technique, Advanced Functional Modelling (AFM) provides substantial improvements in the numerical stability of the converter model during both normal and faulted conditions compared with the original functional modelling technique. In addition, it still provides similar levels of reduction in the computational requirement of simulating power electronic converters. This technique is also completely compatible with the Multi-Level Model Discretization technique described in Chapter 6 and is ideally suited to the network level modelling and simulation of marine and aerospace more-electric architectures.

This chapter will present the core principles of the AFM technique, accommodating aspects such as the representation of time-averaged converter behaviour and the impact of complex network impedances, illustrating these aspects through a simple case study based on a single-phase inverter. The chapter will then move on to develop the core principles of AFM and apply them to other converter topologies, thus demonstrating the versatility of the proposed method. The wider application of the AFM technique to larger marine and aerospace more-electric network architectures and the difficulties associated with this are addressed. A selection of simulation results are then presented to reinforce the core theory presented in the

chapter. Finally, options for developing the AFM technique further are discussed before the chapter concludes with a general review of the technique's potential benefits to the network-level modelling and dynamic simulation of marine and aerospace more-electric network architectures.

This chapter is presented in three parts.

- Part I describes the core concepts of the AFM technique and applies them to a single phase inverter case study.
- Part II applies the core concepts of the AFM technique to other converter topologies to illustrate its versatility.
- Part III investigates the robustness of the AFM technique when it is implemented within models of large electrical networks like those found in marine and aerospace more-electric applications. A case study is also included to illustrate the operation of the AFM.

Part I – The Core Concepts of the Advanced Functional Modelling Technique

7.2. (I) Introduction and Justification for Research

Chapter 5 concluded by expressing the need to develop novel methods for the network-level modelling and dynamic simulation of electrical networks with a significant penetration of power electronics that could address two separate goals. These goals are:

- Develop a method which facilitates the computationally efficient simulation of switched models of power electronic converters.
- Develop a method which improves the numerical stability of functional converter models in order to restore their accuracy during the simulation of normal (i.e. unfaulted) and simulated fault conditions.

The first goal has been addressed in Chapter 6. The technique proposed, Multi-Level Model Discretization (MLMD), allows diode bridge converter models to be simulated efficiently and accurately (which is difficult to achieve with functional models) and is compatible with functional models of other converter topologies. This technique, although not as computationally efficient as the functional modelling technique, is accurate during simulated fault conditions and as such, also provides a useful default position for instances when functional converter models are unreliable. The current chapter will address the second goal by proposing a new method, Advanced Functional Modelling (AFM), which incorporates novel features into the

functional modelling technique to address the numerical stability issues associated with it. The remainder of this chapter shall present the AFM method and evaluate its capabilities and limitations for a range of potential applications.

7.3. (I) The Advanced Functional Modelling (AFM) Concept

This section will introduce the core concepts and design objectives of the Advanced Functional Modelling (AFM) technique. For greater clarity, these concepts will be demonstrated using a single-phase inverter as a case study. Other converter topologies will also be considered later in this chapter.

7.3.1 (I) Review of a Single-Phase Functional Inverter Model

The first stage of developing the AFM is to establish clear design objectives. This can be achieved by first revisiting the stability analysis for a single phase functional inverter model, originally conducted in Chapter 5. By identifying the cause of the numerical instability in this model (and indeed functional models of other converter topologies), a greater appreciation on how to resolve this issue will be gained.

The single phase functional inverter model is based upon the operation of a single-phase switched inverter model. A schematic for this switched model is shown in figure 7.1.

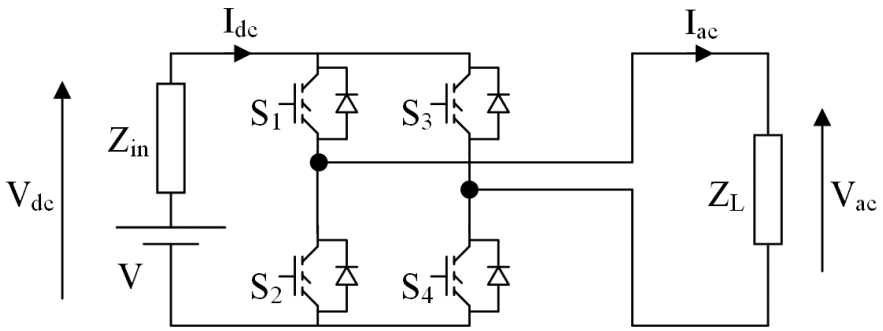

Fig. 7.1. Single-phase switched inverter model

The operation of the single phase switched inverter model is defined by

$$V_{ac} = k_s V_{dc} \tag{7.1}$$

$$V_{dc} = V - I_{dc} Z_{in} \tag{7.2}$$

$$I_{dc} = k_s I_{ac} \tag{7.3}$$

$$I_{ac} = \frac{V_{ac}}{Z_L}, \tag{7.4}$$

where V is the magnitude of the ideal voltage source and is constant. The component Z_{in} is the dc side source impedance and Z_L is the ac side load impedance respectively. The terms V_{ac}, V_{dc}, I_{ac} and I_{dc} are the magnitudes of the ac and dc side voltages and currents respectively. These latter terms are determined by the states of the inverter switches (S_1, S_2, S_3 and S_4). These states are described by the variable k_s, which is defined as

$$k_s = (S_1 - S_3), \tag{7.5}$$

where S_j is the j-th switch state, defined as

$$S_j = \begin{cases} 1 & if \quad closed \\ 0 & otherwise \end{cases} \qquad \text{for } j = 1,2,3,4\,. \qquad (7.6)$$

The states of switches S_2 and S_4 are described by the expressions below,

$$S_2 = 1 - S_1 \qquad (7.7)$$

$$S_4 = 1 - S_3\,. \qquad (7.8)$$

As discussed in Chapter 5, the functional model of the single phase inverter replicates the terminal conditions of the switched inverter model without specifically simulating any of the switching action (utilising controlled voltage and current sources instead). This approach gives rise to significant reductions in the computational requirement of simulations conducted. The schematic of the functional equivalent model of the inverter is illustrated in figure 7.2.

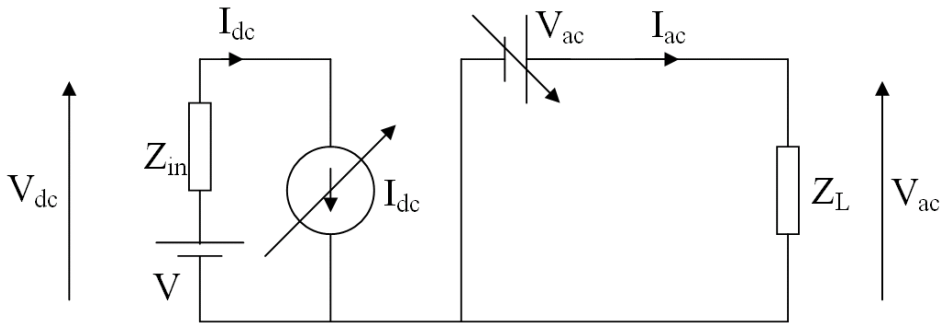

Fig. 7.2. Single-phase functional inverter model

Figure 7.2 illustrates how the terminal conditions of the inverter (V_{ac} and I_{dc}) are now produced by controlled voltage and current sources respectively. Note that it is also necessary to implement a unit delay in the functional model, located in the feedback path of I_{ac}, to remove the algebraic loop present (this was also discussed in Chapter 5). Incorporating this addition, the operation of the functional model is defined as

$$V_{ac}^{(n)} = k_s^{(n)} V_{dc}^{(n)} \tag{7.9}$$

$$V_{dc}^{(n)} = V - I_{dc}^{(n)} Z_{in} \tag{7.10}$$

$$I_{dc}^{(n)} = k_s^{(n)} I_{ac}^{(n-1)} \tag{7.11}$$

$$I_{ac}^{(n)} = \frac{V_{ac}^{(n)}}{Z_L} \tag{7.12}$$

$$k_s^{(n)} = \left(S_1^{(n)} - S_3^{(n)} \right) \tag{7.13}$$

$$S_j^{(n)} = \begin{cases} 1 & \textit{if} \quad \textit{closed at time step (n)} \\ 0 & \textit{otherwise at time step (n)} \end{cases} \qquad \text{for } j = 1,2,3,4 . \tag{7.14}$$

$$S_2^{(n)} = 1 - S_1^{(n)} \tag{7.15}$$

$$S_4^{(n)} = 1 - S_3^{(n)} . \tag{7.16}$$

In this notation, *(n-1)* and *(n)* are subsequent simulation time steps. In this manner, the magnitude of I_{dc} is determined by that of I_{ac} from the previous time step (equation (7.11)). Note that Z_L, Z_{in} and V are assumed to be constant in the analysis conducted in this chapter. While it is possible that these terms may vary from one time step to the next this aspect remains to be studied further. It is anticipated however, that the analysis presented in this and later sections can be readily adapted to accommodate variations in Z_L, Z_{in} and V.

The transfer function of the functional inverter can be derived by combining equations (7.9) through to (7.12) to give

$$V_{ac}^{(n)} = k_s^{(n)} V - \left(k_s^{(n)}\right)^2 V_{ac}^{(n-1)} \frac{Z_{in}}{Z_L}. \qquad (7.17)$$

Equation (7.17) is an example of a first order recurrence relation (see Chapter 5) which has the general solution (for V_{ac} at stage N),

$$V_{ac}^{(N)} = k_s^{(N)} V \sum_{i=0}^{N} \left(-1\right)^i C^i , \qquad (7.18)$$

where

$$C = \left(k_s^{(N)}\right)^2 \frac{Z_{in}}{Z_L}. \qquad (7.19)$$

For numerical stability, it is necessary that $|C|<1$. By considering the range of values for k_s, the condition for stability is only guaranteed if $Z_L>Z_{in}$ (see Chapter 5). A short circuit fault at, or close to the ac terminals of the inverter is unlikely to meet this criterion for stability and that the model will then become inaccurate and possibly even unbounded (resulting in failed simulations). Analyses of other converter topologies conducted also gives rise to similar findings. Hence, despite the attractive characteristics of low computational requirements and ease of implementation, the highlighted shortcoming of functional converter models dictates that they are only of

limited usefulness for application to the network-level modelling and dynamic simulation of marine and aerospace more-electric architectures (where the simulation of fault conditions is often of significance [3, 4]).

Thus, in order for functional converter models to be of any real value to the marine and aerospace applications, numerical stability and accuracy during simulated fault conditions must be restored.

7.3.2 (I) AFM Objectives

Building upon the previous section, this section will identify how the highlighted weakness of the functional modelling approach can be overcome. It will then define the design objectives of the AFM technique accordingly so that this goal might be achieved.

In the case study provided in the previous section, it is the delayed term in the transfer function for V_{ac} that introduces the finite limits to the numerical stability of the single-phase functional inverter model. It is worth reiterating at this stage that that it is possible to run the functional model without a unit delay present in the feedback path of the measured variable. By doing so, the algebraic loop is left intact and no delayed term is present in the transfer function for V_{ac}. As such, the single-phase functional inverter would be numerically stable under simulated ac side fault conditions. Indeed, Chapters 4 and 5 discuss that this is the preferred solution if the network model is small and of a simple nature (and hence readily solved). However, for larger, more complicated networks which are more computationally challenging

to solve (such as marine and aerospace more-electric architectures), the presence of algebraic loops will result in significantly slowed or even failed simulations. Chapter 4 discusses how the use of unit delays to remove these algebraic loops is the only practical solution to this issue. However, as shown in Chapters 4 and 5, the presence of these delays can degrade the numerical stability of the model to unacceptable levels under some operating conditions.

Hence, in order for the functional modelling approach to be viable for use within dynamic models of complex electrical network architectures, such as those found in marine and aerospace more-electric applications, a new method needs to be developed. This method must retain the use of unit delays to remove the algebraic loops present in the model whilst somehow replacing the delayed terms in its transfer function with non-delayed equivalent terms. By doing this, the accuracy of the functional model will be retained whilst its numerical stability under all operating conditions is guaranteed. In this manner, a robust method for reducing the computational requirements of simulating power electronic converters will have been developed.

The design specification outlined above can be achieved by the successful completion of the following two design objectives:

- Incorporate additional delayed feedback terms into the control algorithms of the functional model in order to negate the existing delayed terms in its transfer function.

- Include additional non-delayed terms into the transfer function of the model to restore accuracy to its terminal conditions.

The following section will illustrate how these design objectives can be implemented, using a single-phase functional inverter model for illustration purposes.

7.4. (I) The AFM Concept Applied to a Single-Phase Inverter – Lumped-Parameter Model

As discussed in the previous section, the AFM method aims to replace all the delayed terms in the transfer function of the original functional model with non-delayed equivalents in order to guarantee the numerical stability of this model whilst still accurately representing the terminal conditions of the original switched model. This section will demonstrate how this approach can be implemented, using a single phase inverter as a case study.

There are two variations in the manner in which the AFM can be implemented in a single-phase inverter, each has different merits and drawbacks (these will be addressed in section 7.7). The 'lumped-parameter' model, which introduces the minimum number of new model features, will be introduced first as this is also the simplest configuration. Later, the 'per-phase' model, which distributes the new model features evenly across the terminals of the converter, will be discussed. This

latter format also allows the core AFM concepts to be more easily extrapolated to accommodate three-phase converters.

Consider the single-phase AFM inverter model illustrated in figure 7.3. The converter boundary illustrated in this figure indicates where the ac and dc terminals of the original switched inverter would lie. In this manner, any components inside this boundary are considered part of the converter model and any components located outside of the boundary are parts of the external circuit.

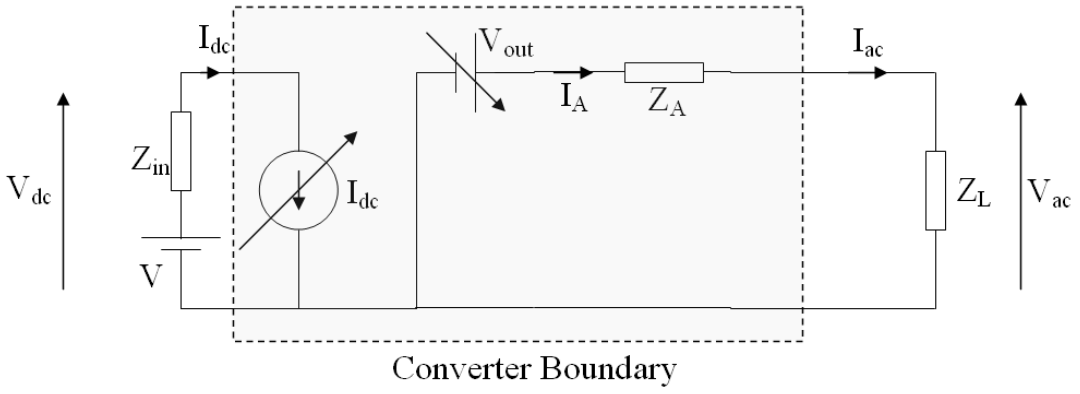

Fig. 7.3. Single-phase 'lumped-parameter' inverter AFM

The following equations define the operation of this model,

$$V_{out}^{(n)} = k_s^{(n)} V_{dc}^{(n)} + X_A^{(n)} \qquad (7.20)$$

$$V_{dc}^{(n)} = V - I_{dc}^{(n)} Z_{in} \qquad (7.21)$$

$$I_{dc}^{(n)} = k_s^{(n)} I_{ac}^{(n-1)} \qquad (7.22)$$

$$I_{ac}^{(n)} = \frac{V_{out}^{(n)}}{Z_L + Z_A^{(n)}}, \qquad (7.23)$$

where *(n-1)* and *(n)* are subsequent simulation time steps and the definition of k_s remains the same as with the original functional model (equation 7.5)). The term X_A is an additional delayed voltage term implemented through the controlled voltage source, V_{out}. The term Z_A is a dynamic impedance component added to the terminals of the AFM. As such, the effective boundary of this AFM inverter is different to the original functional model. The terminals of the controlled voltage source no longer represent the boundary of the model. Instead, V_{ac} now represents the ac voltage output of the AFM model (the notation is deliberately consistent with the original functional model) and is defined by

$$V_{ac}^{(n)} = V_{out}^{(n)} - I_{ac}^{(n)} Z_A^{(n)}. \qquad (7.24)$$

Combining equations (7.20), (7.21), (7.22) and (7.23) gives the transfer function (for V_{out}) of the AFM inverter to be

$$V_{out}^{(n)} = k_s^{(n)} V - \frac{\left(k_s^{(n)}\right)^2 V_{out}^{(n-1)} Z_{in}}{Z_L + Z_A^{(n)}} + X_A^{(n)}. \qquad (7.25)$$

Substituting this into equation (7.24) gives an AFM ac output voltage of

$$V_{ac}^{(n)} = k_s^{(n)} V - \frac{\left(k_s^{(n)}\right)^2 V_{out}^{(n-1)} Z_{in}}{Z_L + Z_A^{(n)}} + X_A^{(n)} - I_{ac}^{(n)} Z_A^{(n)}. \qquad (7.26)$$

Equation (7.26) can now be utilised in the derivation of X_A.

7.4.1 (I) Derivation of the Variable X_A

In keeping with the first objective of the AFM technique (removal of all delayed terms from the converter transfer function) it is desirable to configure the voltage X_A so that it cancels out the delayed term in equation (7.26). Doing this gives X_A as

$$X_A^{(n)} = \frac{\left(k_s^{(n)}\right)^2 V_{out}^{(n-1)} Z_{in}}{Z_L + Z_A^{(n)}}. \qquad (7.27)$$

It is undesirable to implement this expression though, as Z_L and Z_{in} may not be known in complex networks. This position can be improved upon however by recalling the definition of I_{ac} from equation (7.23) and substituting it into equation (7.27), giving

$$X_A^{(n)} = \left(k_s^{(n)}\right)^2 I_{ac}^{(n-1)} Z_{in}. \qquad (7.28)$$

This expression can be further reduced by utilising equation (7.22) to give

$$X_A^{(n)} = k_s^{(n)} I_{dc}^{(n)} Z_{in}. \qquad (7.29)$$

Equation (7.29) represents a much more workable solution as the current I_{dc} has already been derived as part of the functional model output and a knowledge of the load impedance Z_L is no longer required. However, this expression is still dependant on a knowledge of the source internal impedance Z_{in}. In addition to the difficulty of establishing the magnitude of this impedance in complex networks, the requirement

for knowledge about the external electrical network also infringes upon one of the key strengths of the functional modelling technique, its modularity and ease of implementation.

However, it is not possible to readily remove the Z_{in} term from the expression for X_A without creating a further algebraic loop. For example, consider equation (7.21) rearranged to give $I_{dc}Z_{in}$ as the subject:

$$I_{dc}^{(n)} Z_{in} = V - V_{dc}^{(n)}. \qquad (7.30)$$

Substituting this into the expression for X_A in equation (7.29) gives

$$X_A^{(n)} = k_s^{(n)} \left(V - V_{dc}^{(n)} \right). \qquad (7.31)$$

At a first glance, this approach appears to provide the ideal solution, where a knowledge of Z_{in} is no longer required to implement X_A. However, substituting equation (7.31) into the expression for V_{out} given by equation (7.25) creates an algebraic loop. This is a result of the existing direct dependence of V_{dc} upon V_{out} which in turn is now a function of V_{dc}, hence forming the algebraic loop. Given the discussions earlier in this thesis regarding the problems of algebraic loops within functional models of power electronic converters, this is an unacceptable solution. Additionally, a knowledge of the ideal source voltage magnitude is also required to implement this solution, which may be particularly difficult to derive in complex network models or those containing a rectified ac voltage source.

Other approaches investigated to remove the Z_{in} term from X_A result in similar findings. As such, the expression for X_A given in equation (7.29) represents the preferred solution. The noted drawback of the required knowledge of Z_{in} will be re-addressed at a later stage in the chapter where the extent to which this limits the effectiveness of the AFM technique will also be evaluated.

Substituting X_A (equation (7.29)) into the expression for V_{ac} in equation (7.26) gives

$$V_{ac}^{(n)} = k_s^{(n)} V - \frac{\left(k_s^{(n)}\right)^2 V_{out}^{(n-1)} Z_{in}}{Z_L + Z_A^{(n)}} + k_s^{(n)} I_{dc}^{(n)} Z_{in} - I_{ac}^{(n)} Z_A^{(n)} . \tag{7.32}$$

Based on the derivation of X_A (given in equation (7.27)), this can be reduced to

$$V_{ac}^{(n)} = k_s^{(n)} V - I_{ac}^{(n)} Z_A^{(n)} . \tag{7.33}$$

Hence, equation (7.33) illustrates the effectiveness of the X_A term in removing the delayed components from the converter output voltage V_{ac} (and thus from the transfer function of the model too). As such, whilst the single-phase inverter AFM is not necessarily accurate at this stage of its development (this depends on the definition of Z_A), it is no longer at risk of becoming numerically unstable as a result of algebraic loops or unit delays, **regardless of external circuit conditions**. The AFM is hence numerically stable even during simulated fault conditions, where the original functional modelling technique was shown to be unreliable (see Chapter 5).

It is important to note that although the derivation for X_A is based on a scenario where no other system impacts on the magnitude of V_{dc}, the derivation presented is still effective when this is not the case. For example, consider a second scenario where there is additional loading on the dc side of the inverter, drawing a current, I_{other}, from the voltage source. In this manner, the expression for V_{dc} becomes

$$V_{dc}^{(n)} = V - \left(I_{dc}^{(n)} + I_{other}^{(n)}\right) Z_{in}, \qquad (7.34)$$

where I_{dc} is the component of the total dc current being drawn by the inverter. In this manner V_{ac} becomes

$$V_{ac}^{(n)} = k_s^{(n)} \left(V - \left(I_{dc}^{(n)} + I_{other}^{(n)}\right) Z_{in}^{(n)}\right) + X_A^{(n)} - I_{ac}^{(n)} Z_A^{(n)}. \qquad (7.35)$$

Implementing the substitution for X_A (given in equation (7.29)), the expression for V_{ac} reduces to

$$V_{ac}^{(n)} = k_s^{(n)} \left(V - I_{other}^{(n)} Z_{in}^{(n)}\right) - I_{ac}^{(n)} Z_A^{(n)}. \qquad (7.36)$$

Equation (7.36) illustrates how the delayed component in the expression for V_{ac} has been removed, whilst the impact of other dc systems on the magnitude of V_{dc} is still successfully accounted for. In this manner, the case study presented illustrates how the AFM approach maintains the adaptive characteristics of the original functional modelling method, allowing it to be readily and reliably implemented in a variety of applications.

7.4.2 (I) Derivation of Impedance Z_A

The next stage in the development of the AFM is the derivation of impedance Z_A. Whilst the inclusion of X_A guarantees the numerical stability of the AFM, the terminal quantities of this model no longer replicate those of the switched inverter model. This is clearly an unacceptable result.

In order to compensate for the inclusion of X_A, the magnitude of the additional impedance Z_A should be appropriately set so that the ac voltage output of the converter model is an accurate representation of the original switched model again. By doing this, the accuracy will also be restored to all other terminal quantities of the model. This desired output ($V_{ac\text{-}desired}$) is

$$V_{ac-desired}^{(n)} = k_s^{(n)} V_{dc}^{(n)} . \qquad (7.37)$$

Therefore, it is required that

$$V_{ac}^{(n)} = V_{ac-desired}^{(n)} . \qquad (7.38)$$

Substituting for both sides gives

$$k_s^{(n)} V - I_{ac}^{(n)} Z_A^{(n)} = k_s^{(n)} V_{dc}^{(n)} . \qquad (7.39)$$

Substituting for V_{dc} on the right hand side of equation (7.39) gives

$$k_s^{(n)} V - I_{ac}^{(n)} Z_A^{(n)} = k_s^{(n)} \left(V - I_{dc}^{(n)} Z_{in} \right). \qquad (7.40)$$

Now recall from equation (7.3) that the correct relationship between I_{dc} and I_{ac} in a switched model (i.e. one that does not require the use of a unit delay in the feedback path of I_{ac} to remove the algebraic loop) is

$$I_{dc}^{(n)} = k_s^{(n)} I_{ac}^{(n)}. \qquad (7.41)$$

Substituting equation (7.41) into the right hand side of equation (7.40) produces

$$k_s^{(n)} V - I_{ac}^{(n)} Z_A^{(n)} = k_s^{(n)} V - \left(k_s^{(n)} \right)^2 I_{ac}^{(n)} Z_{in}. \qquad (7.42)$$

Therefore, in order for equation (7.42) to be balanced it is necessary that

$$Z_A^{(n)} = S_A^{(n)} Z_{in}, \qquad (7.43)$$

where S_A is defined as

$$S_A = \left(k_s^{(n)} \right)^2. \qquad (7.44)$$

Figure 7.4 illustrates how the expression for Z_A can be implemented within the AFM. The dotted boundary represents the terminals of this impedance element.

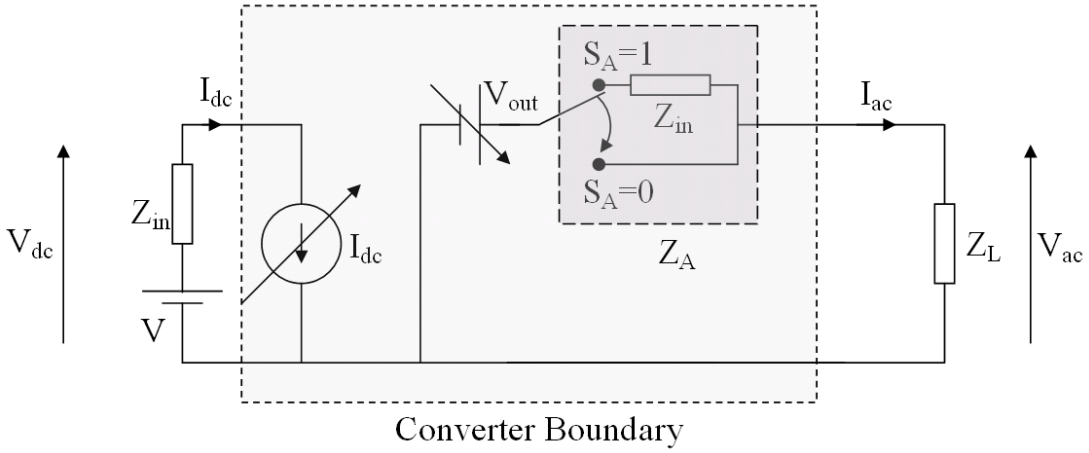

Fig. 7.4. Revised single-phase 'lumped-parameter' inverter AFM

The ac output voltage of the AFM inverter is now defined by

$$V_{ac}^{(n)} = k_s^{(n)} V - \left(k_s^{(n)}\right)^2 I_{ac}^{(n)} Z_{in}, \qquad (7.45)$$

which equates to

$$V_{ac}^{(n)} = k_s^{(n)} V_{dc}^{(n)}. \qquad (7.46)$$

Hence the output of the switched inverter model has been successfully replicated without utilising any delayed terms (hence guaranteeing the numerical stability of the converter model). It should be noted that by restoring the accuracy of V_{ac}, the accuracy of all other terminal quantities of the model is also restored.

It is worth highlighting at this stage that the inclusion of the controlled switch within the AFM will clearly increase the computational burden of the model in comparison

with the original functional model. This increase will be less notable with time-averaged AFM models, where S_A will only operate at considerably lower switching frequency than in pulsed output models. This aspect will be considered in more detail in subsequent sections.

Despite this drawback, by employing the new term X_A and the new impedance Z_A, the AFM has successfully met its objectives of replacing all the delayed terms with non-delayed equivalent terms in the transfer function of the original functional model. By doing this it guarantees numerical stability under all operating conditions whilst accurately replicating the behaviour of the original switched converter model.

7.4.3 (I) Determining the Magnitude of Impedance Z_{in}

The previous section discusses the need to derive internal source impedance, Z_{in}, in order to apply this within the AFM control equations and Z_A, and hence implement the single phase inverter AFM successfully. This section will present the approach for determining the magnitude of this impedance.

The impedance Z_{in} can be found by considering the magnitude of the dc source impedance, as seen by the ac side load. This is effectively the Thevenin equivalent impedance [5] as seen from the relevant converter terminals. To demonstrate this, consider switched inverter model shown in figure 7.5.

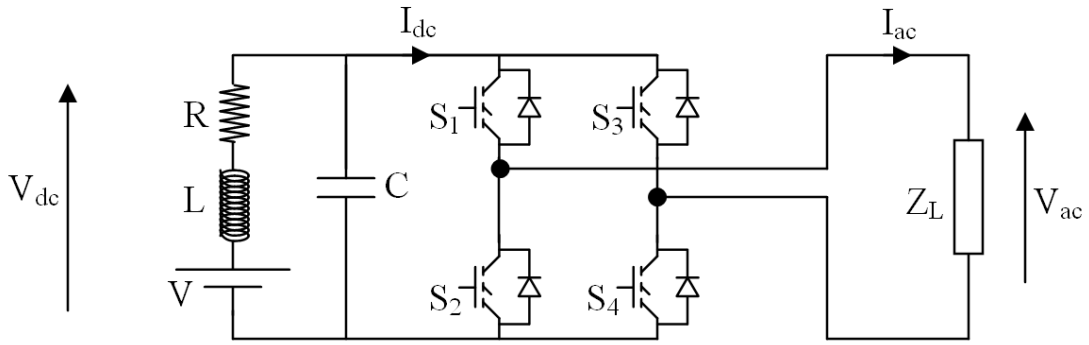

Fig. 7.5. Single-phase inverter with RLC internal impedance

The Thevenin equivalent source impedance is calculated from the dc terminals of the inverter. This process is illustrated in figure 7.6 where all the impedance elements to the left of switches S_1 and S_2 have been accounted for and the ideal voltage source V has been short-circuited (as part of the Thevenin impedance derivation approach).

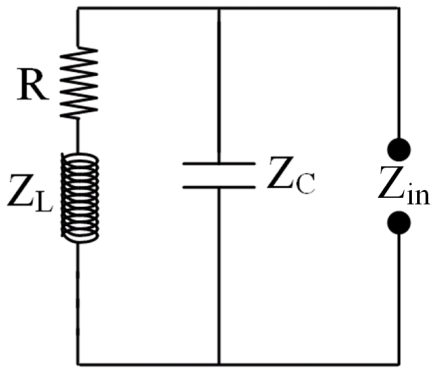

Fig. 7.6. Thevenin equivalent source impedance, Z_{in}

In this arrangement, the Thevenin equivalent impedance, Z_{in}, is the parallel combination of Z_C with R and Z_L, and is defined by

$$Z_{in} = (R + Z_L) // Z_C , \qquad (7.47)$$

where '//' denotes a parallel combination of impedances and '+' denotes a series connection of impedances. The term Z_L is the impedance of the inductor and is defined by

$$Z_L = j\omega L. \qquad (7.48)$$

The term Z_C is the impedance of the capacitor and is defined by

$$Z_C = \frac{1}{j\omega C}. \qquad (7.49)$$

Substituting equations (7.48) and (7.49) into equation (7.47) and expanding gives

$$Z_{in} = \frac{\frac{R}{j\omega C} + \frac{j\omega L}{j\omega C}}{R + j\omega L + \frac{1}{j\omega C}}. \qquad (7.50)$$

By performing some algebra, this expression can be reduced to

$$Z_{in} = \frac{R + j\omega L}{j\omega RC - \omega^2 LC + 1}. \qquad (7.51)$$

Equation (7.51) can be expressed within the Laplace domain to provide easier implementation within power system simulation software packages, giving

$$Z_{in} = \frac{sL + R}{s^2 LC + sRC + 1}, \qquad (7.52)$$

where

$$s = j\omega. \qquad (7.53)$$

Clearly this process becomes more complicated if there are larger numbers of impedances in the circuit. This aspect will be considered later.

Figure 7.7 illustrates how the derived Thevenin equivalent impedance (Z_{in}), given in equation (7.52) can be incorporated into the single phase inverter AFM.

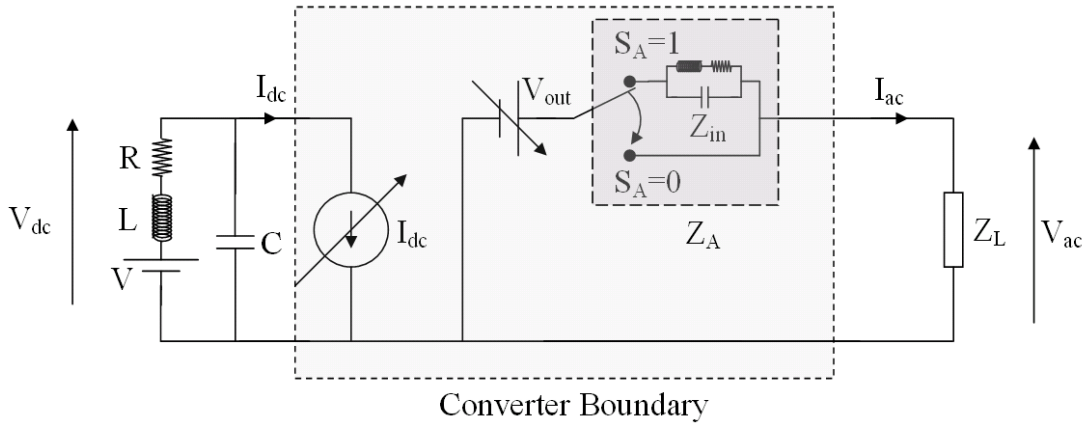

Fig. 7.7. Revised single-phase 'lumped-parameter' inverter AFM with Z_{in} implemented

7.5. (I) Time-averaged AFM Representation

In the analyses of the functional and AFM inverter models presented so far (and indeed of other functional converter models presented in Chapter 5), the equations of operation presented only apply to models with a pulsed output. In order to implement models with time-averaged terminal conditions, subtle modifications must be made to the equations of operation in order to achieve accurate simulation results.

This section will present the modifications necessary to achieve accurate model behaviour, initially for the functional modelling approach and then the AFM approach. A case study of a single phase inverter will be utilised to aid the illustration of this concept.

7.5.1 (I) Modifications to the Functional Model Equations

Consider the equations of operation for the pulsed functional inverter model given earlier in equations (7.9) through to (7.16). The key equations to observe are those for V_{ac} and I_{dc} which are

$$V_{ac} = k_s^{(n)} V_{dc} \tag{7.54}$$

$$I_{dc}^{(n)} = k_s^{(n)} I_{ac}^{(n-1)}, \tag{7.55}$$

where

$$k_s^{(n)} = \left(S_1^{(n)} - S_3^{(n)}\right), \tag{7.56}$$

where *(n-1)* and *(n)* are subsequent simulation time steps. For pulsed models, k_s will only hold values of *1*, *0* or *-1*. However, for time averaged models, k_s will vary continuously between *1* and *-1*, effectively implementing the underlying modulation wave employed in the pulse generation circuit of the converter model [2, 6]. Under these conditions, the expression for V_{ac} given in equation (7.54) is still correct and will now produce the required time-averaged ac voltage. However, the expression for I_{dc} is incorrect. Even in time-averaged conditions, the magnitude of I_{dc} should match that of I_{ac}. In the present expression (equation (7.55)), I_{dc} is (wrongly) attenuated by the multiplying factor of k_s. As such, it is necessary to modify the equations of operation for the functional model, and indeed the associated AFM to properly represent the time-averaged conditions of the converter. This can be achieved by introducing a new variable, k_{dc}, which is defined as

$$k_{dc}^{(n)} = \begin{cases} 1 & \text{for } 0 < k_s^{(n)} \le 1 \\ 0 & \text{for } k_s^{(n)} = 0 \\ -1 & \text{for } -1 \le k_s^{(n)} < 0 \end{cases} . \qquad (7.57)$$

The expression for I_{dc} of the functional model now becomes

$$I_{dc}^{(n)} = k_{dc}^{(n)} I_{ac}^{(n-1)} . \qquad (7.58)$$

Hence, the magnitude of I_{dc} is no longer attenuated and matches that of I_{ac}. In this manner, the accuracy of I_{dc} and indeed all the outputs of the time-averaged model is restored. All other equations of operation for the functional model remain the same as given before. Note that the stability criterion of the functional model is not

affected by this modification as the maximum magnitude of k_{dc} is the same as k_s. Also note that equation (7.58) still holds true for functional models and AFMs with pulsed outputs (where $k_s = k_{dc}$).

7.5.2 (I) Modifications to the AFM Equations

This section will show how the representation of a time-averaged converter output also requires additional changes to be made to the equations of operation for the AFM in order to maintain its accuracy. The impact of these modifications on the numerical stability of the AFM will also be considered and guidelines for the implementation of time-averaged AFMs will be given.

If the updated expression for I_{dc} given in equation (7.58) is implemented in the lumped-parameter AFM model, this impacts on the magnitude Z_A. Note that X_A is not directly affected however (see equation (7.29)). To demonstrate this impact on Z_A, consider the expression for the desired ac voltage output ($V_{ac\text{-}desired}$) of the time-averaged lumped-parameter AFM model (originally given in equation (7.37)).

$$V_{ac-desired}^{(n)} = k_s^{(n)} V_{dc}^{(n)} . \qquad (7.59)$$

Expanding this in the same manner as illustrated in section 7.4.2 but this time accommodating the updated expression for I_{dc} gives

$$V_{ac-desired}^{(n)} = k_s^{(n)} V - k_s^{(n)} k_{dc}^{(n)} I_{ac}^{(n)} Z_{in} . \qquad (7.60)$$

As before, the ac terminal voltage, V_{ac} (given in equation (7.33)) of the AFM inverter should match that of the switched inverter ($V_{ac\text{-}desired}$). This gives

$$k_s^{(n)}V - I_{ac}^{(n)}Z_A^{(n)} = k_s^{(n)}V - k_s^{(n)}k_{dc}^{(n)}I_{ac}^{(n)}Z_{in}. \qquad (7.61)$$

Going through the same process as that used in section 7.4.2 (derivation of Z_A), Z_A is hence required to be

$$Z_A^{(n)} = k_s^{(n)}k_{dc}^{(n)}Z_{in}. \qquad (7.62)$$

Equation (7.62) presents an interesting problem for the successful implementation of the time-averaged AFM. Whilst a variable resistor model can be readily implemented in generic simulation packages (i.e. those which require the specific mathematical modelling of each component of the electrical network and are hence not necessarily suited to simulating complex power systems [7]) it is very difficult to implement in most power systems simulation software packages. These packages only permit the implementation of fixed value resistances. Variable resistor models for these packages involve utilising fast acting feedback loops with controlled sources [8], which inherently involve the creation of algebraic loops (which is clearly undesirable). As such, the requirement to utilise a variable resistor model within a time averaged AFM is not a desirable solution.

It is however, possible to implement an alternative expression for Z_A which is close to that given in equation (7.62) and which is of a form that can be readily

implemented within a power systems simulation package without resulting in the creation of algebraic loops. This alternative is given as

$$Z_A^{(n)} = \left(k_{dc}^{(n)}\right)^2 Z_{in} . \qquad (7.63)$$

Whilst this expression is a simplification of the solution given in equation (7.62), it can however be readily implemented into a power systems simulator package as the magnitude of k_{dc}^2 will only be either 1 or 0. It is acknowledged that there will be some degree of error produced by this solution and as such, it is important to evaluate the potential magnitude of this when the expression for Z_A given in equation (7.63) is implemented. Small errors in time-averaged models are often acceptable because of their low fidelity [1, 2]. As such, depending on the level of error produced and the application in question, the expression for Z_A given in equation (7.63) may represent a viable alternative solution to that given in equation (7.62).

7.5.3 (I) Evaluation of the Error in the Averaged AFM Voltage Output

Implementing the single-phase inverter AFM using the expression for Z_A as defined in equation (7.63), the error in V_{ac} (compared to the switched model) will be

$$V_{error}^{(n)} = V_{ac-desired}^{(n)} - V_{ac}^{(n)}, \qquad (7.64)$$

Substituting for $V_{ac\text{-}desired}$, V_{ac} and Z_A (given in equations (7.60), (7.33) and (7.63) respectively) gives

$$V_{error}^{(n)} = \left(k_s^{(n)} V - k_s^{(n)} k_{dc}^{(n)} I_{ac}^{(n)} Z_{in}\right) - \left(k_s^{(n)} V - \left(k_{dc}^{(n)}\right)^2 I_{ac}^{(n)} Z_{in}\right). \tag{7.65}$$

This expression can be reduced to

$$V_{error}^{(n)} = I_{ac}^{(n)} Z_{in} Y_k^{(n)}, \tag{7.66}$$

where

$$Y_k^{(n)} = \left(k_{dc}^{(n)}\right)^2 - k_s^{(n)} k_{dc}^{(n)}. \tag{7.67}$$

The next stage of this analysis is to consider the potential variation in magnitude of Y_k and its components over the full range of k_s. This is shown in table 7.1.

Table 7.1. Variation of Y_k over the range of k_s.

k_s	k_{dc}	k_{dc}^2	$k_s\, k_{dc}$	Y_k
$0 > k_s \geq -1$	-1	1	$\lvert k_s \rvert$	$1-\lvert k_s \rvert$
$k_s = 0$	0	0	0	0
$1 \geq k_s > 0$	1	1	$\lvert k_s \rvert$	$1-\lvert k_s \rvert$

Table 7.1 shows that there is no error in the voltage V_{ac}, of the time-averaged AFM when k_s is equal to zero (i.e. when $S_1 = S_3$). However, this operating condition usually only arises at a rate of twice per cycle of the fundamental frequency of V_{ac},

and typically lasts for only one simulation time step. Therefore, there is nearly always some error present in the time averaged AFM ac voltage output V_{ac}. As such, it is necessary to further analyse the variation in magnitude of this error, which can now be expressed as

$$V_{error}^{(n)} = I_{ac}^{(n)} Z_{in} \left(1 - \left|k_s^{(n)}\right|\right). \qquad (7.68)$$

By examining equation (7.68) and it can be deduced that the maximum error in V_{ac} will occur when the magnitude of k_s is almost zero. However, in most applications, a very small value for k_s will also give a low magnitude of I_{ac}. Conversely, when I_{ac} is at its greatest, k_s will also be at its maximum value. In this way the error in V_{ac} is largely self attenuating and the behaviour of the time-averaged inverter AFM will be a good representation of the switched model in most applications. For these cases, the alternative form of Z_A derived in equation (7.63) is an acceptable solution.

Note that V_{error} (given in equation (7.68)) is dependant on other circuit parameters such as Z_{in}, V and Z_L, as these variables all serve to affect the magnitude of I_{ac}. It is also worth noting that any error present in V_{ac} will also propagate into an error in I_{ac}, I_{dc} and V_{dc} and so on. In other words, the error is not exclusive to V_{ac}.

There is however, one type of application when the error in V_{ac} is not self attenuating. If the AFM is connected to an additional voltage source on its ac side (either for sourcing or sinking power to/from an external power source) the relationship between k_s and I_{ac} changes. Under these conditions, a low magnitude of

k_s may give a large magnitude of I_{ac} and vice versa, possibly leading to the formation of potentially significant errors. Under these operating conditions, it is highly unlikely that the use of the time-averaged inverter AFM will be acceptable.

As such, the following section will explore the use of additional functionality implemented within the time-averaged AFM model as a method for reducing the level of error in V_{ac} for applications where the level of error defined in equation (7.68) is not acceptable.

7.5.4 (I) Additional Functionality for the Time Averaged Inverter AFM

This section will propose and evaluate a method for reducing the level of error in V_{ac} for the time averaged inverter AFM. It can be employed in applications where V_{error} (see equation (7.68)) is considered too great. The proposed method involves incorporating additional delayed variables into the expression for V_{out}, which up to this point, the AFM approach has previously gone to great lengths to avoid because of the possibility of creating numerical instability. However, this section will go on to show how the numerical stability of the AFM model is still guaranteed under all conditions even with the addition of these particular delayed terms.

It should be noted though that the more generic modelling languages which can accommodate a variable resistor model without creating algebraic loops (as discussed in section 7.5.3) have no requirement for the solution presented here.

The proposed method sees an extra variable term added to the ac voltage output of the AFM (V_{out}) in order to negate the error in V_{ac}. This variable, A_{err}, takes on the magnitude but opposite polarity of the error defined in equation (7.68) and is given by

$$A_{err}^{(n)} = I_{ac}^{(n-1)} Z_{in} \left(- Y_k^{(n)} \right), \qquad (7.69)$$

which gives

$$A_{err}^{(n)} = I_{ac}^{(n-1)} Z_{in} \left(k_s^{(n)} k_{dc}^{(n)} - \left(k_{dc}^{(n)} \right)^2 \right). \qquad (7.70)$$

Notice that the I_{ac} term in equations (7.69) and (7.70) is delayed by one time step in comparison to that of equation (7.68). This use of a delayed I_{ac} term is clearly unattractive as it will have undesirable implications for the numerical stability of the model. However, this position is not easily avoided, as to include a non-delayed measurement of the term I_{ac} would involve introducing an algebraic loop, which is even more undesirable than the presence of a delayed term in equation (7.70). Additionally, this section will go on to show that the numerical stability of the AFM is in fact *not* compromised by the inclusion of the term A_{err}.

It is also worth noting at this stage that with I_{ac} changing from one simulation time step to the next, the use of a delayed I_{ac} term in A_{err} means that the error in V_{ac} will not be completely negated. However, in situations where I_{ac} varies slowly between time steps, like those experienced with time-averaged models, the remaining error in

V_{ac} is likely to be negligible. In most cases, the output of the time-averaged AFM will not be of a high enough fidelity for this level of remaining error to be of any real concern [2].

This section will now consider the operation of the AFM with this delayed term incorporated in order to demonstrate its guaranteed numerical stability.

The full expression for V_{ac} of the time-averaged AFM with the expression for A_{err} (given in equation (7.70)) incorporated is

$$V_{ac}^{(n)} = V_{out}^{(n)} + X_A^{(n)} - A_{err}^{(n)} - I_{ac}^{(n)} Z_A^{(n)} . \qquad (7.71)$$

Using the appropriate substitutions, this can be expanded to

$$V_{ac}^{(n)} = \left(k_s^{(n)} V - k_s^{(n)} I_{dc}^{(n)} Z_{in}\right) + \left(k_s^{(n)} I_{dc}^{(n)} Z_{in}\right) - \left(I_{ac}^{(n-1)} Z_{in} \left(k_s^{(n)} k_{dc}^{(n)} - \left(k_{dc}^{(n)}\right)^2\right)\right) - I_{ac}^{(n)} \left(k_{dc}^{(n)}\right)^2 Z_{in} . \qquad (7.72)$$

Cancelling terms, equation (7.72) can be reduced to

$$V_{ac}^{(n)} = k_s^{(n)} V - I_{ac}^{(n-1)} Z_{in} \left(k_s^{(n)} k_{dc}^{(n)} - \left(k_{dc}^{(n)}\right)^2\right) - I_{ac}^{(n)} \left(k_{dc}^{(n)}\right)^2 Z_{in} . \qquad (7.73)$$

In order to work towards a transfer function for the time-averaged AFM in terms of V_{ac}, the following substitution for I_{ac} will be made

$$I_{ac}^{(n)} = \frac{V_{ac}^{(n)}}{Z_A^{(n)} + Z_L}. \qquad (7.74)$$

This gives

$$V_{ac}^{(n)} = k_s^{(n)} V - \frac{V_{ac}^{(n-1)}}{Z_A^{(n-1)} + Z_L} Z_{in} \left(k_s^{(n)} k_{dc}^{(n)} - \left(k_{dc}^{(n)} \right)^2 \right) - \frac{V_{ac}^{(n)}}{Z_A^{(n)} + Z_L} \left(k_{dc}^{(n)} \right)^2 Z_{in}. \qquad (7.75)$$

Substituting for Z_A and rearranging equation (7.75) gives

$$V_{ac}^{(n)} \left(1 + \frac{\left(k_{dc}^{(n)} \right)^2 Z_{in}}{\left(k_{dc}^{(n)} \right)^2 Z_{in} + Z_L} \right) = k_s^{(n)} V - V_{ac}^{(n-1)} \left(\frac{Z_{in} \left(k_s^{(n)} k_{dc}^{(n)} - \left(k_{dc}^{(n)} \right)^2 \right)}{\left(k_{dc}^{(n-1)} \right)^2 Z_{in} + Z_L} \right), \qquad (7.76)$$

and

$$V_{ac}^{(n)} \left(\frac{2\left(k_{dc}^{(n)} \right)^2 Z_{in} + Z_L}{\left(k_{dc}^{(n)} \right)^2 Z_{in} + Z_L} \right) = k_s^{(n)} V - V_{ac}^{(n-1)} \left(\frac{Z_{in} \left(k_s^{(n)} k_{dc}^{(n)} - \left(k_{dc}^{(n)} \right)^2 \right)}{\left(k_{dc}^{(n-1)} \right)^2 Z_{in} + Z_L} \right). \qquad (7.77)$$

Rearranging equation (7.77) to give V_{ac} as the subject gives

$$V_{ac}^{(n)} = \left(\frac{\left(k_{dc}^{(n)} \right)^2 Z_{in} + Z_L}{2\left(k_{dc}^{(n)} \right)^2 Z_{in} + Z_L} \right) k_s^{(n)} V - V_{ac}^{(n-1)} \left(\frac{Z_{in} \left(k_s^{(n)} k_{dc}^{(n)} - \left(k_{dc}^{(n)} \right)^2 \right)}{\left(k_{dc}^{(n-1)} \right)^2 Z_{in} + Z_L} \right) \left(\frac{\left(k_{dc}^{(n)} \right)^2 Z_{in} + Z_L}{2\left(k_{dc}^{(n)} \right)^2 Z_{in} + Z_L} \right). \qquad (7.78)$$

Adopting a similar approach to the stability analysis conducted on the original functional model earlier in section 7.3.1, it can be shown that this model is numerically stable when

$$\left|\left(\frac{Z_{in}\left(k_s^{(n)}k_{dc}^{(n)}-\left(k_{dc}^{(n)}\right)^2\right)}{\left(k_{dc}^{(n-1)}\right)^2 Z_{in}+Z_L}\right)\left(\frac{\left(k_{dc}^{(n)}\right)^2 Z_{in}+Z_L}{2\left(k_{dc}^{(n)}\right)^2 Z_{in}+Z_L}\right)\right|<1. \tag{7.79}$$

Table 7.2 evaluates this inequality for all combinations of $k_{dc}^{(n-1)}$ and $k_s^{(n)}$, indicating when the criteria for stability is met.

Table 7.2. Evaluation of equation (7.79) over the range of k_s.

$k_{dc}^{(n-1)}$	$k_s^{(n)}$	$k_{dc}^{(n)}$	$\left\|\left(\frac{Z_{in}\left(k_s^{(n)}k_{dc}^{(n)}-\left(k_{dc}^{(n)}\right)^2\right)}{\left(k_{dc}^{(n-1)}\right)^2 Z_{in}+Z_L}\right)\left(\frac{\left(k_{dc}^{(n)}\right)^2 Z_{in}+Z_L}{2\left(k_{dc}^{(n)}\right)^2 Z_{in}+Z_L}\right)\right|$
-1	$0 > k_s \geq -1$	*-1*	< 1
0	$0 > k_s \geq -1$	*-1*	Dependant upon $\|Z_{in}\|$ and $\|Z_L\|$
1	$0 > k_s \geq -1$	*-1*	< 1
-1	$k_s = 0$	*0*	0
0	$k_s = 0$	*0*	0
1	$k_s = 0$	*0*	0
-1	$1 \geq k_s > 0$	*1*	< 1
0	$1 \geq k_s > 0$	*1*	Dependant upon $\|Z_{in}\|$ and $\|Z_L\|$
1	$1 \geq k_s > 0$	*1*	< 1

Table 7.2 illustrates how numerical stability is guaranteed for all but two of the possible operating conditions of the time-averaged inverter. For these two instances, equation (7.79) becomes

$$\left|\left(\frac{Z_{in}\left(\left|k_s^{(n)}\right|-1\right)}{Z_L}\right)\left(\frac{Z_{in}+Z_L}{2Z_{in}+Z_L}\right)\right|<1. \qquad (7.80)$$

From this equation, it would appear that numerical stability is not guaranteed, but is instead a function of the magnitudes of Z_{in}, Z_L and k_s.

Note however, that if k_{dc} at time *(n-1)* is zero, then the magnitude of k_s at time *(n-1)* will also be zero. Substituting these values into equation (7.73) gives $V_{ac} = 0$ at time *(n-1)* under these conditions. As a result of this, the magnitude of the delayed term in equation (7.78) is zero and the time-averaged AFM is in fact completely stable even when the condition set out in equation (7.80) is not met. The implications of the findings presented in this section are discussed in the following section.

7.5.5 (I) Discussion of Alternative Time-Averaged AFM Implementations

The previous sections have shown that two options exist for the implementation of a time-averaged single phase AFM inverter (although the analyses and concepts applied can also be readily extended to other converter topologies). The first is to accept the errors introduced by implementing the impedance Z_A and not include the error correction term A_{err}. The resultant model is numerically stable under all conditions but may not produce acceptable levels of error in some cases. The alternative approach is to implement A_{err} so that the level of error is minimised. This model is also stable under all conditions and will produce less error than the former

method. However, it may exhibit some oscillatory behaviour as a result of the presence of delayed terms in the expression for V_{ac}. Hence, a trade off exists between these two methods and care must be taken when selecting which one to implement.

7.6. (I) The AFM concept applied to a Single-Phase Inverter – Per-Phase Model

This section will present an alternative approach to implementing the AFM technique on a single-phase inverter, the per-phase approach. The core concepts and the manner in which they are implemented will be described before the effectiveness of this AFM approach is evaluated.

Additionally, the following section will build on the material presented thus far in this chapter by considering the comparative advantages and disadvantages of the two alternative AFM methods presented in sections 7.4 and 7.6. The purpose of this comparison will be to illustrate the need for two separate AFM methods and to provide guidelines on their use.

Like the previously described lumped-parameter AFM, the per-phase model aims to replace all the delayed terms in the transfer function of the original functional model with non-delayed equivalents in order to guarantee its numerical stability whilst still accurately representing the terminal conditions of the original switched model. However, the key difference between the per-phase and 'lumped-parameter' approaches is that the former method only utilises one source and thus implements

X_A and Z_A in series with this source, whilst the latter method utilises two controlled voltage sources and evenly distributes the additional AFM features into both of these output lines. This approach adopted in the per-phase AFM has some advantages over the 'lumped-parameter' model (as will be discussed in section 7.7) and is more readily transferable to a three-phase inverter. However, it is also a more complex model architecture and as such has a higher computational requirement.

Figure 7.8 illustrates the circuit schematic of the 'per-phase' representation of a single-phase inverter AFM. As with the lumped-parameter AFM, the converter boundary illustrated in this figure indicates where the terminals of the original switched converter model would lie. In this manner, any components inside this boundary are considered part of the converter model and any components located outside of the boundary are parts of the external circuit.

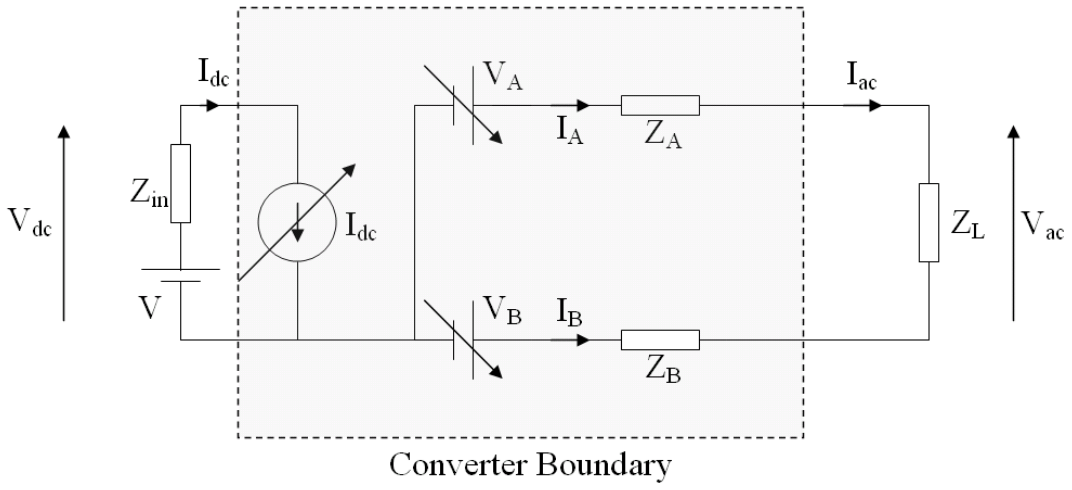

Fig. 7.8. Single-phase 'per-phase' inverter AFM

The operation of this per-phase inverter AFM is governed by the following equations

$$V_A^{(n)} = S_1^{(n)} V_{dc}^{(n)} + X_A^{(n)} \qquad (7.81)$$

$$V_B^{(n)} = S_3^{(n)} V_{dc}^{(n)} + X_B^{(n)} \qquad (7.82)$$

$$V_{dc}^{(n)} = V - I_{dc}^{(n)} Z_{in} \qquad (7.83)$$

$$I_{dc}^{(n)} = S_1^{(n)} I_A^{(n-1)} + S_3^{(n)} I_B^{(n-1)} \qquad (7.84)$$

$$V_{ac}^{(n)} = V_A^{(n)} - V_B^{(n)} - I_A^{(n)} Z_A^{(n)} + I_B^{(n)} Z_B^{(n)}, \qquad (7.85)$$

where *(n-1)* and *(n)* are subsequent simulation time steps, X_A and X_B are additional delayed voltage terms implemented through the controlled voltage sources, V_A and V_B respectively. The definitions of V_{dc}, V_{ac}, I_{dc}, Z_L and Z_{in} remain the same as for the lumped-parameter inverter AFM described in section 7.4. The ac side currents I_A and I_B are artificial variables added in order to simplify later derivations of AFM variables. Note that $I_A = I_{ac} = -I_B$ at any instant in time. The term S_j is the *j*-th switch state at time step *(n)* and is defined as

$$S_j^{(n)} = \begin{cases} 1 & if \quad closed \\ 0 & otherwise \end{cases} \qquad \text{for } j = 1,2,3,4\,. \qquad (7.86)$$

As with the previous case, these equations already take account of the delays in the feedback paths of I_A and I_B which have been added to eliminate the algebraic loops present. Also note that V_{ac} represents the effective ac terminals of the AFM model. Substituting equation (7.83) into equations (7.81) and (7.82) gives expressions for the ac side controlled voltage sources V_A and V_B as

$$V_A^{(n)} = S_1^{(n)} V - S_1^{(n)} I_{dc}^{(n)} Z_{in} + X_A^{(n)} \qquad (7.87)$$

$$V_B^{(n)} = S_3^{(n)} V - S_3^{(n)} I_{dc}^{(n)} Z_{in} + X_B^{(n)}. \qquad (7.88)$$

Equations (7.87) and (7.88) can now be used to derive the voltages X_A and X_B.

7.6.1 (I) Derivation of X_A and X_B

In keeping with the first objective of the AFM technique (removal of all delayed terms from the converter transfer function) it is desirable to configure the voltages X_A and X_B so that they cancel out the middle terms ($S_1 I_{dc} Z_{in}$ and $S_3 I_{dc} Z_{in}$) in equations (7.87) and (7.88), as these derive from the delayed measurements of I_A and I_B (as illustrated in section 7.4.1). Doing this gives X_A and X_B as

$$X_A^{(n)} = S_1^{(n)} I_{dc}^{(n)} Z_{in} \qquad (7.89)$$

$$X_B^{(n)} = S_3^{(n)} I_{dc}^{(n)} Z_{in}. \qquad (7.90)$$

As with the lumped-parameter AFM, these solutions are considered convenient since I_{dc} is already derived as part of the operation of the original functional model. Substituting these expressions into equations (7.87) and (7.88) successfully removes the delayed terms in these equations. As with the lumped-parameter AFM, the per-phase AFM is not accurate at this stage of its development (this still depends on the definition of Z_A and Z_B), but it will not become numerically unstable as a result of algebraic loops or unit delays, regardless of external circuit conditions. As such, the

per-phase AFM is numerically stable even during simulated fault conditions, successfully meeting the first of its design criteria.

7.6.2 (I) Derivation of Z_A and Z_B

As with the lumped parameter AFM, the next stage in the development of the per-phase AFM is the derivation of additional impedances Z_A and Z_B to negate the errors created in its governing equations by the introduction of the terms X_A and X_B. By doing this, the ac voltage output of the AFM will once again be an accurate representation of the original switched model.

From the earlier lumped-parameter example, it is known that the desired ac voltage output (i.e. that which is produced by the original switched model) of the AFM model ($V_{ac\text{-}desired}$) should be

$$V_{ac-desired}^{(n)} = \left(S_1^{(n)} - S_3^{(n)}\right)V_{dc}^{(n)}. \qquad (7.91)$$

Expanding V_{dc} in equation (7.91) in a similar manner to that performed in the derivation of the 'lumped-parameter' inverter AFM gives

$$V_{ac-desired}^{(n)} = \left(S_1^{(n)} - S_3^{(n)}\right)V - \left(S_1^{(n)} - S_3^{(n)}\right)\left(S_1^{(n)} I_A^{(n)} + S_3^{(n)} I_B^{(n)}\right)Z_{in}. \qquad (7.92)$$

Expanding this equation even further allows $V_{ac\text{-}desired}$ to be expressed in the following manner (which will later aid the derivation of expressions for Z_A and Z_B)

$$V_{ac-desired}^{(n)} = \left(S_1^{(n)} - S_3^{(n)}\right)V - \left(\left(S_1^{(n)}\right)^2 - S_1^{(n)}S_3^{(n)}\right)I_A^{(n)}Z_{in} + \left(\left(S_3^{(n)}\right)^2 - S_1^{(n)}S_3^{(n)}\right)I_B^{(n)}Z_{in}. \quad (7.93)$$

Now consider the AFM ac terminal voltage, V_{ac}, incorporating revised expressions for voltages V_A and V_B,

$$V_{ac}^{(n)} = S_1^{(n)}V - S_3^{(n)}V - I_A^{(n)}Z_A^{(n)} + I_B^{(n)}Z_B^{(n)}. \quad (7.94)$$

In order for the ac voltage of the AFM (V_{ac}) given in equation (7.94) to match that of the switched model ($V_{ac\text{-}desired}$) given in equation (7.93), it is necessary that

$$Z_A^{(n)} = S_A^{(n)}Z_{in} \quad (7.95)$$

$$Z_B^{(n)} = S_B^{(n)}Z_{in}, \quad (7.96)$$

where

$$S_A^{(n)} = \left(S_1^{(n)}\right)^2 - S_1^{(n)}S_3^{(n)} \quad (7.97)$$

$$S_B^{(n)} = \left(S_3^{(n)}\right)^2 - S_1^{(n)}S_3^{(n)}. \quad (7.98)$$

The resulting magnitudes of Z_A and Z_B are shown in table 7.3.

Table 7.3. Magnitudes of impedances Z_A and Z_B

S_1	S_3	Z_A	Z_B
0	0	**0**	**0**
0	1	**0**	Z_{in}
1	0	Z_{in}	**0**
1	1	**0**	**0**

Hence, Z_A and Z_B can be readily implemented using a two-state switch and a fixed impedance of magnitude Z_{in}, which is the desired result. The magnitude of the internal impedance, Z_{in}, is calculated in the same manner as shown for the lumped-parameter model (section 7.4.3).

Figure 7.9 shows the revised 'per-phase' arrangement for a single-phase inverter AFM, illustrating the implementation of Z_A and Z_B.

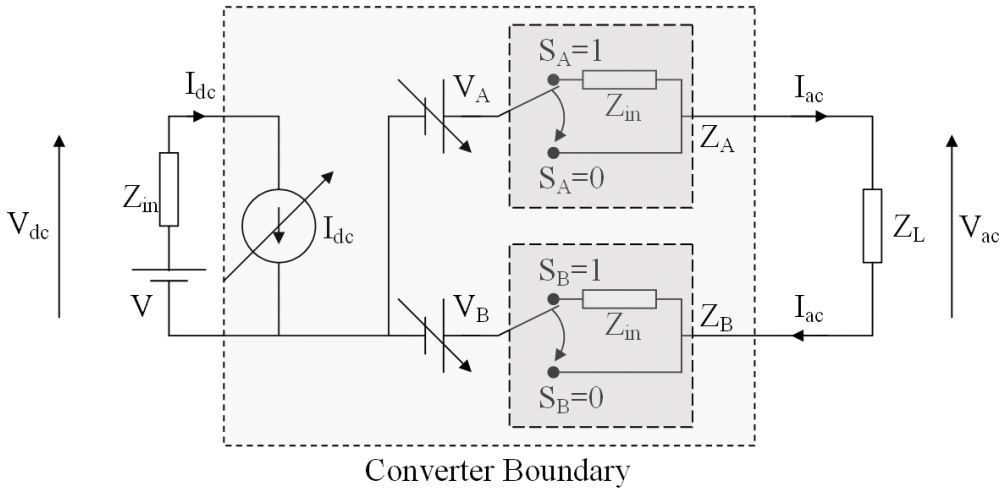

Fig. 7.9. Revised single-phase 'per-phase' inverter AFM

As with the lumped-parameter model, it is undesirable (although unavoidable) to utilise controlled switches in this AFM model, as these will decrease the AFM's computational efficiency. Also in line with lumped-parameter model, these

additional controlled switches will have a much lower impact on the computational efficiency of the AFM when a time averaged converter output is implemented.

Note that the time averaged 'per-phase' AFM inverter model can be implemented in a similar manner to that described in sections 7.5.2 through to 7.5.5.

Through the inclusion of the new terms X_A and X_B, and the new impedances Z_A and Z_B, the per-phase AFM has successfully met its objectives of replacing all the delayed terms in the transfer function of the original functional model with non-delayed equivalent terms. By doing this it guarantees numerical stability under all operating conditions whilst accurately replicating the behaviour of the original switched converter model.

In addition to these benefits, the next section illustrates how the per-phase AFM provides increased fidelity in its output, when compared to the lumped-parameter AFM, although at the expense of increased computation.

7.7. (I) Comparison of Lumped-Parameter and Per-Phase AFM Inverter Models

This section will discuss the comparative advantages and disadvantages of the two alternative AFM representations presented in sections 7.4 and 7.6. By doing this, it is intended that the need for two separate AFM methods will be illustrated and that guidelines on their use will be provided.

7.7.1 (I) Computational Requirements

The first aspect to consider is the computational requirement of both AFM representations. The lumped-parameter approach contains fewer additional controlled switches than the per-phase representation and as such, will require less computation to solve. In large networks with multiple converter models, this difference in the computational requirement could have a notable impact on the execution time of simulations conducted. Hence, on this basis, the lumped-parameter model is the preferred option for applications involving multi-converter networks.

If the AFMs are used to implement the time-averaged behaviour of the power electronic converters, the typical operating frequencies of the additional controlled switches contained within the models will be significantly lower. As such, the lumped-parameter approach will be only marginally more computationally efficient than the per-phase approach. Hence, in applications considering time-averaged converter behaviour, the differences in simulation execution time are unlikely to be significant enough that this aspect would be a key factor in choosing between the two AFM approaches.

7.7.2 (I) Specific AC Side Accuracy

The second key difference between the lumped-parameter and per-phase AFM representations is the difference in ac voltage potentials. Whilst the rail to rail output voltage, V_{ac}, of both converters is the same as the original switched converter model (taken as the benchmark for accuracy), the voltage potential of each ac terminal with respect to the dc side of the converter varies between the two representations.

The following case studies will illustrate how the lumped-parameter model is designed to achieve accuracy only in the reproduction of rail-to-rail voltages on the ac side of the converter model, but per-phase approach is designed to produce accurate specific ac voltage potentials (with respect to the dc side of the converter) in addition to this.

Figure 7.10 shows the schematics of a single-phase switched inverter model, the 'lumped-parameter' AFM equivalent and the 'per-phase' AFM equivalent (with additional annotations). Using the switched model as a benchmark for accuracy, the potentials between points **A**, **B** and **M** will be considered for both the lumped-parameter and per-phase AFM models in order to illustrate the accuracy of these models under a variety of operating conditions.

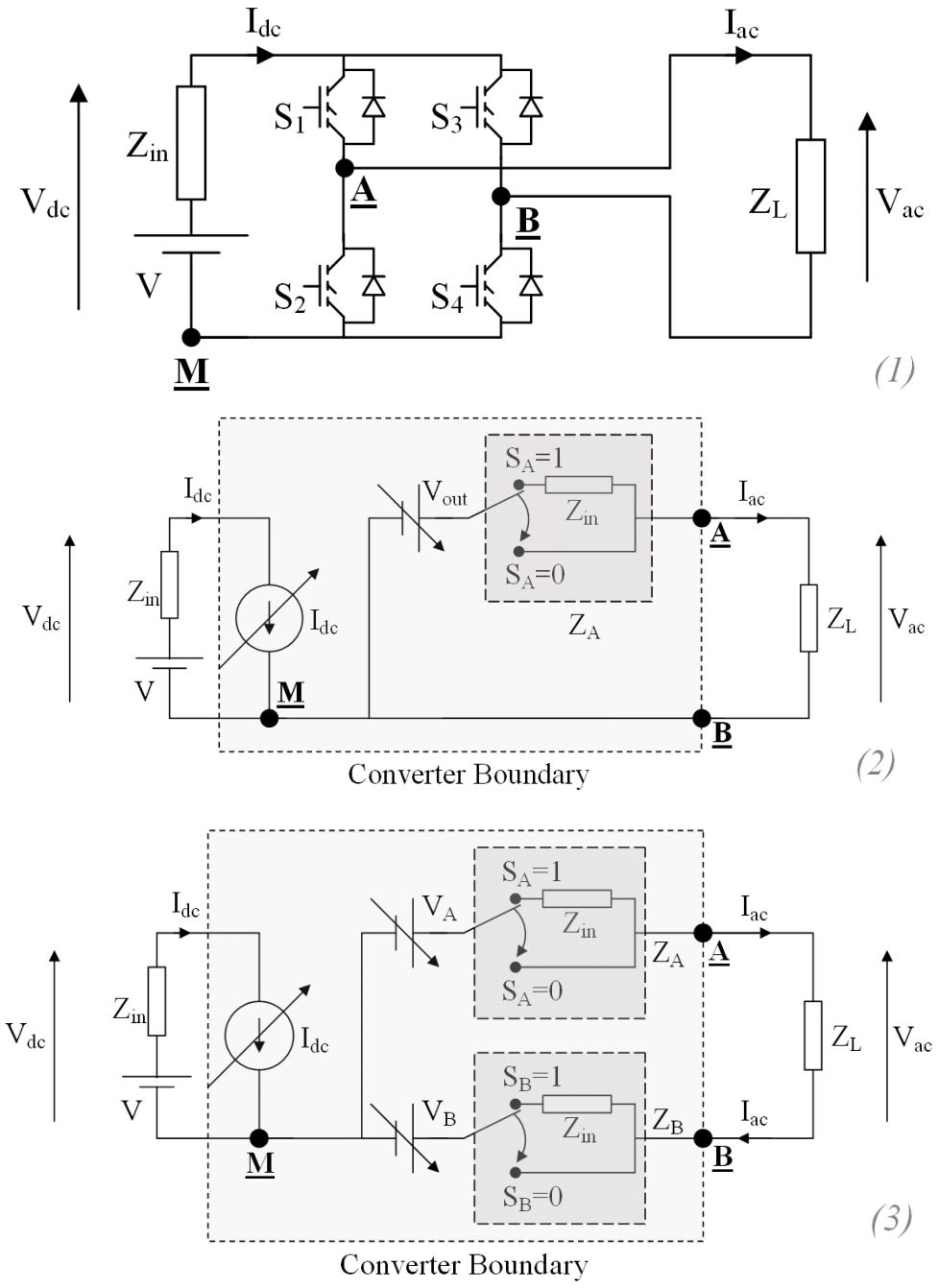

Fig. 7.10. *(1)* Schematics of a single-phase switched inverter, *(2)* 'lumped-parameter' AFM and *(3)* 'per-phase' AFM

The schematics shown in figure 7.10 will now form the basis for a number of comparative studies to illustrate the accuracy of both AFM approaches for a variety of different converter operating states. The findings of these studies will form the

core guidelines for the application of both AFM methods, which will be given in section 7.7.5.

7.7.3 (I) Switches S_1 and S_4 Closed

With reference to figure 7.10 (1), if the switched inverter is in an operating state such that switches S_1 and S_4 are closed, and switches S_2 and S_3 are open, the potential of point **A** with respect to point **M** will be $+V_{dc}$. The potential of point **B** will be the same as point **M** (neglecting any voltage loss across the semiconductor switches of the converter).

The lumped-parameter AFM representation (figure 7.10 (2)) will operate with $V_{out} = V$ and $S_A = 1$ in order to replicate the operating state of the switched inverter. In this manner, the potential of point **A** with respect to point **M** will be $+V_{dc}$ (as with the switched model). Point **B** will share the same potential as point **M** (again, in line with the switched model).

The per-phase AFM representation (figure 7.10 (3)) will operate with $V_A = V$, $S_A = 1$, $V_B = 0$ and $S_B = 0$ in order to replicate the operating state of the switched inverter. In this manner, the potentials of points **A** and **B** will once again match that of the switched converter.

Therefore, for the given operating state, the true potentials of both AFM representations match those of the switched model. The implications of these results will be discussed in section 7.7.5.

7.7.4 (I) Switches S_1 and S_4 Open

It will now be shown that not both AFM representations are accurate however if the switched model (figure 7.10 (1)) is in an operating state such that switches S_1 and S_4 are open, and switches S_2 and S_3 are closed. Under these conditions, the potential of point **B** with respect to point **M** will now be $+V_{dc}$ and the potential of point **A** will be same as **M**.

In order to match the operating state of the switched inverter, the lumped-parameter AFM (figure 7.10 (2)) will operate with $V_{out} = -V_{dc}$ and $S_A = 1$. In this case, the potential of point **A** with respect to point **M** is actually $-V_{dc}$ and the potential of point **B** is still equal to that of point **M**. Hence, although the line-to-line output voltage (V_{ac}) of the AFM remains accurate, an effective common-mode voltage [6] of $-V_{dc}$ (which is erroneous) has been created in this case. Note that a similar error would also be created if the original functional model architecture described in Section 7.3.1 was utilised.

The per-phase AFM (figure 7.10 (3)) will operate with $V_A = 0$, $S_A = 0$, $V_B = 1$ and $S_B = 1$ in order to match the operating state of the switched inverter. Thus the true potentials of points **A** and **B** with respect to **M** are correct with reference to the switched inverter model (figure 7.10 (1)).

Therefore, for this operating state, the true potentials of the per-phase AFM representation match those of the switched model but this is not the case with the

lumped-parameter AFM. The implications of these results will be discussed in section 7.7.5.

7.7.5 (I) Switches S_1 and S_3 Closed – Zero Voltage Vector

Consider the instance when the switched inverter (figure 7.10 (3)) is operating in a state such that switches S_1 and S_3 are equal. These conditions are classed as zero voltage switching vectors because the ac side rail to rail voltage of the inverter is zero. The first zero voltage vector case to consider is when switches S_1 and S_3 are both closed and switches S_2 and S_4 are both open. Under these conditions, the potential of points **A** and **B** with respect to point **M** in the switched model will now be $+V$ (I_{dc} is zero for the configuration of Z_{in} illustrated in figure 7.10 (1)).

In order to match the operating state of the inverter, the lumped-parameter model (figure 7.10 (2)) operates with $V_{out} = 0$ and $S_A = 0$. In this manner, points **A** and **B** will erroneously both adopt the same potential as point **M**. Again, this error would also occur if the original functional model architecture was utilised.

The per-phase model (figure 7.10 (3)) operates with $V_A = V$, $V_B = V$, $S_A = 0$ and $S_B = 0$ in order to match the operating state of the switched inverter. In this manner, the true potentials of both points **A** and **B** are correct.

Therefore, for this converter operating state, the per-phase AFM representation accurately reproduces the specific ac side potentials (with reference to the switched model), whilst the lumped-parameter AFM only achieves accuracy in the line to line

voltage output (V_{ac}). The implications of these results will be discussed in section 7.7.5.

7.7.6 (I) Switches S_1 and S_3 Open – Zero Voltage Vector

In this case, the operating state of the switched inverter (figure 7.10 (1)) is such that switches S_1 and S_3 are open and switches S_2 and S_4 closed. Under this condition, the potentials of points **A** and **B** in the switched model are both equal to that of **M**.

The lumped-parameter model (figure 7.10 (2)) operates with $V_{out} = 0$ and $S_A = 0$ so that its operating state matches that of the switched inverter. Under this operating condition, the true potentials of points **A** and **B** within this model are equal to **M** and are hence correct.

In order to match the operating state of the switched inverter, the per-phase model (figure 7.10 (3)) operates with $V_A = 0$, $V_B = 0$, $S_A = 0$ and $S_B = 0$. Under this condition, the potentials of points **A** and **B** with respect to point **M** are also correct.

Hence, for this operating state, both the lumped-parameter and per-phase AFM approaches are accurate for both the line to line ac side voltages and true ac side voltage potentials. The implications of these results will be discussed in section 7.7.5.

7.7.7 (I) Discussions on the Comparison of AFM Representations

This section will review the findings of the case studies presented in sections 7.7.1, 7.7.2, 7.7.3 and 7.7.4 in order to establish guidelines for the application of both the lumped-parameter and per-phase AFM representations.

As discussed in section 7.7, the lumped-parameter inverter AFM (figure 7.10 (2)) is more computationally efficient than the per-phase model. However, the case studies above have illustrated that it can only provide guaranteed accuracy in the rail to rail voltage output (V_{ac}) of the converter. For other voltages that are referenced to the dc side of the converter, such as common mode voltages (depending on the earthing arrangement of the network considered), accuracy is not guaranteed. In order to investigate these aspects, it is necessary to utilise the less computationally efficient per-phase AFM (figure 7.10 (3)), which provides accuracy in these desired output quantities. However, in multi-converter network models, the additional computational requirement associated with the per-phase AFM representation may lead to a significant increase in simulation execution time. Hence, this representation should only be utilised if the true ac side voltage potentials are to be studied, otherwise the lumped-parameter representation should be employed to realise the maximum reductions in simulation computation.

At this stage, it is also worth noting that the true potentials of points **A** and **B** in the per-phase model (figure 7.10 (3) remain correct for the other configurations of Z_{in} considered (but not presented). For example, if there is some capacitance in parallel with the ideal voltage source V and its internal impedance Z_{in}, the magnitude of V_{dc}

would not necessarily become V when I_{dc} is zero (i.e. during the application of zero voltage vectors). The per-phase model however, still accounts for this by measuring the dc terminal voltage of the converter. Hence whilst X_A and X_B negate the impact of the delayed measurements of the ac side currents, they do not cancel out variations in V_{dc} caused by current flow internal to the source impedance, Z_{in}.

Also note that, like the original functional model, neither AFM representation can accommodate conditions where the states of switches S_1 and S_2 are equal or where the states of switches S_3 and S_4 are equal. These operating conditions are generally not utilised though as they cause the dc voltage source (V_{dc}) to be short circuited which is generally undesirable.

Part II - AFM Applied to Other Converter Topologies

In the following sections, the core principles of the AFM technique will be applied to a selection of converter topologies in order to demonstrate its versatility. It is acknowledged that there are other converter topologies utilised within marine and aerospace more-electric architectures [9, 10] in addition to those considered in this section. However, to address each of these on a case by case basis offers only limited additional benefit. Instead, it is intended that the selection provided will be a demonstration of the versatility and capability of the AFM technique.

In line with the two inverter AFM representations already presented in Part I of this chapter, all the converter AFM representations presented in Part II aim to replace the delayed terms in the transfer function of the original functional model with non-delayed equivalents in order to guarantee its numerical stability whilst still accurately representing the terminal conditions of the original switched model.

7.8 (II) Single-Phase Switched Rectifier – Lumped-Parameter Model

Like the single phase inverter, there are two variations of the single-phase switched rectifier AFM, the 'lumped-parameter' model and the 'per-phase' model. This chapter will consider both, starting with the 'lumped-parameter' model. This is illustrated in figure 7.11.

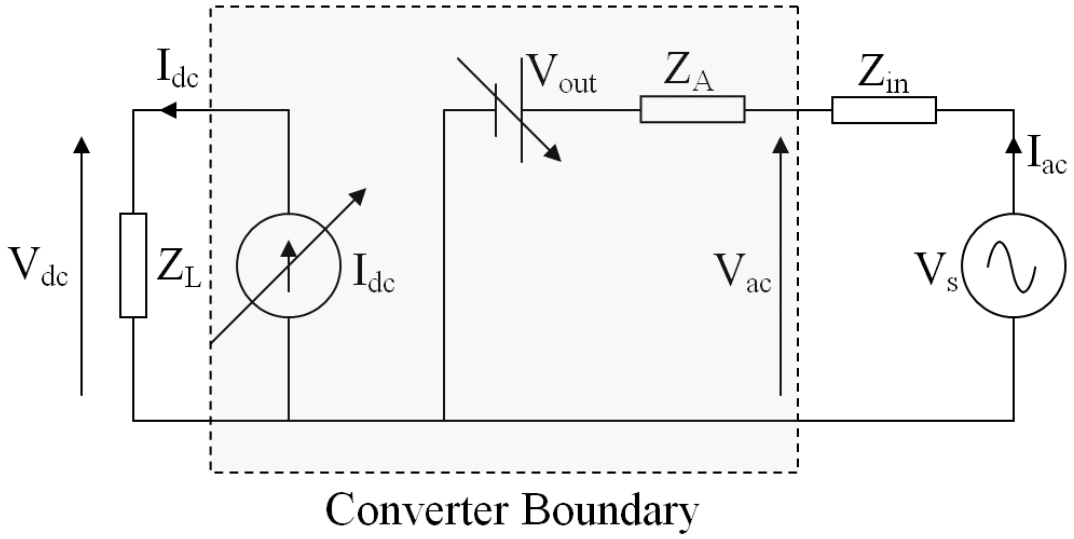

Fig. 7.11. Single-phase lumped-parameter switched rectifier AFM

As with inverter AFM, the converter boundary illustrated in figure 7.11 indicates where the terminals of the original switched model would be located. In this manner, any components within this boundary are part of the converter AFM and any components external to this boundary are parts of the surrounding electrical network.

The equations governing the behaviour of this model are

$$V_{out}^{(n)} = k_s^{(n)} V_{dc}^{(n)} + X_A^{(n)} \qquad (7.99)$$

$$V_{dc}^{(n)} = I_{dc}^{(n)} Z_L \qquad (7.100)$$

$$I_{dc}^{(n)} = k_s^{(n)} I_{ac}^{(n-1)} \qquad (7.101)$$

$$I_{ac}^{(n)} = \frac{V_s^{(n)} - V_{out}^{(n)}}{Z_{in} + Z_A^{(n)}}, \qquad (7.102)$$

where the definitions of *(n-1)*, *(n)* and k_s remain the same as previous models. The variables V_{ac}, I_{ac}, V_{dc} and I_{dc} are the ac side voltage and current and the dc side voltage and current respectively. Terms V_s, Z_{in}, and Z_L are the magnitudes of the voltage source, internal impedance and the load impedance. The term X_A is an additional voltage implemented with the controlled voltage source, V_{out}, to negate the delayed terms in its output. The impedance Z_A is the additional impedance utilised to restore the accuracy in the AFM ac side voltage output.

Following the same principles as previous AFMs, the governing equations for this switched rectifier can be developed to give the following definitions of X_A and Z_A as

$$X_A^{(n)} = -k_s^{(n)} I_{dc}^{(n)} Z_L , \qquad (7.103)$$

$$Z_A^{(n)} = \left(k_s^{(n)}\right)^2 Z_L . \qquad (7.104)$$

From equation (7.104), it is possible to implement Z_A using a fixed impedance of magnitude Z_L and a controlled switch. This approach is necessary if the application of the AFM within power systems simulation packages is to be achieved. This implementation of Z_A is illustrated in figure 7.12.

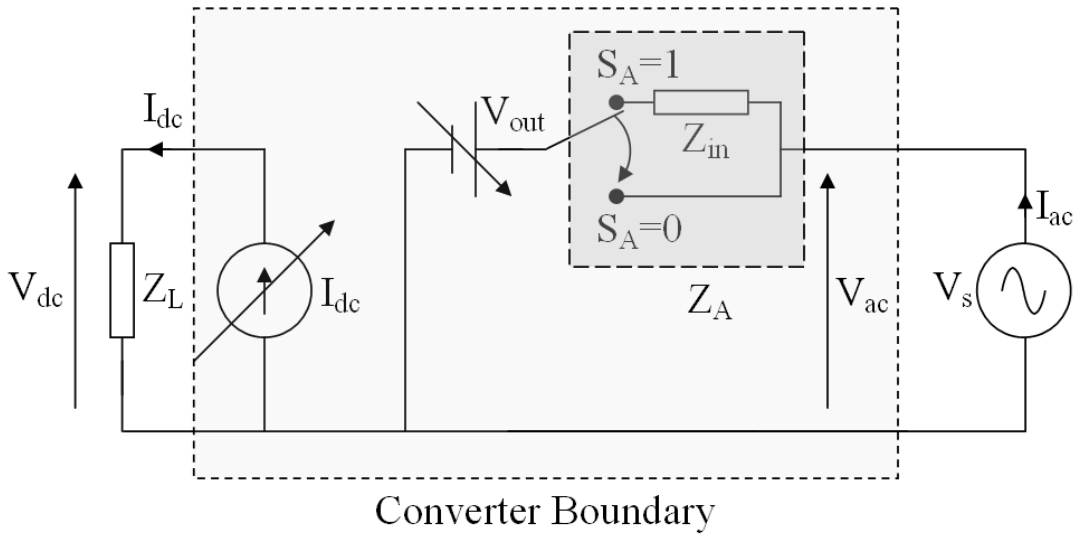

Fig. 7.12. Single-phase lumped-parameter switched rectifier AFM with revised Z_A

Implementing X_A and Z_A and performing some algebra gives the ac side voltage output of the switched rectifier AFM as

$$V_{ac}^{(n)} = \left(S_1^{(n)} - S_3^{(n)}\right)V_{dc}^{(n)}. \qquad (7.105)$$

Note, that in line with the inverter AFMs presented in sections 7.4 and 7.6, the V_{dc} term present in equation (7.105) is now made up of non-delayed terms. Hence, through the inclusion of the new term X_A and the new impedance Z_A, the AFM has successfully met its objectives of replacing all the delayed terms with non-delayed equivalent terms in the transfer function of the original functional model. By doing this it guarantees numerical stability under all operating conditions whilst accurately replicating the behaviour of the original switched converter model.

7.9 (II) Single-Phase Switched Rectifier – Per-Phase Model

This section will present the AFM concept applied to the single-phase switched rectifier in a per-phase arrangement. The design objectives of this AFM model are the same as those for the other AFMs previously presented in this chapter. Additionally, the advantages and disadvantages of the lumped-parameter (described in the previous section) and per-phase AFM representations of a switched rectifier are the same as those for a single-phase inverter (discussed in section 7.7.5).

Consider the single-phase, 'per-phase' switched rectifier AFM illustrated in figure 7.13.

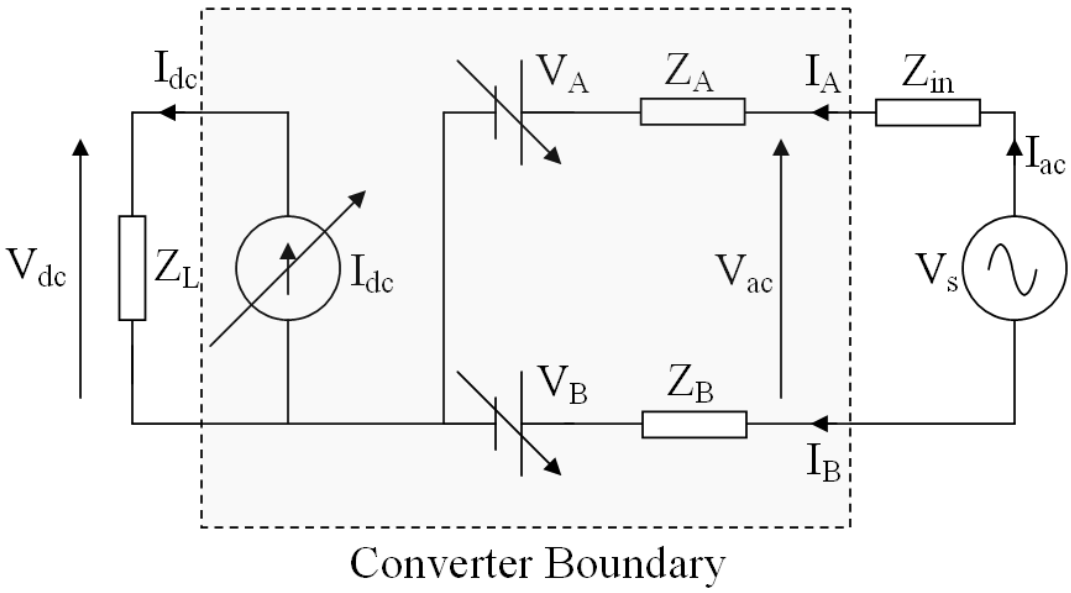

Fig. 7.13. Single-phase, per-phase switched rectifier AFM

In keeping with earlier AFMs, the converter boundary illustrated in figure 7.11 indicates where the terminals of the original switched model would be located. The equations governing the behaviour of this model are

$$V_A^{(n)} = S_1^{(n)} V_{dc}^{(n)} + X_A^{(n)} \tag{7.106}$$

$$V_B^{(n)} = S_3^{(n)} V_{dc}^{(n)} + X_B^{(n)} \tag{7.107}$$

$$V_{dc}^{(n)} = I_{dc}^{(n)} Z_L \tag{7.108}$$

$$I_{dc}^{(n)} = S_1^{(n)} I_A^{(n-1)} + S_3^{(n)} I_B^{(n-1)} \tag{7.109}$$

$$I_{ac}^{(n)} = \frac{V_s^{(n)} + V_B^{(n)} - V_A^{(n)}}{Z_{in} + Z_A^{(n)} + Z_B^{(n)}}. \tag{7.110}$$

$$V_{ac}^{(n)} = V_A^{(n)} - V_B^{(n)} + I_A^{(n)} Z_A^{(n)} - I_B^{(n)} Z_B^{(n)}, \tag{7.111}$$

The definitions of *(n-1)* and *(n)* remain the same as previous models. Terms X_A and X_B are additional voltages implemented with the controlled voltage sources, V_A and V_B. The variables V_{ac}, I_{ac}, V_{dc} and I_{dc} are the ac side voltage and current and the dc side voltage and current respectively. The ac side currents I_A and I_B are artificial notations added in order to simplify later derivations of AFM variables. It is assumed that $I_A = I_{ac} = -I_B$ at any instant in time. Impedances Z_A and Z_B are dynamic components added to restore the accuracy of the AFM.

Following the same principles as previous AFMs, the governing equations for this per-phase switched rectifier AFM can be developed to give the following definitions of X_A, X_B, Z_A and Z_B.

$$X_A^{(n)} = -S_1^{(n)} I_{dc}^{(n)} Z_L \qquad (7.112)$$

$$X_B^{(n)} = -S_3^{(n)} I_{dc}^{(n)} Z_L . \qquad (7.113)$$

$$Z_A^{(n)} = \left(\left(S_1^{(n)} \right)^2 - S_1^{(n)} S_3^{(n)} \right) Z_L \qquad (7.114)$$

$$Z_B^{(n)} = \left(\left(S_3^{(n)} \right)^2 - S_1^{(n)} S_3^{(n)} \right) Z_L . \qquad (7.115)$$

Table 7.4 shows the variation in magnitude of Z_A and Z_B for all possible combinations of S_1 and S_3.

Table 7.4. Impact of the states of S_1 and S_3 on Z_A and Z_B.

S_1	S_3	Z_A	Z_B
0	0	0	0
0	1	0	Z_L
1	0	Z_L	0
1	1	0	0

From Table 7.4, it can be seen that it is possible to implement Z_A and Z_B using fixed impedances of magnitude Z_L and controlled switches (this is in line with the lumped-parameter model). This approach is necessary to achieve the application of the AFM within power systems simulation packages. This implementation of Z_A and Z_B is illustrated in figure 7.14.

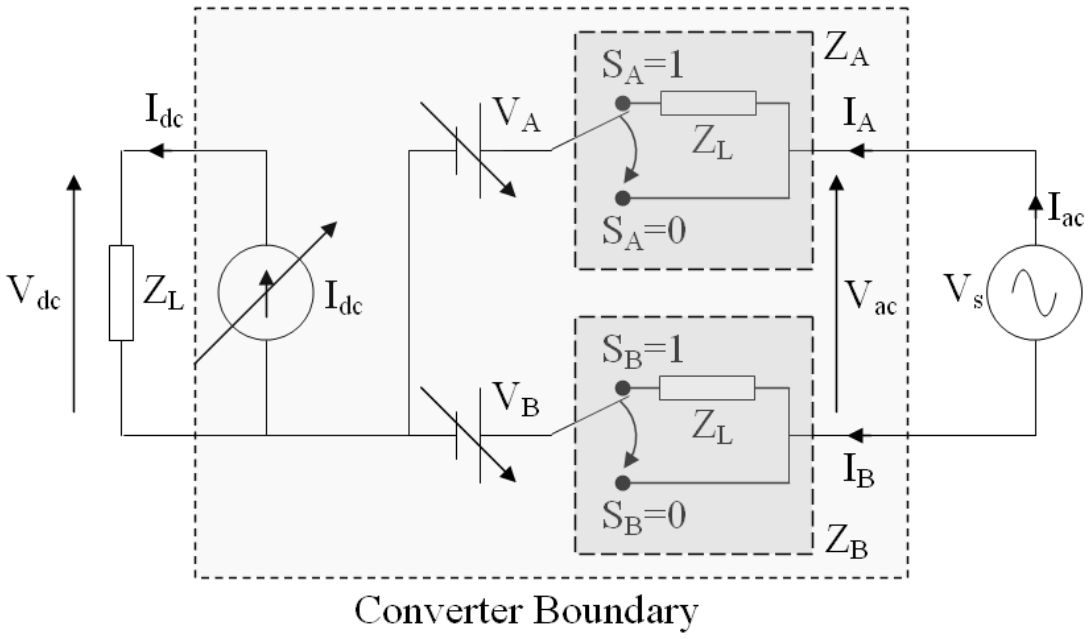

Fig. 7.14. Single-phase per-phase switched rectifier AFM with revised Z_A and Z_B

By following the same process as that presented for the per-phase inverter AFM, the ac side voltage output of the per-phase switched rectifier AFM can be expressed as

$$V_{ac}^{(n)} = \left(S_1^{(n)} - S_3^{(n)}\right) V_{dc}^{(n)} . \qquad (7.116)$$

Note, that in line with the inverter AFMs presented in sections 7.4 and 7.6, the V_{dc} term present in equation (7.105) is now made up of non-delayed terms. Hence, the AFM has successfully met its objectives of replacing all the delayed terms with non-delayed equivalent terms in the transfer function of the original functional model. By doing this it guarantees numerical stability under all operating conditions whilst accurately replicating the behaviour of the original switched converter model.

Additionally, the per-phase model is accurate even when common-mode voltages are studied (as discussed in section 7.5.5), where the lumped-parameter model is not. However, because of the increased number of additional controlled switches in comparison to the lumped-parameter model, the per-phase model is more computationally demanding than the lumped-parameter model. Hence, in order to minimise the computational requirement of any particular simulation utilising switched rectifier AFMs, the per-phase representation should only be utilised ahead of the lumped-parameter representation when specifically studying the variables described above.

7.10 (II) DC-DC Forward Converter AFM

Unlike the inverter and switched rectifier topologies studied, the AFM of the dc-dc forward converter considered in Chapter 5 can only be represented in one form as there is only one switch controlling the output of this converter. Otherwise, the design objectives of this AFM model are the same as those for the other AFMs previously presented in this chapter.

The schematic of the dc-dc forward converter AFM is illustrated in figure 7.15.

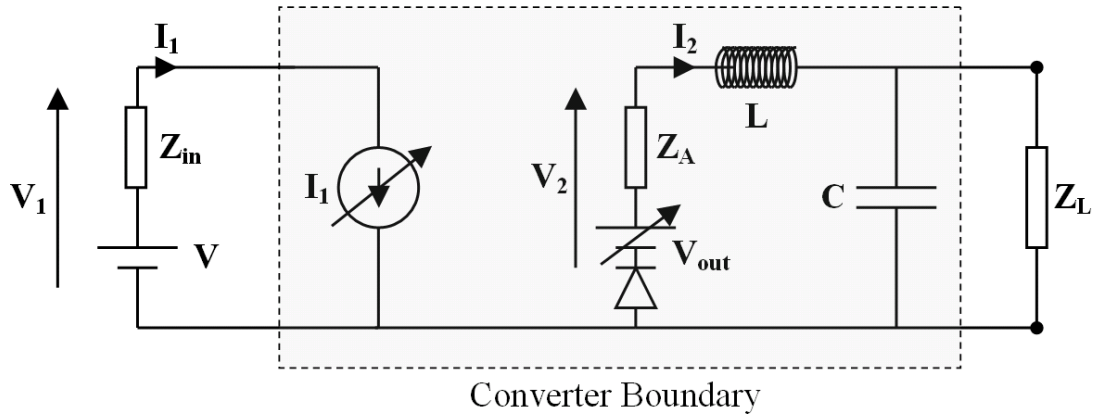

Fig. 7.15. DC-DC Forward Converter AFM

As before, the converter boundary illustrated in figure 7.15 indicates where the terminals of the original switched model would be located.

The equations governing the behaviour of this model are

$$V_{out}^{(n)} = S^{(n)} V_1^{(n)} + X_A^{(n)} \qquad (7.117)$$

$$V_1^{(n)} = V - I_1^{(n)} Z_{in} \qquad (7.118)$$

$$I_1^{(n)} = S^{(n)} I_2^{(n-1)} \qquad (7.119)$$

$$I_2^{(n)} = \frac{V_2^{(n)}}{Z_{out} + Z_A^{(n)}} \qquad (7.120)$$

$$V_2^{(n)} = V_{out}^{(n)} - I_2^{(n)} Z_A^{(n)}, \qquad (7.121)$$

where the definitions of *(n-1)* and *(n)* remain the same as with previous models. The term *S*, is the state of the single switch in the original switched converter model and is defined as

$$S^{(n)} = \begin{cases} 1 & if \quad closed \\ 0 & otherwise \end{cases} . \qquad (7.122)$$

The term X_A is an additional voltage implemented with the controlled voltage source, V_{out}. Impedance Z_A is a dynamic component added to restore the accuracy of the AFM. The impedance Z_{out} is the combined impedance of components L, C and Z_L. The terms V and Z_{in} are the magnitudes of the source voltage and source impedance respectively. The terms V_1, I_1, V_2 and I_2 represent the input and output voltages and currents of the dc-dc converter AFM respectively.

Following the same principles as previous AFMs, the governing equations for this dc-dc forward converter can be developed to give the following definitions of X_A and Z_A.

$$X_A^{(n)} = S^{(n)} I_1^{(n)} Z_{in} \qquad (7.123)$$

$$Z_A^{(n)} = \left(S^{(n)}\right)^2 Z_{in} . \qquad (7.124)$$

In line with earlier AFMs, it can be seen that it is possible to implement Z_A using fixed impedances of magnitude Z_{in} and a controlled switch. Again, this approach is necessary to achieve the application of the AFM within power systems simulation packages. This implementation of Z_A is illustrated in figure 7.16.

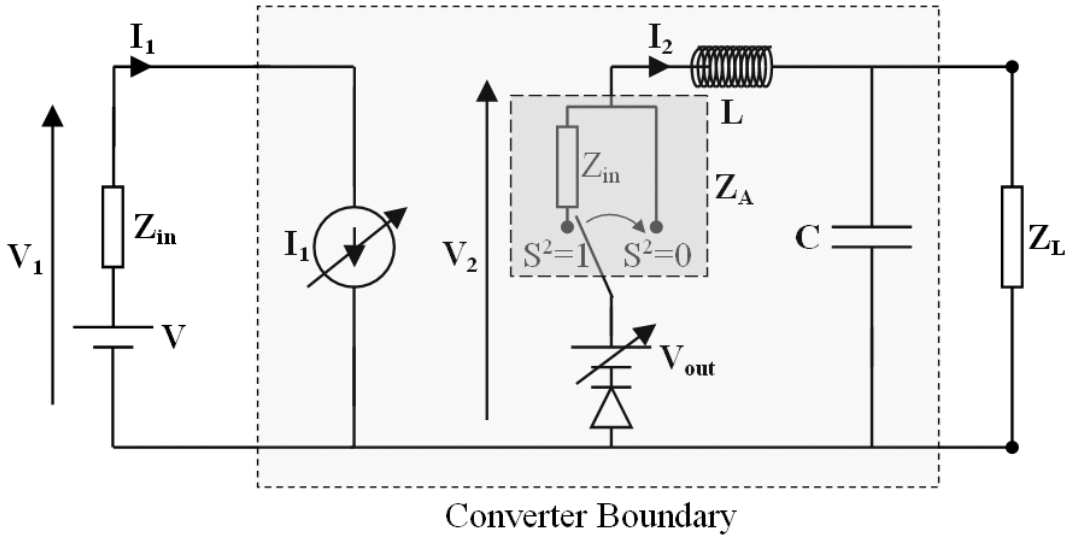

Fig. 7.16. Revised single-phase DC-DC forward converter AFM

Implementing X_A and Z_A and performing some algebra gives the output voltage of the dc-dc forward converter AFM as

$$V_2^{(n)} = S^{(n)} V_1^{(n)}. \qquad (7.125)$$

Note that in line with previous AFM topologies presented in this chapter, the V_1 term present in equation (7.105) is now made up of non-delayed terms. Hence, the AFM has successfully met its objectives of replacing all the delayed terms with non-delayed equivalent terms in the transfer function of the original functional model. By doing this it guarantees numerical stability under all operating conditions whilst accurately replicating the behaviour of the original switched converter model.

7.11 (II) Three-Phase Inverter

This section will present the three phase inverter AFM. Like the DC-DC forward converter AFM, the three-phase inverter AFM only has one form. The higher number of phases of this converter means that it cannot be easily represented using the lumped-parameter approach, requiring the per-phase approach to be used instead. Otherwise, the design objectives of this AFM model are the same as those of other AFMs previously presented in this chapter.

The schematic of a three-phase inverter AFM is illustrated in figure 7.17.

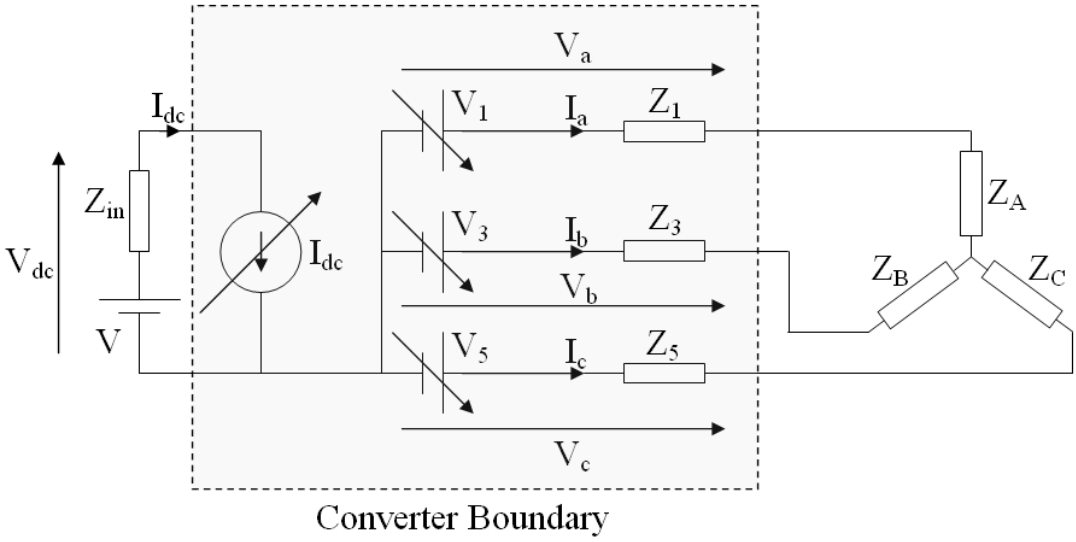

Fig. 7.17. Three-phase Inverter AFM

As before, the converter boundary illustrated in figure 7.17 indicates where the terminals of the original switched model would be located.

The equations governing the behaviour of this model are

$$V_1^{(n)} = S_1^{(n)} V_{dc}^{(n)} + X_A^{(n)} \quad (7.126)$$

$$V_3^{(n)} = S_3^{(n)} V_{dc}^{(n)} + X_B^{(n)} \quad (7.127)$$

$$V_5^{(n)} = S_5^{(n)} V_{dc}^{(n)} + X_C^{(n)} \quad (7.128)$$

$$V_{dc}^{(n)} = V - I_{dc}^{(n)} Z_{in} \quad (7.129)$$

$$I_{dc} = S_1^{(n)} I_a^{(n-1)} + S_3^{(n)} I_b^{(n-1)} + S_5^{(n)} I_c^{(n-1)} . \quad (7.130)$$

$$V_a^{(n)} = V_1^{(n)} - I_a^{(n)} Z_1^{(n)} \quad (7.131)$$

$$V_b^{(n)} = V_3^{(n)} - I_b^{(n)} Z_3^{(n)} \quad (7.132)$$

$$V_c^{(n)} = V_5^{(n)} - I_c^{(n)} Z_5^{(n)} \quad (7.133)$$

The definitions of V, V_{dc}, Z_{in}, I_{dc}, *(n-1)* and *(n)* remain the same as the single phase inverter AFMs. Impedances Z_A, Z_B and Z_C are the three-phase load impedances. Terms X_A, X_B and X_C are additional voltages implemented with the controlled voltage sources, V_1, V_3 and V_5. Impedances Z_1, Z_3 and Z_5 are dynamic components added to the AFM to restore its accuracy. The voltages V_a, V_b and V_c represent the effective ac side output voltages of the AFM converter. The terms S_1, S_3, S_5 derive from the states of the switches of the original switched inverter model in the same manner as the single phase inverter AFM.

Following the same principles as previous AFMs, the governing equations for this converter can be developed to give the following definitions of X_A, X_B and X_C.

$$X_A^{(n)} = S_1^{(n)} I_{dc}^{(n)} Z_{in} \tag{7.134}$$

$$X_B^{(n)} = S_3^{(n)} I_{dc}^{(n)} Z_{in} \tag{7.135}$$

$$X_C^{(n)} = S_5^{(n)} I_{dc}^{(n)} Z_{in} . \tag{7.136}$$

As a result of these changes, V_a, V_b and V_c become

$$V_a^{(n)} = S_1^{(n)} V - I_a^{(n)} Z_1^{(n)} \tag{7.137}$$

$$V_b^{(n)} = S_3^{(n)} V - I_b^{(n)} Z_3^{(n)} \tag{7.138}$$

$$V_c^{(n)} = S_5^{(n)} V - I_c^{(n)} Z_5^{(n)} . \tag{7.139}$$

Hence, the delayed terms have been removed from these expressions indicating that this model is numerically stable under all operating conditions.

In line with other AFMs, the next stage of the development process is the derivation of the additional controlled impedances Z_1, Z_3 and Z_5 in order to compensate for the errors introduced by the inclusion of the voltages X_A, X_B and X_C. However, Z_1, Z_3 and Z_5 cannot be derived in the same manner as was shown for other AFM models. This is due to the additional complexity of the physical relationships governing the behaviour of the three-phase inverter in comparison to the other converters studied in this thesis. This aspect can be illustrated by considering the desired ac side voltage outputs ($V_{a\text{-}desired}$, $V_{b\text{-}desired}$ and $V_{c\text{-}desired}$) from the three-phase inverter AFM (i.e. those voltages which would be produced by the original switched converter model). These can be defined as

$$V_{a-desired}^{(n)} = S_1^{(n)} V_{dc}^{(n)} \quad (7.140)$$

$$V_{b-desired}^{(n)} = S_3^{(n)} V_{dc}^{(n)} \quad (7.141)$$

$$V_{c-desired}^{(n)} = S_5^{(n)} V_{dc}^{(n)} . \quad (7.142)$$

By substituting for V_{dc}, equations (7.140), (7.141) and (7.142) can be expanded to

$$V_{a-desired}^{(n)} = S_1^{(n)} V - S_1^{(n)} I_{dc}^{(n)} Z_{in} \quad (7.143)$$

$$V_{b-desired}^{(n)} = S_3^{(n)} V - S_3^{(n)} I_{dc}^{(n)} Z_{in} \quad (7.144)$$

$$V_{c-desired}^{(n)} = S_5^{(n)} V - S_5^{(n)} I_{dc}^{(n)} Z_{in} . \quad (7.145)$$

In other AFM models, substituting for I_{dc} in the equations for the desired output voltages leads to a workable solution for the additional dynamic impedance components. However, with the three-phase inverter, I_{dc} is a function of the currents in all three ac side phases. Substituting for I_{dc} in equations (7.143), (7.144) and (7.145) would lead to the development of expressions for Z_1, Z_3 and Z_5 which could not be implemented with switches and fixed impedances, and thus could not be readily implemented within power systems simulation software packages. As a result, a different approach must be adopted.

7.11.1 (II) Derivation of Additional Impedances Z_1, Z_3 and Z_5

This section will present the alternative approach utilised to derive expressions for the additional impedances Z_1, Z_3 and Z_5 of the three-phase inverter AFM.

Consider the operation of the switched three-phase inverter shown in figure 7.18. The marked points ***a***, ***b***, ***c*** and ***d*** are highlighted for later use.

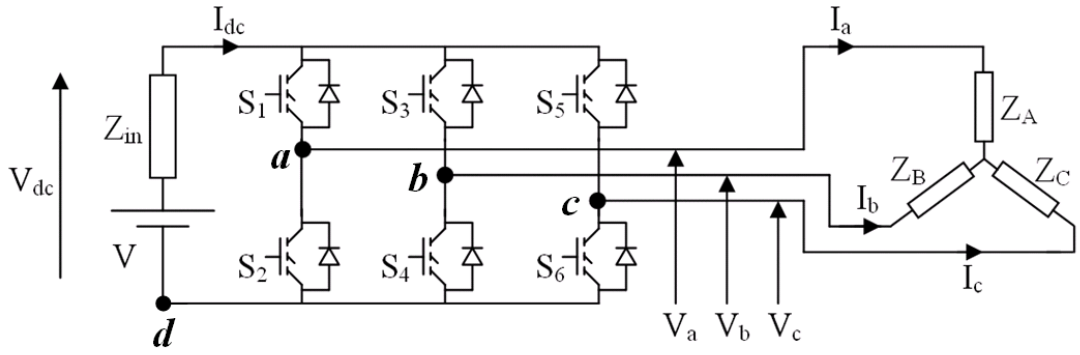

Fig. 7.18. Three-phase inverter (switched) model

The magnitudes of the ac side output voltages V_a, V_b and V_c illustrated in this figure will now be considered for all the possible operating states of the inverter in order to work towards deriving expressions for Z_1, Z_3 and Z_5 of the AFM equivalent model (shown in figure 7.17).

In this figure, if switches S_1, S_3 and S_5 are either all open or all closed, there will be no voltage lost across Z_{in} as a result of the ac side currents. In order for the AFM to replicate this behaviour, the magnitudes of impedances Z_1, Z_3 and Z_5 should be zero.

In all the other operating states of the switched inverter, two of the three ac phase voltages of the inverter (i.e. V_a, V_b and V_c) will adopt the same magnitude. For the AFM to replicate this behaviour, the magnitude of its additional impedance elements (i.e. Z_1, Z_3 and Z_5) for these matched phases must be zero. This is so that the voltages produced by the unequal ac side currents (i.e. I_a, I_b and I_c) flowing through these

impedance elements do not lead to the creation of errors in V_a, V_b and V_c. Under these operating conditions, the magnitude of the current in the remaining phase will be equal to I_{dc} and as such, the magnitude of the additional impedance element in this remaining phase must be equal to Z_{in} so that the voltage drop across it is equal to that experienced in the switched converter.

The operating logic for Z_1, Z_3 and Z_5 described above is summarised in table 7.5.

Table 7.5. Derived values of Z_1, Z_3 and Z_5.

S_1	S_3	S_5	Z_1	Z_3	Z_5
0	0	0	0	0	0
0	0	1	0	0	Z_{in}
0	1	0	0	Z_{in}	0
0	1	1	Z_{in}	0	0
1	0	0	Z_{in}	0	0
1	0	1	0	Z_{in}	0
1	1	0	0	0	Z_{in}
1	1	1	0	0	0

In line with earlier AFMs, it can be seen that the approach presented facilitates the implementation of Z_1, Z_3 and Z_5 using fixed impedances of magnitude Z_{in} and controlled switches. Again, this approach is necessary to achieve the application of the AFM within power systems simulation packages. The implementation of Z_1, Z_3 and Z_5 within the three-phase inverter AFM is illustrated in figure 7.19.

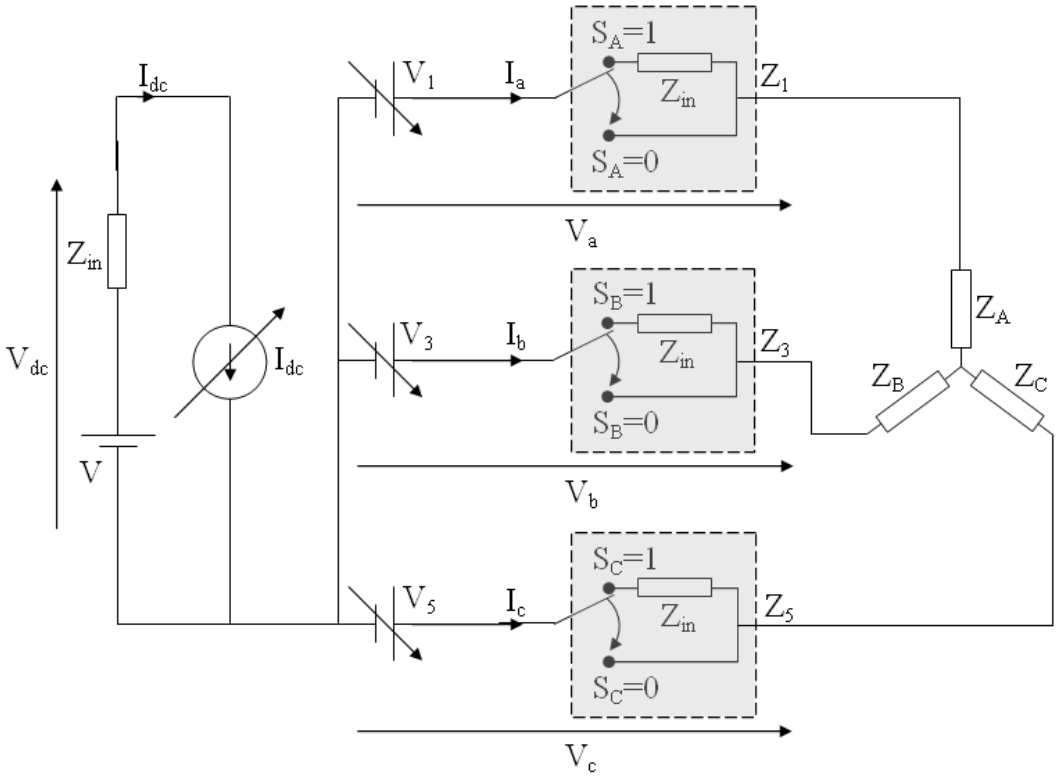

Fig. 7.19. Revised three-phase inverter AFM

Unlike previous AFM models, presenting equations for the ac side voltage outputs of the converter (V_a, V_b and V_c) will not be an effective method for illustrating the accuracy restored to the AFM by the inclusion of Z_1, Z_2 and Z_3. Instead, this will be achieved by considering V_a, V_b and V_c for the different operating states of the three-phase inverter. This analysis will be presented in the following section.

7.11.2 (II) Illustration of Three-Phase Inverter AFM Accuracy

This section will use three case studies to illustrate how the three-phase inverter AFM accurately replicates the line to line voltage output voltages ($V_{a\text{-}b}$, $V_{b\text{-}c}$ and $V_{c\text{-}a}$) of the original switched converter. It should be noted however, that the accuracy of

specific phase voltages (V_a, V_b and V_c) with respect to any point on the dc side of the converter or the neutral point of the load is not always guaranteed. Based on the analysis presented, this section discusses the potential applications for the three-phase inverter AFM.

The case studies presented are based on the switched model of a three-phase inverter shown in figure 7.20 (which is reproduced from figure 7.18), upon which the AFM equivalent given in figure 7.19 is based.

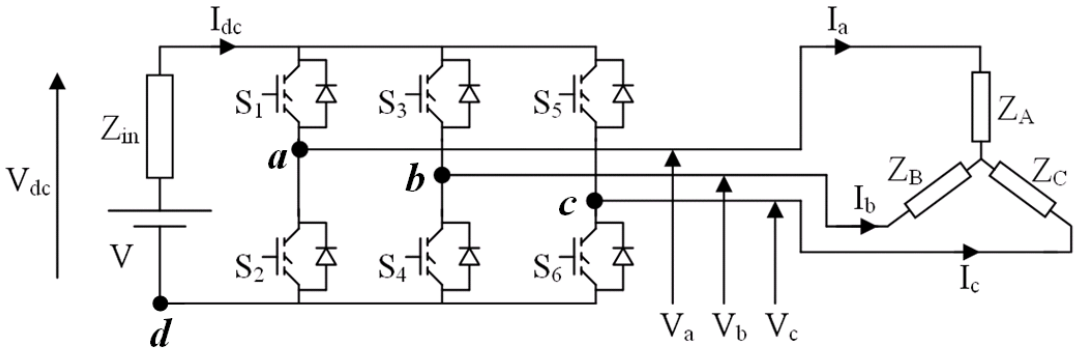

Fig. 7.20. Switched model of a three-phase inverter with load and source

Case Study 1

If the switched model three-phase inverter shown in figure 7.20 is in an operating state at time *(n)* such that $S_1 = 1$, $S_3 = 1$ and $S_5 = 0$, the equivalent circuit of this converter will be of the form illustrated in figure 7.21 (neglecting the on-state resistance and forward voltage of all semi-conductor switches).

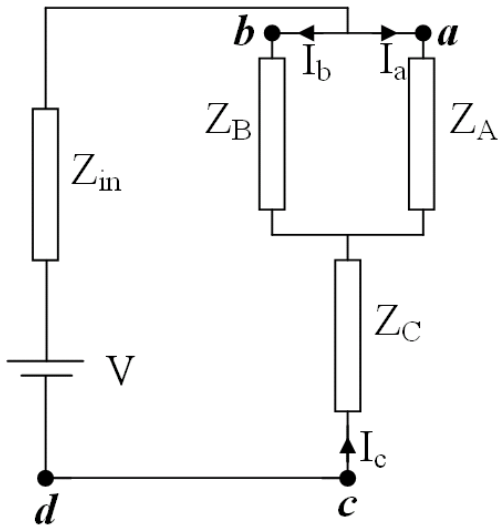

Fig. 7.21. Equivalent circuit of the switched model three-phase inverter for case study 1

By summing the individual voltage components between points **c** and **a**, the voltage between these points ($V_{a\text{-}c}$) at time *(n)* can be expressed as

$$V_{a-c}^{(n)} = V + I_c^{(n)} Z_{in}, \qquad (7.146)$$

where $V_{a\text{-}c}$ is the effective line to line voltage between phases ***a*** and ***c***. Note that $V_{b\text{-}c}$ also holds the same magnitude as $V_{a\text{-}c}$, and $V_{a\text{-}b}$ is zero.

In order to replicate the operating state of the switched model, the three-phase inverter AFM operates such that an additional impedance, Z_{in} will be switched into the ***c*** phase of the inverter (as according to table 7.5) and $V_1 = V$, $V_2 = V$, $V_3 = 0$. The equivalent circuit of the AFM under these conditions is illustrated in figure 7.22.

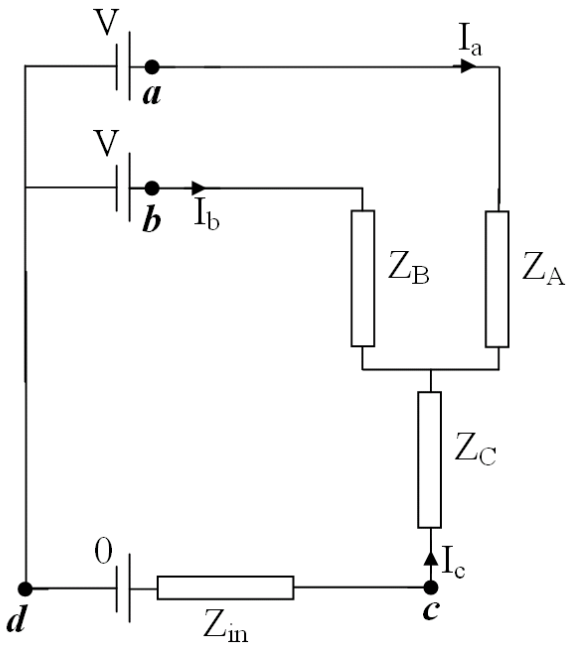

Fig. 7.22. Equivalent circuit of the three-phase inverter AFM for case study 1

Using a similar approach to that illustrated for the switched inverter model shown in figure 7.21, it can be seen that all line to line voltages of the AFM ($V_{a\text{-}b}$, $V_{b\text{-}c}$ and $V_{c\text{-}a}$) at time *(n)* are consistent with the original switched model. However, that there is some error in the voltage potentials of points ***a***, ***b*** and ***c*** with respect to point ***d*** (e.g. the phase voltages $V_{a\text{-}d}$, $V_{b\text{-}d}$ and $V_{c\text{-}d}$). All three voltage potentials are a magnitude of I_cZ_{in} less than those of the switched model. More simply put, an artificial common mode voltage [6] of $-I_cZ_{in}$ has been created in the phase voltages of the AFM converter.

Hence, operating under the conditions given for this case study, the three-phase inverter AFM provides valid results for line to line voltages ($V_{a\text{-}b}$, $V_{b\text{-}c}$ and $V_{a\text{-}c}$) but not for specific phase voltages (V_a, V_b and V_c). The following two operating conditions also produce this result:

- When the inverter's state is such that $S_1 = 1$, $S_3 = 0$ and $S_5 = 1$.
- When the inverter's state is such that $S_1 = 0$, $S_3 = 1$ and $S_5 = 1$.

The implications of this finding will be discussed at the end of this section when the other operating states of the three-phase inverter have been considered.

Case Study 2

If the three-phase switched inverter shown in figure 7.20 is in an operating state such that $S_1 = 0$, $S_3 = 0$ and $S_5 = 1$, the equivalent circuit of this converter will be of the form illustrated in figure 7.23 (neglecting the on-state resistance and forward voltage of all semi-conductor switches).

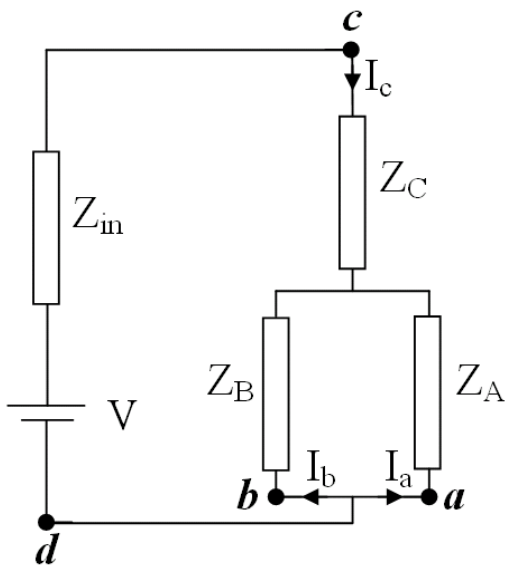

Fig. 7.23. Equivalent circuit of the switched model three-phase inverter for case study 2

By summing the individual voltage components between points **c** and **a**, the voltage between these points ($V_{a\text{-}c}$) at time *(n)* can be expressed as

$$V_{a-c}^{(n)} = -V + I_c^{(n)} Z_{in} . \qquad (7.147)$$

The voltage $V_{b\text{-}c}$ holds the same magnitude as $V_{a\text{-}c}$, and $V_{a\text{-}b}$ is zero.

In order to replicate the operating state of the switched model, the three-phase inverter AFM operates such that an additional impedance, Z_{in} will be switched into the ***c*** phase of the inverter (as according to table 7.5) and $V_1 = 0$, $V_2 = 0$, $V_3 = V$. The equivalent circuit of the AFM under these conditions is illustrated in figure 7.24.

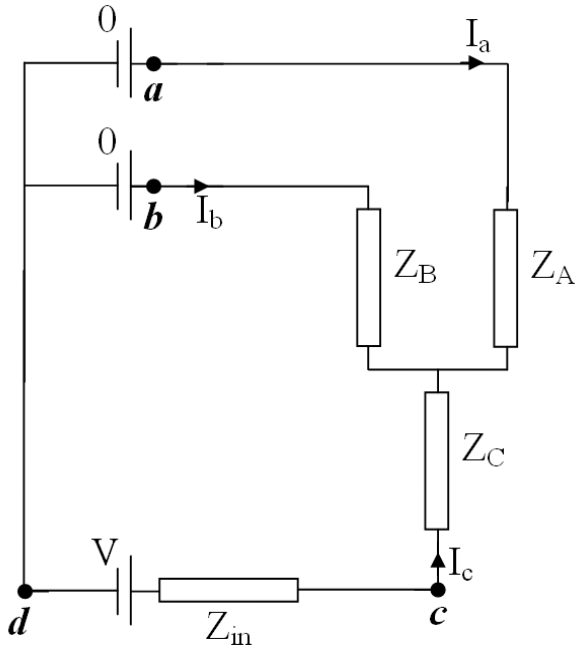

Fig. 7.24. Equivalent circuit of the three-phase inverter AFM for case study 2

Using a similar approach to that illustrated for the switched inverter model shown in figure 7.21, it is observed that all line to line voltages ($V_{a\text{-}b}$, $V_{b\text{-}c}$ and $V_{c\text{-}a}$) produced by the AFM are again consistent with the original switched model. Additionally, the phase voltages ($V_{a\text{-}d}$, $V_{b\text{-}d}$ and $V_{c\text{-}d}$) produced by the AFM also match those of the switched inverter model.

Hence, operating under the conditions given for this case study, the three-phase inverter AFM provides valid results both for line to line ($V_{a\text{-}b}$, $V_{b\text{-}c}$ and $V_{c\text{-}a}$) voltages and phase voltages (V_a, V_b and V_c). This observation holds also true all for the following two operating conditions:

- When the inverter's state is such that $S_1 = 1$, $S_3 = 0$ and $S_5 = 0$.
- When the inverter's state is such that $S_1 = 0$, $S_3 = 1$ and $S_5 = 0$.

Note that for the other two operating states of the three-phase inverter ($S_1 = S_3 = S_5 = 1$ and $S_1 = S_3 = S_5 = 0$) the AFM accurately replicates both the line to line voltages and the phase voltages of the original switched model. The analyses of these states will not be presented however, as they only serve to provide a limited benefit.

Discussion of Findings

By considering all the possible operating states of the three-phase inverter, it is observed that the AFM produces accurate results for the line to line output voltages ($V_{a\text{-}b}$, $V_{b\text{-}c}$ and $V_{a\text{-}c}$) of the three-phase inverter (i.e. matching those results produced by the switched inverter model). This ensures that the desired accuracy in the

modelled ac side currents is achieved and as a result, the dc side variables of the AFM inverter are also accurate (as shown by considering the derivation of the three-phase inverter ac side current magnitudes in Appendix A).

However, the case studies presented show that the AFM does not always produce accurate results for the specific phase voltages of the inverter. If the magnitude of the phase currents (I_a, I_b and I_c) and the dc voltage source internal impedance (Z_{in}) are small compared to the magnitude of the dc voltage source, the error in the phase voltages will be negligible. Otherwise, the three-phase inverter AFM can not be reliably utilised for studying these variables.

This outcome is clearly undesirable as the three-phase inverter AFM would ideally be valid for all types of studies conducted. However, this is a small sacrifice to make in order to achieve guaranteed numerical stability even during simulated fault conditions. In addition, the model is still of great benefit for the many types of studies conducted on marine and aerospace electrical network architectures which only require accuracy in the line to line voltages of the inverter model.

Note that other three-phase converters would require a similar implementation approach to that illustrated in this section.

Part III – Assessing the Robustness of AFM

7.12 (III) Impact of Inaccurate Derivation of AFM Variables

In the earlier sections of this thesis, it was shown that the developed AFMs of each converter topology are dependant on an accurate derivation of certain network impedances in order to function correctly. Given the complexity of marine and aerospace more-electric networks, this derivation may be difficult to achieve (this aspect is explored in more detail in section 7.13). As a result, it is important to consider the impact of an incorrect derivation of one or more of these impedances on the accuracy and numerical stability of the AFM.

This concept will be investigated in this section using the lumped-parameter single-phase inverter AFM (developed in section 7.4) as a case study. The accuracy and numerical stability will be considered for a varying level of error in the derivation of the dc side internal impedance. The analysis methods and findings presented in this section are also readily transferable to other AFM converter topologies.

For the lumped-parameter single-phase inverter shown in section 7.4, consider the case where the derived magnitude of Z_{in}, is different to the actual Z_{in} by a factor of A, such that

$$Z_{in-derived} = AZ_{in} \qquad (7.148)$$

Where the term $Z_{in\text{-}derived}$ is the derived magnitude of the dc source impedance and Z_{in} is the actual dc source impedance. The term A is a positive real number. Implementing the derived value of Z_{in} in the equations of operation for the inverter leads to the following expressions for the additional voltage X_A and the additional controlled impedance Z_A:

$$X_A^{(n)} = k_s^{(n)} I_{dc}^{(n)} A Z_{in} \qquad (7.149)$$

$$Z_A^{(n)} = \left(k_s^{(n)}\right)^2 A Z_{in}\,. \qquad (7.150)$$

As a result of the change to X_A, the expression for V_{out} becomes

$$V_{out}^{(n)} = k_s^{(n)} V - k_s^{(n)} I_{dc}^{(n)} Z_{in}\left(1 - A\right). \qquad (7.151)$$

By incorporating the revised expressions for Z_A and V_{out} given in equations (7.150) and (7.151), the ac terminal voltage of the inverter AFM now becomes

$$V_{ac}^{(n)} = k_s^{(n)} V - \left(k_s^{(n)}\right)^2 I_{ac}^{(n-1)} Z_{in}\left(1 - A\right) - \left(k_s^{(n)}\right)^2 I_{ac}^{(n)} Z_{in} A\,. \qquad (7.152)$$

From this equation, when Z_{in} is accurately derived (i.e. $A = 1$), equation (7.152) reverts back to the desired form for V_{ac} of the AFM (given in section 7.4). Also, if $A = 0$, equation (7.152) is equal to that for V_{ac} of the original functional model (as described in Chapter 5). However, for inaccurate derivations of Z_{in} (i.e. $A \neq 1$), an error is introduced into the magnitude of V_{ac}. Note however, that if there is little

change in the magnitude I_{ac} between time (*n-1*) and (*n*), V_{ac} will be a close approximation to the desired ac terminal voltage.

In addition to the error in V_{ac}, the presence of the delayed term in equation (7.149) indicates that the numerical stability of this model is no longer guaranteed and that V_{ac} may also become oscillatory under some operating conditions. This section will now assess the impact of this degradation in accuracy and numerical stability on the performance of the AFM and its ability to meet its objectives.

Substituting for I_{ac} in equation (7.152) gives the transfer function (in V_{ac}) for the AFM as

$$V_{ac}^{(n)} = BV - CV_{ac}^{(n-1)}, \qquad (7.153)$$

where

$$B = \frac{k_s^{(n)} Z_L}{Z_L + \left(k_s^{(n)}\right)^2 Z_{in} A}, \qquad (7.154)$$

and

$$C = \frac{\left(k_s^{(n)}\right)^2 Z_{in}(1-A)}{Z_L + \left(k_s^{(n)}\right)^2 Z_{in} A}, \qquad (7.155)$$

where the terms k_s, Z_{in} and Z_L have the same definition as given in section 7.4. In order for numerical stability to be guaranteed, it is necessary that $|C| < 1$. Hence, when k_s is zero, the AFM is stable regardless of the magnitude of the other terms within the expression for, C. However, when the magnitude of k_s is equal to 1, this is no longer the case. Under this operating condition, the expression for C becomes

$$C = \frac{(1 - A) Z_{in}}{Z_L + A Z_{in}}. \qquad (7.156)$$

Considering equation (7.156) more closely, it can be observed that the magnitude of C is less than unity when $A > 0.5$, regardless of the magnitudes of Z_{in} and Z_L (even if Z_L is zero) and the AFM will be numerically stable in all operating conditions. However, at much larger magnitudes of A, such that AZ_{in} is much greater than Z_L, the resulting magnitude of C will be very close to unity. Under these conditions, although it will be numerically stable, the AFM behaviour will become very oscillatory (see equation (7.153)).

For $|A| \leq 0.5$, the magnitude of C may be greater than unity (depending on the relative magnitudes of Z_{in} and Z_L) and as such, numerical stability is not guaranteed. Indeed, when the inverter is subjected to ac side short circuit conditions (where the effective magnitude of Z_L is expected to be lower than Z_{in}), the AFM is likely to suffer from the same instability problems as the original functional model (as described in Chapter 5).

Figure 7.25 summarises this analysis by illustrating the resulting magnitude of *C* for the range of *A*. The implications this analysis has for the application of the AFM method will be discussed at the end of this section.

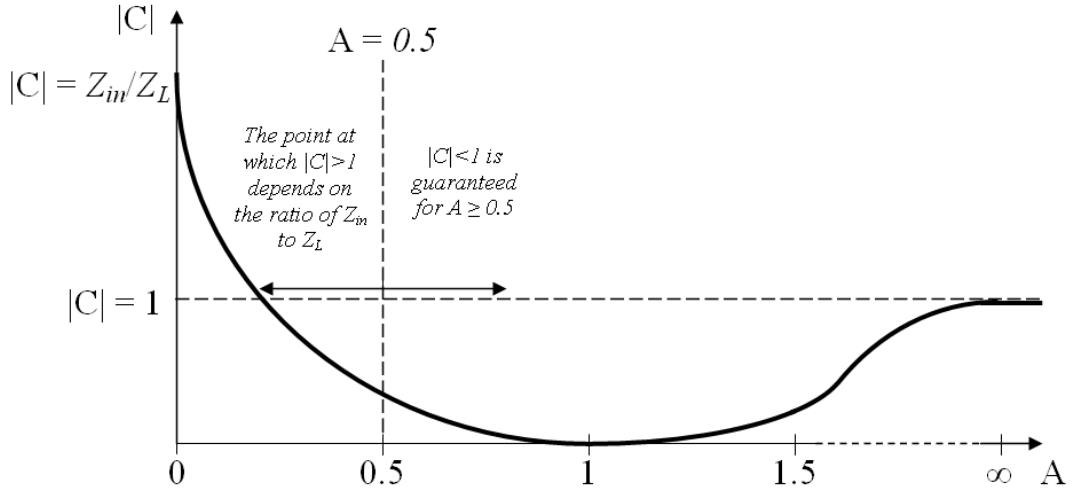

Fig. 7.25. Variation of the magnitude of *C* over the range of *A*

Figure 7.25 illustrates how the magnitude of *C* is zero when *A* has a unity magnitude (i.e. the AFM has been correctly implemented and there is no error in the derivation of Z_{in}). The magnitude of *C* increases either side of this point, due to the error in the derivation of Z_{in}. It also illustrates that the magnitude of *C* grows towards unity as the magnitude of A approaches infinity (i.e. when the derived Z_{in} is significantly large). Lastly, the figure shows that the magnitude of *C* can only be greater than unity in the region $0 < A \leq 0.5$ (i.e. when the derived Z_{in} is too small). However, the point at which $C = 1$ depends the ratio of the impedances Z_{in} and Z_L.

This section has shown that in complex networks where the derivation of Z_{in} may be more difficult, AFMs of different converters are likely to remain numerically stable under all operating conditions even with a modest error in the derivation of Z_{in}. For larger errors in this derivation however, the AFMs will become more oscillatory in behaviour and possibly even unbounded as the effective magnitude of the term C, approaches or even exceeds unity. Such findings would indicate that the AFM method is a robust and reliable method, whose successful operation does not depend on a perfect derivation of circuit parameters. This is an important finding, as it means that the AFM can be used in complex networks even if an accurate derivation of the required circuit impedance (e.g. Z_{in}) is difficult to achieve. That is, the method is not restricted to simpler applications where the required circuit impedance can be readily derived.

However, this analysis is not yet complete. In order to fully demonstrate the robustness of the AFM method, it is necessary to consider the likely sources of error in the derivation of the required circuit impedance (i.e. Z_{in}) and quantify as best possible the impact they will have on the overall accuracy of this derivation. This aspect will be considered in the following section.

7.13 (III) Impact of Network Architectures on the Inaccurate Derivation of AFM Variables

The next stage of the assessment into poor derivation of AFM circuit impedances (e.g. Z_{in}) is to consider the impact of the network architecture and size. This aspect

will be considered in this section using a model of a representative more-electric aircraft network as a case study [11, 12]. Figure 7.26 illustrates the schematic of this modelled network.

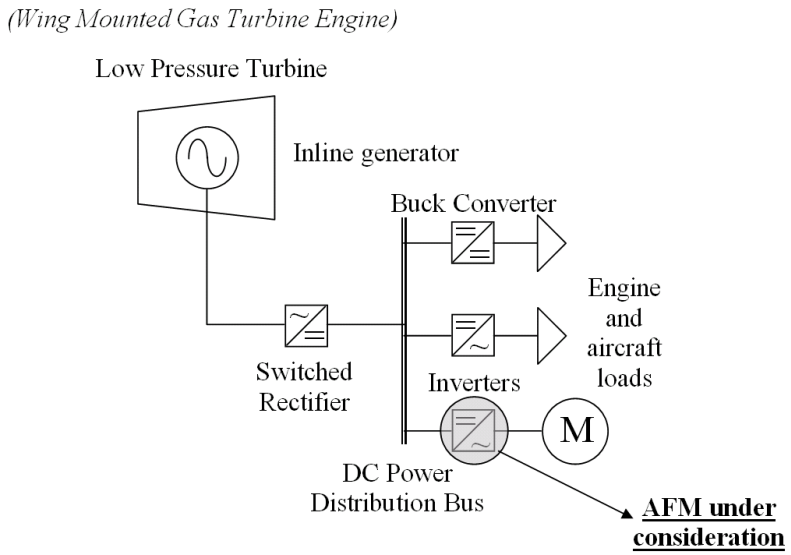

Fig. 7.26. More-electric aircraft network model

The network illustrated in figure 7.26 shows a dc power distribution system being supplied by a single generator interfaced through a switched rectifier interface. Multiple ac and dc loads are connected through power electronics interfaces to the dc power distribution bus.

This case study will consider the derivation of circuit impedance Z_{in} for the motor drive inverter AFM highlighted in figure 7.26. As described in section 7.4.3, this impedance is found by evaluating the Thevenin equivalent impedance [5] considered from the dc terminals of the converter model. Figure 7.27 illustrates the individual impedances of the network that combine to form the Thevenin impedance, Z_{in} for this

particular example. Note that in keeping with the Thevenin method, the voltage source representing the generator is not included in this network.

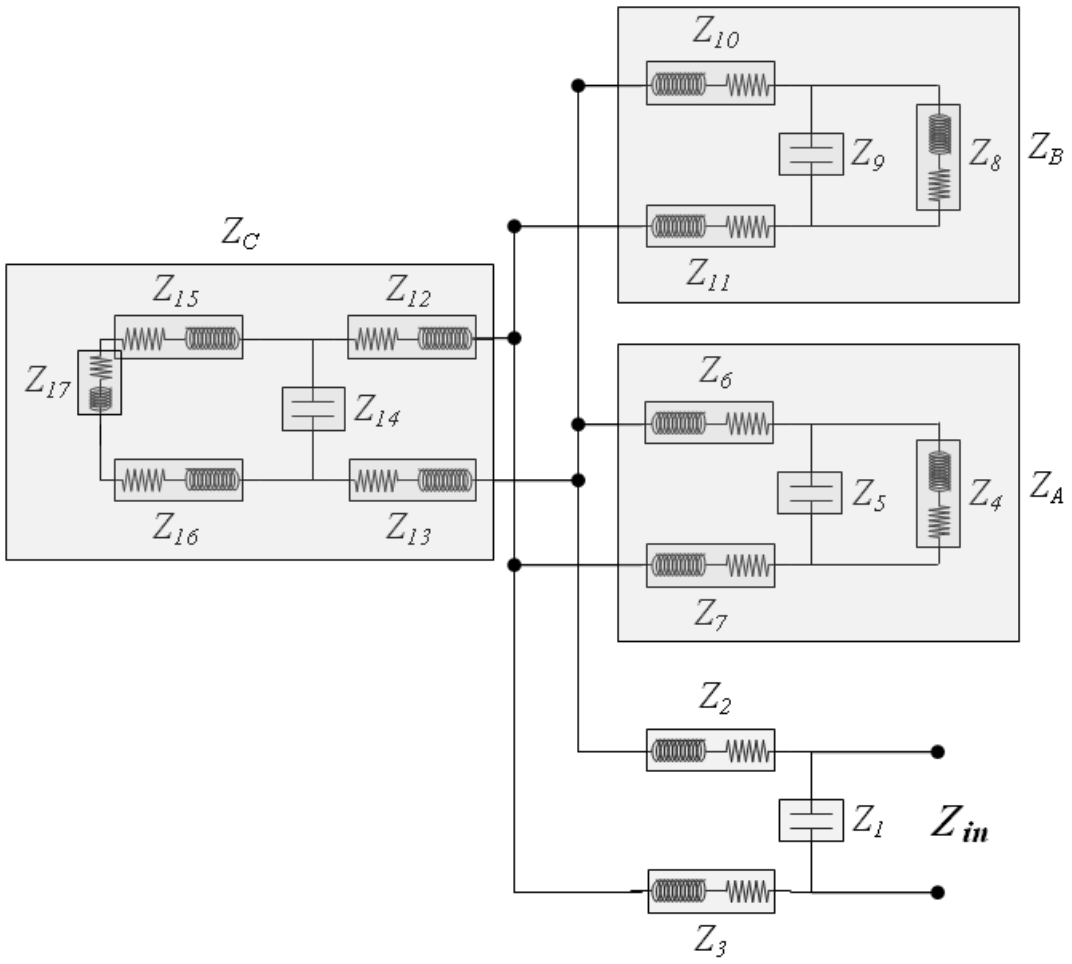

Fig. 7.27. Equivalent impedance network

In figure 7.27:

- Z_{in} is the Thevenin equivalent impedance as considered from the dc terminals of the motor drive inverter AFM.
- Z_1, Z_5, Z_9 and Z_{14} are filter capacitors for the power electronic converters and should be readily obtainable from the network model.

- Z_2, Z_3, Z_6, Z_7, Z_{10}, Z_{11}, Z_{12}, Z_{13} are cable impedances within the dc section of the network and should also be readily obtainable from the network model.
- Z_{15} and Z_{16} are ac side cable impedances. These will be more difficult to evaluate as they will vary with the switching state of the associated converter
- Z_4 and Z_8 are load impedances of the other dc bus connected systems. Again, these will be difficult to evaluate as they will vary with the switching state of the associated converter.
- Z_{17} is the internal impedance of the voltage source. This will be difficult to evaluate as it will vary with the switching state of the associated converter.

Z_A, Z_B and Z_C are equivalent grouped impedances and are defined as follows:

$$Z_A = Z_6 + Z_7 + \left(Z_5 \,//\, Z_4\right) \qquad (7.157)$$

$$Z_B = Z_{10} + Z_{11} + \left(Z_8 \,//\, Z_9\right) \qquad (7.158)$$

$$Z_C = Z_{12} + Z_{13} + \left(Z_{14} \,//\left(Z_{15} + Z_{16} + Z_{17}\right)\right) \qquad (7.159)$$

where '+' denotes a series connection and '//' denotes a parallel connection of impedances.

The effective magnitude of the Thevenin impedance Z_{in} will now be considered in order to evaluate the most influential terms of its magnitude.

The required AFM variable Z_{in} is defined as

$$Z_{in} = Z_1 // \left(Z_2 + Z_3 + Z_{ABC}\right) \qquad (7.160)$$

where

$$Z_{ABC} = Z_A // Z_B // Z_C \,. \qquad (7.161)$$

The expression for Z_{ABC} can be expanded as

$$Z_{ABC} = \frac{Z_A Z_B Z_C}{\left(Z_A Z_B + Z_B Z_C + Z_A Z_C\right)} \,. \qquad (7.162)$$

The expression for Z_{in} given in equation (7.160) can also be expanded as

$$Z_{in} = \frac{Z_1 Z_2 + Z_1 Z_3 + Z_1 Z_{ABC}}{Z_1 + Z_2 + Z_3 + Z_{ABC}} \,. \qquad (7.163)$$

Based on equation (7.163), the impedances Z_1, Z_2 and Z_3 are the key determining terms for Z_{in}. In particular, the magnitude of Z_1 impacts on this variable with the greatest influence. Other circuit impedances have a diminishing influence on the overall value of Z_{in}.

Overall, it is a good outcome that the three most influential terms in Z_{in} are readily known and that any uncertainty in the other terms has a much lower impact on the determination of Z_{in}. More generally, Z_{in} is most sensitive to impedances 'close to' the AFM converter (i.e. those connected to the terminals of the converter), which are

also the most likely to be accurately derived. Additionally, Z_{in} is less sensitive to impedances which are 'more distant' from the converter (i.e. those not directly connected to the converter), which are less likely to be accurately derived. These findings are also transferable to AFMs of other converter topologies.

On the basis of the findings of this and the previous sections, it is evident that the AFM method is a robust method even if there is some error introduced in the derivation of Z_{in}.

It is worth noting at this stage though that there will be additional difficulties associated with implementing AFMs in complex electrical network architectures. High order impedances will be difficult to implement with fixed impedances and controlled switches and this arrangement will also be more computationally demanding to simulate. Clearly there is scope for further work in addressing the aspects of applying AFM within larger networks (details of this work will be discussed later in the chapter). However, the analysis conducted in this and the previous section indicates that when fully developed, the AFM method will be particularly suited for application within models of complex electrical network architectures, such as those found in marine and aerospace more-electric systems.

7.14 (III) Demonstration of a Single-Phase Inverter AFM

This section will illustrate the operation of a lumped-parameter single-phase inverter AFM model implemented within a power systems simulation package. Its output

under normal and faulted conditions is validated against that of a switched model in order to illustrate the accuracy and robustness of the AFM technique.

7.14.1 (III) Model Description and Parameters

Figure 7.28 shows the schematic of the modelled converter system.

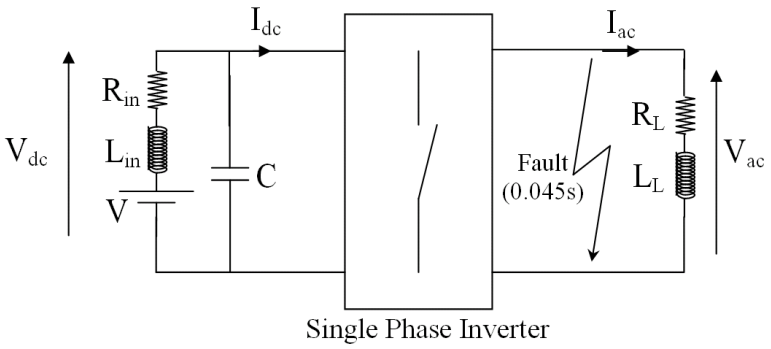

Fig. 7.28. Schematic of the modelled network

Note that the converter shown in figure 7.28 operates with an open loop control scheme and as such will not alter its operation following the application of the fault. This approach has been taken to avoid masking the response of the implemented software models to the application of the fault. The parameters of this network and the inverter are described in table 7.8.

Table 7.6 Network and inverter parameters.

Parameter	**Value**
V	100V
C	100μF
R_{in}	0.1Ω
L_{in}	10μH
R_L	5Ω
L_L	1mH
Fault impedance	50mΩ (applied at 0.045s)
PWM carrier frequency	2000Hz

Figure 7.29 shows the single phase inverter switched model implemented within the SimPowerSystems block set of Matlab Simulink [8].

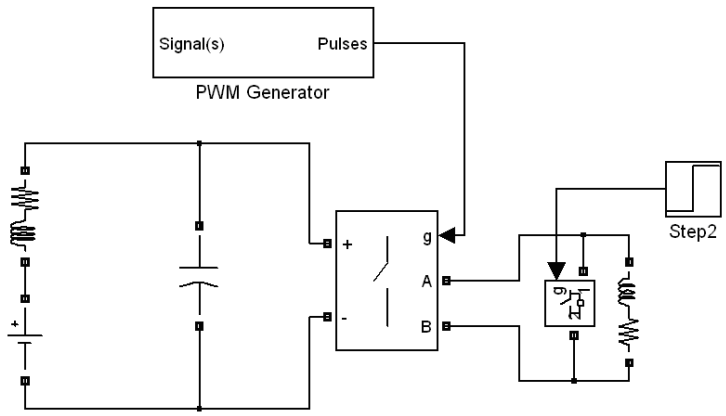

Fig. 7.29. Implemented switched model

Figure 7.30 shows the top-level schematic of the equivalent lumped-parameter single phase inverter AFM also implemented within SimPowerSystems.

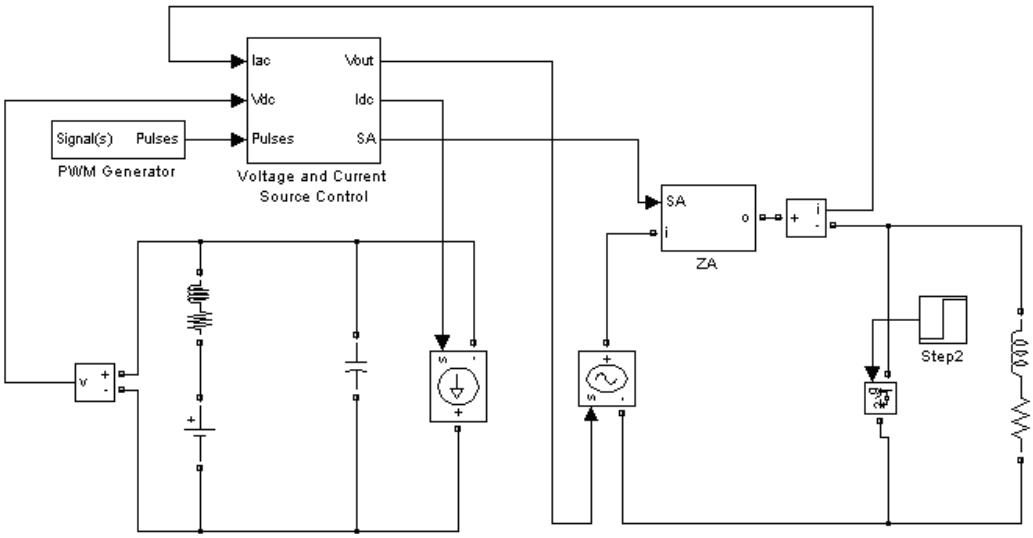

Fig. 7.30. Implemented AFM – main schematic

A comparison of figures 7.29 and 7.30 illustrates how the AFM utilises a controlled voltage source and a controlled current source in place of the inverter's switches. Figure 7.30 also illustrates the location of the additional controlled impedance Z_A (defined in section 7.4). The internal components of this controlled impedance are shown in figure 7.31.

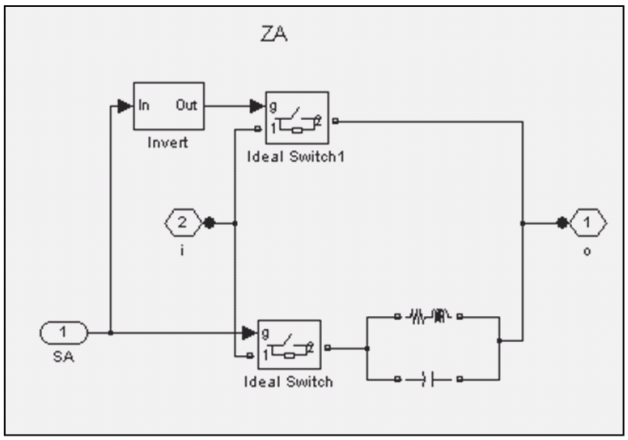

Fig. 7.31. Implemented AFM – internal components of Z_A

Figure 7.31 shows how the expression for Z_A has been implemented using fixed impedance components and controlled switches (as described in Section 7.4).

Figure 7.32 illustrates how the control of the AFM voltage and current sources is achieved.

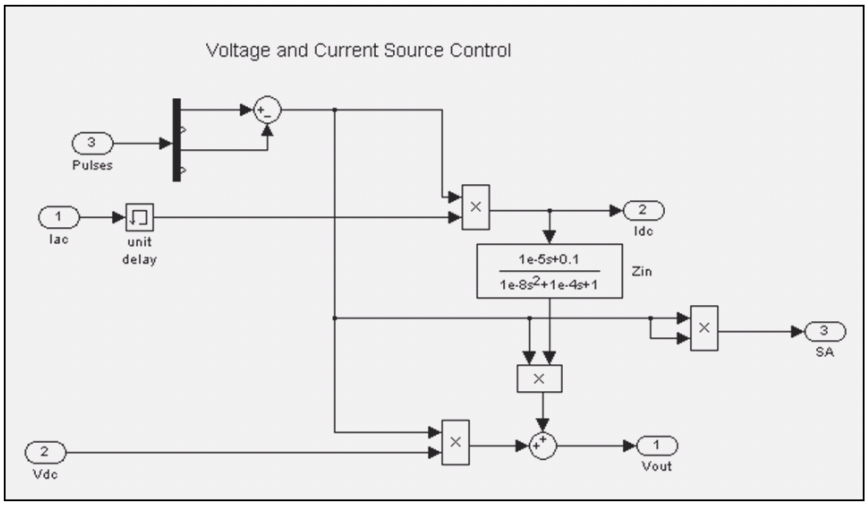

Fig. 7.32. Implemented AFM – voltage and current source control

This figure illustrates how the AFM retains the unit delay, inherited from the original functional inverter model control architecture. As explained in section 7.4, this approach is taken so that no algebraic loops are present in the model.

7.14.2 (III) Simulation Results

Figures 7.33, 7.34 and 7.35 illustrate the steady state ac current between 0 and 0.02 seconds of simulation time for the switched model, AFM and time-averaged AFM respectively. These plots show the behaviour of the converter models during normal (i.e. unfaulted) operating conditions supplying an ac load of fixed impedance. Note that the time-averaged model utilised to produce these results does not make use of the additional error reduction term A_{err} (discussed in Section 7.5.4) because there is no additional voltage source on the ac side of the inverter and as such, the error in V_{ac} produced by the AFM under these conditions should be negligible.

Additional figures showing plots of ac side voltage, and dc side voltage and current for each of the inverter models listed above can be found in Appendix D.

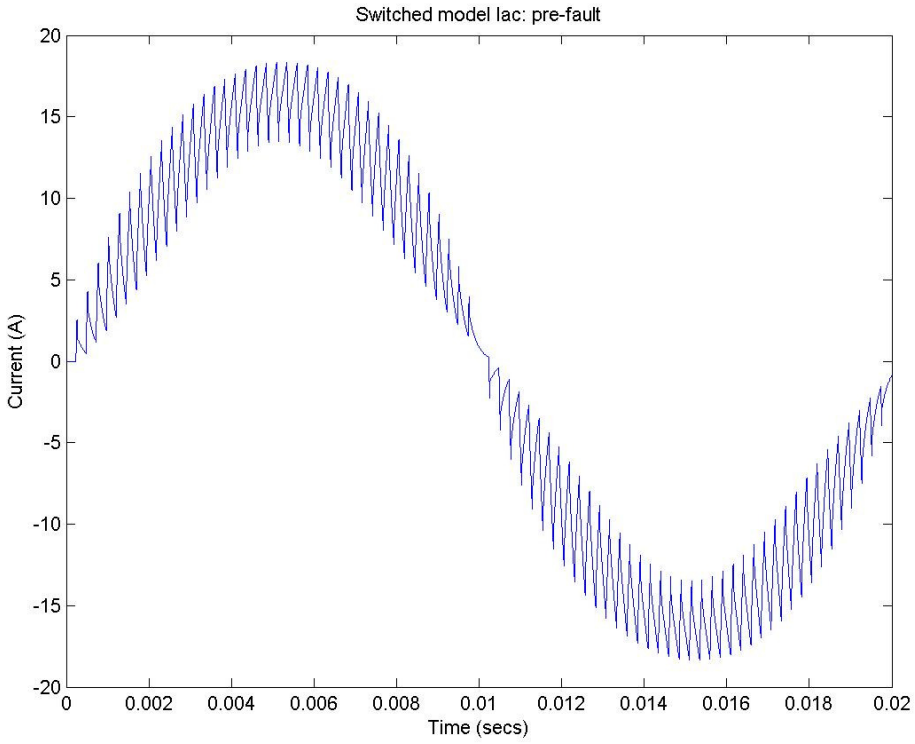

Fig. 7.33. Switched model Iac – Pre-fault

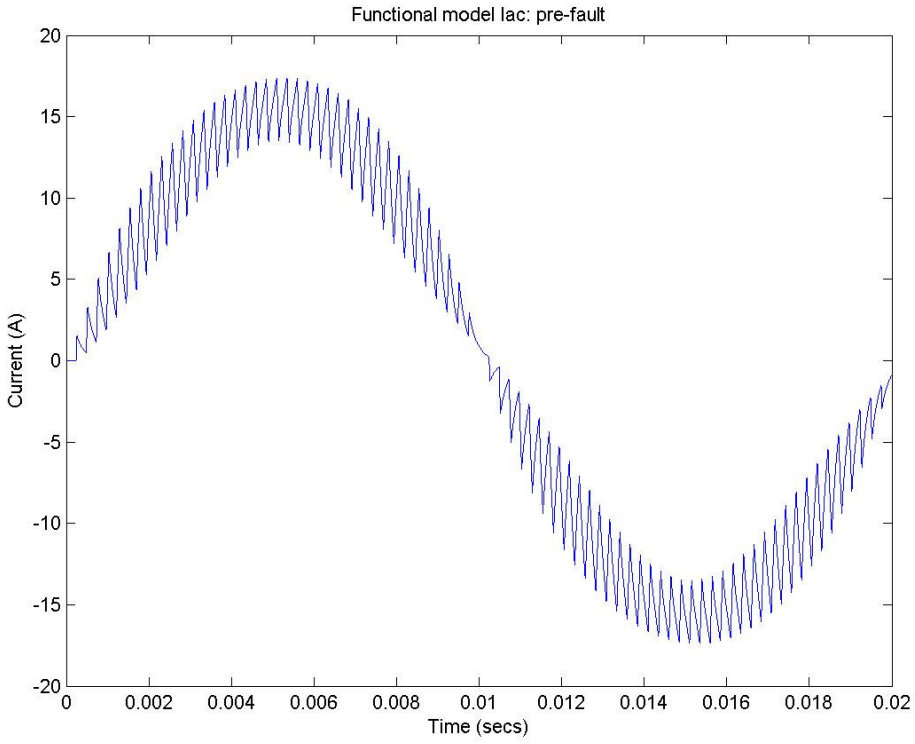

Fig. 7.34. AFM Iac – Pre-fault

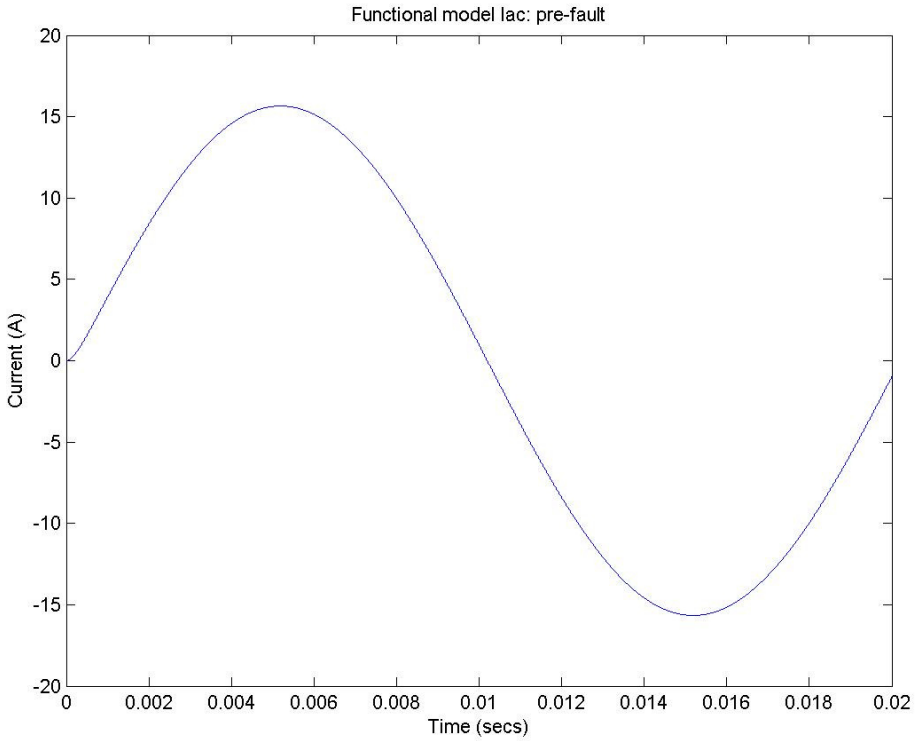

Fig. 7.35. Time-averaged AFM Iac – Pre-fault

Figures 7.36, 7.37 and 7.38 illustrate the steady state ac current between 0.06 and 0.08 seconds of simulation time for the switched model, AFM and time-averaged AFM respectively. This second group of plots shows the behaviour of the converter models after a low impedance rail to rail fault has occurred across the ac terminals of the inverter. Additional figures showing plots of ac side voltage, and dc side voltage and current for each of the inverter models listed above can be found in Appendix D.

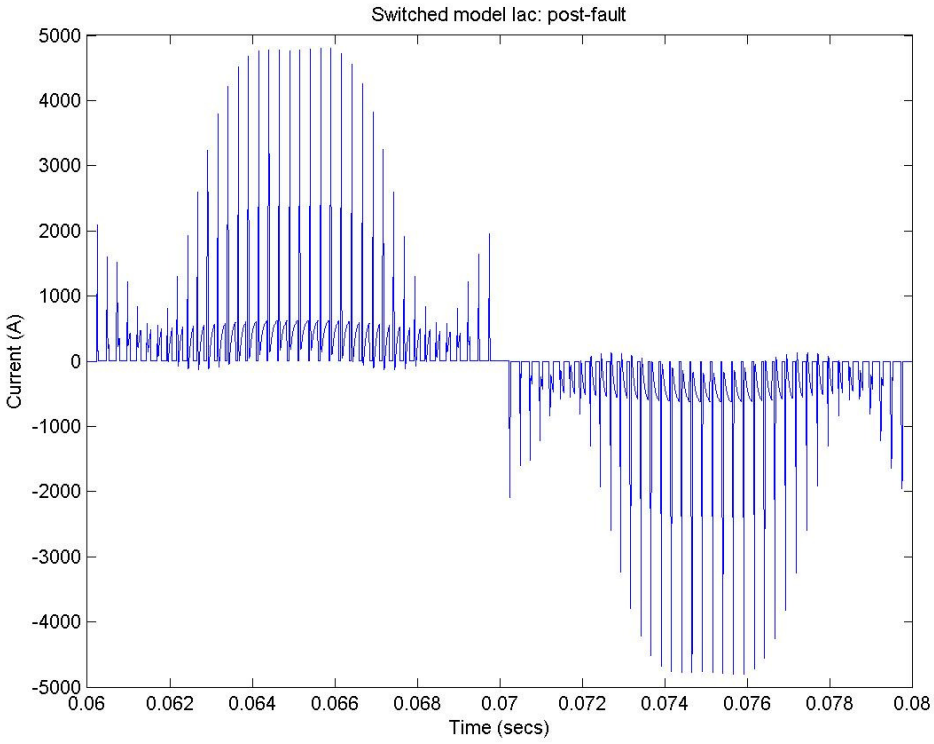

Fig. 7.36. Switched model Iac – Post-fault

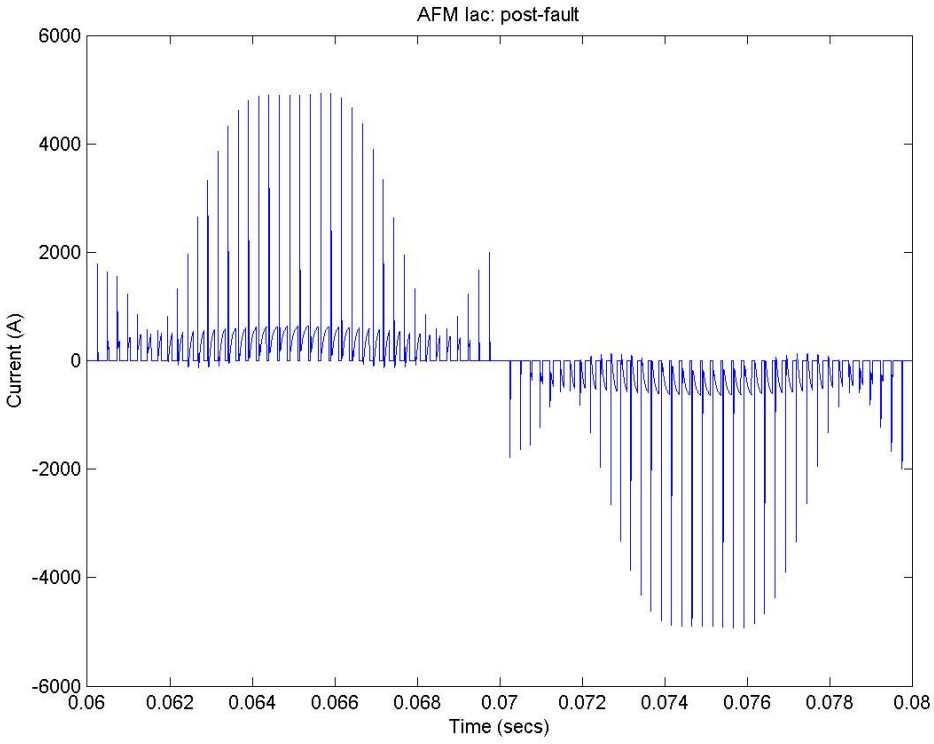

Fig. 7.37. AFM Iac – Post-fault

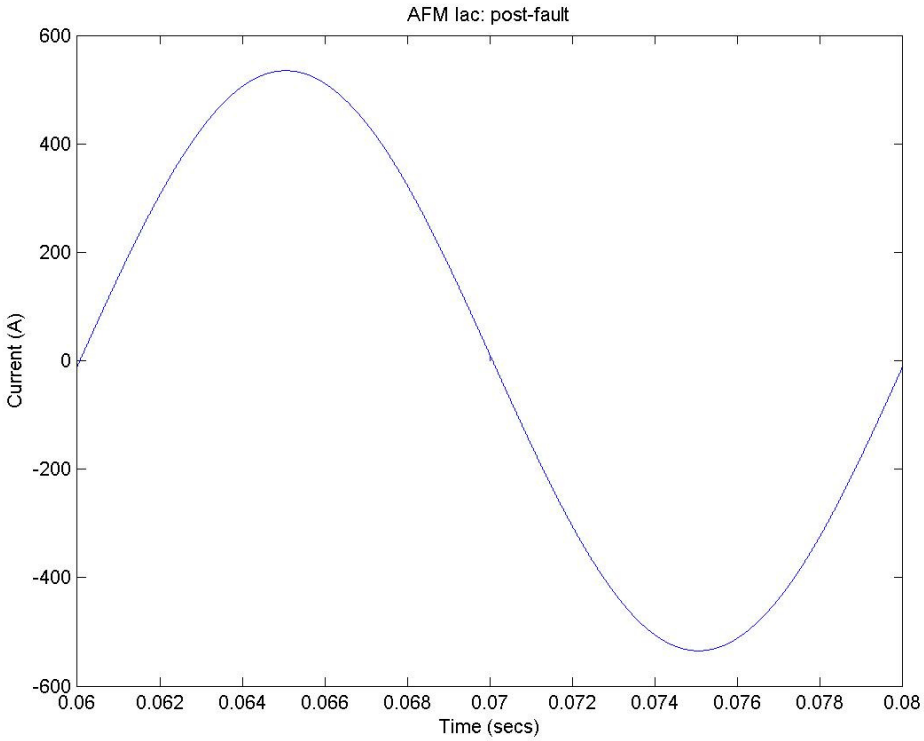

Fig. 7.38. Time-averaged AFM Iac – Post-fault

7.14.3 (III) Summary of Findings

By comparing the simulation results produced by the AFM representations (figures 7.34, 7.35, 7.37, 7.38) to those produced by the switched inverter (figures 7.33 and 7.36), the accuracy of the AFM and time-averaged AFM can be assessed. It is observed that inverter AFM representations successfully replicate the terminal behaviour of the switched model. This is still the case during simulated fault conditions, where the original functional model has been shown to be numerically unstable and inaccurate (as shown in Chapter 5).

Overall, this case study illustrates the success of the AFM approach in achieving its key objectives under this operating condition. That is, by replacing all the delayed terms in the transfer function of the original functional model with non-delayed equivalents, the numerical stability of the model has been maintained whilst the terminal conditions of the original switched model have still been represented accurately.

These findings reinforce the key outcomes of the analyses conducted earlier in this chapter.

7.14.5 (III) Additional Simulation Results – Erroneous Derivation of Z_{in}

In order to provide an illustration of the robustness of the AFM method even when the magnitude of Z_{in} is inaccurately derived, this section considers the response of the AFM converter when it is implemented with a 50% error in the derivation of C, R_{in} and L_{in}, such that the derived C = 50μF, the derived R_{in} = 0.05Ω and the derived L_{in} = 5μH (see Table 7.8 for original values). Section 7.12 highlighted this level of error as the maximum allowable error that would still guarantee numerically stable (although very oscillatory) simulation results. Hence, it is a worthwhile investigative exercise to assess the impact on the behaviour of the AFM with this level of error present in the derivation of Z_{in}.

Figures 7.39 and 7.40 illustrate the steady state ac current between 0 and 0.02 seconds, and between 0.06 and 0.08 seconds of simulation time respectively. These

plots show the behaviour of the converter models during normal (i.e. unfaulted) and faulted operating conditions supplying an ac load of fixed impedance. Additional figures showing plots of ac side voltage, and dc side voltage and current can be found in Appendix D.

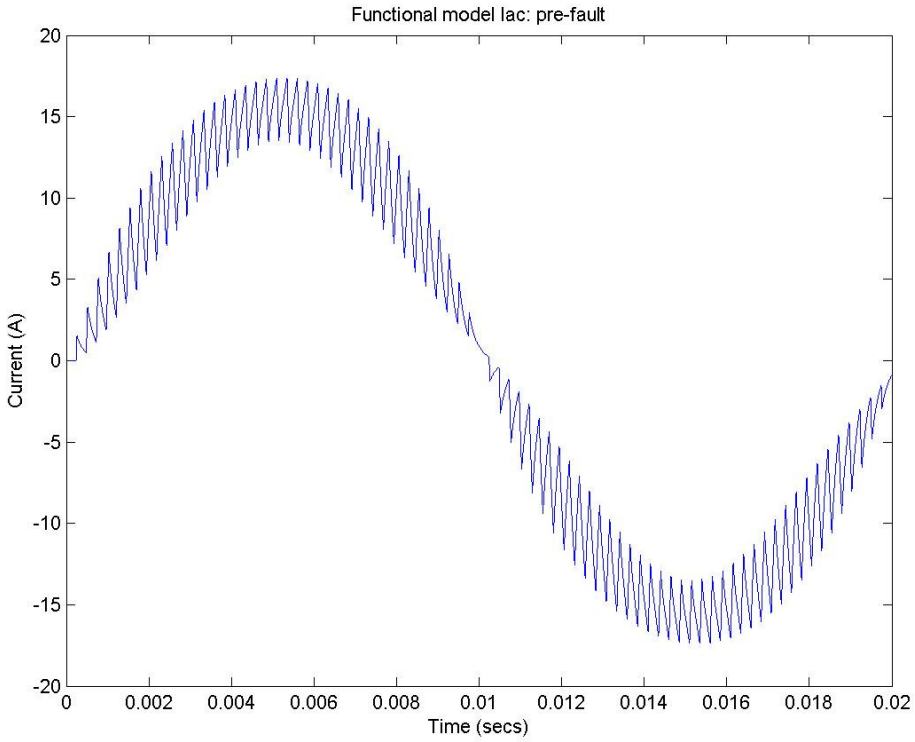

Fig. 7.39. Erroneous AFM Iac – Pre-fault

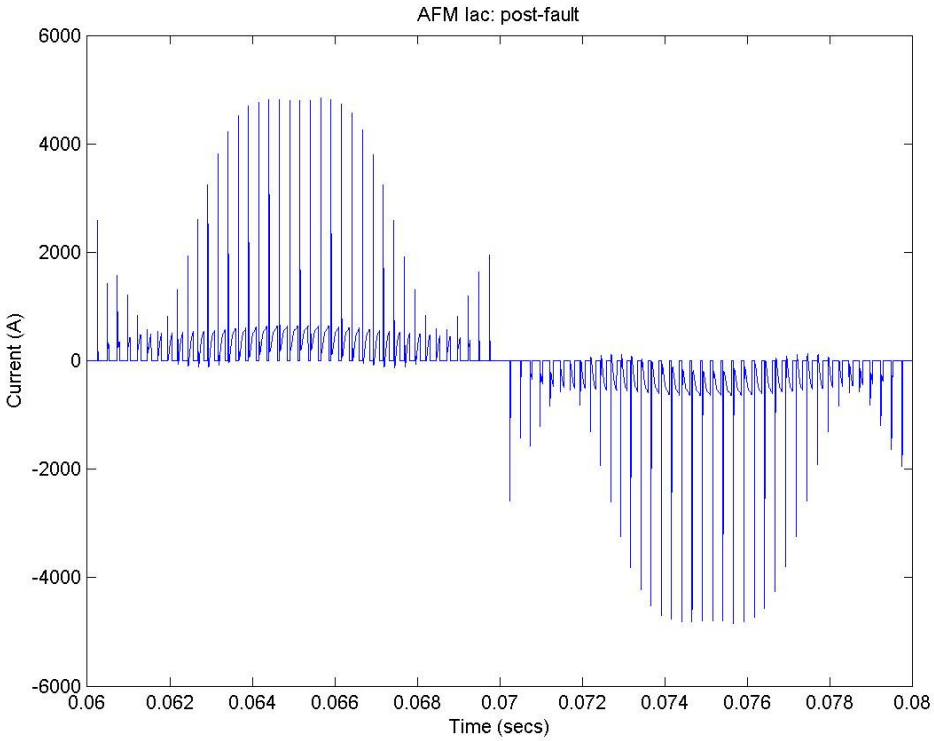

Fig. 7.40. Erroneous AFM Iac – Post-fault

As with the previous cases, by comparing the simulation results for this case (figures 7.39 and 7.40) to those produced by the switched inverter figures 7.33 and 7.36), it is observed that the AFM still accurately replicates the behaviour of the switched inverter model even when it is implemented with a 50% error in the derivation of Z_{in}. Any oscillatory behaviour in the model is not noticeable at this level of examination although it becomes more pronounced as the magnitude of either the term A (as defined in section 7.12) or the fault impedance decreases (this finding is in line with the analysis presented in section 7.12 regarding equation (7.156)).

While it is acknowledged that the accuracy of AFMs in other applications may vary compared to this case, the results presented in figures 7.39 and 7.40 once again

illustrate the robustness of this method even when the accurate derivation of the required circuit impedance (Z_{in}) is difficult to achieve.

7.15 (III) Computational Efficiency Comparisons

In order to evaluate the impact of the AFM's novel features on its computational efficiency (in comparison to the original functional modelling method), table 7.6 shows the comparative run times (averaged over multiple simulations) of the switched model, AFM, time-averaged AFM, functional model and averaged functional model for the case study presented in Appendix D. Note that all simulations were conducted using a $2^{nd}/3^{rd}$ order Runge-Kutta variable step solver [13] and the completion times were measured using Matlab functionality [8].

Table 7.7 Details of comparative simulation completion times

Model	**Average Completion Time for a 0.08s Simulation**	**Completion Time as a % of Switched Model**
Switched	8.664s	100%
AFM	2.016s	23.2%
Time-averaged AFM	0.797s	9.2%
Functional model	1.594s	18.4%
Time-averaged functional model	0.75s	8.7%

Table 7.6 illustrates how the completion times achieved with the pulsed and time-averaged AFM models are only slightly greater than those of the original functional models. This indicates that the presence of the additional features within the AFMs has not lead to a significant increase in computational burden.

It should also be noted that the difference between the completion times of the time-averaged functional model and time-averaged AFM is much smaller than for the pulsed output (i.e. non-averaged) models. This finding is in line with the observations made in Section 7.4. There it was stated that the additional controlled switches within the time-averaged AFM operate at a much lower frequency than within the pulsed model. This produces only a very small increase in the computational requirement compared to that of the time-averaged functional model.

If the network shown in figure D.1 of Appendix D is modelled using the Multi-Level Model Discretization (MLMD) technique presented in Chapter 6, operating with a fixed step size of 10μs, the average simulation completion time is 3.1 seconds. This is comparable to the pulsed functional and AFM models but is much slower than the time-averaged versions. Note however, that the level of error produced by MLMD will be often be significantly higher than that produced by the AFM method due to the use of discrete models and fixed solver time steps (this aspect is discussed in Chapter 6).

Additionally, larger comparative time savings with regards to the original switched model are presented for the MLMD technique in the case study given in Chapter 6.

This is a reflection of the cumulative effect on the simulation completion time produced by reducing the computational burden of every converter model within a multi-converter network model. Similar cumulative effects can be expected from the functional and AFM techniques also.

7.16 (III) Further Work

Based on the analyses of the AFM concept provided in this chapter, and its recognised limitations, the following further work is suggested in order to improve the capabilities of this method.

- Expand the AFM concept to accommodate converter topologies not presented in this chapter. In particular, address the unique challenges that will arise in the implementation of AFMs of multi-level or multi-phase converters (i.e. greater than three ac phases). This will facilitate the use of the AFM method for the modelling of advanced propulsion drives in marine-electrical applications [14, 15] and novel generation technologies in aerospace-electrical applications [10, 11].
- Develop a robust methodology to accommodate the effects of other converters' switching effects (for both switched models and AFMs) on the derivation of the required circuit impedances (e.g. Z_{in}). For example, given that sections 7.13 and 7.14 have shown the AFM to be accurate with small errors in the derived AFM circuit impedance, this methodology may involve selecting an appropriate fixed impedance which produces the smallest error in the total derived circuit impedance.

- Develop a software tool which automatically derives the Thevenin equivalent impedance for different points in a network. This should account for other active devices in the network (for example utilising a methodology similar to the one described above) and even quantify the maximum error in the derived impedance to allow the numerical stability of the AFM converter to be assessed.
- Develop a methodology for reducing the order of the derived AFM impedance. It is likely that higher order terms in the expression for the derived impedance could be neglected without introducing any significant errors. Reducing the order of the derived impedance would simplify the implementation of the AFM and improve its computational efficiency.
- Validate the behaviour of a network with multiple converter AFMs against that of a similar network with switched models when all of the above suggestions for further work have been addressed. This task would give increased confidence in the use of the AFM for applications involving complex electrical network architectures, such as marine and aerospace more-electric systems.
- Re-address the time-averaged AFM with a view to reducing the errors generated in terminal conditions. This may be achievable through a more complex arrangement for the derived AFM impedance.
- Consider alternative approaches to implementing the AFM concepts in three-phase converters such that accuracy in the phase voltages with respect to the dc side of the converter is achieved, thereby allowing earth fault studies to be conducted with this particular AFM.

- Adapt the AFM concept for use in behavioural models of other fast acting devices or systems. The surge arrestor model discussed in Chapters 3 and 4 is a good example of this, where the algebraic loop present within the model creates convergence and numerical stability issues similar to those faced in the use of behavioural converter models. Adapting the AFM method and applying it to this model may provide a solution to the noted challenges of modelling a surge arrestor.

7.17 (III) Conclusions

This chapter has demonstrated a novel technique, Advanced Functional Modelling (AFM), for the modelling and simulation of power electronics converters which is based on the functional modelling technique described in Chapter 5. This technique provides excellent computational reductions compared to switched converter models whilst maintaining numerical stability during simulated fault conditions, where the functional modelling technique has been shown to be unreliable. The core principles of this technique have been described, its application to a range of converter topologies has been demonstrated and guidelines on its implementation within larger electrical network models have been provided.

As it stands, the AFM technique presented in this chapter provides an immediate and significant contribution to the stable and efficient modelling and dynamic simulation of individual power electronic converter systems operating in both normal and faulted networks. Further work is required to develop the technique to a stage where multiple AFMs can be readily employed in models of complex electrical network

architectures with a significant penetration of power electronics (such as those found in marine and aerospace more-electric systems). However, the concepts and analysis conducted in this chapter indicate that the AFM concept can become a very useful tool for these applications with further developmental effort applied. Additionally, the compatibility of this approach with the Multi-Level Model Discretization technique is also a key strength given its incomplete development as well as the difficulties associated with implementing functional models of diode bridges (as discussed in Chapter 5). Indeed, the use of both techniques in harmony will provide a strong foundation for efficient and robust modelling and dynamic simulation of marine and aerospace more-electric network architectures.

7.18 References

[1] H. Jin, "Behaviour-mode simulation of power electronic circuits," *IEEE Trans. on Power Electronics*, Vol. 12, no. 3, pp. 443 – 452, May 1997.

[2] J. Clare, P. Zanchetta, P. Wheeler, L. Empringham, "Modelling and design of matrix converter solutions for shipboard applications," *Proc. IMarEST Electric Warship IX Seminar*, December 2003, pp. 20 – 34.

[3] C. Booth, G. Dudgeon, J.R. McDonald, A. Kinson, J. Hill, "Protection of modern marine power systems: challenges and solutions", Proc. *Eighth IEE International Conference on Developments in Power System Protection,* pp. 825 – 828, April 2004.

[4] P. J. Norman, S. J. Galloway, and J. R. McDonald, "Simulating electrical faults within future aircraft networks," *IEEE Trans. on Aerospace and Electronic Systems*, Vol. 44, no. 1, pp. 99-110, January 2008.

[5] R. Nave, "Thevenin's Theorem." Available at: http://hyperphysics.phy-astr.gsu.edu/hbase/electric/thevenin.html (accessed 11/05/2009)

[6] Barry W. Williams, *Power electronics: devices, drivers, applications, and passive components*. Available http://www.eee.strath.ac.uk/~bwwilliams (accessed 11/05/2009)

[7] A. M. Gole, A. Keri, C. Nwankpa, E. W. Gunther, H. W. Dommel, I. Hassan, J. R. Marti, J. A. Martinez, K. G. Fehrle, L. Tang, M. F. McGranaghan, O. B. Nayak, P. F. Ribeiro, R. Iravani, Lasseter, "Guidelines for modeling power electronics in electric power engineering applications," *IEEE Trans. on Power Delivery*, Vol. 12, No. 1, pp. 505 – 514, January 1997.

[8] *Using Matlab*, The Mathworks Inc., 3 Apple Hill Drive, Natick, MA, USA, 2002.

[9] CDR John V. Amy Jr, "Modern, high-converter-populations argue for changing how to design naval electric power systems," *Proc. 2005 IEEE Electric Ship Technologies Symposium (ESTS)*, Philadelphia, July 2005, pp 280 – 283.

[10] Lester F. Faleiro, "Trends towards a more electrical aircraft," Liebherr-Aerospace. Available: http://www.poa-project.com/53.asp (accessed 13/10/2008)

[11] Richard Newman, "The more electric engine concept," *SAE Technical Papers*, document number: 2004-01-3128.

[12] Liebherr Aerospace, "Power Optimised Aircraft", Available at: www.poa-project.com (accessed 13/10/2008)

[13] J. Arrillaga, N. R. Watson, *Computer modelling of electrical power systems*" 2nd Edition, Wiley, 2001.

[14] David Gritter, Swarn S. Kalsi, Nancy Henderson, "Variable speed electric drive options for electric ships," *Proc. IEEE Electric Ship Technologies Symposium (ESTS)*, Philadelphia, Pennsylvania, USA, July 2005, pp. 347 – 354.

[15] C. G. Hodge, "Modern applications of power electronics to marine propulsion systems," Proc. *2002 IEEE International Symposium on Power Semiconductor Devices and ICs (ISPSD).* Available: http://www.ship.org.tw/Upload/ISPSD_2002_Paper.pdf (accessed 11/05/2009)

Chapter 8 – Thesis Conclusions

8.1 Chapter Overview

This chapter will summarise the key conclusions reached within this thesis and discuss the potential application of the novel methods presented for use within the modelling and simulation of marine and aerospace more-electric networks.

8.2 Key Thesis Conclusions

The key conclusions reached within this thesis are as follows:

Chapter 2:

- Due to the large proportion of novel technologies incorporated, the behaviour of many marine and aerospace more-electric network architectures is not fully understood and as such, there are many research challenges still outstanding within these fields. As a result, it is important to support their design and implementation with informed modelling and simulation to de-risk the technologies employed. In particular, network-level dynamic simulations are required to assess the behaviour and interactions within electrical power distribution networks for operation during both healthy and faulted conditions.
- Due to the complex nature of the models utilised for network-level dynamic simulations, the associated computational overhead is significant, often

resulting in impractically long simulation completion times (typically in the order of several hours or more). To overcome this, it is usually necessary to abstract the models to the lowest level of detail required. In particular, power electronic converter models can be especially computationally intensive and require appropriate levels of abstraction.

Chapter 3:

- The abstraction of power electronic converter models has been recognised as a matter of some significance in existing literature. A detailed review concludes that functional modelling techniques are the most suited to marine and aerospace dynamic simulations because they can be readily implemented and offer significant gains in computational efficiency (i.e. simulations complete up to 30 times quicker than those with detailed converter models).
- However, the literature review also raises questions about the validity of these models in some operating circumstances, such as electrical fault studies. The ability to simulate fault scenarios is a key requirement of the dynamic marine and aerospace electrical system models and this noted drawback is of particular concern. A more detailed investigation is necessary in order to fully assess the capabilities of functional modelling techniques and their applicability to marine and aerospace, network-level dynamic simulations.

Chapter 4:

- Algebraic loops occur within many models, including those of marine and aerospace electrical power distribution networks. A conceptual analysis

indicates that these are also present within functional models. Algebraic loops are undesirable as they increase the computational overhead of simulations. As such, whilst algebraic loops cause few difficulties in smaller, more easily computed models, their presence in large and more complex marine and aerospace network models causes slow running simulations and possible convergence problems.

- Although there are three main techniques discussed in existing literature that facilitate the removal of algebraic loops, detailed analysis shows that in fact, only two of these; reduction to a feed forward equivalent system and the insertion of a small delay, actually achieve this. The third method (insertion of a low pass filter) is instead shown to reduce additional computational burden of algebraic loops by aiding numerical convergence.
- In complex models, such as those of marine and aerospace more-electric architectures, the option of reducing the feedback loop to a feed forward equivalent is rarely applicable and so the insertion of a small delay into the algebraic loops is the only viable solution for their removal. However, a detailed analysis shows that this approach introduces finite limits to the numerical stability of the model, which are determined by a number of its parameters. Therefore it is essential that the impact of this solution on the functional modelling technique is quantified in order to fully assess its potential applicability to the dynamic simulation of marine and aerospace electrical networks.

Chapter 5:

- Numerical analysis shows functional converter models to be at a high risk of becoming inaccurate and unbounded during many simulated electrical fault conditions. This represents a particular limitation in the application of functional models to marine and aerospace network-level simulations, where many studies of this type will be conducted.
- A need hence exists to develop novel power electronics model abstraction techniques which are suited to the modelling and simulation of marine and aerospace more-electric networks and which are also numerically stable during simulated fault conditions.

Chapter 6:

- Given the desire to avoid techniques which are build-intensive or inaccurate during some operating circumstances (e.g. fault studies), an alternative approach for the efficient and yet accurate simulation of electrical power networks with a significant penetration of power electronics is proposed. This technique is numerically stable under all operating conditions and is hence reliable during simulated electrical fault conditions. It is also readily implemented, thereby providing additional value.
- The technique, Multi-Level Model Discretization (MLMD), applies the discretization of the modelled electrical and control signals, not for accuracy, but to improve the computational efficiency of simulations, reducing overall completion times to around 1% of that taken by equivalent detailed models.

The fixed step size of the simulation solver is used as a means to achieve varying levels of model abstraction.

- Through case studies and conceptual analysis, it is shown that MLMD provides the greatest increase in simulation speed when applied to models of multi-converter networks and so is particularly suited to network-level modelling and dynamic simulation of marine and aerospace more-electric network architectures.

Chapter 7:

- The Advanced Functional Modelling (AFM) technique developed as part of this thesis runs up to four times quicker than MLMD whilst still maintaining numerical stability under all operating conditions (based on the implementation of time-averaged converter behaviour)
- Areas for further development and refinement of the AFM technique are identified in order to enhance its value and applicability to the specified application areas.

8.3 Chapter Conclusions

Overall, this thesis has investigated options for computationally efficient, but accurate methods for the network-level modelling and dynamic simulation of more-electric marine and aerospace networks, with a particular emphasis on power electronic converter representation. The novel techniques presented have significantly increased the options to achieve these aims. Equally as important, these techniques can be readily implemented within existing electrical system models, a

feature which has been a key emphasis throughout the thesis. This aspect is largely not considered for many of the techniques proposed in existing literature, although this reflects the only recently emerging need for dynamic network-level simulation of novel electrical network architectures.

Appendices

Appendix A – Derivation of Three-Phase Inverter AC Current Variables

A.1 Formation of Basic Equations

Consider the functional model representation of a three-phase inverter shown in figure A.1.

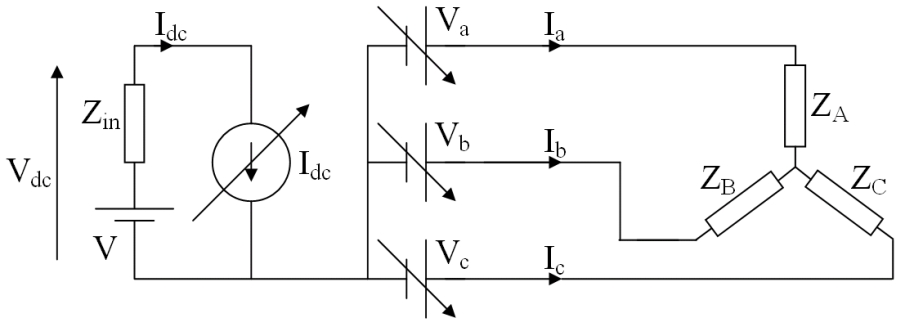

Fig. A. 1. Three-phase functional inverter model

In three-phase power electronic systems, the neutral point of ac load is not balanced and as such does not hold a zero potential (with reference to the negative terminal of the dc source) during normal operating conditions [1, 2]. As a result, the ac line currents I_a, I_b and I_c cannot be simply derived from V_a/Z_a, V_b/Z_b and V_c/Z_c. To demonstrate this, consider the inverter model in figure A.1 operating with $V_a = V_{dc}$, $V_b = 0$ and $V_c = 0$. Figure A.2, shows the ac side network under these conditions.

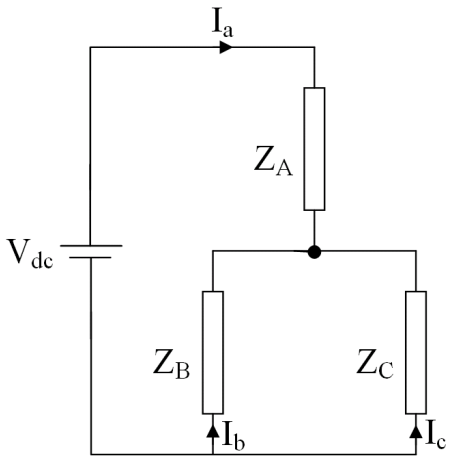

Fig. A. 2. Equivalent ac side circuit

In this circuit arrangement, the ac side phase currents I_a, I_b and I_c are hence defined as

$$I_a = \frac{V_{dc}}{Z_A + \dfrac{Z_B Z_C}{Z_B + Z_C}}, \qquad \text{(A.1)}$$

$$I_b = -I_a \frac{Z_C}{Z_B + Z_C}, \qquad \text{(A.2)}$$

$$I_c = -I_a \frac{Z_B}{Z_B + Z_C}. \qquad \text{(A.3)}$$

Note that in all parts of the analysis conducted, there are no delayed terms within the expressions presented. As such, notation of *(n)* has been omitted from all the non-constant terms in these expressions to simplify the appearance of the equations presented.

If the ac side load is assumed as balanced, such that Z_A, Z_B, $Z_C = Z$, equations (A.1), (A.2) and (A.3) can be reduced to

$$I_a = \frac{2}{3}\frac{V_{dc}}{Z}, \qquad \text{(A.4)}$$

$$I_b = -\frac{1}{3}\frac{V_{dc}}{Z}, \qquad \text{(A.5)}$$

$$I_c = -\frac{1}{3}\frac{V_{dc}}{Z}. \qquad \text{(A.6)}$$

The unequal current magnitudes of this example hence demonstrate the necessity to derive expressions for the ac side line currents from first principles. Figure A.3 shows the circuit diagram of the ac side of the converter with two loops and a node labelled for later analysis using Kirchoff's laws.

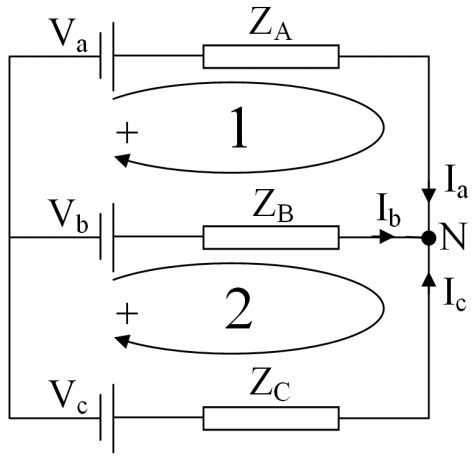

Fig. A.3. AC side of the three-phase functional inverter

As there are three unknowns (I_a, I_b and I_c), three distinct equations must be developed to obtain a unique solution. The first of these is achieved by considering Kirchoff's Current Law ("the algebraic sum of the current meeting at any point in a circuit is zero" [3]) around node N.

$$I_b = -I_a - I_c\,, \qquad \text{(A.7)}$$

In order to form the second equation, Kirchoff's Voltage Law ("in travelling round any closed mesh (section) of a network (circuit), the algebraic sum of the emfs (voltages) acting in the mesh is equal to the algebraic sum of the *IR* voltage drops for the individual resistance in the mesh" [3]) is applied to loop number 1. The sign convention adopted in this summation is given in figure A.3.

$$V_a - I_a Z_A + I_b Z_B - V_b = 0\,. \qquad \text{(A.8)}$$

Similarly, performing Kirchoff's Voltage Law on loop number 2 gives

$$V_b - I_b Z_B + I_c Z_C - V_c = 0\,. \qquad \text{(A.9)}$$

The next stage of the derivation process is to solve equations (A.7), (A.8) and (A.9) to yield expressions for I_a, I_b and I_c.

A.2 Formation of Expressions for I_a, I_b and I_c

Substituting equation (A.7) into (A.9) gives

$$V_b + I_a Z_B + I_c\left(Z_B + Z_C\right) - V_c = 0. \qquad \text{(A.10)}$$

Rearranging (A.10) to give I_a as the subject gives

$$I_a = \frac{V_c}{Z_B} - \frac{V_b}{Z_B} - I_c\left(\frac{Z_B + Z_C}{Z_B}\right). \qquad \text{(A.11)}$$

Substituting equation (A.7) into equation (A.8) gives

$$V_a - I_a\left(Z_A + Z_B\right) - I_c Z_B - V_b = 0. \qquad \text{(A.12)}$$

Substituting equation (A.11) into (A.12) gives

$$V_a - V_b - I_c Z_B - \left(Z_A + Z_B\right)\left(\frac{V_c}{Z_B} - \frac{V_b}{Z_B} - I_c\left(\frac{Z_B + Z_C}{Z_B}\right)\right) = 0. \qquad \text{(A.13)}$$

Expanding and rearranging equation (A.13) to give I_c as the subject gives

$$I_c = \frac{V_c\left(1 + \frac{Z_A}{Z_B}\right) - V_a - V_b\left(\frac{Z_A}{Z_B}\right)}{\left(Z_A + Z_C + \frac{Z_A Z_C}{Z_B}\right)}. \qquad \text{(A.14)}$$

In order to move towards a more manageable solution format, equation (A.14) is multiplied by

$$I_c = \frac{Z_B}{Z_A + Z_B}, \qquad \text{(A.15)}$$

which gives

$$I_c = \frac{V_c - V_a\left(\frac{Z_B}{Z_A + Z_B}\right) - V_b\left(\frac{Z_A}{Z_A + Z_B}\right)}{\frac{Z_A Z_B + Z_B Z_C + Z_A Z_C}{Z_A + Z_B}}. \qquad \text{(A.16)}$$

Further simplifications can be made to equation (A.16) by accommodating additional expressions for V_a, V_b and V_c derived in Chapter 5. Thus

$$V_a = S_1 V_{dc} \qquad \text{(A.17)}$$

$$V_b = S_3 V_{dc} \qquad \text{(A.18)}$$

$$V_c = S_5 V_{dc}, \qquad \text{(A.19)}$$

where V_{dc} is the magnitude of the voltage source depicted in figure A.3 and S_1, S_3 and S_5 represent the state of the inverter switches represented by the functional model and are defined by

$$S_j = \begin{cases} 1 & if \quad closed \\ 0 & otherwise \end{cases} \qquad \text{for } j = 1,3,5\,. \qquad \text{(A.20)}$$

Substituting equations (A.17), (A.18) and (A.19) into (A.16) gives

$$I_c = \frac{V_{dc}\left(S_5 - S_1\left(\frac{Z_B}{Z_A + Z_B}\right) - S_3\left(\frac{Z_A}{Z_A + Z_B}\right)\right)}{\frac{Z_A Z_B + Z_B Z_C + Z_A Z_C}{Z_A + Z_B}}. \qquad \text{(A.21)}$$

By introducing additional substitutions, equation (A.21) can be further simplified to

$$I_c = \frac{S_C V_{dc}}{Z_{ABC} \big/ Z_A + Z_B}, \qquad \text{(A.22)}$$

where

$$Z_{ABC} = Z_A Z_B + Z_B Z_C + Z_A Z_C \qquad \text{(A.23)}$$

and

$$S_C = S_5 - S_1\left(\frac{Z_B}{Z_A + Z_B}\right) - S_3\left(\frac{Z_A}{Z_A + Z_B}\right). \qquad \text{(A.24)}$$

Performing similar algebra to that laid out in equations (A.10) through to (A.24) produces expressions for I_a and I_b. These are given below.

$$I_a = \frac{S_A V_{dc}}{Z_{ABC} \big/ Z_B + Z_C} \tag{A.25}$$

$$I_b = \frac{S_B V_{dc}}{Z_{ABC} \big/ Z_A + Z_C} \tag{A.26}$$

where

$$S_A = S_1 - S_3\left(\frac{Z_C}{Z_B + Z_C}\right) - S_5\left(\frac{Z_B}{Z_B + Z_C}\right) \tag{A.27}$$

$$S_B = S_3 - S_1\left(\frac{Z_C}{Z_A + Z_C}\right) - S_5\left(\frac{Z_A}{Z_A + Z_C}\right). \tag{A.28}$$

The validity of the derived expressions for I_a, I_b and I_c has been confirmed using numerical analyses on examples of three-phase inverters for each of their eight possible operating states.

A.3 References

[1] Barry W. Williams, *Power electronics: devices, drivers, applications, and passive components*. Available http://www.eee.strath.ac.uk/~bwwilliams (accessed 11/05/2009)

[2] Mario Cacciato, Alfio Consoli, Giuseppe Scarcella, Antonio Testa, "Reduction of Common-Mode Currents in PWM Inverter Motor Drives," *IEEE Trans. on Industry Applications*, vol. 35, no. 2, pp. 469 – 476, March/April 1999.

[3] Simon Carter, "Kirchoff's Laws." Available at: http://www.electronics2000.co.uk/data/itemsgl/Kirchoff.htm (accessed 11/05/2009)

Appendix B – Derivations of Functional Inverter Model Stability Criteria under Different Short Circuit Conditions

B.1 Introduction

Consider the three-phase inverter functional model shown in figure B.1.

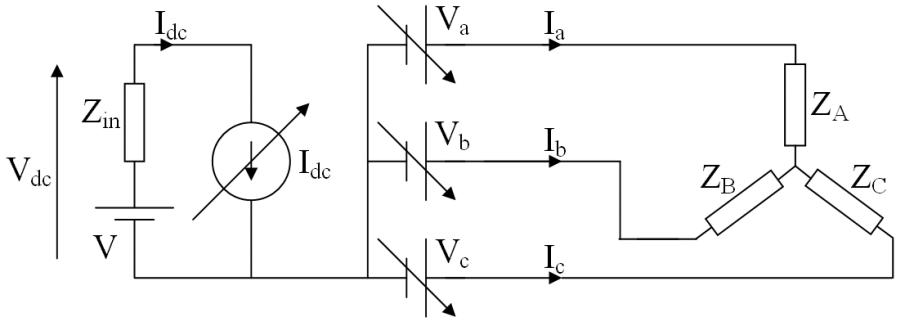

Fig. B.1. Three-phase functional inverter model

Chapter 5 showed that this model is numerically stable when $|C| < 1$, where

$$C = Z_{in}\left(\frac{S_1^{(n)}S_A^{(n-1)}}{Z_{ABC}/Z_B + Z_C} + \frac{S_3^{(n)}S_B^{(n-1)}}{Z_{ABC}/Z_A + Z_C} + \frac{S_5^{(n)}S_C^{(n-1)}}{Z_{ABC}/Z_A + Z_B}\right). \quad \text{(B.1)}$$

and

$$Z_{ABC} = Z_A Z_B + Z_B Z_C + Z_A Z_C \quad \text{(B.2)}$$

$$S_A^{(n)} = S_1^{(n)} - S_3^{(n)}\left(\frac{Z_C}{Z_B + Z_C}\right) - S_5^{(n)}\left(\frac{Z_B}{Z_B + Z_C}\right) \quad \text{(B.3)}$$

$$S_B^{(n)} = S_3^{(n)} - S_1^{(n)}\left(\frac{Z_C}{Z_A + Z_C}\right) - S_5^{(n)}\left(\frac{Z_A}{Z_A + Z_C}\right) \quad \text{(B.4)}$$

$$S_C^{(n)} = S_5^{(n)} - S_1^{(n)}\left(\frac{Z_B}{Z_A + Z_B}\right) - S_3^{(n)}\left(\frac{Z_A}{Z_A + Z_B}\right). \quad \text{(B.5)}$$

The terms Z_A, Z_B and Z_C are the ac side load impedances and Z_{in} is the dc side source impedance. The variables S_1, S_3 and S_5 refer to the states of the corresponding semiconductor switches of the inverter (see figure 5.1 in Chapter 5), where

$$S_j = \begin{cases} 1 & \textit{if} \quad \textit{closed} \\ 0 & \textit{otherwise} \end{cases} \qquad \text{for } j = 1,2,3,4,5,6\,. \quad \text{(B.6)}$$

Chapter 5 shows that under balanced load conditions, where Z_A=Z_B=Z_C=Z_L, and accounting for the impact of the inverter switching state (where the states of all switches are considered constant over the interval *(n-1)* to *(n)*, *C* is reduced to

$$C = \frac{2}{3}\frac{Z_{in}}{Z_L}. \quad \text{(B.7)}$$

Therefore, to guarantee the numerical stability of the model, it is necessary that

$$Z_L > \frac{2}{3} Z_{in} . \qquad \text{(B.8)}$$

Under normal load conditions, this condition is readily met. However, under low impedance fault conditions on the ac side of the converter, the effective magnitude of Z_L will be lower, hence producing a higher risk of numerical instability. The following sections will evaluate the impact of three-phases-to-neutral, two-phases-to-neutral and phase-to-neutral fault conditions (where neutral is the star point of the load). In each case, the analysis conducted will maintain the assumption that the inverter switch states are constant over the period from *(n-1)* to *(n)* which is assumed small.

B.2 Three Phases to Neutral Fault

In this case, all three output phases of the inverter are subjected to a short circuit fault of impedance Z_F, as shown in figure B.2.

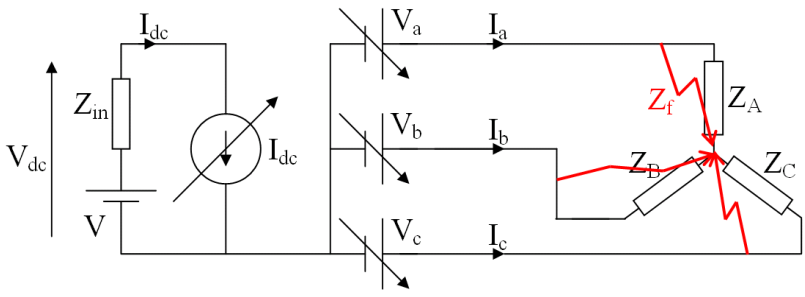

Fig. B.2. Three-phase fault applied to functional inverter

As the fault impedance Z_F, is considered much lower than the load impedance, the parallel combination of these can be taken as Z_F. By simple substitution of Z_F for Z_A, Z_B, and Z_C, the numerical stability of the model can be shown to be guaranteed if

$$Z_F > \frac{2}{3} Z_{in}. \qquad \text{(B.9)}$$

This criterion is unlikely to be met in most short circuit fault circumstances.

B.3 Single Phase to Neutral Fault

In this case, a single phase (phase A) of the three inverter output is subjected to a short circuit fault of impedance Z_F, as shown in figure B.3. The remaining two phases maintain an impedance of Z_L.

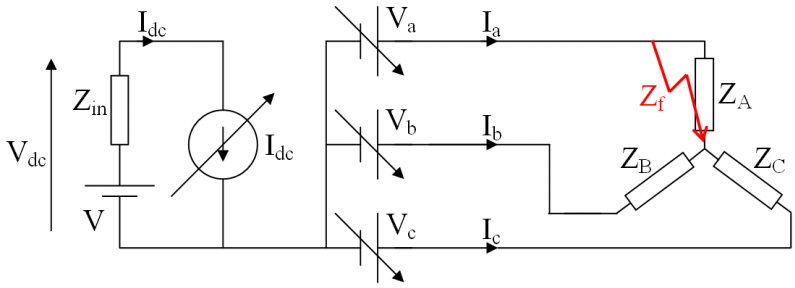

Fig. B.4. Two-phase fault applied to functional inverter

Substituting $Z_A = Z_F$ and $Z_B = Z_C = Z_L$ into equations (B.2), (B.3), (B.4) and (B.5) gives

$$Z_{ABC} = 2Z_F Z_L + Z_L^2 \qquad \text{(B.10)}$$

$$S_A = S_1 - \frac{S_3}{2} - \frac{S_5}{2} \qquad \text{(B.11)}$$

$$S_B = S_3 - S_1\left(\frac{Z_L}{Z_F + Z_L}\right) - S_5\left(\frac{Z_F}{Z_F + Z_L}\right) \qquad \text{(B.12)}$$

$$S_C = S_5 - S_1\left(\frac{Z_L}{Z_F + Z_L}\right) - S_3\left(\frac{Z_F}{Z_F + Z_L}\right). \qquad \text{(B.13)}$$

Substituting equations (B.10), (B.11), (B.12) and (B.13) into equation (B.1) gives

$$C = Z_{in}\left[\frac{S_1^2 - \frac{S_1 S_3}{2} - \frac{S_1 S_5}{2}}{\frac{Z_F Z_L + Z_L^2 + Z_F Z_L}{2Z_L}} + \frac{S_3^2 - S_1 S_3\left(\frac{Z_L}{Z_F + Z_L}\right) - S_3 S_5\left(\frac{Z_F}{Z_F + Z_L}\right)}{\frac{Z_F Z_L + Z_L^2 + Z_F Z_L}{Z_F + Z_L}} + \frac{S_5^2 - S_1 S_5\left(\frac{Z_L}{Z_F + Z_L}\right) - S_3 S_5\left(\frac{Z_F}{Z_F + Z_L}\right)}{\frac{Z_F Z_L + Z_L^2 + Z_F Z_L}{Z_F + Z_L}}\right]. \qquad \text{(B.14)}$$

For low impedance short circuit conditions, it can be assumed that the magnitude of Z_F is negligible when compared to Z_L. This assumption allows equation (B.14) to be further simplified, yielding

$$C = Z_{in}\left[\frac{S_1^2 - \frac{S_1 S_3}{2} - \frac{S_1 S_5}{2}}{\frac{Z_L}{2}} + \frac{S_3^2 - S_1 S_3}{Z_L} + \frac{S_5^2 - S_1 S_5}{Z_L}\right]. \qquad \text{(B.15)}$$

Extracting the common term Z_L and rearranging gives

$$C = \frac{Z_{in}}{Z_L}\left[2S_1^2 + S_3^2 + S_5^2 - 2S_1S_3 - 2S_1S_5\right]. \qquad \text{(B.16)}$$

Equation (B.16) can be rewritten as

$$C = \frac{Z_{in}}{Z_L}k_A\,, \qquad \text{(B.17)}$$

where

$$k_A = 2S_1^2 + S_3^2 + S_5^2 - 2S_1S_3 - 2S_1S_5\,. \qquad \text{(B.18)}$$

In order to simplify equation (B.17) any further it is necessary to consider all the possible magnitudes of k_A. This evaluation of k_A is given in Table B.1.

Table B.1. Evaluation of k_A for different switch states

(S_1, S_3, S_5)	$k_A = 2S_1^2 + S_3^2 + S_5^2 - 2S_1S_3 - 2S_1S_5$
(0, 0, 0), (1, 1, 1)	***0***
(0, 0, 1), (0, 1, 0), (1, 0, 1), (1, 1, 0)	***1***
(0, 1, 1), (1, 0, 0)	***2***

The worst case criterion for numerical stability occurs when the magnitude of k_A equals 2. Substituting this value into equation (B.17) gives

$$C = 2\frac{Z_{in}}{Z_L}. \qquad \text{(B.19)}$$

Given that numerical stability of the three-phase functional inverter model occurs when $|C| < 1$, the condition for the numerical stability of this model under single phase to neutral fault conditions can be expressed as

$$Z_L > 2Z_{in}. \qquad \text{(B.20)}$$

B.4 Two Phases to Neutral Fault

In this case, two of the three inverter output phases are subjected to a short circuit fault of impedance Z_F, as shown in figure B.4. The remaining phase (phase C) has an impedance of Z_L.

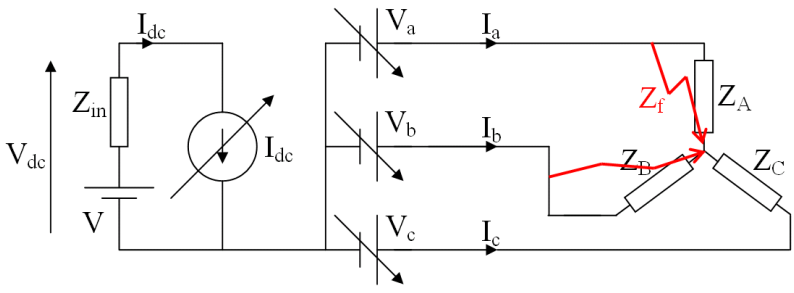

Fig. B.4. Two phase fault applied to functional inverter

Substituting $Z_A = Z_B = Z_F$ and $Z_C = Z_L$ into equations (B.2), (B.3), (B.4) and (B.5) gives

$$Z_{ABC} = Z_F^2 + 2Z_F Z_L \qquad \text{(B.21)}$$

$$S_A = S_1 - S_3\left(\frac{Z_L}{Z_F + Z_L}\right) - S_5\left(\frac{Z_F}{Z_F + Z_L}\right) \qquad \text{(B.22)}$$

$$S_B = S_3 - S_1\left(\frac{Z_L}{Z_F + Z_L}\right) - S_5\left(\frac{Z_F}{Z_F + Z_L}\right) \qquad \text{(B.23)}$$

$$S_C = S_5 - \frac{S_1}{2} - \frac{S_3}{2}. \qquad \text{(B.24)}$$

Substituting equations (B.21), (B.22), (B.23) and (B.24) into equation (B.1) gives

$$C = Z_{in}\left[\frac{S_1^2 - S_1 S_3\left(\frac{Z_L}{Z_F + Z_L}\right) - S_1 S_5\left(\frac{Z_F}{Z_F + Z_L}\right)}{\frac{Z_F(Z_F + 2Z_L)}{Z_F + Z_L}} + \frac{S_3^2 - S_1 S_3\left(\frac{Z_L}{Z_F + Z_L}\right) - S_3 S_5\left(\frac{Z_F}{Z_F + Z_L}\right)}{\frac{Z_F(Z_F + 2Z_L)}{Z_F + Z_L}} + \frac{S_5^2 - \frac{S_1 S_5}{2} - \frac{S_3 S_5}{2}}{\frac{Z_F + 2Z_L}{2}}\right], \qquad \text{(B.25)}$$

The simplification of the expression for C is more complex here than in the single phase to neutral fault case however. If the assumption is made that the magnitude of Z_L dominates over Z_F to the extent that Z_F is assumed to be zero, this will produce a division by zero in the first two fractions of equation (B.25). Clearly, more careful

consideration of an appropriate substitution must be utilised to yield a meaningful result.

Hence, for this case it is assumed that the magnitude of Z_L dominates over Z_F to the extent that Z_F is assumed to be zero when compared to Z_L, but not to the extent that the product of Z_F and Z_L is zero. This yields the following substitutions

$$Z_F + Z_L \approx Z_L, \tag{B.26}$$

$$Z_F\left(Z_F + 2Z_L\right) \approx 2Z_F Z_L. \tag{B.27}$$

Substituting equations (B.26) and (B.27) into (B.25) gives

$$C = Z_{in}\left[\frac{S_1^2 - S_1S_3 - S_1S_5\left(\frac{Z_F}{Z_L}\right)}{\frac{2Z_FZ_L}{Z_L}} + \frac{S_3^2 - S_1S_3 - S_3S_5\left(\frac{Z_F}{Z_L}\right)}{\frac{2Z_FZ_L}{Z_L}} + \frac{S_5^2 - \frac{S_1S_5}{2} - \frac{S_3S_5}{2}}{\frac{2Z_L}{2}}\right], \tag{B.28}$$

and after some rearranging yields

$$C = Z_{in}\left[\frac{S_1^2 + S_3^2 - 2S_1S_3 - S_1S_5\left(\frac{Z_F}{Z_L}\right) - S_3S_5\left(\frac{Z_F}{Z_L}\right)}{2Z_F} + \frac{S_5^2 - \frac{S_1S_5}{2} - \frac{S_3S_5}{2}}{Z_L}\right]. \tag{B.29}$$

Given that Z_L is assumed to be large compared to Z_F, the first fraction in the brackets will have the greatest magnitude and will hence be the dominant term in determining the numerical stability of the functional inverter model under this operating condition. As a result of the assumptions made, equation (B.29) can be reduced to

$$C = \frac{Z_{in}}{Z_F}\left[\frac{S_1^2 + S_3^2 - 2S_1S_3 - S_1S_5\left(\frac{Z_F}{Z_L}\right) - S_3S_5\left(\frac{Z_F}{Z_L}\right)}{2}\right]. \qquad \text{(B.30)}$$

The assumption that Z_L is assumed to be large compared to Z_F also implies that the last two terms of the numerator in equation (B.30) will have a negligible magnitude in comparison to the first three, allowing equation (B.30) to be further simplified to

$$C = \frac{Z_{in}}{Z_F}\left[\frac{S_1^2 + S_3^2 - 2S_1S_3}{2}\right], \qquad \text{(B.31)}$$

which can be rewritten as

$$C = \frac{Z_{in}}{2Z_F}k_B, \qquad \text{(B.32)}$$

where

$$k_B = S_1^2 + S_3^2 - 2S_1S_3. \qquad \text{(B.33)}$$

In order to develop this stability analysis any further it is necessary to consider all the possible magnitudes of k_B. This evaluation of k_B is given in Table B.2.

Table B.2. Evaluation of k_B.

(S_1, S_3)	$k_B = S_1^2 + S_3^2 - 2S_1S_3$
(0, 0), (1, 1)	***0***
(0, 1), (1, 0)	***1***

The worst case criterion for numerical stability occurs when the magnitude of k_B equals 1. Substituting this value into equation (B.33) gives

$$C = \frac{Z_{in}}{2Z_F}. \qquad \text{(B.34)}$$

Given that numerical stability of the three-phase functional inverter model occurs when $|C| < 1$, the condition for the numerical stability of this model with a two phases to neutral fault applied can be expressed as

$$\frac{Z_{in}}{2Z_F} < 1, \qquad \text{(B.35)}$$

or more simply,

$$Z_F > \frac{1}{2} Z_{in}. \qquad \text{(B.36)}$$

In summary, the stability criteria for a three-phase function inverter model under normal (unfaulted), single-phase-to-neutral, two-phases-to-neutral and three-phases-to-neutral ac side short circuit fault conditions are given below.

No Fault

$$Z_L > \frac{2}{3} Z_{in} . \qquad \text{(B.37)}$$

Phase-to-Neutral Fault

$$Z_L > 2Z_{in} \qquad \text{(B.38)}$$

Two Phases-to-Neutral Fault

$$Z_F > \frac{1}{2} Z_{in} \qquad \text{(B.39)}$$

Three Phases-to-Neutral Fault

$$Z_F > \frac{2}{3} Z_{in} , \qquad \text{(B.40)}$$

By considering these equations more closely, it can be seen that the requirements for numerical stability become more difficult to meet as the severity of the simulated fault increases. Additionally, it is acknowledged that other fault conditions could occur, but the analyses of these have been omitted as they would provide little additional benefit at this stage. However, if required, the methods and procedures

presented could be readily applied to other fault conditions in order to derive the stability criterion for each.

Appendix C – Demonstration of Functional Model Behaviour under Normal and Faulted Conditions – Additional Simulation Results

C.1 Switched Model Simulation Results

Figures C.1and C.2 illustrate the steady state ac current and voltage outputs between 0 and 0.02 seconds of simulation time for the switched inverter model. Figures C.3 and C.4 illustrate the dc current and voltage outputs also over this period. These plots show the behaviour of the switched converter model during normal (i.e. unfaulted) operating conditions supplying an ac load of fixed impedance.

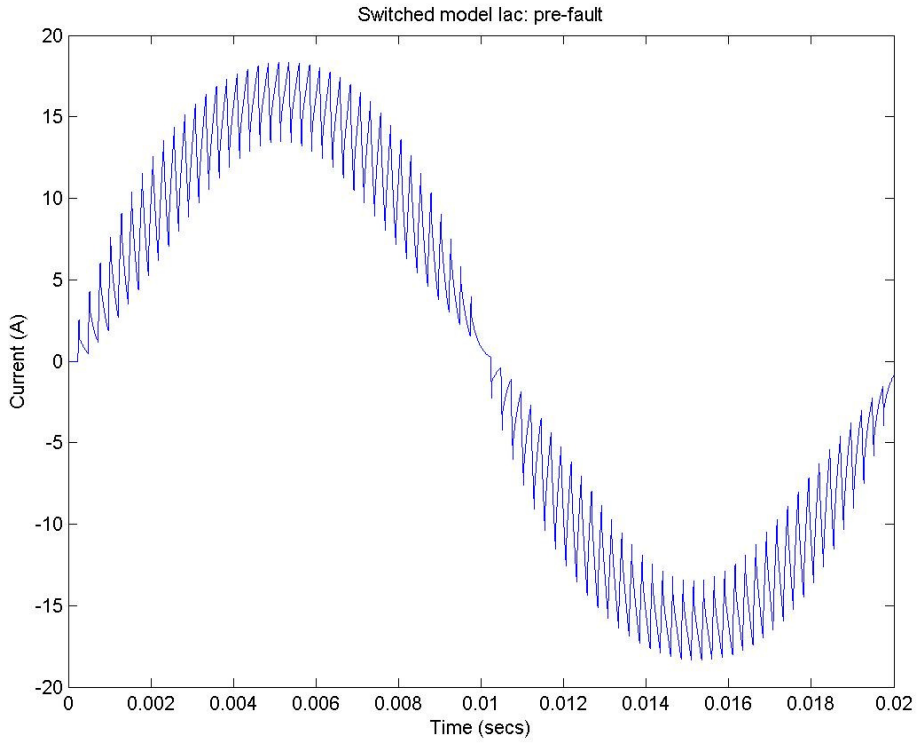

Fig. C.1. Switched model Iac – Pre-fault

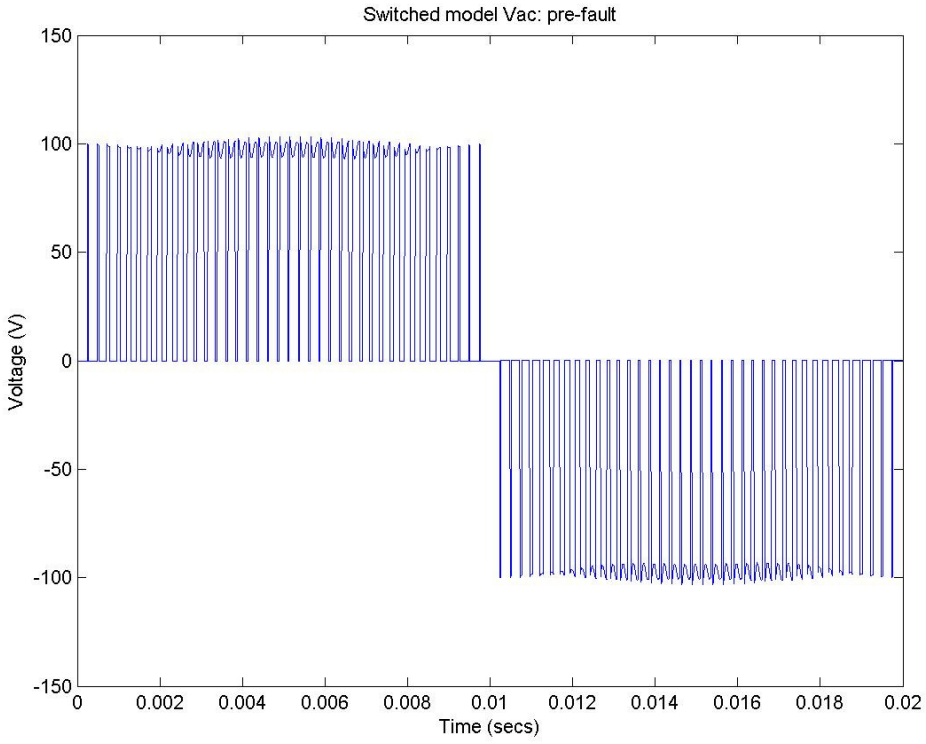

Fig. C.2. Switched model Vac – Pre-fault

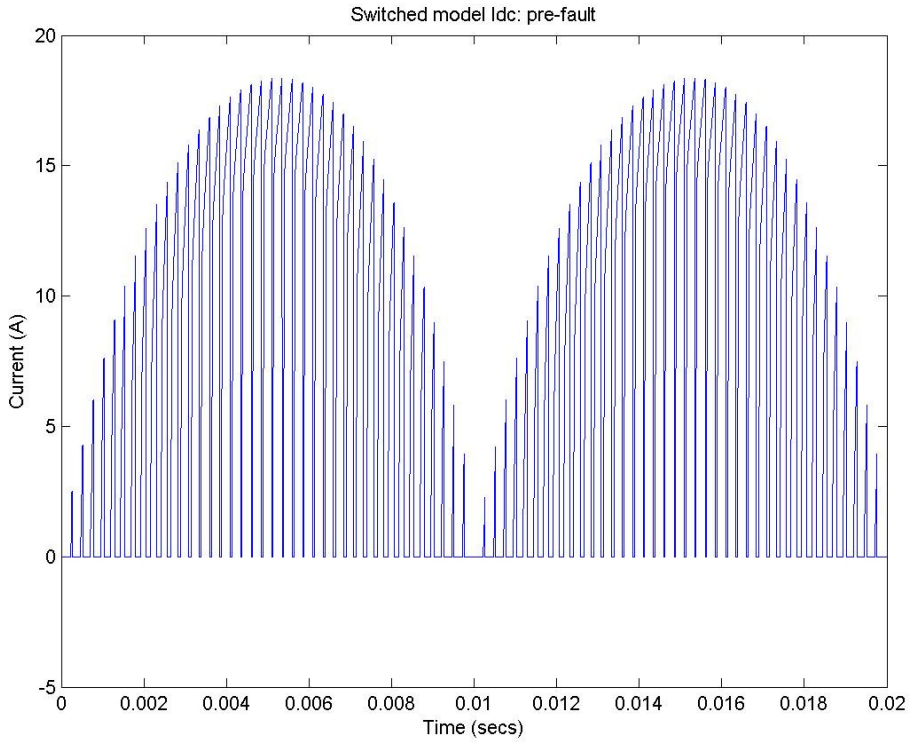

Fig. C.3. Switched model Idc – Pre-fault

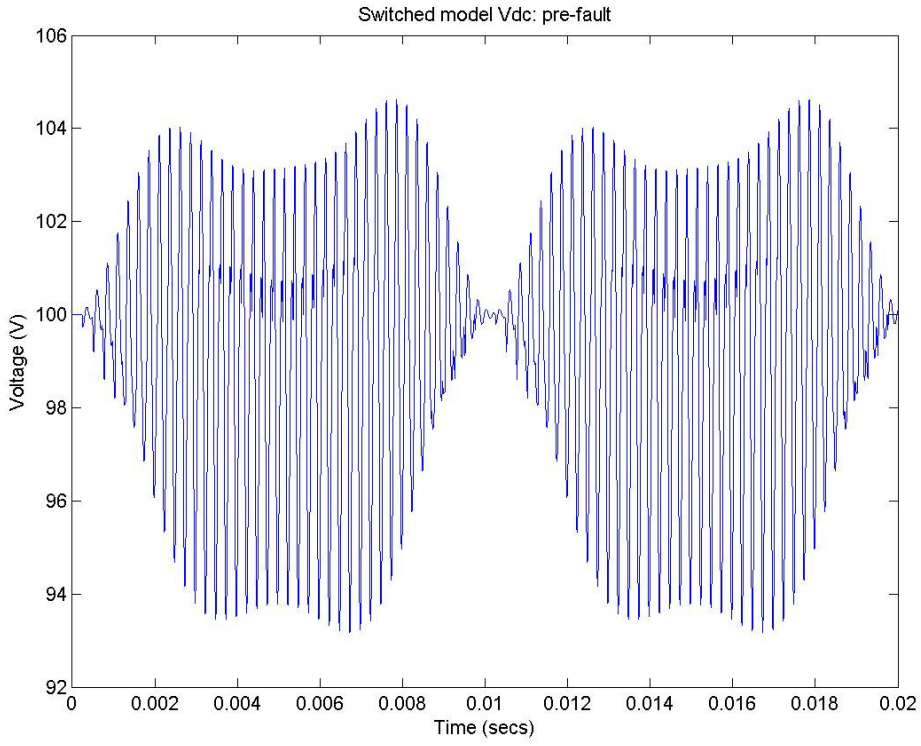

Fig. C.4. Switched model Vdc – Pre-fault

Figures C.5 and C.6 illustrate the steady state ac current and voltage outputs between 0.06 and 0.08 seconds of simulation time. Figures C.7 and C.8 illustrate the dc current and voltage outputs for this period.

This second group of plots shows the behaviour of the switched converter model after a low impedance rail to rail fault has occurred across the ac terminals of the inverter.

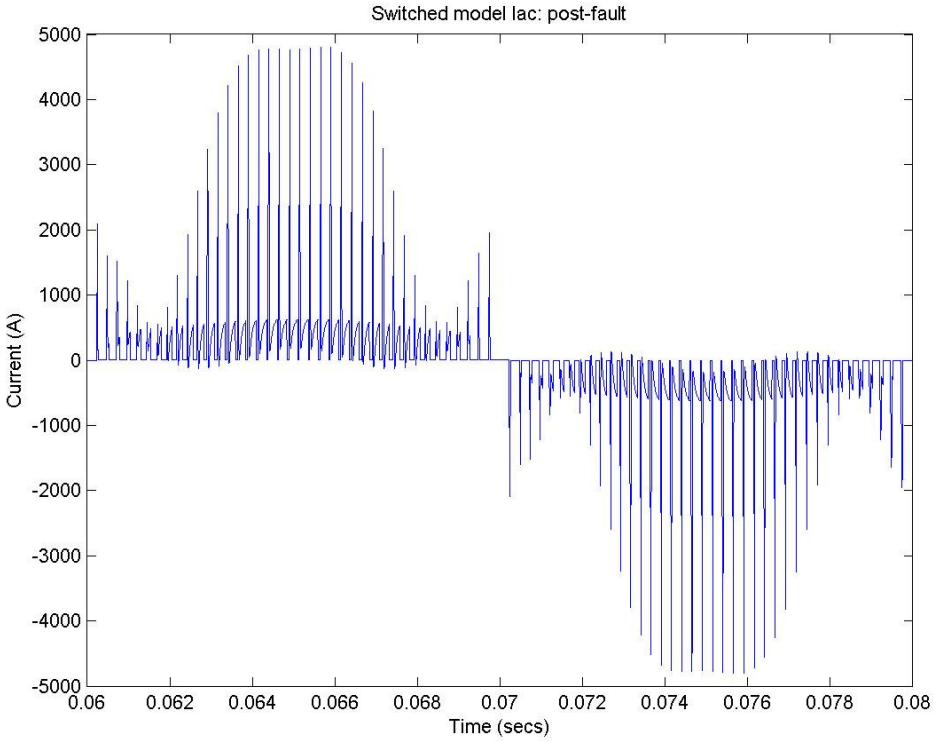

Fig. C.5. Switched model Iac – Post-fault

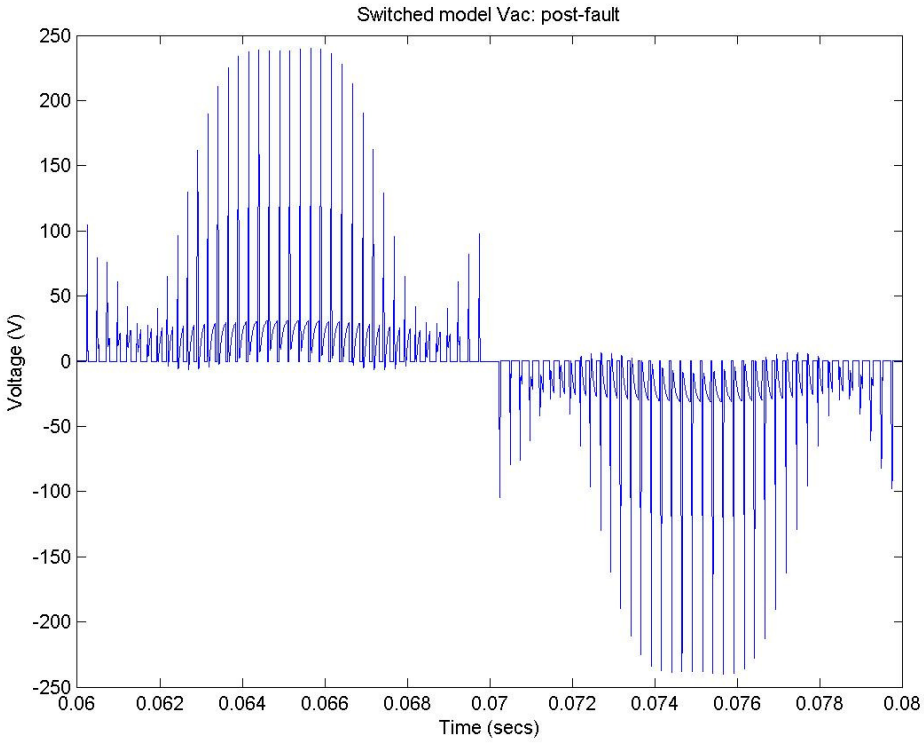

Fig. C.6. Switched model Vac – Post-fault

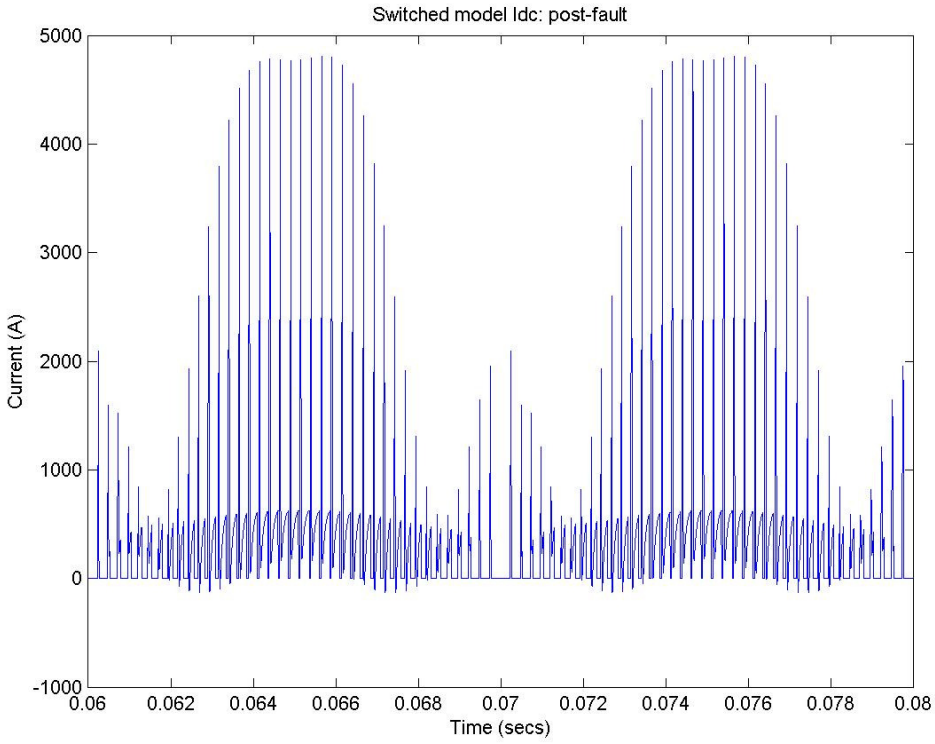

Fig. C.7. Switched model Idc – Post-fault

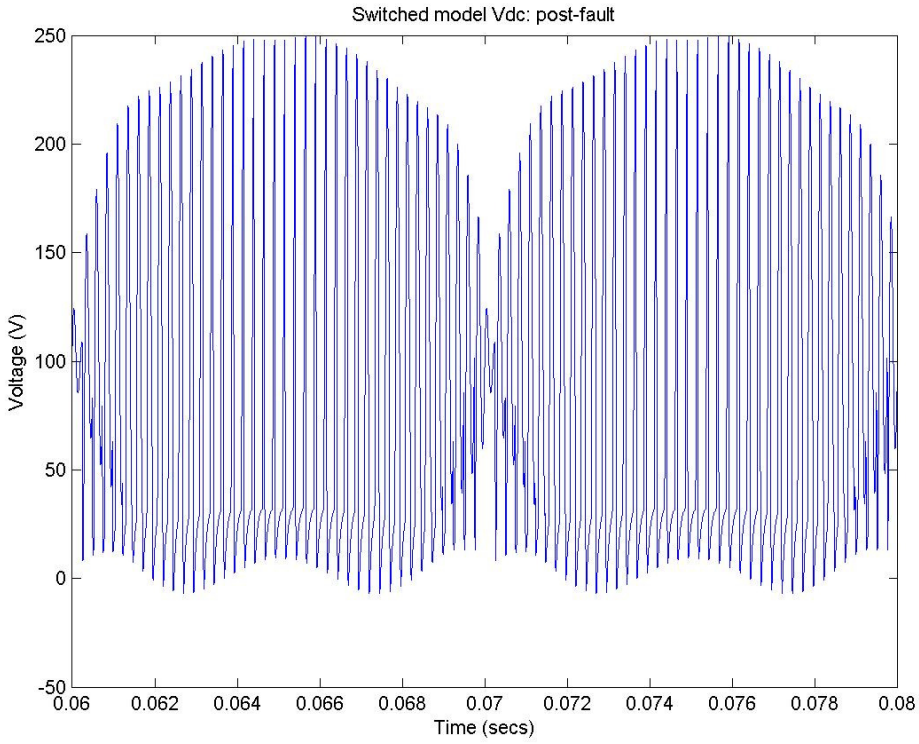

Fig. C.8. Switched model Vdc – Post-fault

C.2 Functional Model Simulation Results

Figures C.9 and C.10 illustrate the steady state ac current and voltage outputs between 0 and 0.02 seconds of the simulation time. Figures C.11 and C.12 illustrate the dc current and voltage outputs also over this period. These plots show the behaviour of the functional inverter model during normal (i.e. unfaulted) operating conditions supplying an ac load of fixed impedance.

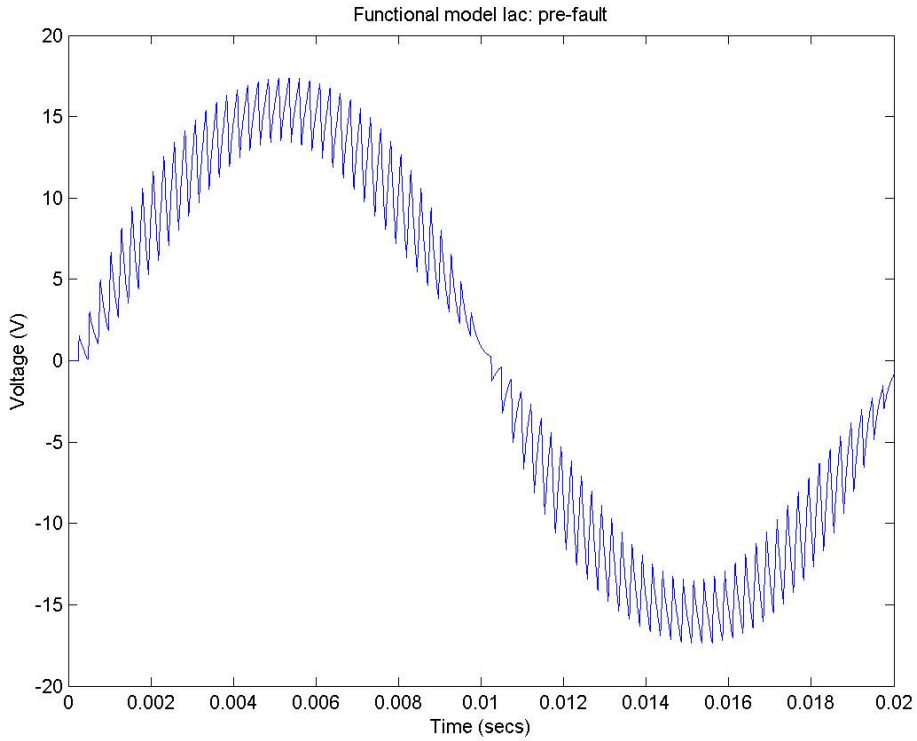

Fig. C.9. Functional model Iac – Pre-fault

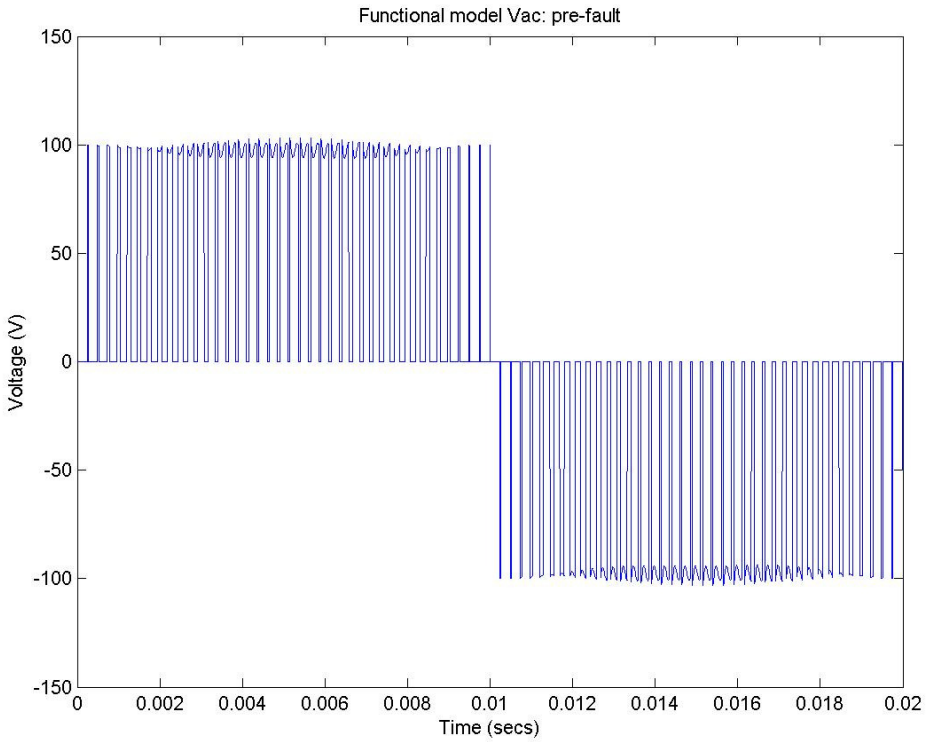

Fig. C.10. Functional model Vac – Pre-fault

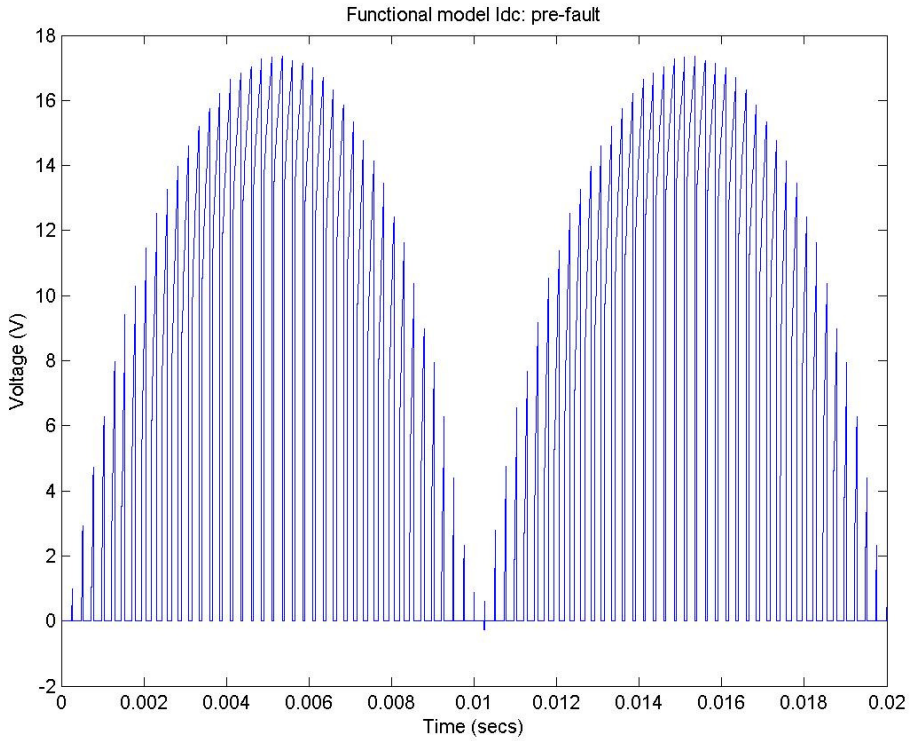

Fig. C.11. Functional model Idc – Pre-fault

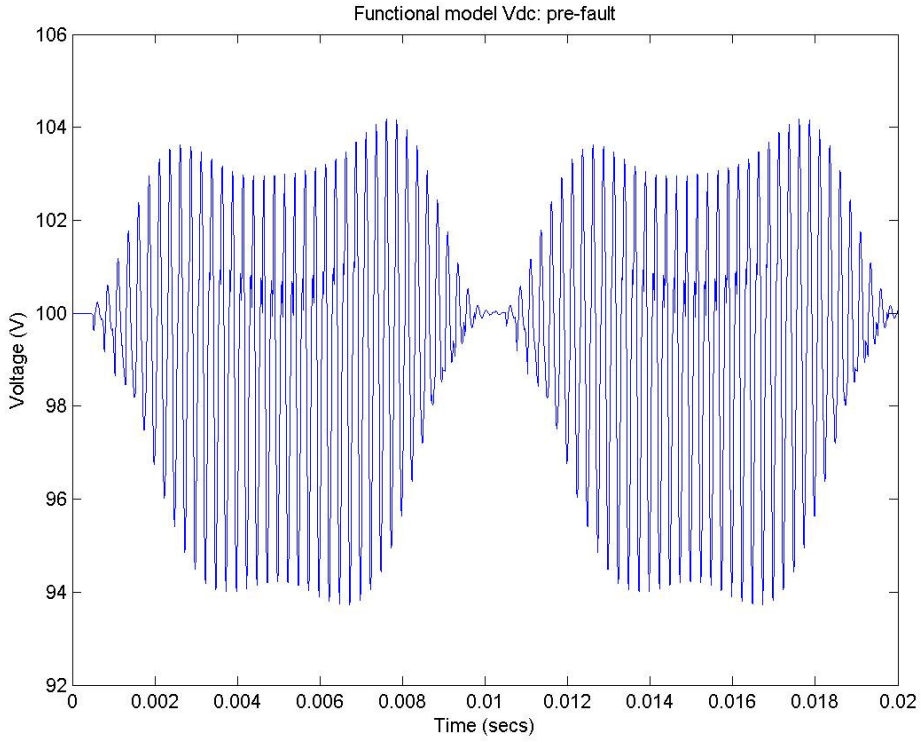

Fig. C.12. Functional model Vdc – Pre-fault

Figures C.13 and C.14 illustrate the steady state ac current and voltage outputs between 0.06 and 0.08 seconds of simulation time. Figures C.15 and C.16 illustrate the dc current and voltage outputs also over this period. This second group of plots shows the behaviour of the functional model after a low impedance rail to rail fault has occurred across the ac terminals of the inverter.

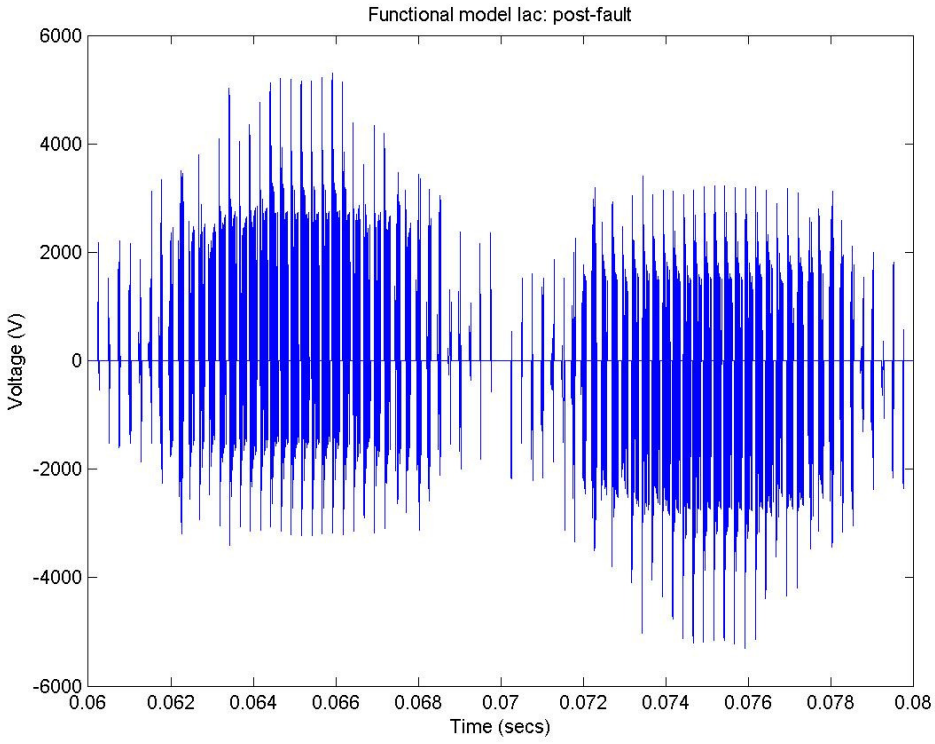

Fig. C.13. Functional model Iac – Post-fault

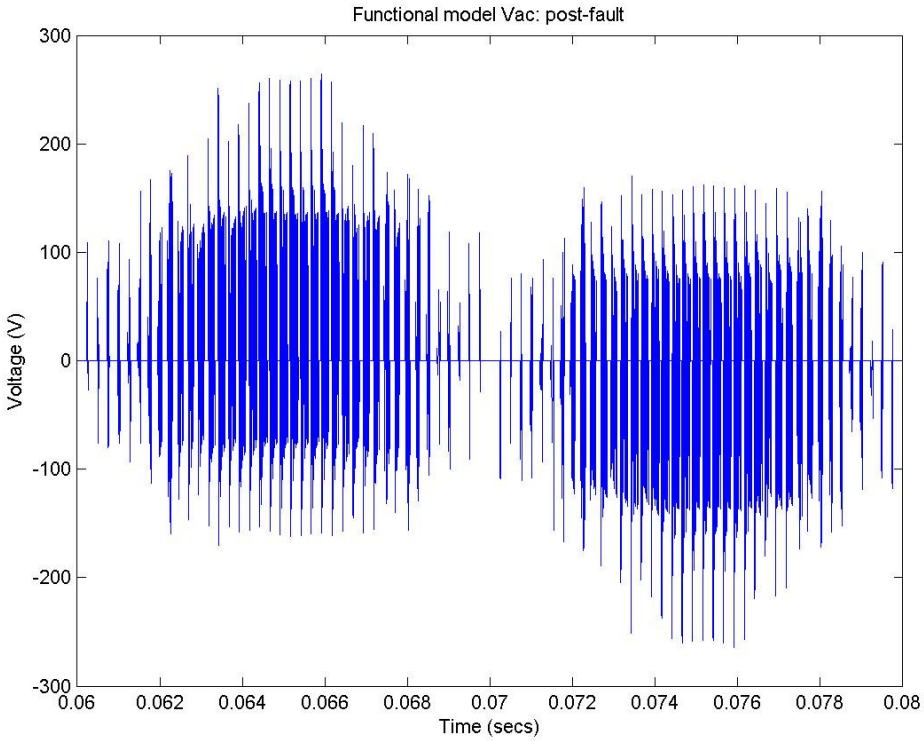

Fig. C.14. Functional model Vac – Post-fault

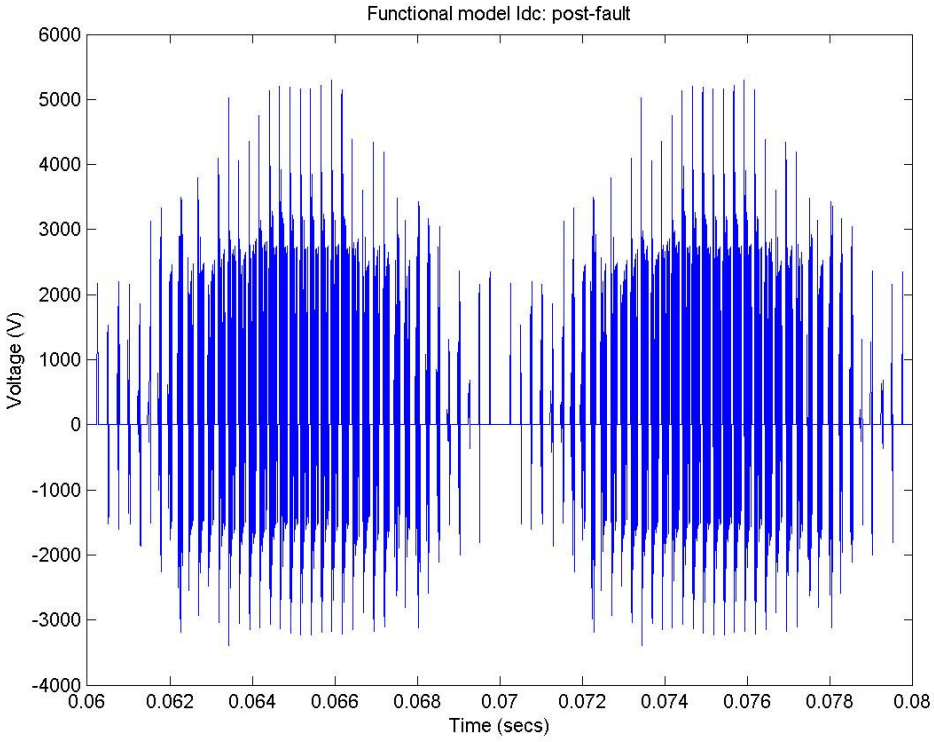

Fig. C.15. Functional model Idc – Post-fault

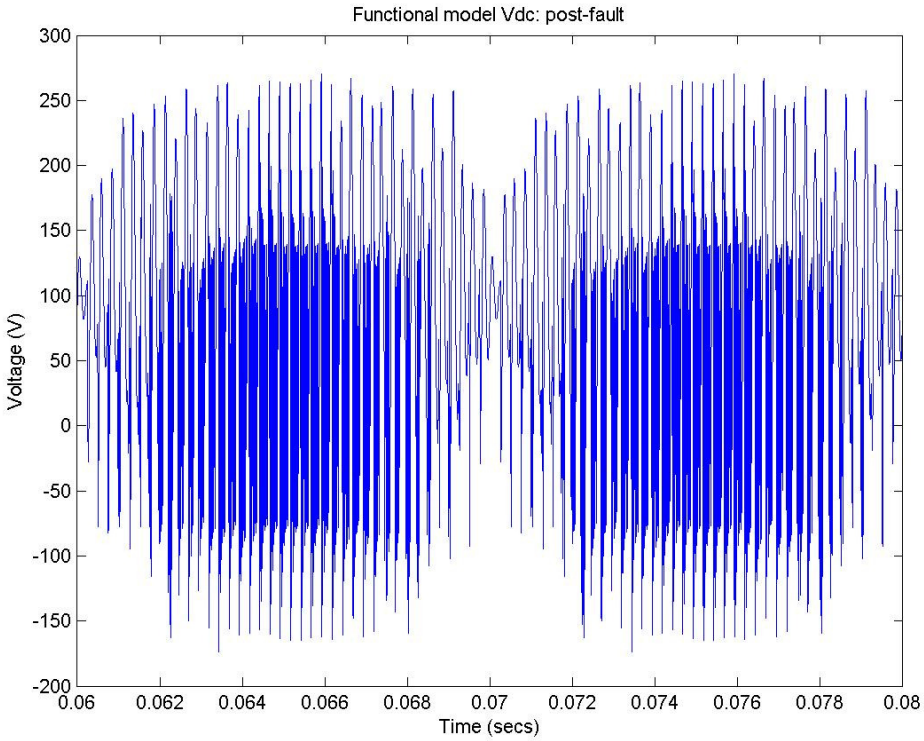

Fig. C.16. Functional model Vdc – Post-fault

C.3 Time-Averaged Functional Model Simulation Results

Figures C.17 and C.18 illustrate the steady state ac current and voltage outputs between 0 and 0.02 seconds of simulation time. Figures C.19 and C.20 illustrate the dc current and voltage outputs also over this period. These plots show the behaviour of the functional model during normal (i.e. unfaulted) operating conditions supplying an ac load of fixed impedance.

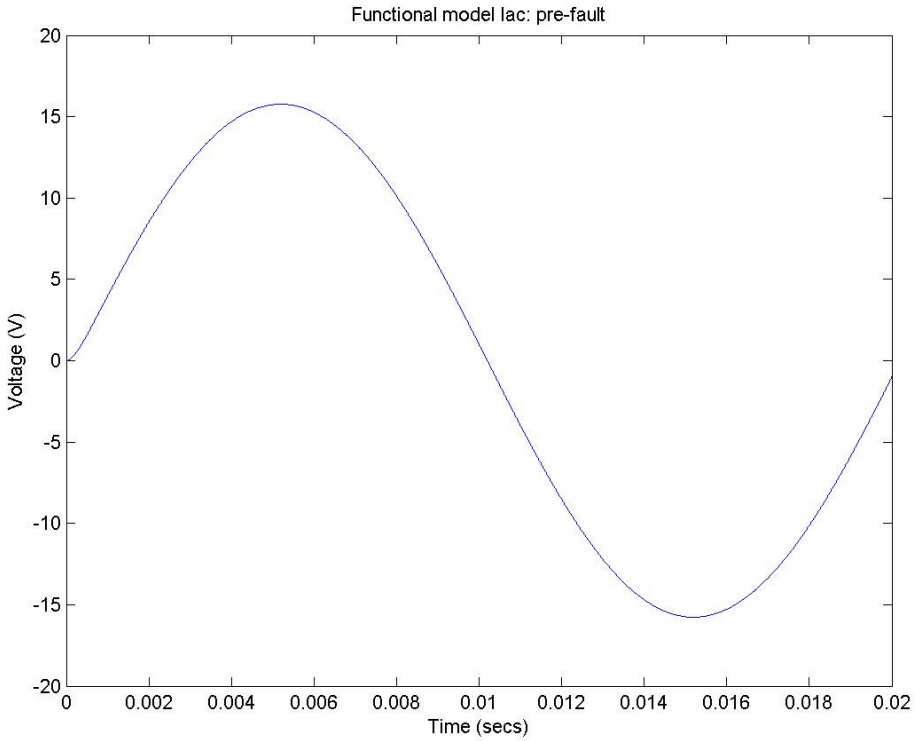

Fig. C.17. Time-averaged functional model Iac – Pre-fault

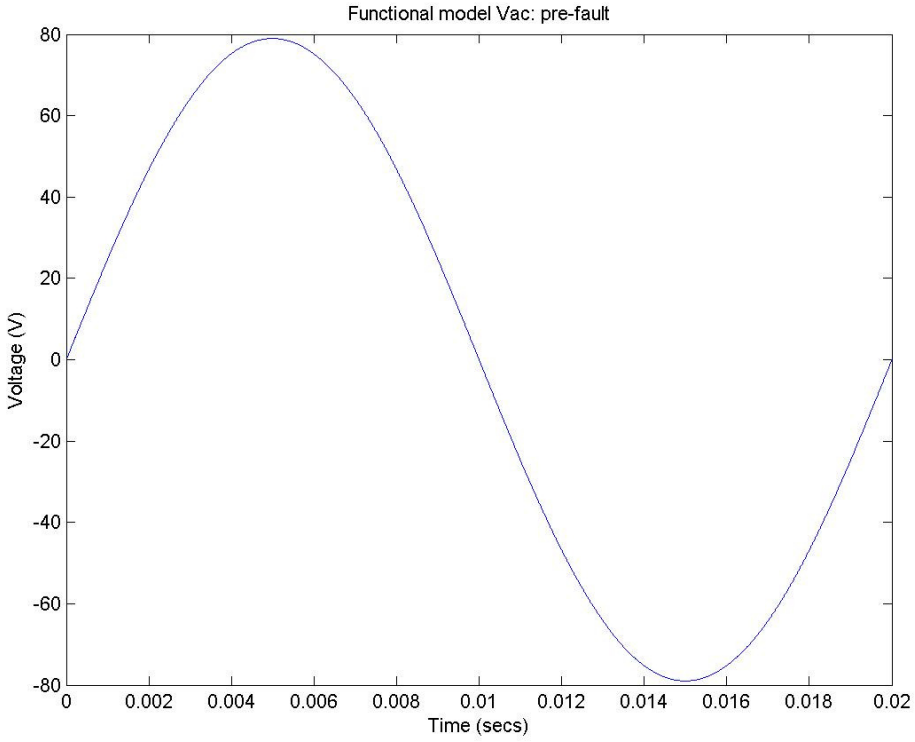

Fig. C.18. Time-averaged functional model Vac – Pre-fault

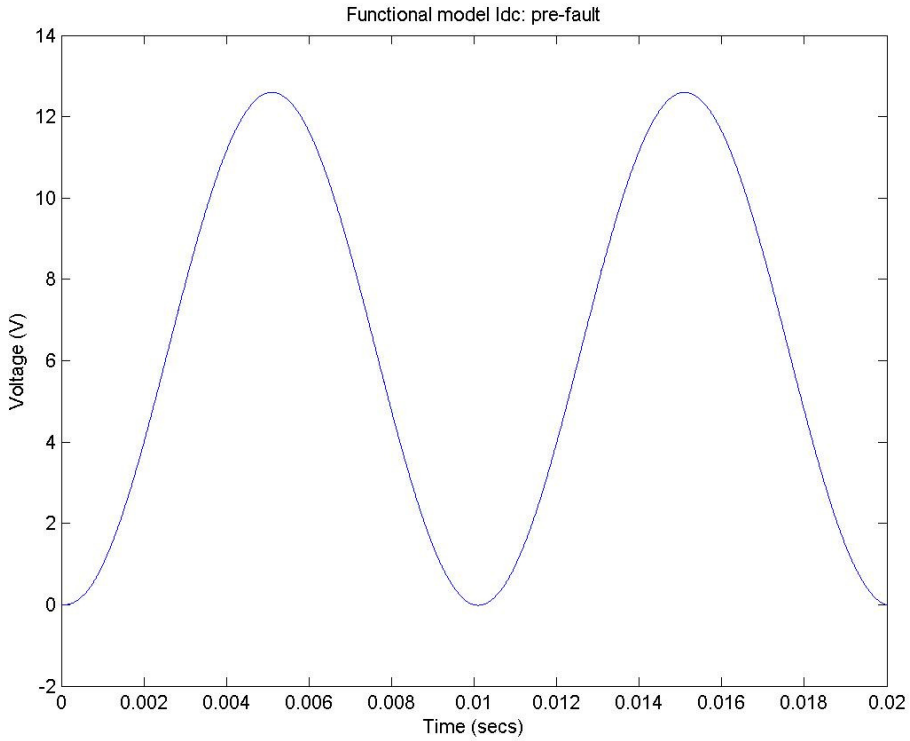

Fig. C.19. Time-averaged functional model Idc – Pre-fault

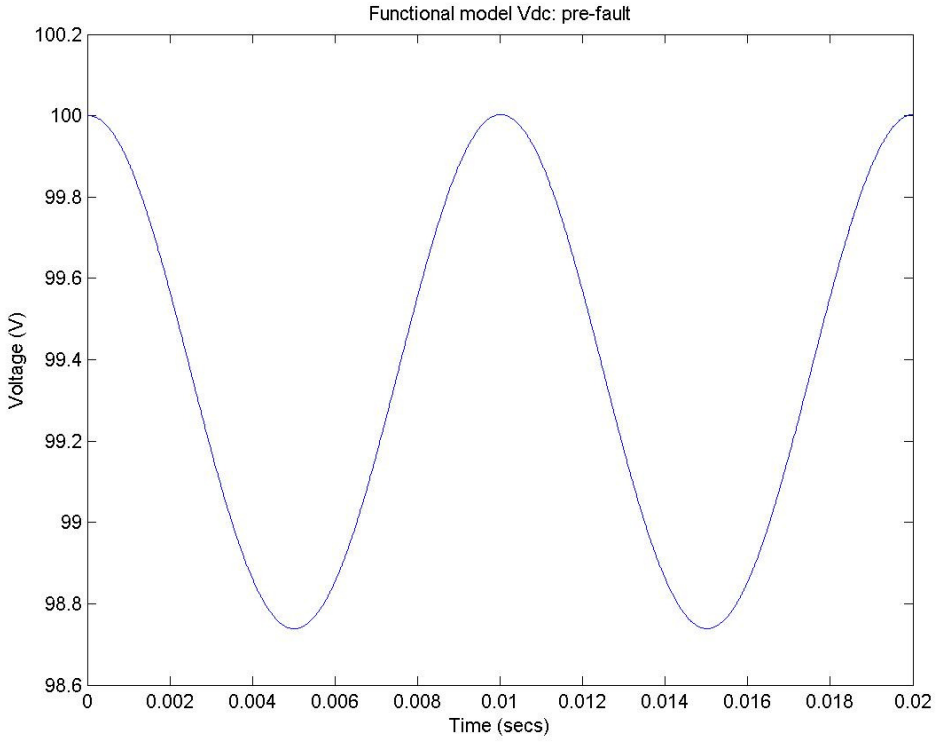

Fig. C.20. Time-averaged functional model Vdc – Pre-fault

Figures C.21 and C.22 illustrate the steady state ac current and voltage outputs between 0.06 and 0.08 seconds of simulation time. Figures C.23 and C.24 illustrate the dc current and voltage outputs also over this period. This second group of plots shows the behaviour of the time-averaged functional model after a low impedance rail to rail fault has occurred across the ac terminals of the inverter.

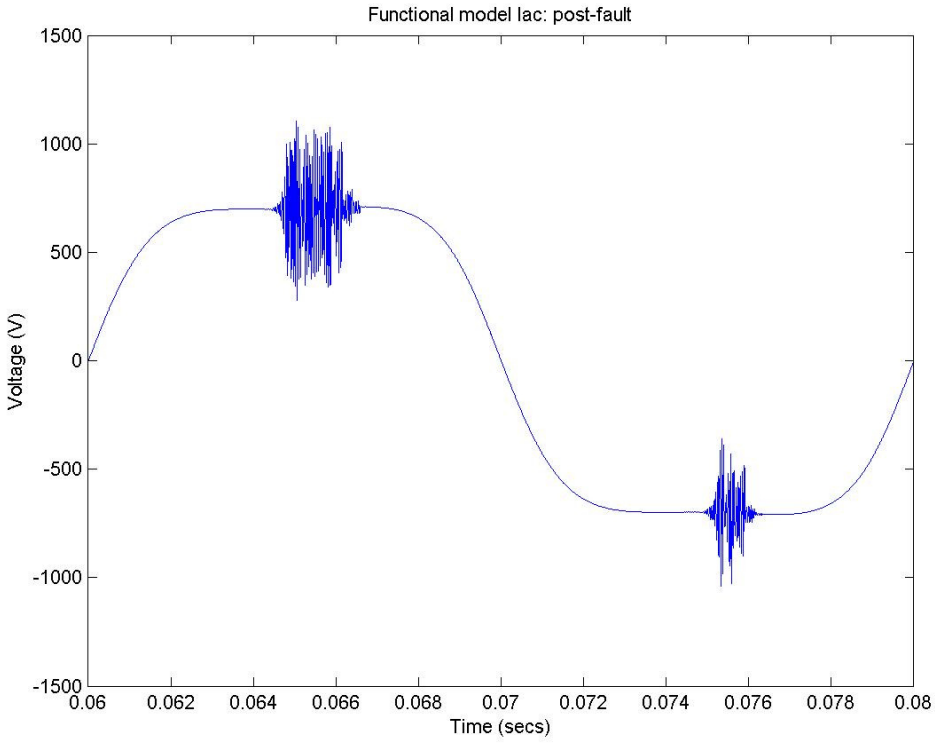

Fig. C.21. Time-averaged functional model Iac – Post-fault

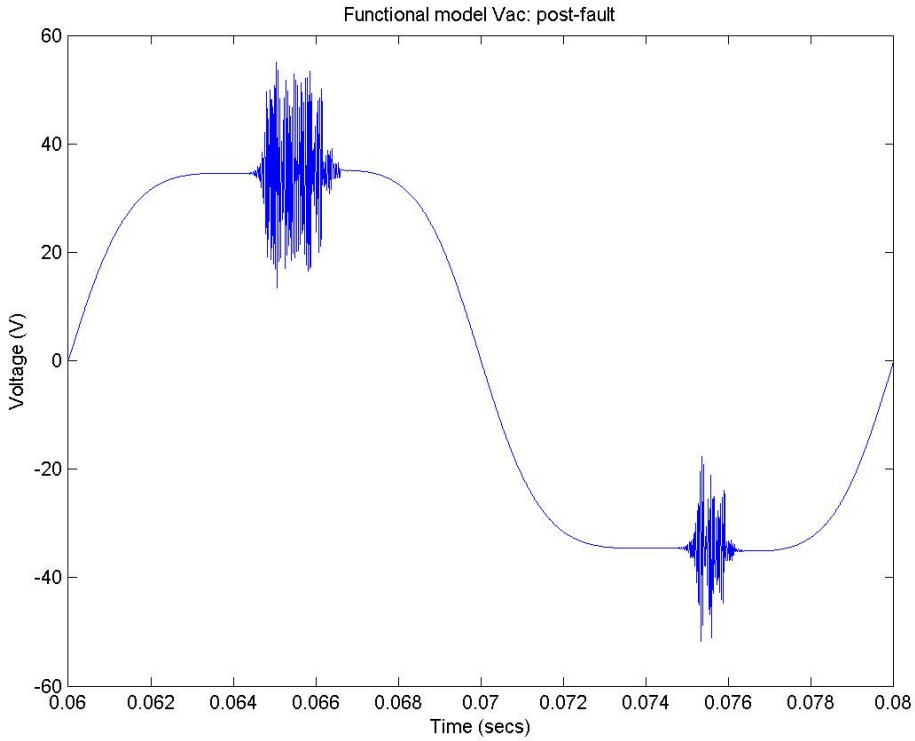

Fig. C.22. Time-averaged functional model Vac – Post-fault

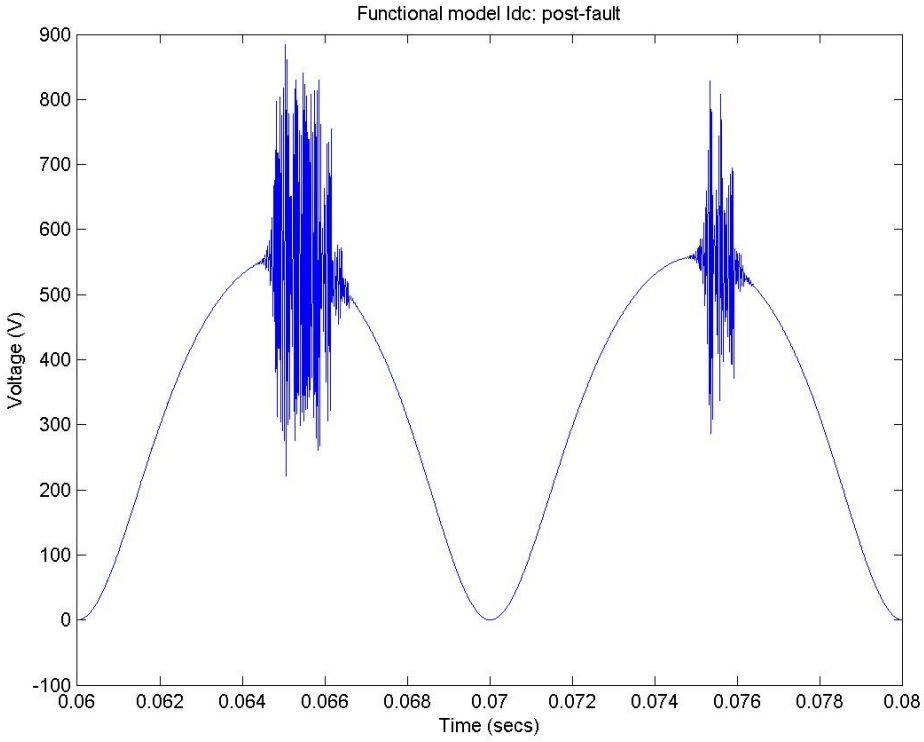

Fig. C.23. Time-averaged functional model Idc – Post-fault

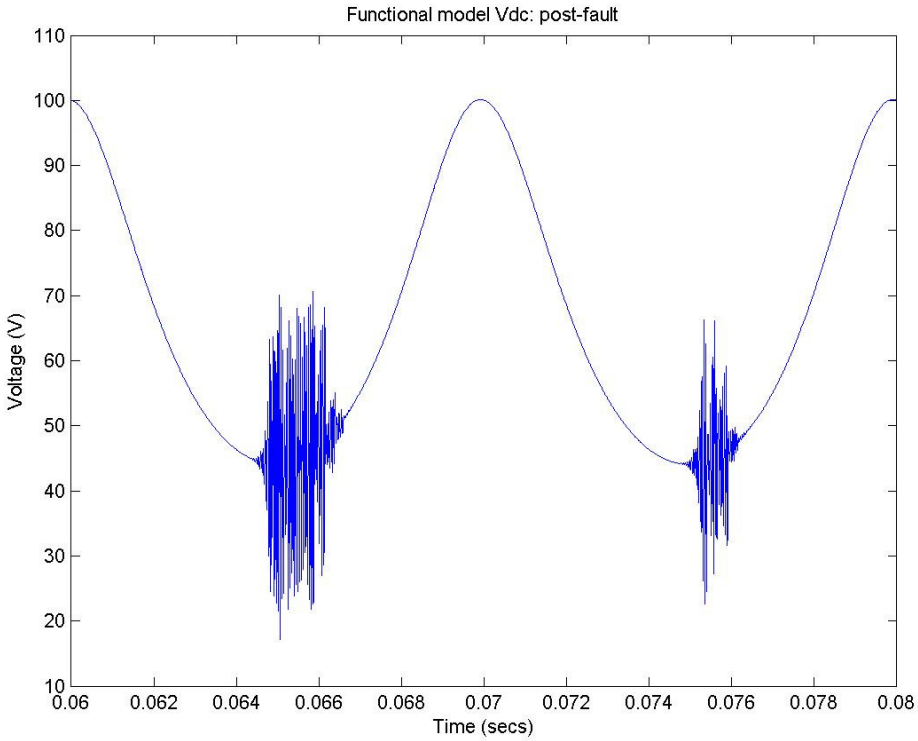

Fig. C.24. Time-averaged functional model Vdc – Post-fault

Appendix D – Demonstration of Single-Phase Inverter AFM

D.1 Switched Model Simulation Results

Figures D.1 and D.2 illustrate the steady state ac current and voltage outputs between 0 and 0.02 seconds of simulation time. Figures D.3 and D.4 illustrate the dc current and voltage outputs also over this period. These plots show the behaviour of the switched converter model during normal (i.e. unfaulted) operating conditions supplying an ac load of fixed impedance.

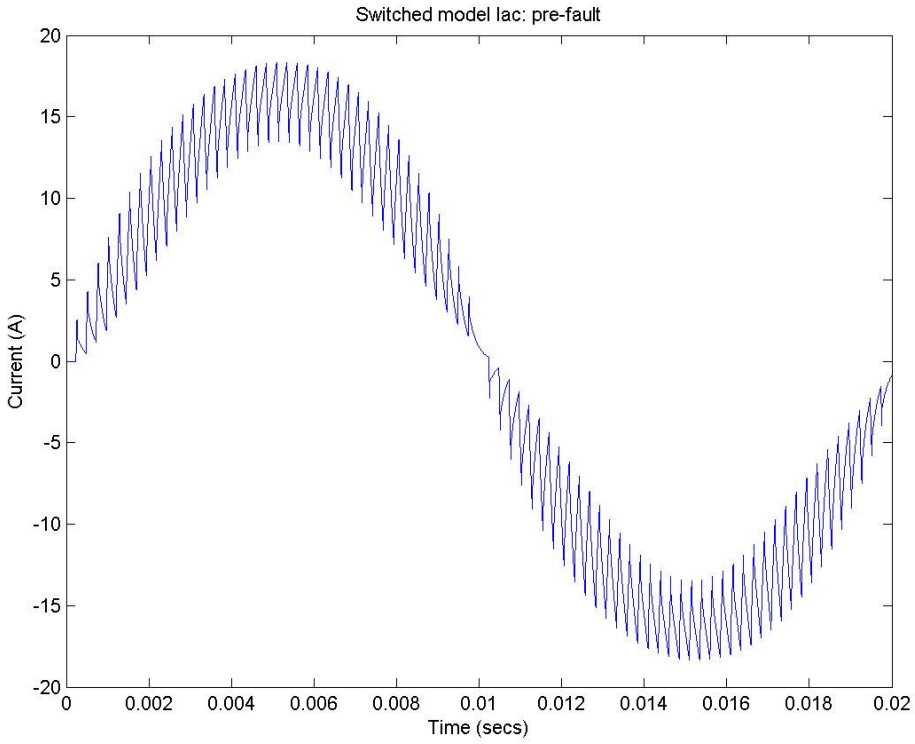

Fig. D.1. Switched model Iac – Pre-fault

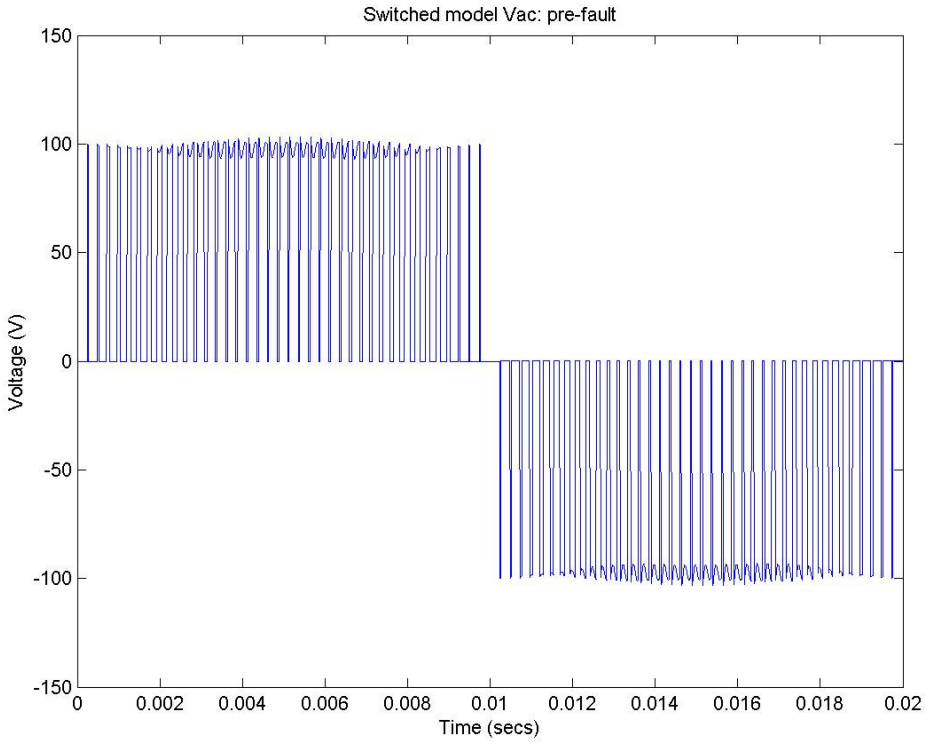

Fig. D.2. Switched model Vac – Pre-fault

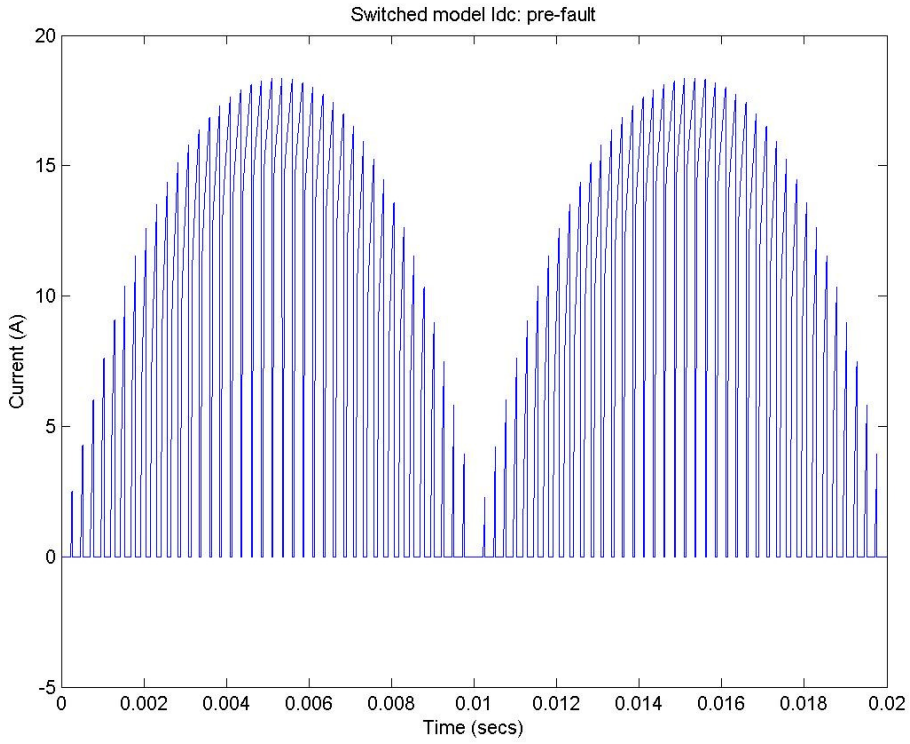

Fig. D.3. Switched model Idc – Pre-fault

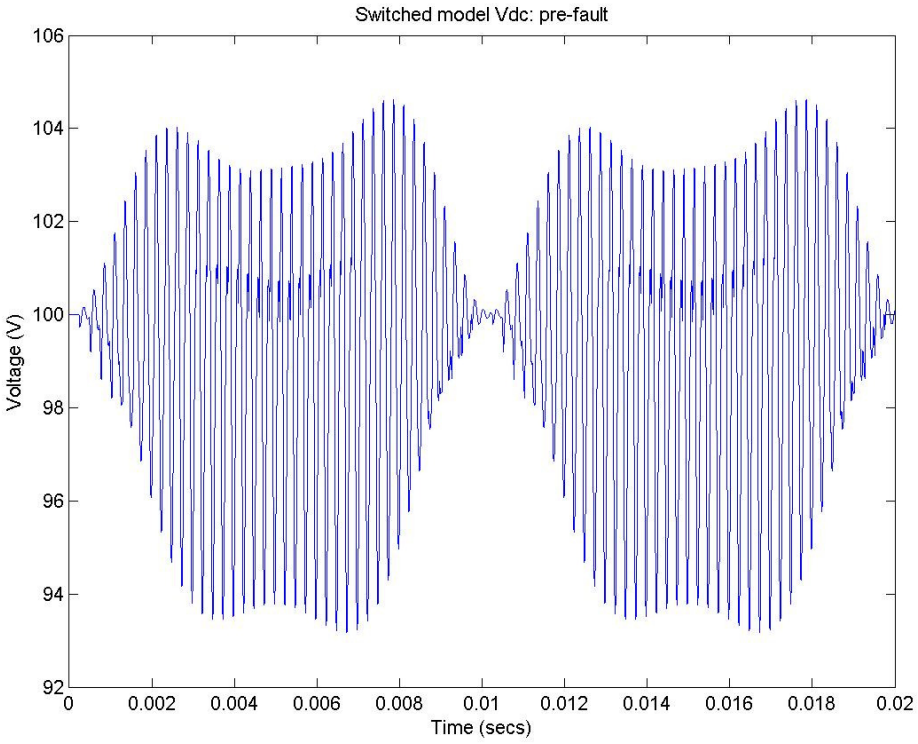

Fig. D.4. Switched model Vdc – Pre-fault

Figures D.5 and D.6 illustrate the steady state ac current and voltage outputs between 0.06 and 0.08 seconds of simulation time. Figures D.7 and D.8 illustrate the dc current and voltage outputs for this period.

This second group of plots shows the behaviour of the switched converter model after a low impedance rail to rail fault has occurred across the ac terminals of the inverter.

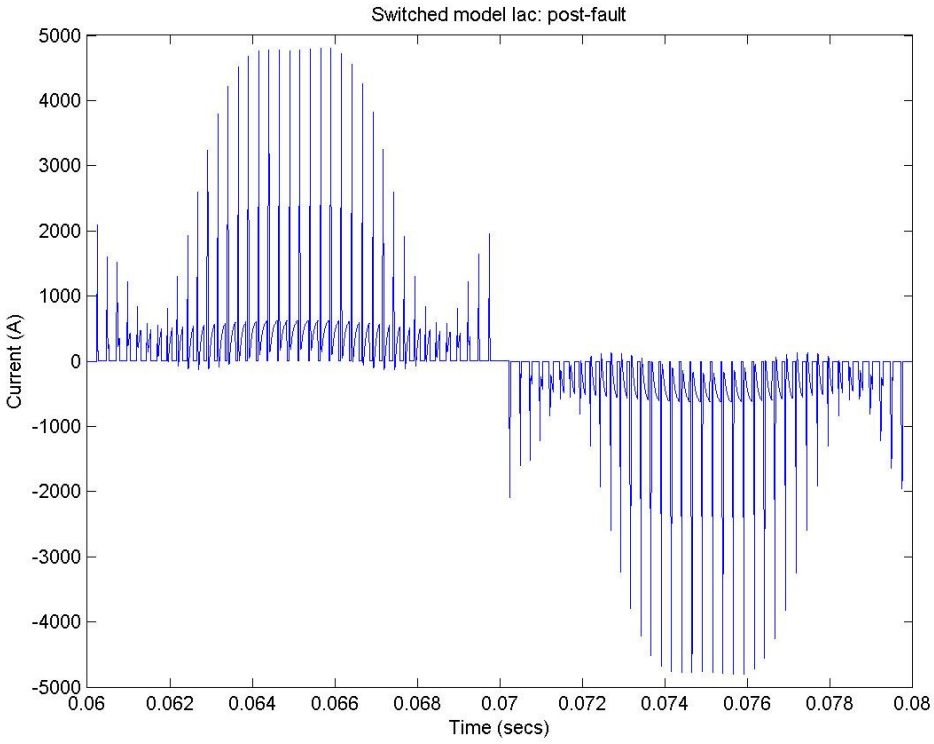

Fig. D.5. Switched model Iac – Post-fault

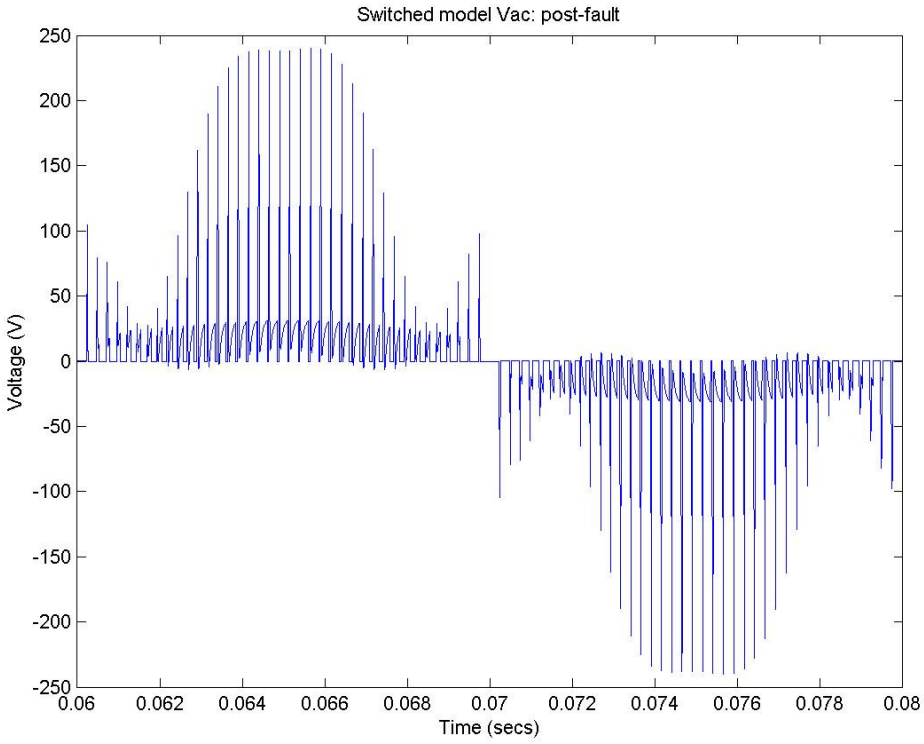

Fig. D.6. Switched model Vac – Post-fault

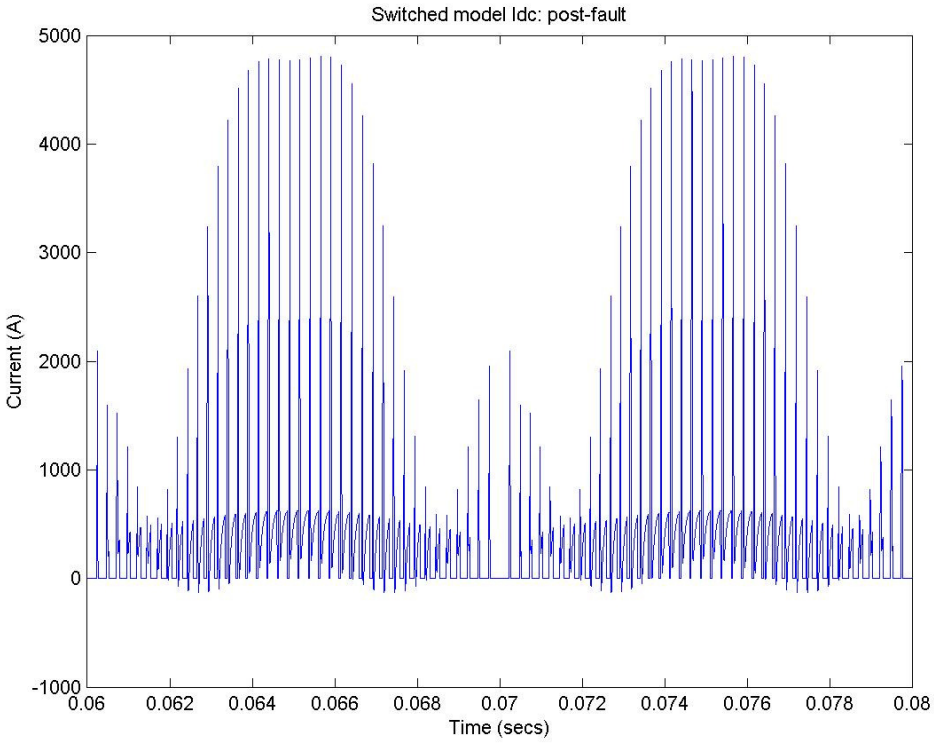

Fig. D.7. Switched model Idc – Post-fault

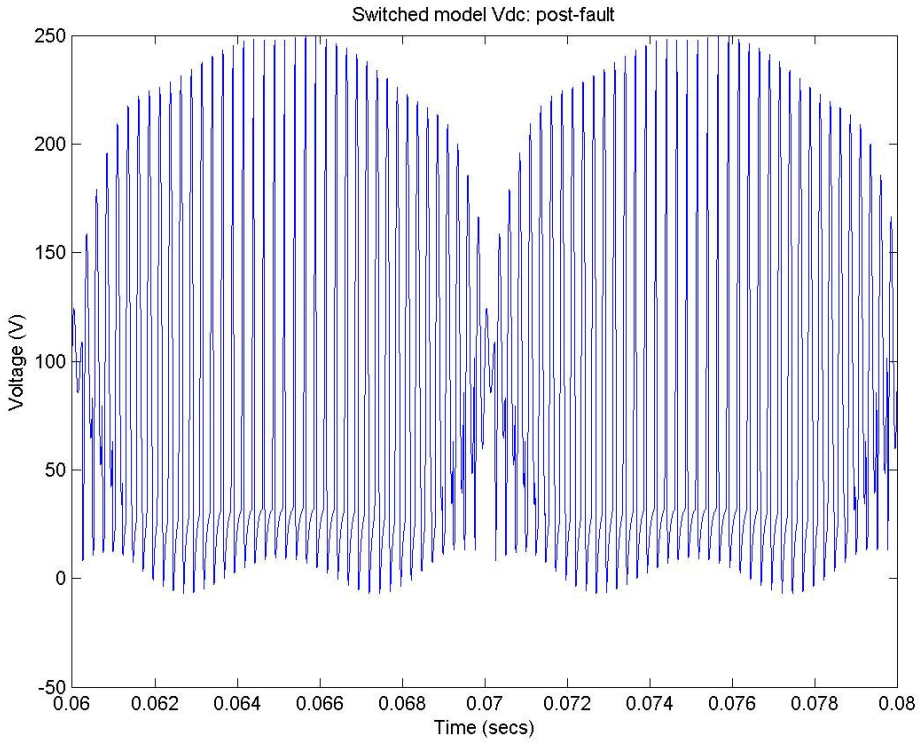

Fig. D.8. Switched model Vdc – Post-fault

D.2 AFM Simulation Results

Figures D.9 and D.10 illustrate the steady state ac current and voltage outputs between 0 and 0.02 seconds of the simulation time. Figures D.11 and D.12 illustrate the dc current and voltage outputs also over this period. These plots show the behaviour of the AFM during normal (i.e. unfaulted) operating conditions supplying an ac load of fixed impedance.

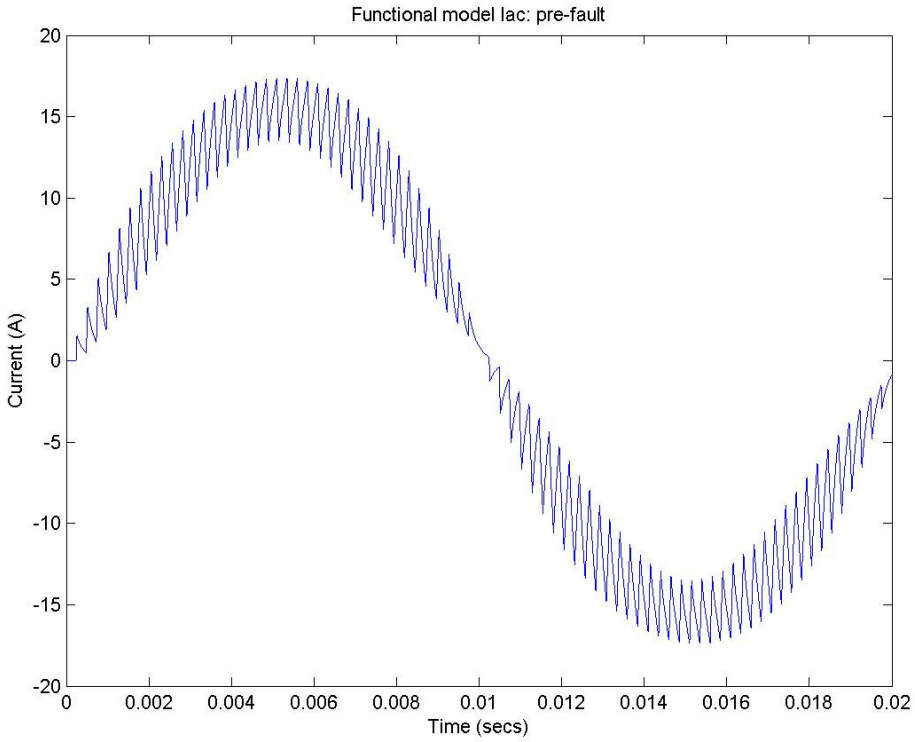

Fig. D.9. AFM Iac – Pre-fault

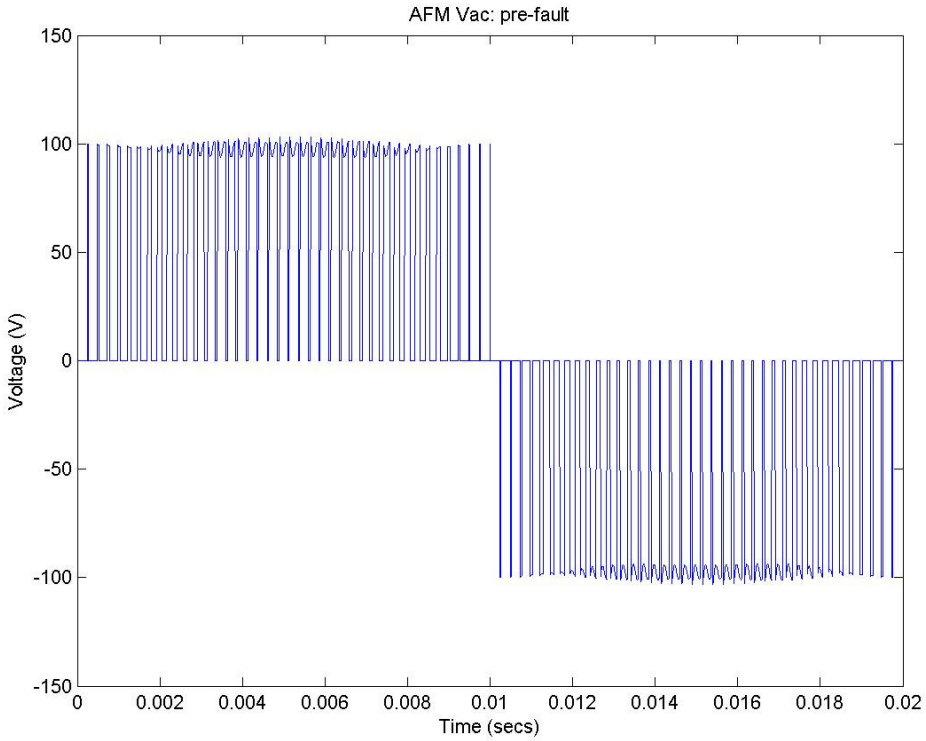

Fig. D.10. AFM Vac – Pre-fault

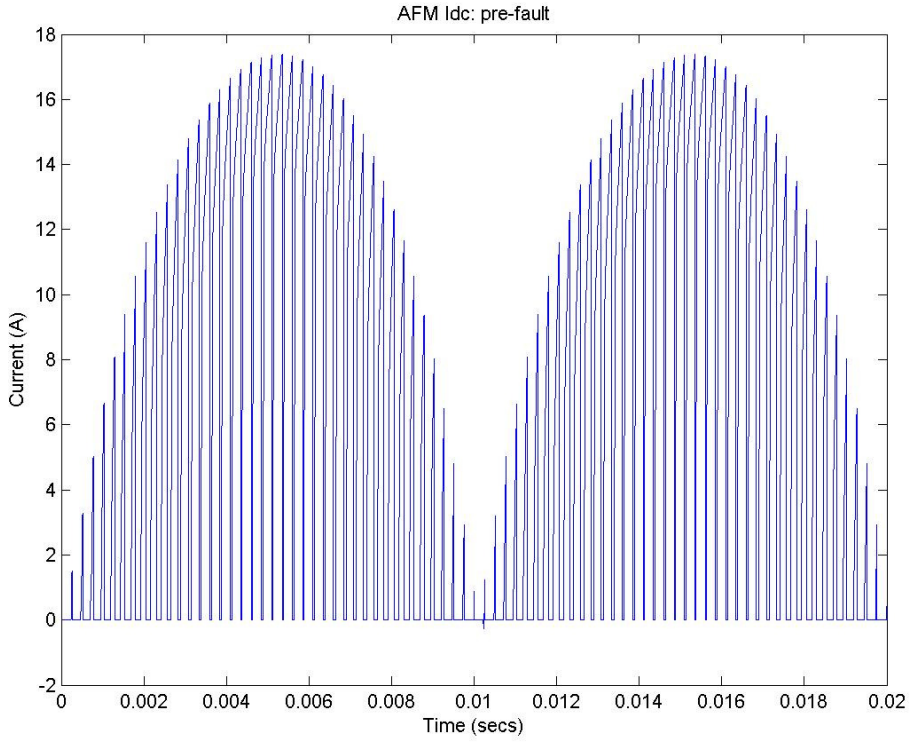

Fig. D.11. AFM Idc – Pre-fault

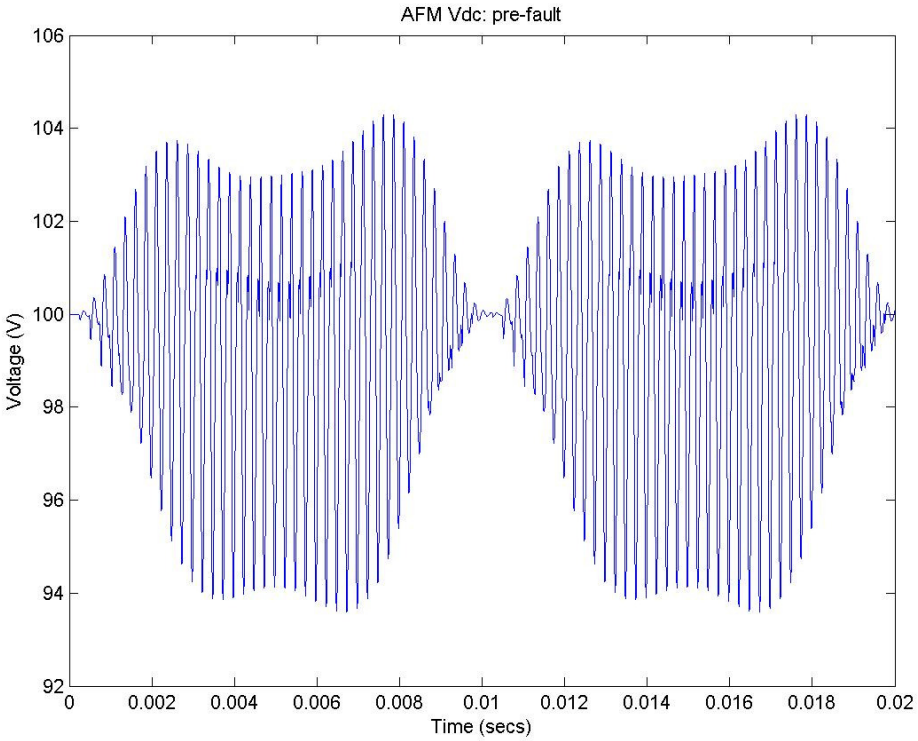

Fig. D.12. AFM Vdc – Pre-fault

Figures D.13 and D.14 illustrate the steady state ac current and voltage outputs between 0.06 and 0.08 seconds of simulation time. Figures D.15 and D.16 illustrate the dc current and voltage outputs also over this period. This second group of plots show the behaviour of the AFM after a low impedance rail to rail fault has occurred across the ac terminals of the inverter.

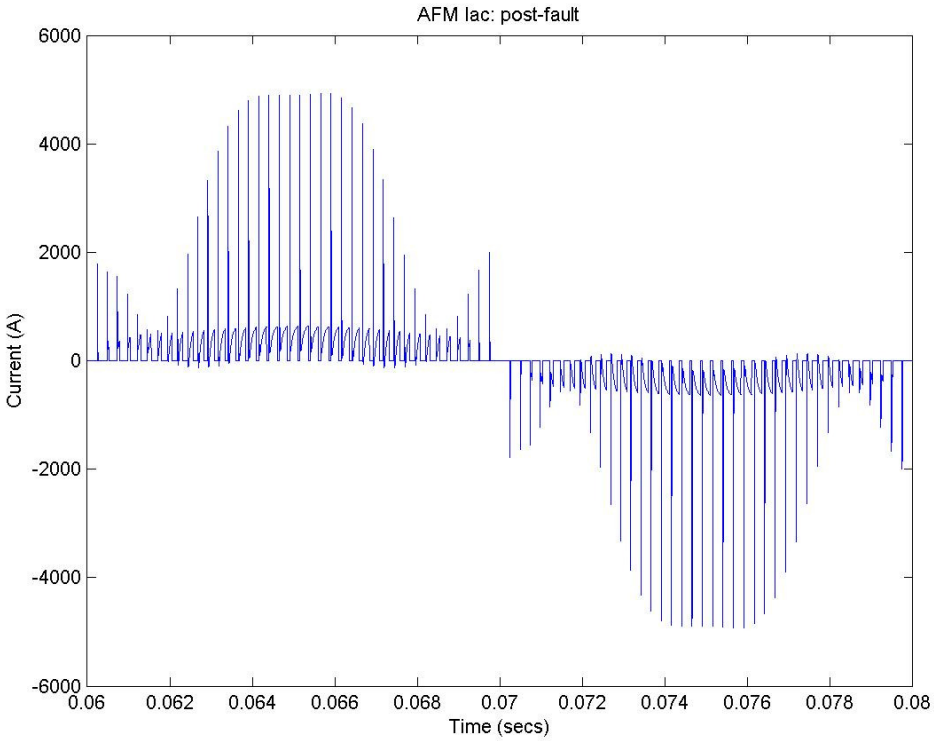

Fig. D.13. AFM Iac – Post-fault

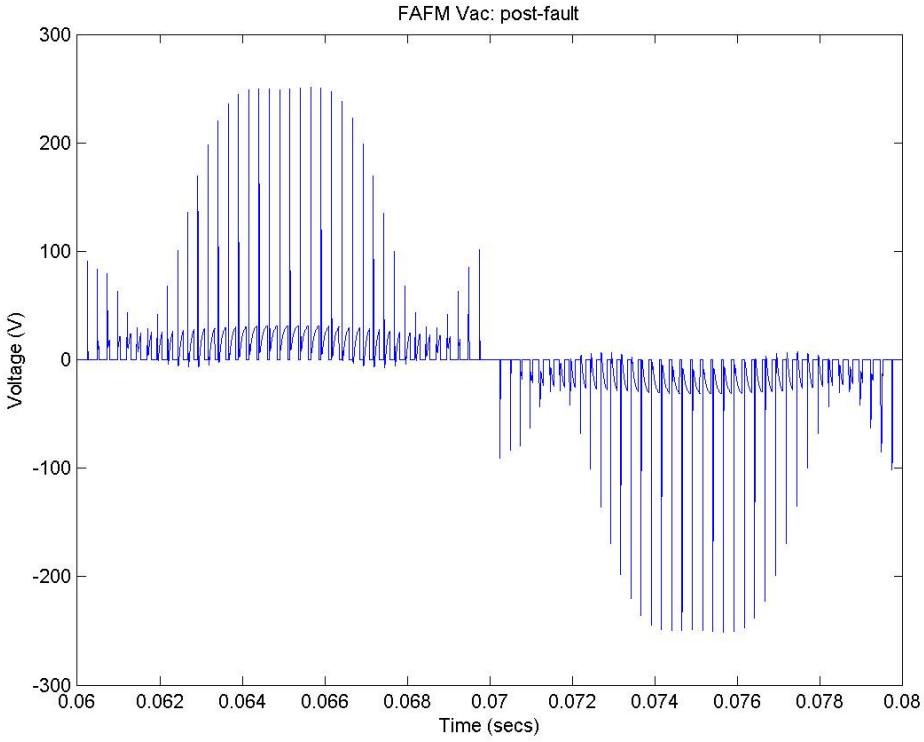

Fig. D.14. AFM Vac – Post-fault

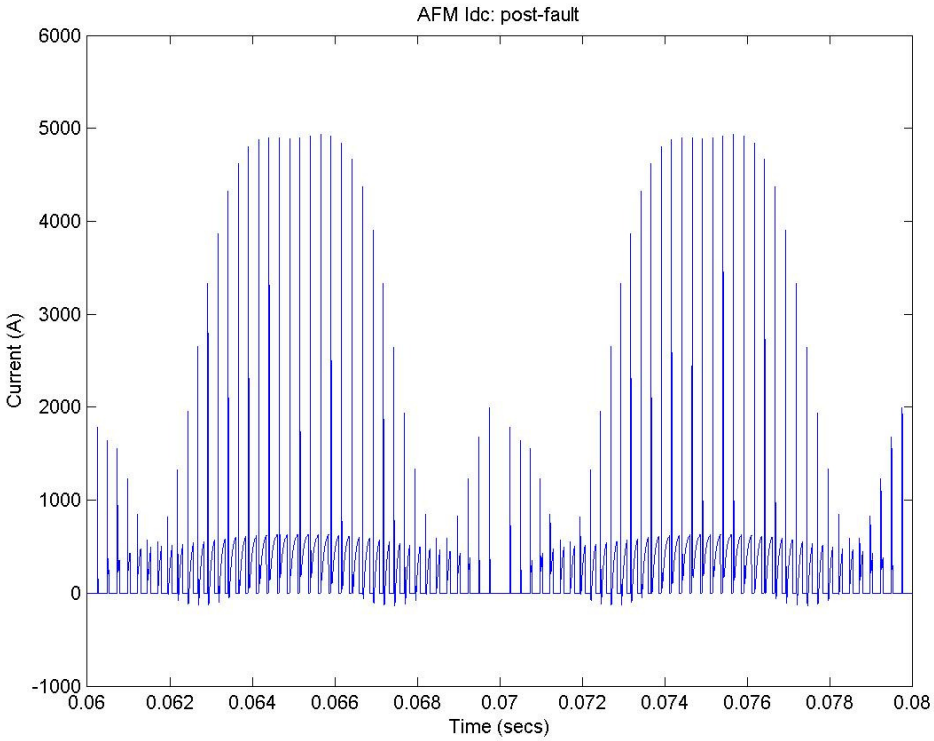

Fig. D.15. AFM Idc – Post-fault

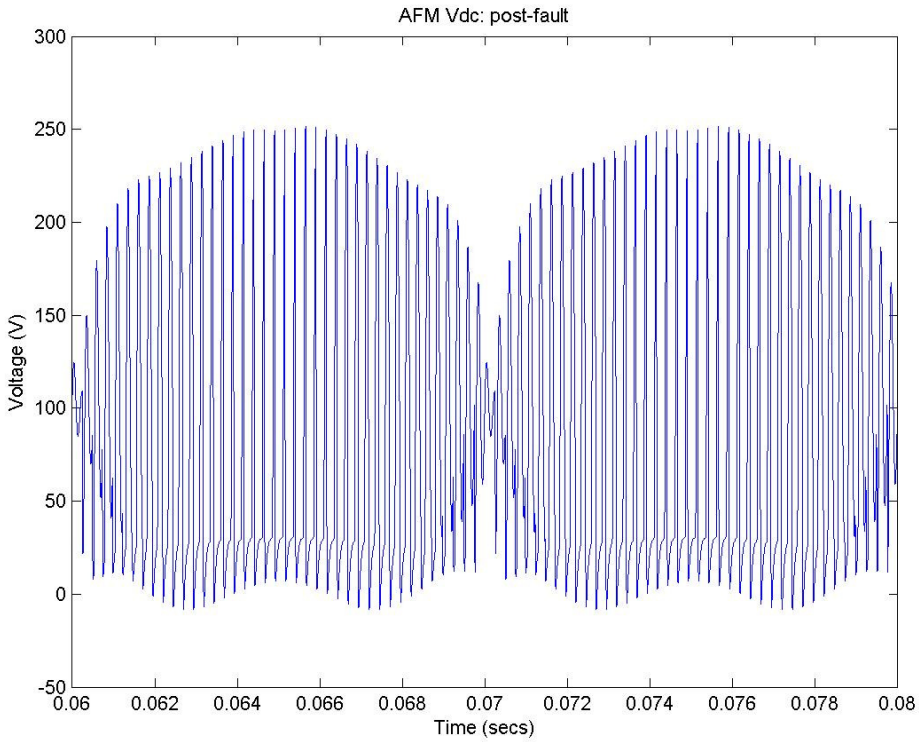

Fig. D.16. AFM Vdc – Post-fault

D.3 Time-Averaged AFM Simulation Results

Figures D.17 and D.18 illustrate the steady state ac current and voltage outputs between 0 and 0.02 seconds of simulation time. Figures D.19 and D.20 illustrate the dc current and voltage outputs also over this period. These plots show the behaviour of the AFM during normal (i.e. unfaulted) operating conditions supplying an ac load of fixed impedance.

Note that the time-averaged model utilised to produce these results does not make use of the additional error reduction term A_{err} (discussed in Chapter 7, Section 7.5.4) because there is no additional voltage source on the ac side of the inverter and as such, the error in V_{ac} produced by the AFM under these conditions should be negligible.

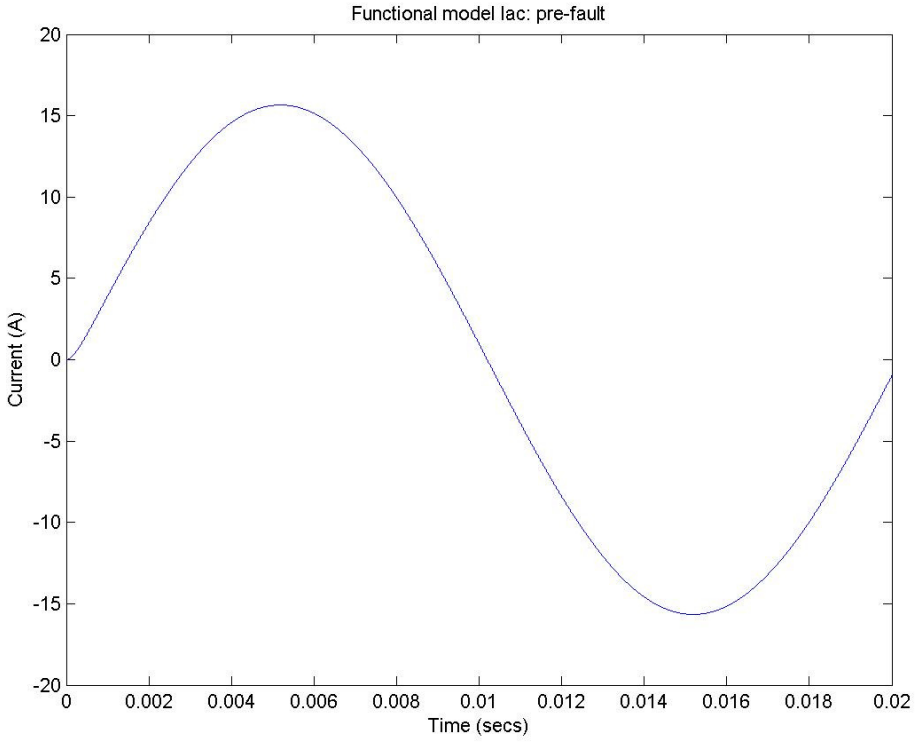

Fig. D.17. Time-averaged AFM Iac – Pre-fault

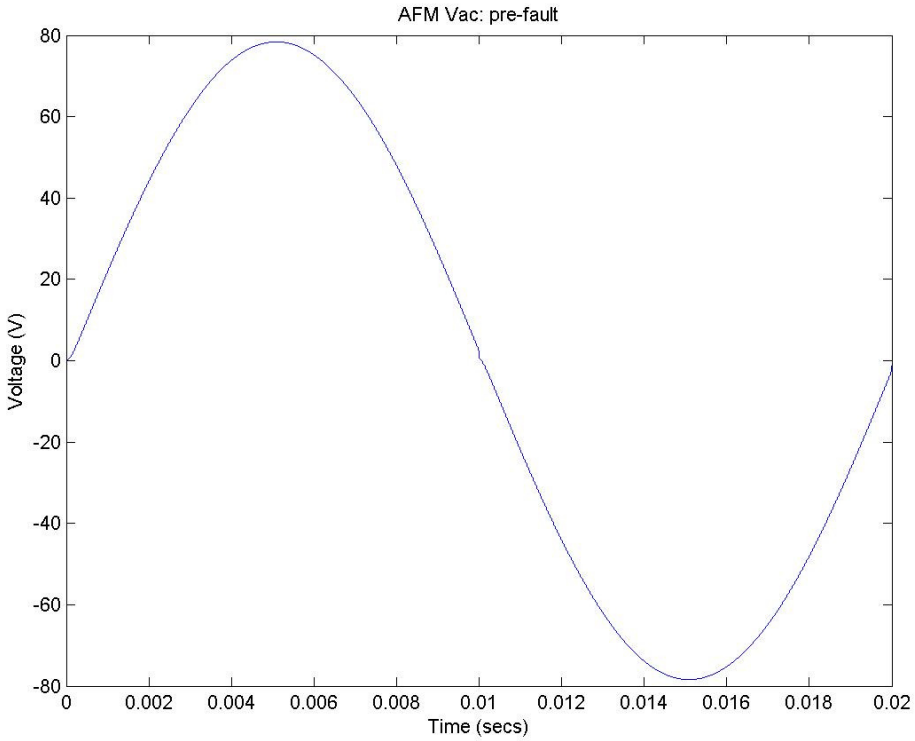

Fig. D.18. Time-averaged AFM Vac – Pre-fault

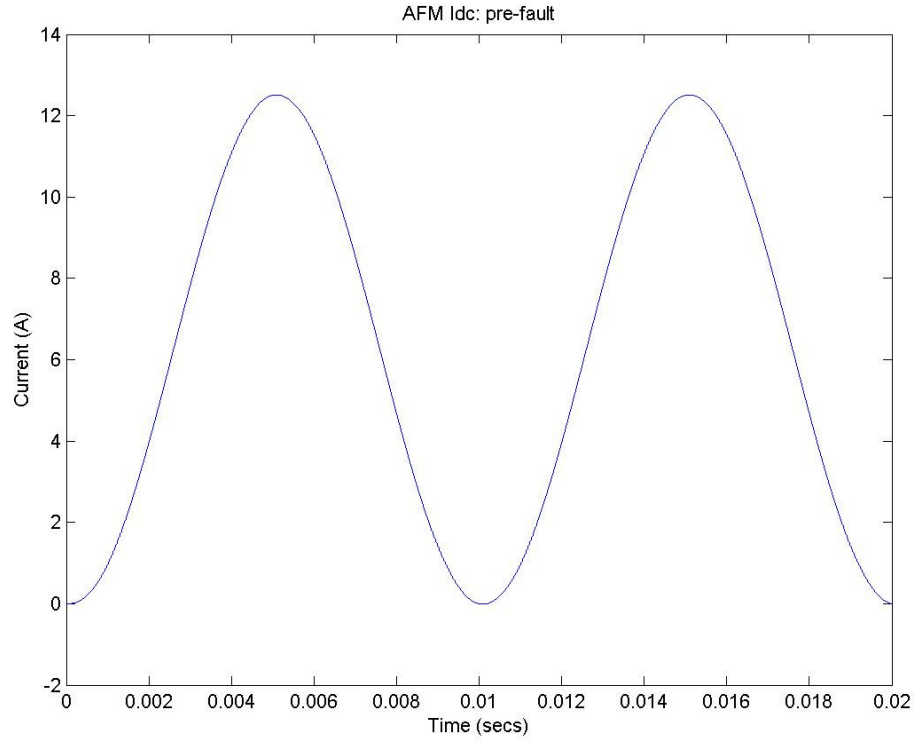

Fig. D.19. Time-averaged AFM Idc – Pre-fault

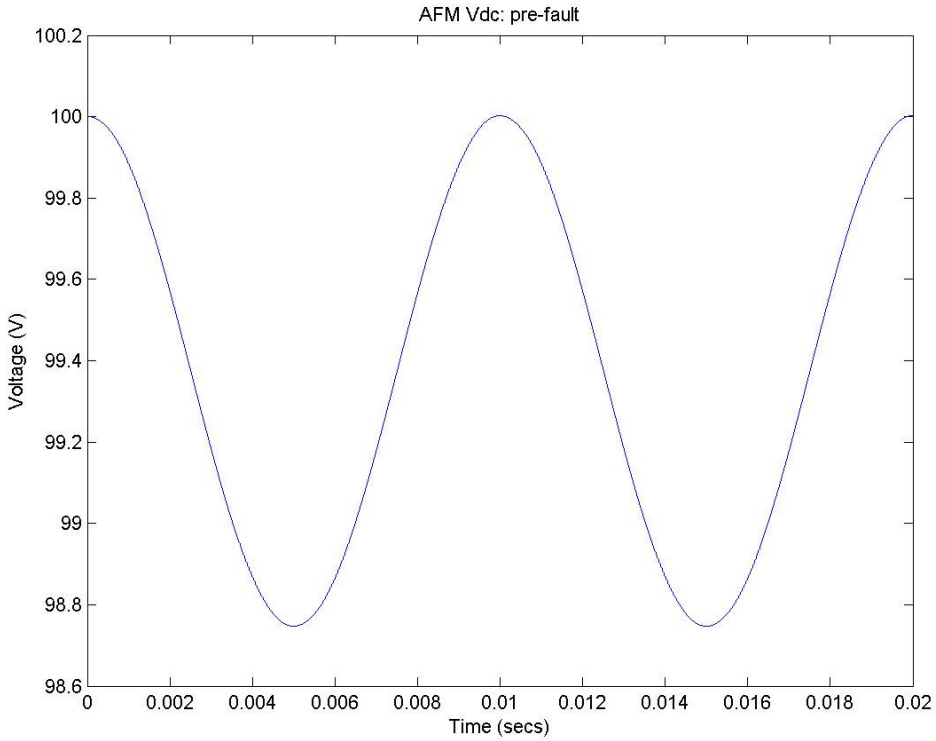

Fig. D.20. Time-averaged AFM Vdc – Pre-fault

Figures D.21 and D.22 illustrate the steady state ac current and voltage outputs between 0.06 and 0.08 seconds of simulation time. Figures D.23 and D.24 illustrate the dc current and voltage outputs also over this period. This second group of plots shows the behaviour of the time-averaged AFM after a low impedance rail to rail fault has occurred across the ac terminals of the inverter.

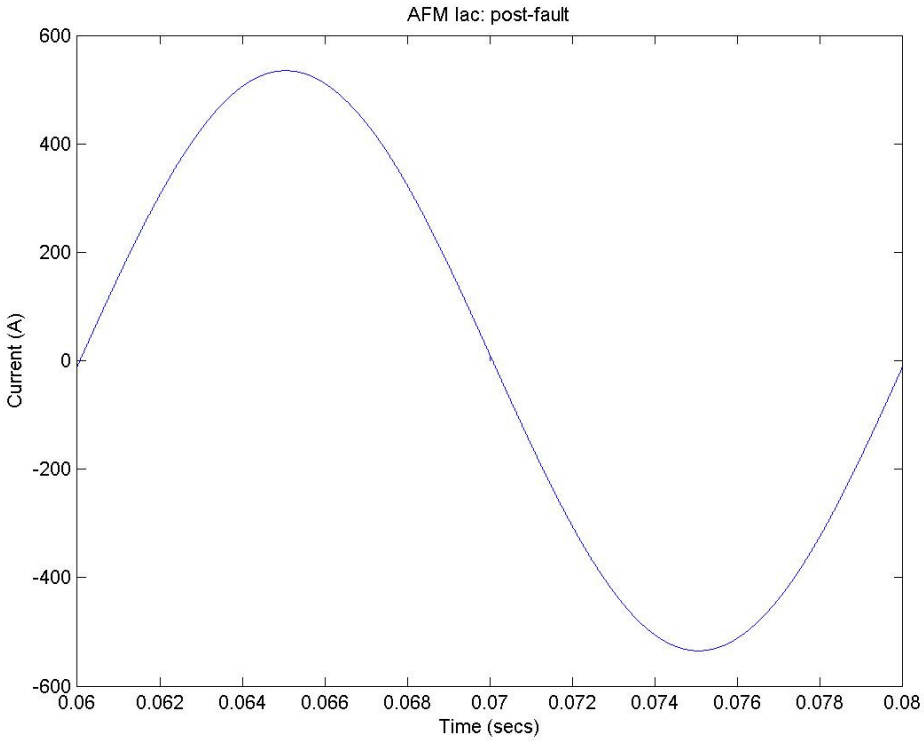

Fig. D.21. Time-averaged AFM Iac – Post-fault

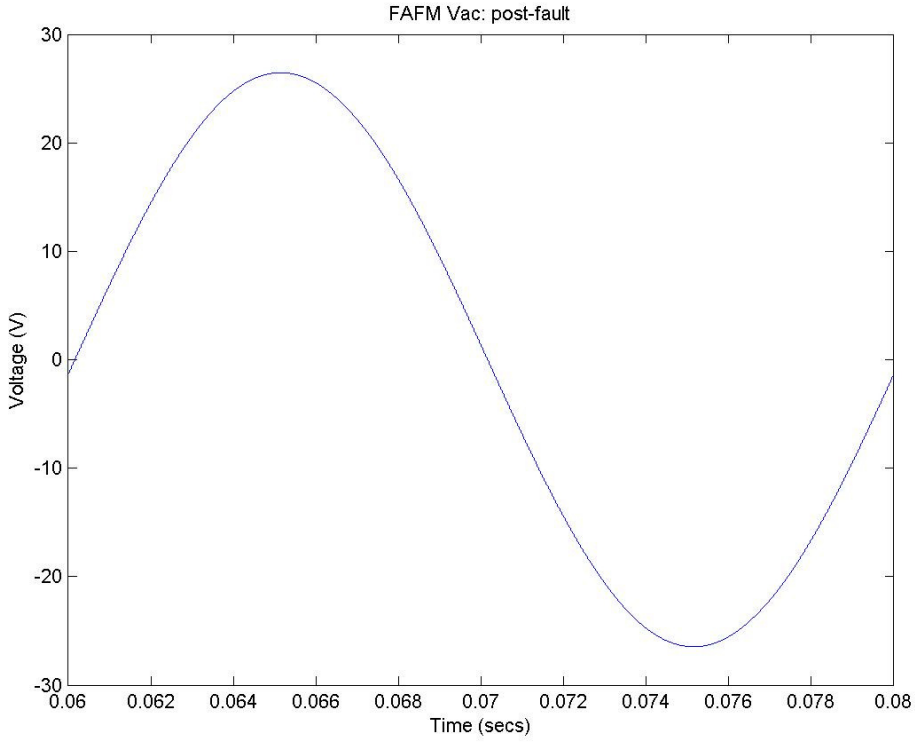

Fig. D.22. Time-averaged AFM Vac – Post-fault

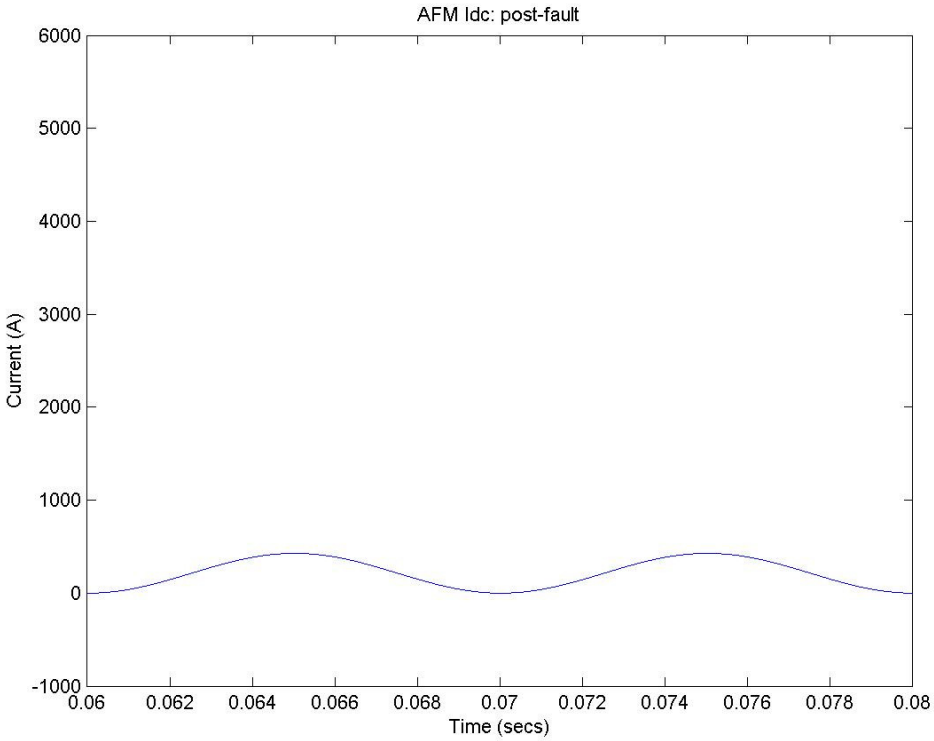

Fig. D.23. Time-averaged AFM Idc – Post-fault

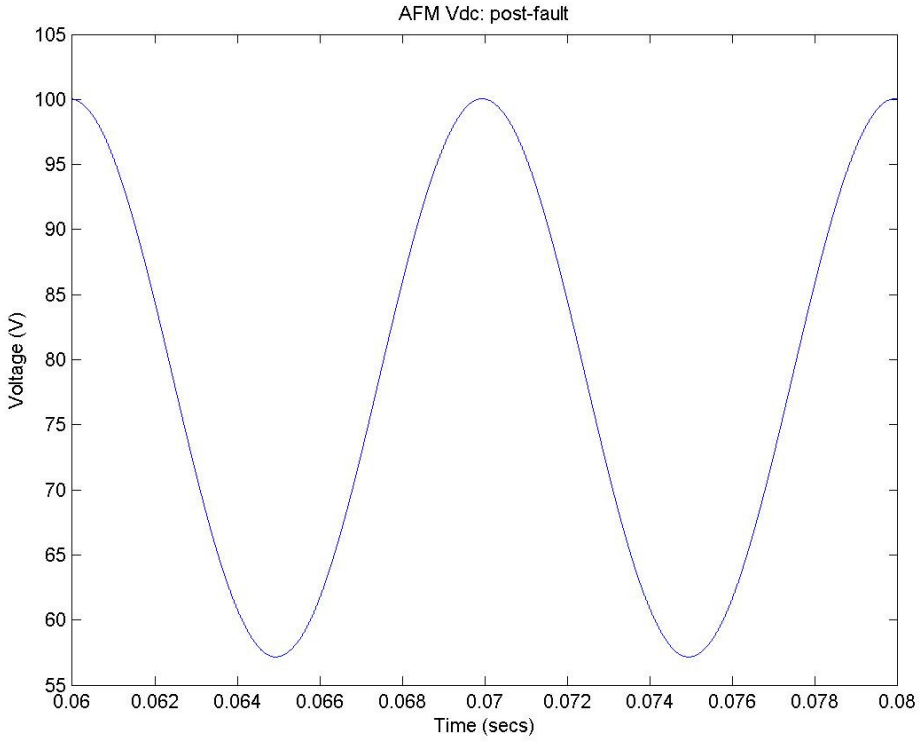

Fig. D.24. Time-averaged AFM Vdc – Post-fault

D.4 AFM Simulation Results – Erroneous Derivation of Z_{in}

Figures D.25 and D.26 illustrate the steady state ac current and voltage outputs between 0 and 0.02 seconds of simulation time. Figures D.27 and D.28 illustrate the dc current and voltage outputs also over this period. These plots show the behaviour of the case study AFM during normal (i.e. unfaulted) operating conditions supplying an ac load of fixed impedance.

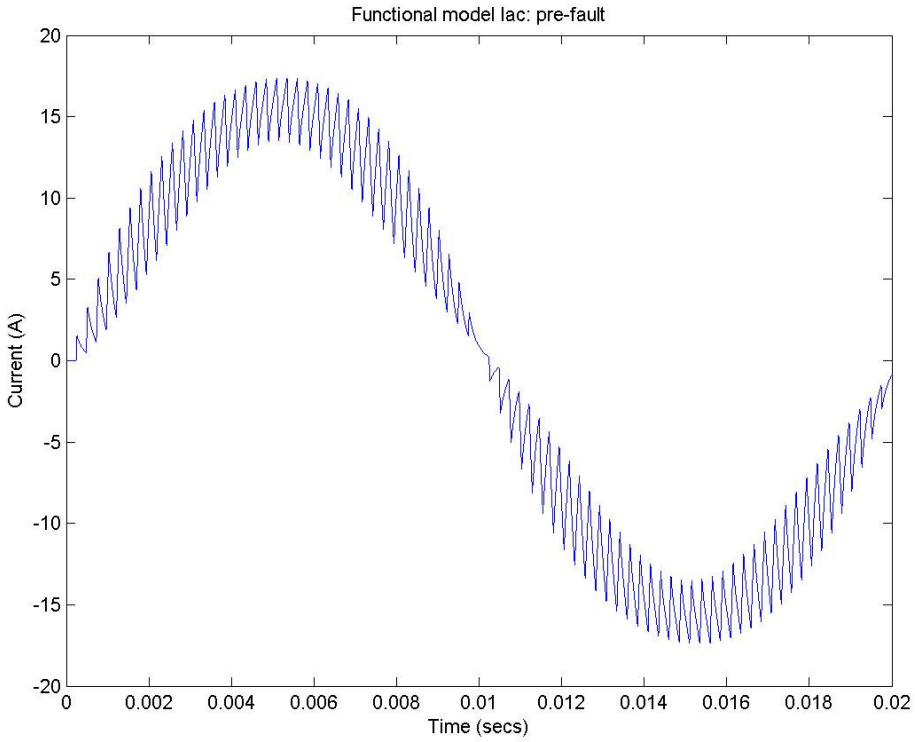

Fig. D.25. Erroneous AFM Iac – Pre-fault

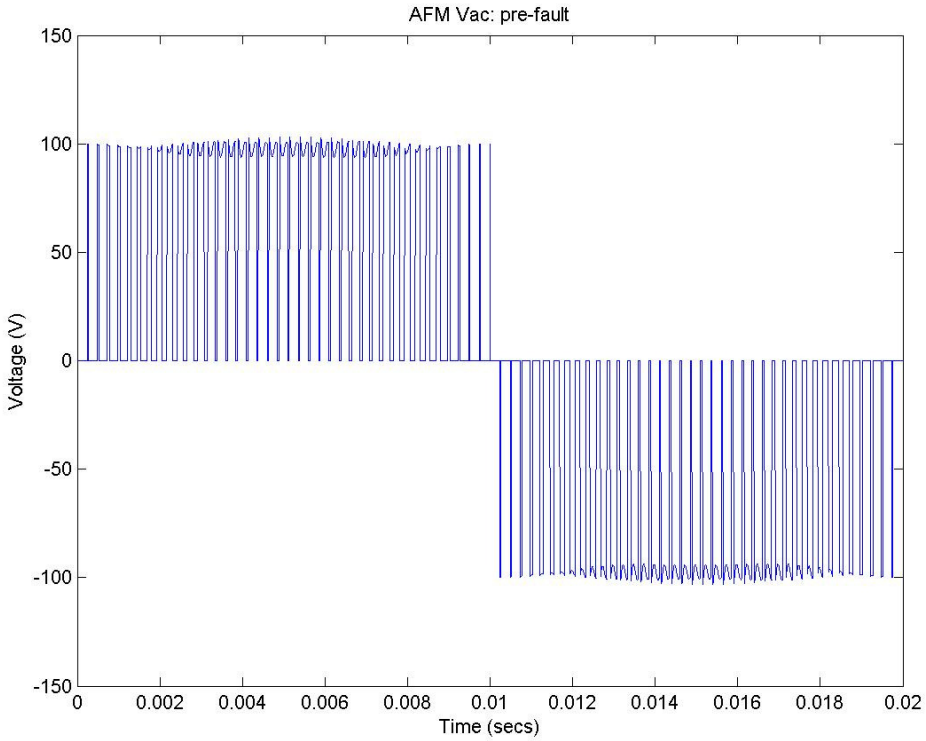

Fig. D.26. Erroneous AFM Vac – Pre-fault

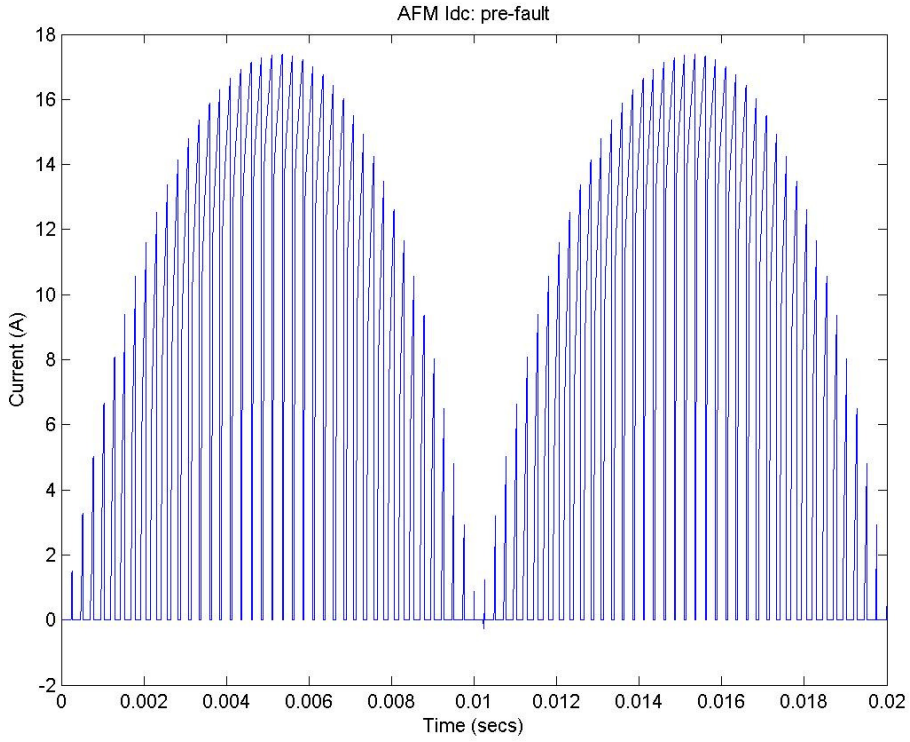

Fig. D.27. Erroneous AFM Idc – Pre-fault

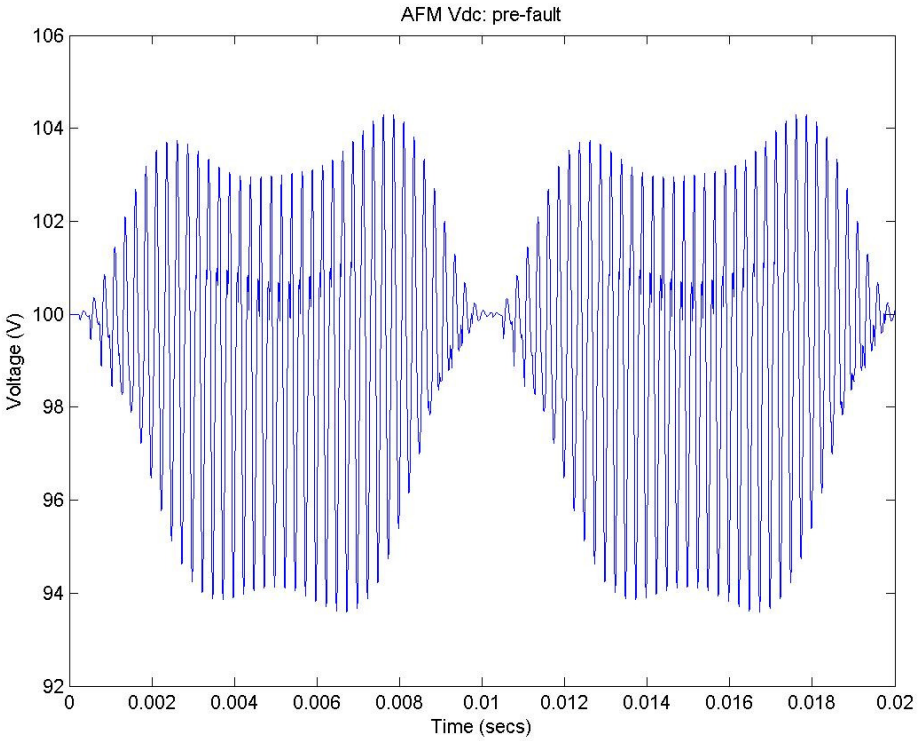

Fig. D.28. Erroneous AFM Vdc – Pre-fault

Figures D.29 and D.30 illustrate the steady state ac current and voltage outputs between 0.06 and 0.08 seconds of simulation time. Figures D.31 and D.32 illustrate the dc current and voltage outputs for this same period. This second group of plots shows the behaviour of the very erroneous AFM after a low impedance rail to rail fault has occurred across the ac terminals of the inverter.

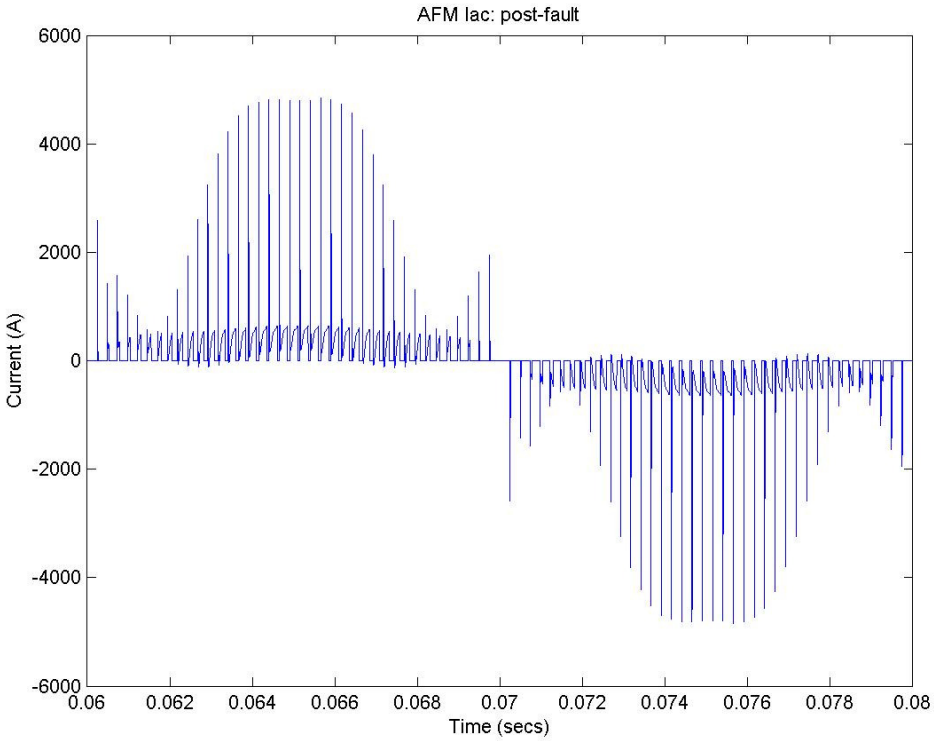

Fig. D.29. Erroneous AFM Iac – Post-fault

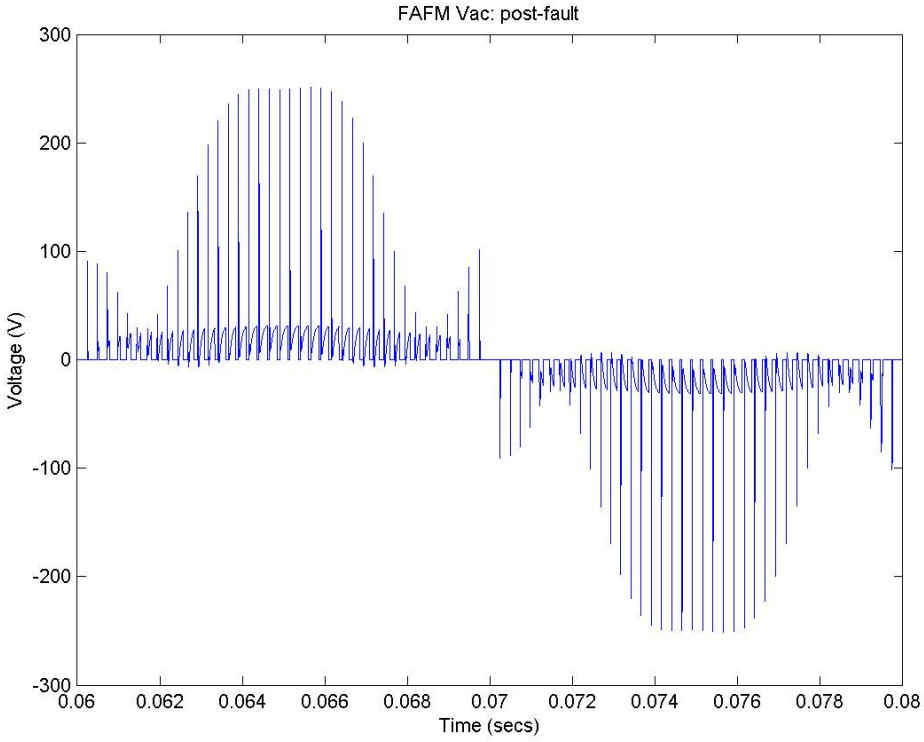

Fig. D.30. Erroneous AFM Vac – Post-fault

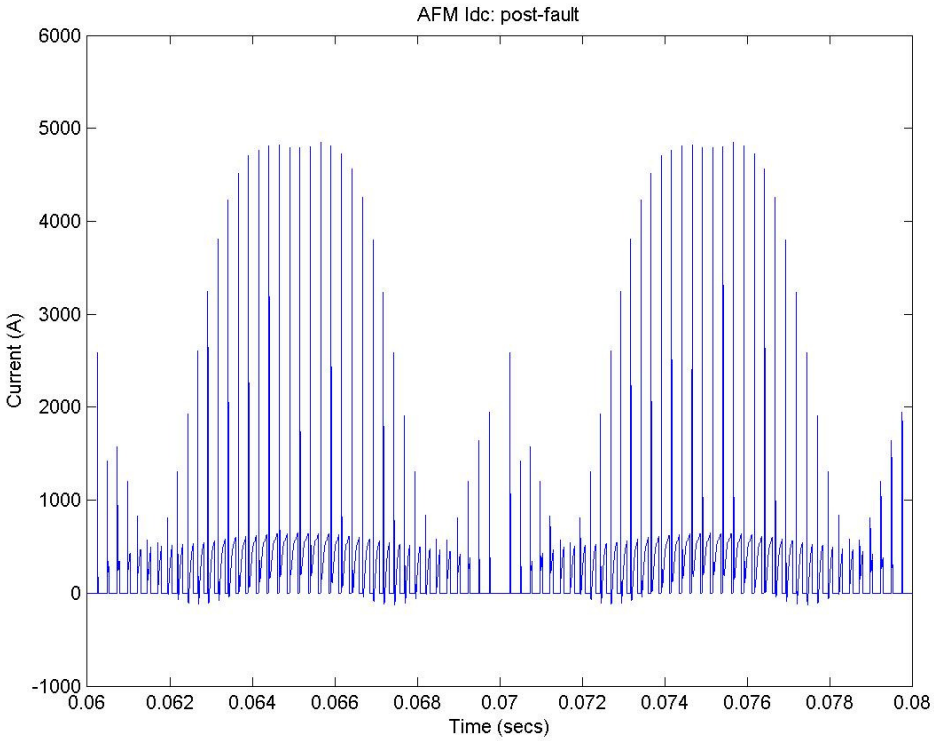

Fig. D.31. Erroneous AFM Idc – Post-fault

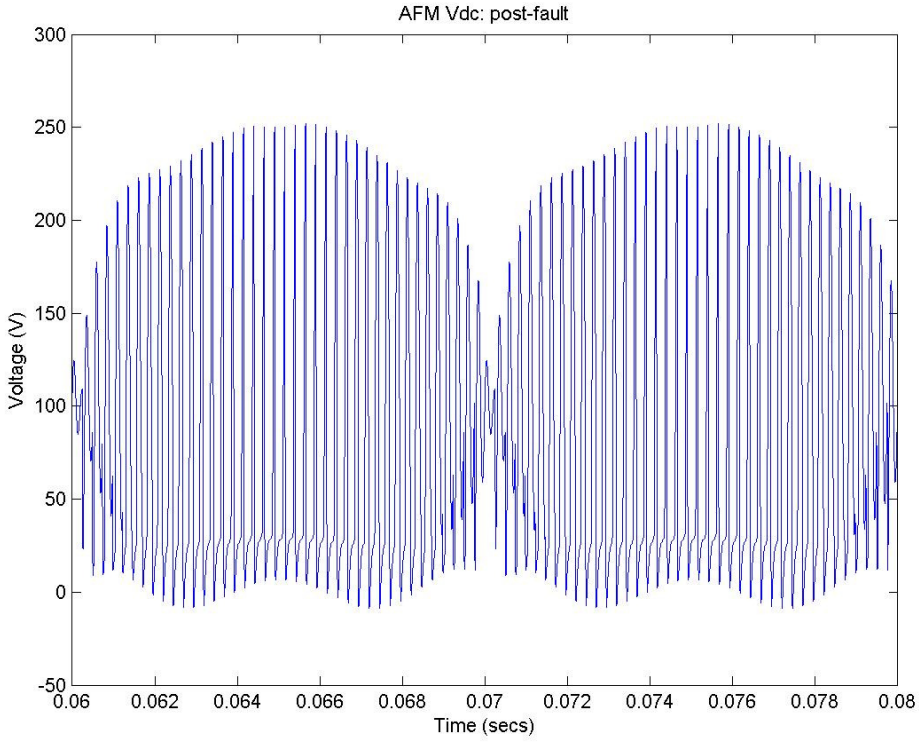

Fig. D.32. Erroneous AFM Vdc – Post-fault